Separation & Purification Reviews
Publication details, including instructions for authors and subscription information:
http://www.informaworld.com/smpp/title~content=t713597294

Expression of Fluid from Biological Solids

H. G. Schwartzberg[a]
[a] Science Department, University of Massachusetts, Amherst, Massachusetts

To cite this Article Schwartzberg, H. G.(1997) 'Expression of Fluid from Biological Solids', Separation & Purification Reviews, 26: 1, 1 — 213
To link to this Article: DOI: 10.1080/03602549708014156
URL: http://dx.doi.org/10.1080/03602549708014156

SEPARATION AND PURIFICATION METHODS, 26(1), 1–213 (1997)

EXPRESSION OF FLUID FROM BIOLOGICAL SOLIDS

H.G. Schwartzberg
Food Science Department
University of Massachusetts
Amherst, Massachusetts 01003

TABLE OF CONTENTS

1. INTRODUCTION

Expression: Expression or pressing is a process in which liquid contained in pores in a solid matrix or contiguous array of solid matrices or particles is expelled by compaction or squeezing. The pressed mixture is often called a "presscake", or "cake" for short. Mechanically-, hydraulically- and pneumatically-driven moving surfaces provide compaction in most expression equipment. Incidental compaction of solid-fluid mixtures also causes expression. Fluid is pressed out of moist soils when added soil or structures are placed on top of them. If gas pressure acts on a soft cake whose pores are so fine that capillary "suction" pressure exceeds the applied pressure, the gas

won't displace fluid directly; but the applied pressure will compact the cake and express fluid.

Weight-driven expression occurs in piles of moist solids and in sediments at the bottom of bodies of fluid. Centrifugal force compacts solids and expels fluid in centrifuges. Fluid drag also causes compaction. Attractive forces between particles in cakes cause expulsion of fluid during syneresis. Forces induced by electrical fields can also cause expression. Thus expression can be caused by mechanical and pneumatic force, gravity, centrifugal force, drag forces, electrical fields and attractive forces between solids.

Scope of Review: This review covers how theory, expression equipment and its operation apply to expression of fluid from biological solids, particularly cellular biological solids. Expression behavior of non-biological solids will also be reviewed for comparison purposes.

Alternative Processes: Solutes in fluids expressed from cellular biological solids often can also be recovered by extraction, which generally provides higher yields, but requires removal of solvents, resulting in higher energy costs. Multi-stage, countercurrent combinations of imbibition and expression can sometimes provide solute yields close to those obtained by solid-liquid extraction. Combinations of expression and solvent extraction are frequently used to recover vegetable oils. Expression is preferred for simply removing water or other fluids from cellular biological solids or for recovering organelles and sparingly soluble intracellular materials from such solids.

Enzymes that convert cell wall solids and other insoluble solids into soluble matter are now used to increase juice solids yields and reduce or eliminate solid pressing residues and needs for expression. However, these processes may change the taste of juices.

2. USES OF EXPRESSION

Expression is used to recover valuable fluids, e.g. vegetable oil and fruit juice and organelles. It is also used to reduce fluid contents of solids that are going

to be dried and used for fuel, feed or paper, or to reduce the mass and volume of moist processing and municipal wastes. Expression also occurs when curds are compacted and fused together, when filtered fiber slurries are compacted into felts and paper, and when slurries of fine particles are compacted to form molded parts.

Table I lists biological press feeds, estimated amounts of feed pressed per year and resultant products generated by pressing.

3. EXPRESSION EQUIPMENT

Single-Screw Presses; In this common type of press, a screw turns inside a perforated barrel. Examples are shown in figs. 1, 2 and 3. Cake, fed in at one end of the barrel, moves down the screw because friction between the cake and barrel or baffles prevents the cake from turning in the barrel. The cake compacts because either: a) the screw's root diameter progressively increases; b) its pitch progressively decreases; c) the diameter of the barrel decreases; d) cake outflow is throttled; or e) combinations of these actions occur. Expressed fluid flows out through openings in the barrel. Barrels made of perforated sheet metal (see fig. 1) are used when pressing relatively soft fruits. Screws for pressing crushed wine grapes often extend only part way down the barrel; pressing also occurs in the screw-free zone because of solids-outflow throttling. Medium weight presses with barrels with coarse perforations lined with finer screens on their inside are used to press apples. Units with 7,000 to 8,000 kg/hr pressing capacity require 9.3 kW (12.5 HP) to drive and provide 69% to 74% juice yield for apples[1]. Large-diameter screw presses are used to dewater pulp and paper sludges, e.g. a 0.9-m diameter unit can handle 50,000 kg/day of sludge.

Screws designed to handle very wet feeds, e.g. bleached paper pulp, may operate with their axes tilted 60° up from the horizontal, and are driven at their upper (discharge) end[2]. Dilute slurry enters the open, bottom of the barrel. Fluid drains through perforations in the barrel and the solids thickens as they move upward, forming a plug near the top of the barrel. The plug compacts, is

TABLE I Expressed Materials, Annual Amount Processed Worldwide, and Products Obtained

Material	Amount Processed Per Year 10^9 kg/year	Products
Cellular Biological Solids		
Sugar Cane	676	sugar juices
Spent sugar beet shreds	242	cattle feed
Oranges	27	orange juice, peel oil
Grapefruit	1.9	grapefruit juice
Citrus pulp and peel	13.1	cattle feed
Wine Grapes (initial pressing)	50.5	grape juice, pomace
Grape Pomace	8.5	alcohol production stock
Pineapple trimmings, small fruit		pineapple juice
Apples (grated or milled)	3.8	apple juice
Cooked apple pomace		pectin liquor
Alfalfa	1.9	alfalfa protein, feed
Moistened cassava shreds		cyanogen-free cassava
Shredded tobacco		regenerated tobacco leaf
Shredded leather		regenerated leather
Dyed, bleached or washed cloth		moist cloth, dyes, bleach
Spent coffee grounds	1.5	partly dried fuel
Waste treatment sludge	rough est. 250	partly dewatered sludge
Flaxseed (34% oil)	1.8	linseed oil, presscake
Peanuts (45% oil)	8.5	peanut oil, extractor feed
Copra (63% oil)	5.0	coconut oil, extractor feed
Palm kernels (47% oil)	3.6	palm oil, extractor feed
Rapeseed (35% oil)	26	oil, extractor feed
Sesame seed (45% oil)	1.5	sesame oil, extractor feed
Corn germ	1.8	corn oil, cattle feed

(continued)

TABLE I Continued

Material	Amount Processed Per Year 10^9 kg/year	Products
Olives (20-25% oil)	8.6	olive oil
Oil-rich fish (e.g. menhaden)	21	fish oil, fish meal
Cocoa	1.7	cocoa butter, cocoa kibble
Cooked meat scraps	7.5	tallow, grease, meat meal
77%-90% moisture paper webs	1,360	60%-70% moisture paper
bleached paper pulp		high consistency pulp
waste paper pulp		partly dewatered pulp
wet bark from debarking drums		fuel
Degraded Cellular Material		
Peat		partly dried fuel
Brown Coal		partly dried fuel
Curds and Flocs		
Cut, cheese curds (94% liquid)	100	immersed curd cubes
Fully drained curd cubes	11	pressed blocks of cheese 31% to 50.3% moisture
Alum precipitated pectin		12.5% solids pectin ppt.

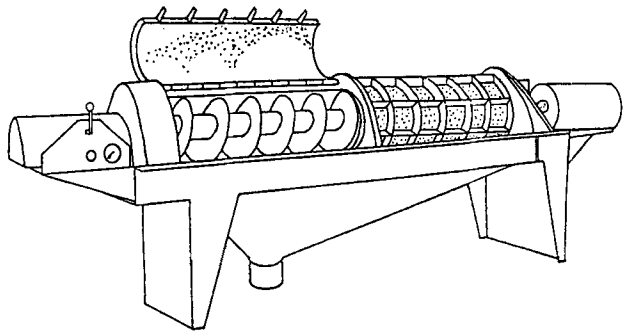

FIGURE 1 Light-weight, single-screw press (Brown International)

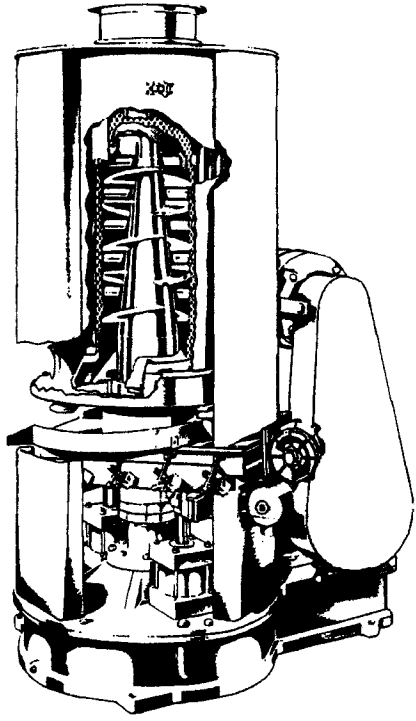

FIGURE 2 Medium-weight, single-screw press (Beloit-Jones)

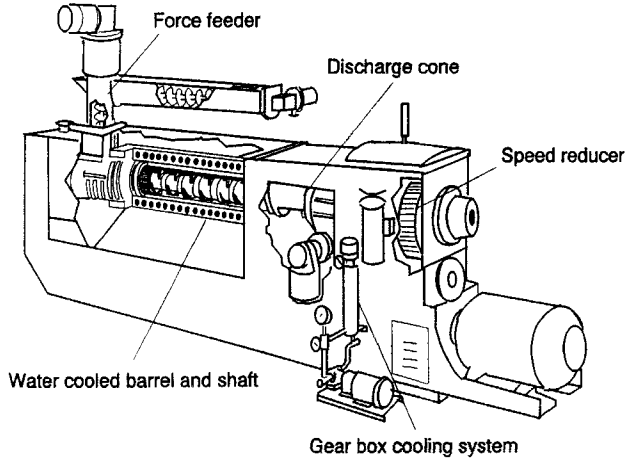

FIGURE 3 Heavy-weight, single-screw press (oil expeller) with breaker bars, baffles and wedge-bar cage (French Oil Machinery Company)

forced out of the barrel by the screw, and is broken up by breaker bars on the screw drive shaft and discharges. Expression occurs only near the top of the barrel, filtration near the bottom.

Moderately heavy barrels (see fig. 2) are used when pressing harder materials, materials with thick cell walls (e.g. spent coffee grounds, bleached paper pulp), materials that can stand intense pressing (e.g. grapes used to produce juice for sweetening) and solid residues from less stringent pressing operations, (e.g. grape pomace left after juice recovery for wine, citrus peels and pulp left after juice recovery).

Solids often discharge through flow constrictions that provide back pressure, which is adjusted by varying opening size, or by pressing a spring-loaded or hydraulically or pneumatically loaded throttling element, e.g. a cone, against the advancing cake. A motor-driven, rotating cone that turns at a different speed than the screw may be used. Its face may be perforated to permit added outflow of fluid.

Heavy Duty Screw Presses: Oil is expressed from cooked, pretreated oil seeds in screw presses (expellers) with cages made of heavy case-hardened bars (see fig. 3). To prevent extruded solids from plugging openings between the bars, the openings widen in the direction of oil outflow. 0.5 mm openings and 4% open area may be used near a press's feed end, and 0.13 mm openings and 1% open area near its discharge end. Most of the expelled oil flows radially outward, but, if the cage openings are too narrow or the rate of compaction is too great, oil flows back down the screw towards its feed end. This reduces friction between the cake and the barrel wall so that the cake sometimes turns en-masse; and the screw no longer conveys the cake, a condition known as "oiling up". Breaker bars and baffles that project inward from the barrel wall and fit between gaps in the screw are used to prevent hard-to-press cakes from turning en-masse. The bars and baffles also reduce cake blinding by breaking up the cake and inducing solids turnover.

Pressures up to 110 MPa (16,000 psi) are generated in oil expellers. Expellers may be equipped with meters that indicate power use or screw-drive

torque. Solids output throttling can be adjusted to provide drive power expenditures or torques that provide good pressing.

Two expellers may be connected in series, e.g. a vertical first screw and a horizontal second screw, or two, coaxial screws driven at different speeds inside a common housing. The first screw has a constant root diameter, turns faster (e.g. at 122 rpm) than the second, expels entrained air, expresses 40% to 50% of the oil in the feed and forces material into the second section. The second screw has an expanding root diameter, flights interrupted by breaker bars, turns at a slower speed (e.g. 42 rpm) and can expel up to 85% of the remaining oil. A large oil expeller may handle 17,400 kg feed/hr, have a 2.5-m long cage and an average ID of 0.38-m and require a 447 kW (600 HP) drive[3].

Oil seeds that contain 25% oil, or less, are usually flaked and directly subjected to solvent extraction. Screw presses, used to recover oil from plant matter with higher oil contents, can provide residual oil contents as low as 3.5%. Fines expelled with oil are separated from it and recycled to the press. To minimize wear and problems caused by fines recycling, high-oil-content feeds are usually prepressed rather than fully pressed[4]. Prepressing removes two thirds of the oil and generates cake containing 15% to 18% oil. 95% to 98% of the residual oil is recovered by subsequent solvent extraction. Throughput can be doubled when full-press expellers are used as prepresses, but it is preferable to use units specifically designed for prepressing. Most oil screw presses in the U.S. are prepresses; thousands of full-press units are still used in developing and underdeveloped countries[4].

Porous, vapor-puffed, cylindrical "collets" produced in heated, single-screw extruders[5] are now often used instead of flakes to facilitate solvent extraction of oil. Flaked or unflaked oil seeds or prepressed cake are used to feed the extruder. The discharge end of some extruders is fitted with a cage where oil is expressed, yielding collets containing less than 30% oil when high-oil-content feeds are used. Such extruders act as prepresses as well as puffing devices.

Heavy-duty, single-screw presses are also used to press juice from sugar cane and remove water from paper pulps, from styrene-butadiene rubber and from bagasse discharged from cane sugar extraction systems.

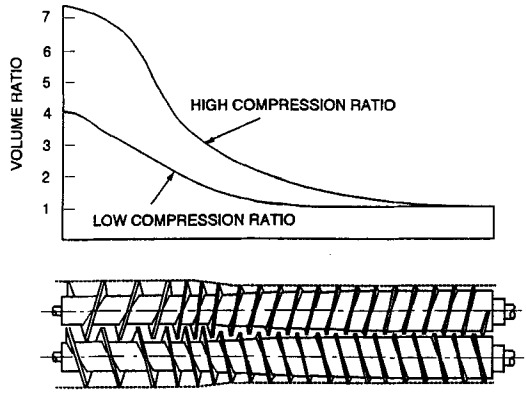

FIGURE 4 Axial cross section of twin-screw press and graph showing volume-reduction during pressing (Stord-Bartz[6,7])

Twin-Screw Presses: These presses contain intermeshing counter-rotating twin screws housed in a close-fitting perforated casing, shaped like a broad-waisted figure eight. The intermeshing screws provide positive conveying. Cake compacts as it moves down the screws because the casing diameter decreases and screws' root diameters increase. Fig. 4 shows a cross-section of a twin screw press and illustrates how cake volume changes during pressing[6]. Twin-screw presses with capacities up to 85,000 kg/hr are available. More than 2,300 are in use today: roughly 65% for dewatering spent sugar beet pulp, 30% for expelling oil and water from cooked oil-rich fish, and smaller percentages for expelling protein-rich juices from alfalfa, dewatering sugar beet trash, tails and leaves, pressing spent brewers and distillers grains, expelling hydrocolloid juices and pressing fat from cooked/dried meat scraps or from heated moist meat scraps in rendering operations[7]. Pressures around 7 MPa are generated. 1.5 to 1.9 kWh of energy are required per 1000 kg of feed; up to 3 kWh/ton of feed may be required for pressing alfalfa[7]. Operation when pressing spent sugar beets has been improved so that dry solids contents of 32% are now obtained versus only 20% in 1976 [8].

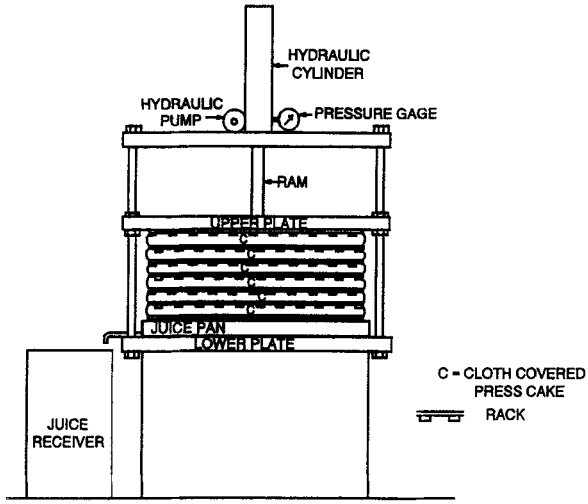

FIGURE 5 Rack-and-cloth press

Rack-and-Cloth Presses: In these presses, series of cloth pouches sandwiched between wooden, plastic or metal racks are pressed between heavy plates, one of which is driven by a screw or screws, or, more often, by a hydraulic ram (see fig. 5). Ground or milled fruit is deposited on and spreads across a cloth. The corners of the cloth are folded over, forming a pouch, called a "cheese", which is placed on a rack; and another rack is placed on top of it. The process is repeated until there is a stack of 10 or 12 cheeses and racks. The stack is placed between the plates. Then the top and bottom plate are driven together at roughly constant speed with the stack between them, until a desired maximum pressure is reached. The stack is held at that pressure for 5 to 20 minutes, during which the moving plate advances at a progressively diminishing rate. Juice pressed out of the fruit flows through the cloths and gaps or depressions in the racks into a juice collection system. Then pressure is released, the plates are separated, and the racks and cheeses are unloaded. A typical pressing cycle takes 30 minutes. The process is repeated as often as needed. Often, two sets of cloths and racks are used. One is dumped, filled

and assembled on a transfer trolley or rotating table while the other is being pressed. The cloths are washed and sterilized frequently to prevent fouling and bacterial buildup. A press with 12, 0.76-m square cheeses can process roughly 800 kg apples/hr and requires 1.1 kW to operate.

Rack-and-cloth presses are widely used by small-scale apple-juice producers, and can provide roughly a 75% yield of juice of high quality using 50-mm to 75-mm deep cheeses and maximum cake pressures as small as 0.35 kPa; but require large amounts of labor to operate. Presses that can provide up to 1.5 MPa pressures and handle 90-mm deep cheeses are available. They usually provide only slightly greater yields than presses operating at 0.35 MPa.

To improve productivity, readily fillable, preformed pouches are sometimes used instead of cheeses. Grooved plastic or corrugated stainless-steel plates may be used instead of wooden frames. In some systems, plates and pouches are mounted in frames that permit quick assembly and disassembly and are pressed together by platens that move horizontally. Nevertheless, the process remains laborious.

Presses containing a single pair of hydraulically-driven, 0.8-m square, vertical plates, have been used to reduce labor requirements. The plates, made of stainless steel slats with 0.25-mm gaps between them, are enclosed in a 140-mm wide perforated cage[9]. The presses are fed with milled fruit through an opening at the top of the cage. The opening is closed and the plates are pressed together by the rams, forcing juice out of the perforations in the plates and cage. The maximum pressure used, 3.1 MPa, is much higher than those used in rack and cloth presses. At the end of the press, the plates are pulled back; the latched bottom of the press opens; and the pressed cake drops out. The pressing cycle is illustrated in fig. 6. Thirty to one-hundred pressing cycles are carried out per hour. The presses are used mainly to press apples. Large amounts of rice hulls, a filter aid, have to be added to provide good pressability. Juice yields of 92% are claimed; but costs are high because of the rice hulls used. Only 20 units of this type have been sold.

Box and Pot Presses: Presses in which feeds were wrapped in pouches and placed on perforated mats and grids of drainage channels in a series of boxes

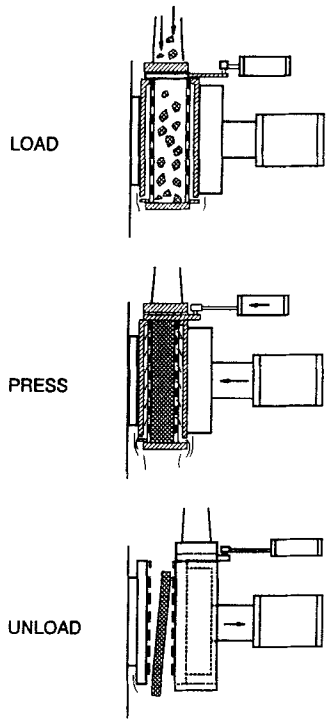

FIGURE 6 Pressing cycle for rapid-cycling, perforated-plate press (Stoll II Press) (Hubert C. Stollenwerk Inc.[9])

were once used to express oil from materials such as conditioned cottonseeds. Pressures up to 11 MPa were used. Similar systems that contained series of cylindrical frames into which mat-, cloth- or metal screen-lined drainage plates could slide (see fig. 7) were once used to press oil out of slurried milled cocoa and milled palm nuts, but have been almost completely replaced by screw presses for this purpose. They are still used in small olive oil mills and for production of specialty oils. Vertical or horizontal arrays of plates and frames are placed between platens that are then driven together by hydraulic rams. Pressures up to 42 MPA (6000 psi) are applied to the cake. The frames may be manually cleaned, assembled and filled; more often they are filled with fluid-

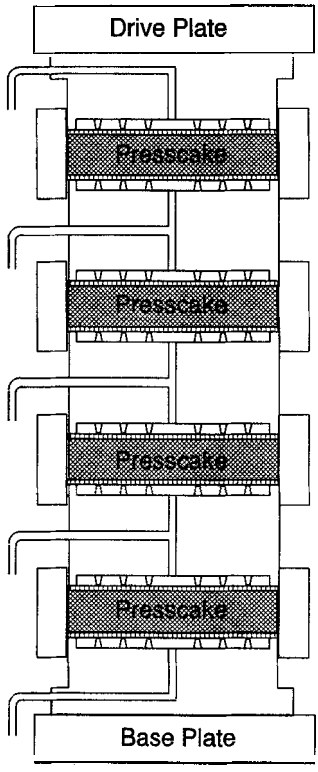

FIGURE 7 Pot press

like slurry, similar to the way frames are filled in plate-and-frame filter presses. Partly automated unloading is also provided[10]. Except for the higher pressures used, the basic process is similar to that used with rack and cloth press. Milled cocoa was pressed in units of this type. The feed contained 54% cocoa butter; the discharged cake, "cocoa kibble" contained 10 to 12% cocoa butter. Cocoa kibble is used to make chocolate.

Curb Presses: Milled or crushed fruit is often pressed between plates in cylindrical cages made of wood slats, metal bars or rib-reinforced perforated

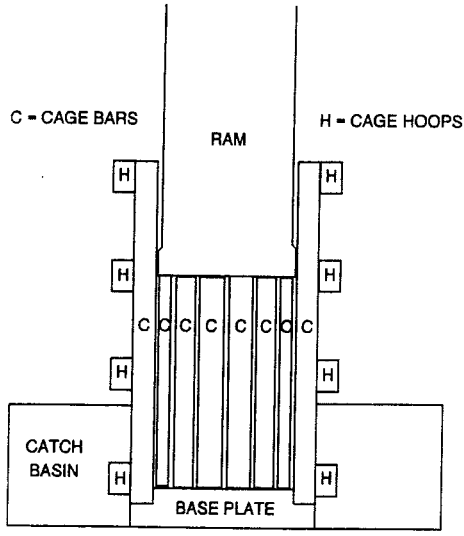

FIGURE 8 Curb press

sheet metal in units called curb presses (see fig. 8). Vertical curb presses have been used for centuries to press grapes and are still used in some wineries and for home production of cider and wine. Heavy-weight curb presses were once used to press oil seeds. Crushed wine grapes are pressed between vertical plates in horizontal perforated cylinders in large-scale modern curb presses called spindle presses[11]. The plate are driven together by long screws or hydraulic rams that often project beyond the end of the cylinder (see fig. 9).

Cheese Presses: Cheese is pressed to: a) knit curds together into a block, b) form rinds, and c) regulate their water content by expelling whey. Relatively little whey is expelled, but pressing should provide blocks with prescribed, uniform moisture contents. Milled curds for semi-hard cheeses are loaded into perforated, cylindrical or rectangular metal or plastic molds; curds for hard cheese are loaded into cloth-lined hoops[12]. Large, hard cheeses are pressed at 0.4 to 0.8 kPa up to 24 hours; semi-hard cheeses at 0.1 to 0.3 kPa up to four

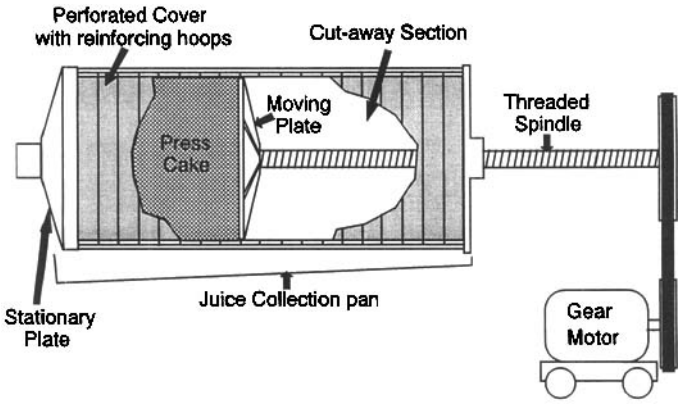

FIGURE 9 Spindle press (Troost[11]. Reprinted with permission of Verlag Eugen Ulmer.)

hours. Low pressures are used at first to allow whey to run off slowly. Full pressure is applied later to fuse curds together and form the rind. Platens driven by pneumatic or hydraulic rams do the pressing. Often groups of molds mounted in a single frame are pressed at the same time. Rams may press up to seven curd-filled hoops stacked one on top of the other. Cheeses are often soaked in brine after pressing and lose more water by osmosis.

Flexible Outflow Tubes Plates move together within a cylindrical shell in highly automated presses made by Bucher-Geyer. Cloth covered, grooved rubber tubes run between the plates and are attached to them at each end (see fig. 10)[13]. Milled fruit mash is pumped into the cylinder through a pipe at the center of one plate. The inlet valve automatically closes when the cylinder is full. Then a hydraulic ram pushes the opposing plate toward the feed plate at a programmed rate over a 1 to 1.5 hour period, pressing juice out of the mash into the grooves on the cloth-covered, contorting tubes. The juice runs down the grooves into manifolds in the end plates, and from there into a juice collection tank. Pressing is often interrupted by temporarily pulling back the ram and rotating the cylinder to break up the cake and reduce outflow-surface

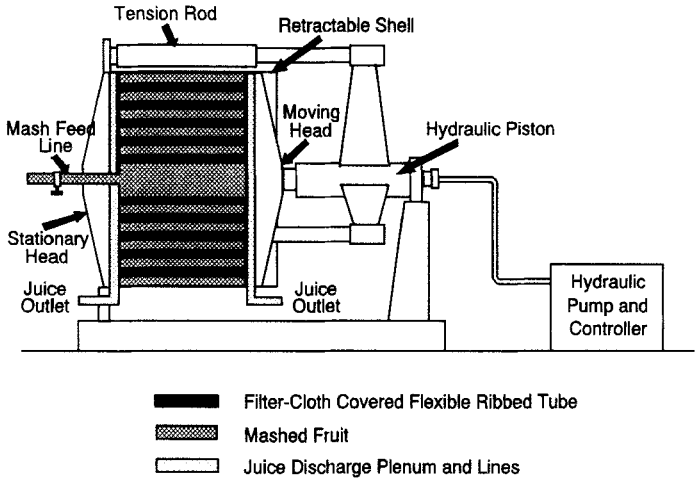

FIGURE 10 Press with flexible outflow tubes (Bucher-Guyer Ltd[13])

blinding. After the pressing is complete, the cylindrical shell and the ram are pulled back by hydraulic jacks. The tubes straighten, breaking up and discharging the cake. Then the internal parts are washed, the cylinder is reclosed, and the cycle is repeated. Press chambers up to 1.7-m in diameter with a capacity of 6 m^3 are available. Pressures up to 1.4 MPa are used. 80% juice yield is obtained.

Pomace (pressed fruit) is sometimes repulped with weak juice and repressed. Then it is repulped again with water and repressed again to provide the weak juice used in the previous step[14]. This effectively subjects the pomace to countercurrent expression, yielding added juice solids that bring the juice-solids yield up to 95%. Up to four stages of repulping and repressing have been used.

Roll Mills: Juice is pressed out of chopped and shredded sugar cane in roughly 5,000, three-roll mills, like the unit depicted in fig. 11. The residual solid is called bagasse. Hard, cast-iron rolls, up to 1.38-m in diameter and 2.75-m

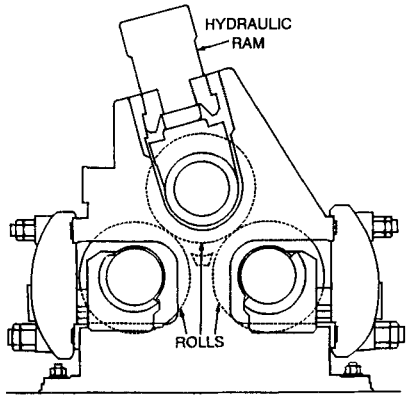

FIGURE 11 Three-roll mill (Fulton Iron Works.[16])

long, are used[15]. Rolls as small as 0.32-m in diameter and 0.63-m long may be used in small mills. Two-roll mills are sometimes used, particularly for initially crushing cane; and mills containing four, five or six rolls have come into use. Friction between rolls and the cane, or bite provided by grooves on the rolls, drags the cane through the nips between rolls. In three-roll mills, cane is pressed between the top roll and the first bottom roll (feed or cane roll) and then between the top roll and the second bottom roll (bagasse or discharge roll). A turn plate directs cane leaving the first pair into the second pair. Hydraulic rams, one above each bearing of the "floating" top roll, press the roll down on the cane. The force applied per unit length of roll ranges between 1.2×10^6 Newtons/m for small mills to 2.7×10^6 Newtons/m for large mills[16].

Modern roll mills are usually driven by geared-down steam turbines. Electric motors are also used; reciprocating steam engines may be used in older plants. A large mill processing 120 kg cane/s (11,500 tons cane/day) requires 950 kW of drive power.

No matter how hard cane is pressed, the bagasse leaving a mill still contain roughly 45% fluid. A process called compound imbibition is used to obtain high sugar yields. Cane and resulting bagasse are pressed by five or six roll

mills in series. Roughly 0.27 kg water/kg of original cane is sprayed on and absorbed by bagasse leaving the next-to-last mill. The dilute juice expelled in the last mill is sprayed on and mixes with discharged bagasse two mills ahead. This pattern is repeated in all mills from the third mill on. Juice expressed in a mill is sprayed on and mixes with discharged bagasse two mills ahead (in the direction of liquid flow), effectively providing countercurrent imbibition and expression. The extra press liquor provided by this process leaves the second mill and is combined with juice from the first mill, raising the yield of sugar from 71% to more than 95%. 0.5 kg of sprayed bagasse is pressed for every unit of fresh cane pressed. Around 680×10^9 kg of cane is pressed each year. Since bagasse produced from that cane is pressed four to five times, roughly $2{,}200 \times 10^9$ kg of material per year is pressed in sugar cane mills. Sugar is also recovered from cane by diffusive extraction instead of pressing; but bagasse leaving the extractor is pressed; pressed cane is also often used as extractor feed.

Closely-spaced 12-mm deep, V-shaped grooves circle around most rolls (see fig. 12). Wider and deeper grooves may be used on the first and second mills of milling trains. Feed rolls also often contain thin, 30-mm deep channels every sixth groove to facilitate juice drainage. Grooves that cross encircling groves at right angles or in a chevron pattern are also used. Perforated top rolls, called Lotus rolls, are starting to be used. Liquid pressed through small holes on the roll's grooved surface runs out of holes in the roll's end plates.

Rolls turn at 3 to 6 rpm. Linear speeds at the rolls periphery range between 0.08 and 0.46 m/s. Nip clearances between top rolls and feed rolls during pressing are larger than clearances between the top rolls and discharge rolls; clearances also decrease going from the first to last mill. Typical feed and discharge clearances in first mills in trains are 57 mm and 29 mm respectively. In last mills, the corresponding figures are 38 mm and 8 mm. Pressures peak about 5° ahead of the center of the nip. Based on pin-gauge measurements, peak pressures of roughly 40 MPa (6,000 psi) may be reached at the crowns of groove teeth[17]. Fig. 13 depicts how pressures at a tooth crown vary with angular position close to the center of a nip (0°) for different compression ratios. Local pressures averaged over the whole groove surface are roughly 0.33 to 0.45 times as great as the crown pressure.

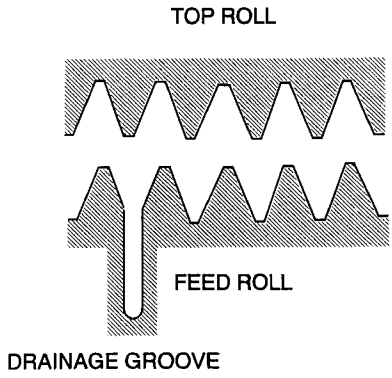

FIGURE 12 Groove arrangement for roll mills used to press sugar cane (Chen[15])

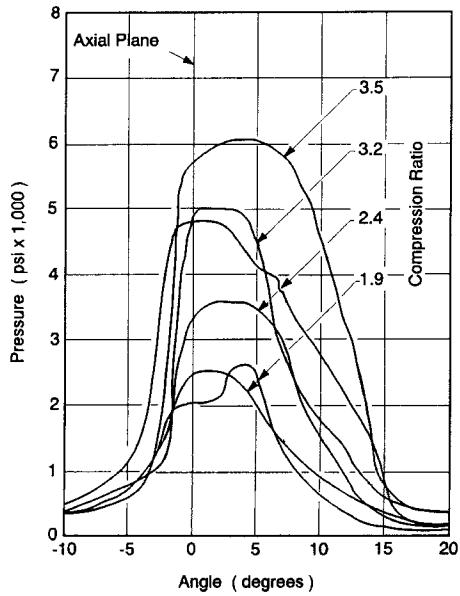

FIGURE 13 Pressure versus angular position in roll mill during pressing of finely shredded sugar cane containing 12.8% fiber. Roll diameter: 0.66 m. Roll Surface Speed: 0.15 m/s (Murry and Holt[17])

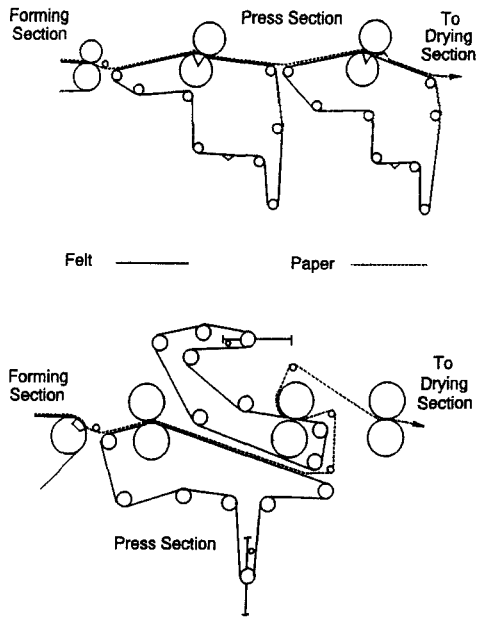

FIGURE 14 Press roll arrangements in press sections of paper-making machines. Reprinted by permission of Van Nostrand Reinhold, copyright © 1970.

Roll mills are also used to press washed wood chips, knots, bark, wood fiber clumps, flax pulp and bleached wood pulp.

Paper Mill Presses: Thin aqueous slurries of cellulose fibers are converted into a continuous, moving sheet of moist paper by filtering off water in paper-making machines. The sheet is pressed between apposing pairs of rotating cylinders (press rolls) to remove more water; finally it is dried. The moist sheet is carried through the pressing section and gaps between rolls on moist felt belts at speeds ranging 0.05 m/s to 25 m/s (usually 2.5 to 15 m/s). Fig. 14 shows examples of roll pressing arrangements. Usually, two or three pairs of pressing rolls are used; up to nine pairs may be used in "cylinder" machines

that make heavy papers. Rolls range between 0.25- and 1.5-m in diameter and are up to 10.7-m long.

Both rolls may be solid, or a solid roll may be paired with a perforated suction roll. In fig. 14, the rolls with sectors drawn near their nips are suction rolls. At least one roll in a pair is covered with a thick layer (e.g. 25 mm) of rubber; often both are. Solid rolls may be made of steel or cast iron covered with rubber or hard plastic; some used to be made of granite. Granite rolls occasionally explode, so their use is being phased out. Suction rolls are made of bare or rubber-covered bronze or stainless steel perforated by evenly spaced, 4- to 4.8-mm diameter holes covering 18 to 25% of their surface.

Bottom rolls have fixed bearings; bearings of top rolls slide in tracks and are loaded to apply 8.8- to 53-kN of force per meter of roll length[18]. This causes the rubber coating to flatten at the nip, producing a 25- to 50-mm long pressing zone. Average pressures acting on paper and felt in this zone range from 0.18 to 2.1 MPa. The pressure forces water out of the paper into and through the felt. Expression rates depend on the initial moisture content of the paper; they are much greater for the first pair of rolls in a series than for the second pair. Respective first and second roll water removal rates reported[19] for Kraft paper containing 0.10 kg dry fiber/m^2 were 17.65 kg/s and 4.83 kg/s. Assuming each nip was 50-mm wide, these respectively correspond to nip-area-based expression rates of 50 kg/(m^2·s) and 13.6 kg/(m^2·s). Similar nip-area-based expression-rate figures for first and second rolls for newsprint containing 0.052 kg dry fiber/m^2 were 33.3 kg/m^2·s and 6.8 kg/m^2·s respectively. Transit times (for a 50-mm nip) were six milliseconds for Kraft and four milliseconds for newsprint. The first rolls expressed 45% to 53% of the water that entered them; second rolls expressed roughly 23% of the water that entered them.

When paired plain rolls are used, expressed water flows out of the saturated felt and is caught by a vacuum scoop (see fig. 15). The flow path in the felt is roughly 25- to 35-mm long and roughly as wide as the felt is thick, i.e. 0.7- to 1.4- mm wide. When a suction roll is used, most of the expelled water flows directly across felt just ahead of the nip, where the suction box of the roll is placed (see fig. 16). Since suction boxes are 125- to 250-mm wide

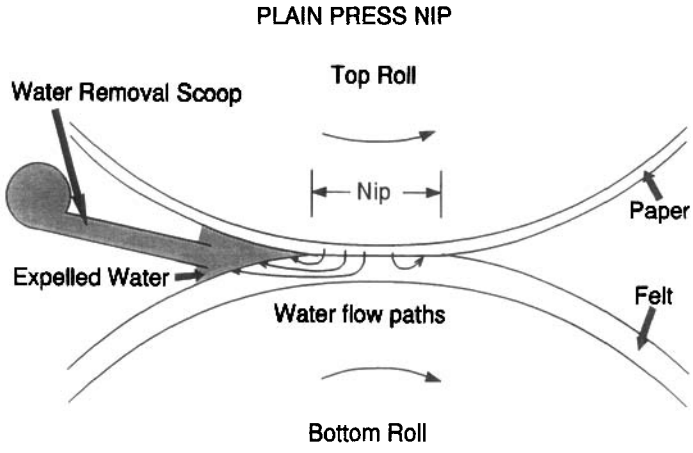

FIGURE 15 Flows in the vicinity of the nip of a pair of plain pressing rolls in a paper-making machine

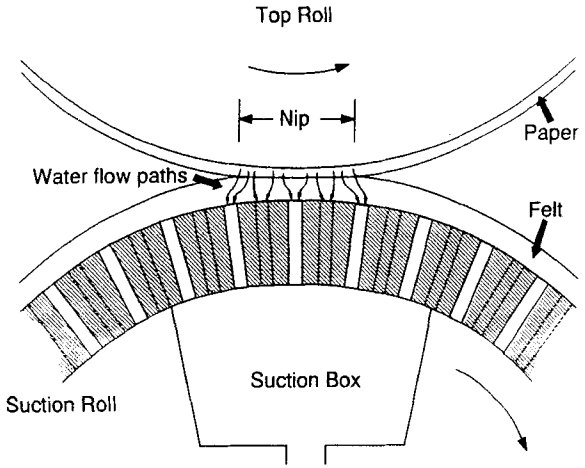

FIGURE 16 Flows in the vicinity of the nip between a plain pressing roll and a suction roll in a paper-making machine

and nips are 25- to 50-mm wide, flow paths for water passing directly through the felt are 0.7 to 1.4- mm long and at least 25- to 50-mm wide. Most of the flow resistance is in the paper rather than in the felt.

51 to 74 KPa (15 to 22-in Hg) of vacuum are applied to suction boxes, which are isolated from the rest of the suction roll's interior by wiper blades. Suction draws expelled water through the felt and into the holes in the roll. In fast-turning rolls, water is thrown out of the holes by centrifugal force after the holes leave the suction zone. In slow-turning rolls, water may be drawn into the suction box.

Capillaries in papers are much smaller than in felts. If felts and papers do not separate when they leave a nip, capillarity will draw water out of the felt back into the paper as soon as nip pressure is released. Therefore, at low pressing speeds, fine felts, which exert more capillary action, provide greater water removal than coarse felts[20]. Water removal peaks at intermediate pressing speeds. At low speeds there is time for capillary pull-back of water from the felt; at high speeds there is not enough time for water to flow out of the paper.

Long rolls supported at both ends deflect. To even out nip pressure, paper-machine press rolls are crowned, i.e. have a slightly larger diameter in the middle of their span. Most rolls are smooth. In Venti-Nip rolls, 2.5- to 3-mm deep, 0.25 to 0.3-mm wide grooves, spaced 3.2-mm apart spiral around the roll and vent it, permitting higher pressures to be used[19]. This results in an added 2 to 8% reduction in water content without crushing the paper.

Other Roll Mills: Pairs of rubber-covered rolls are also used to press water or process liquid out of cloth during dyeing, bleaching and drying operations. Small pairs of rubber covered rolls were used for water removal from washed clothes in old-fashioned washing machines. Pairs of counter-rotating grooved rolls are used to crush wine grapes and expel grape juice. The rolls are sometimes driven at different speeds to tear the grape skins. Intermeshing lobed rolls are also used for the same purpose (see fig. 17). Large clearances are used between crushing roll surfaces so as to avoid crushing seeds and stems and consequent release of extractable tannins.

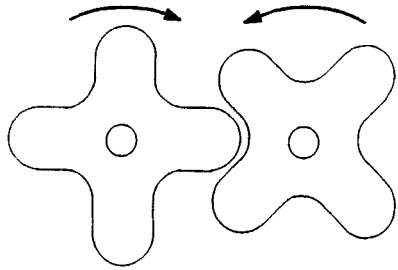

FIGURE 17 Lobed rolls for crushing wine grapes (Troost[11]. Reprinted with permission of Verlag Eugen Ulmer.)

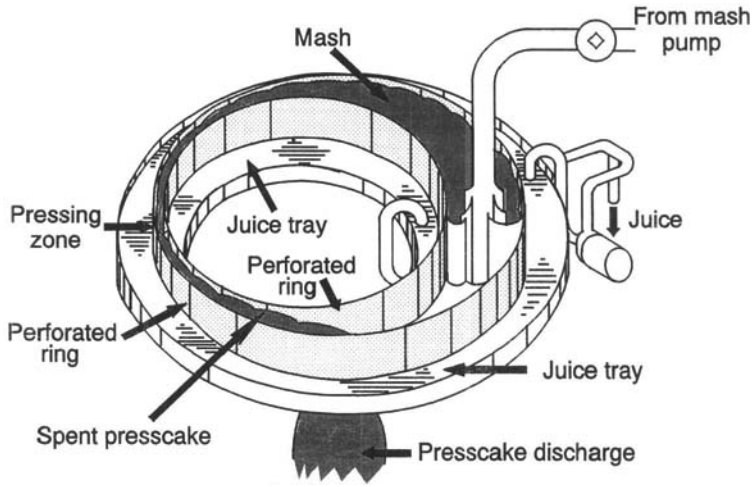

FIGURE 18 Graham press: an internal double-roll press used for pressing wine grapes (Troost[11]. Reprinted with permission of Verlag Eugen Ulmer.)

Pairs of shallow perforated cylinders with vertical axes (see fig. 18) are used to press juice out of crushed wine grapes[11]. One cylinder runs inside the other so that their surfaces nearly come together in a pinch zone where pressing occurs. Juice pressed out of the crushed grapes passes through the perforated cylinders into shallow catch basins and is removed by pumping. A

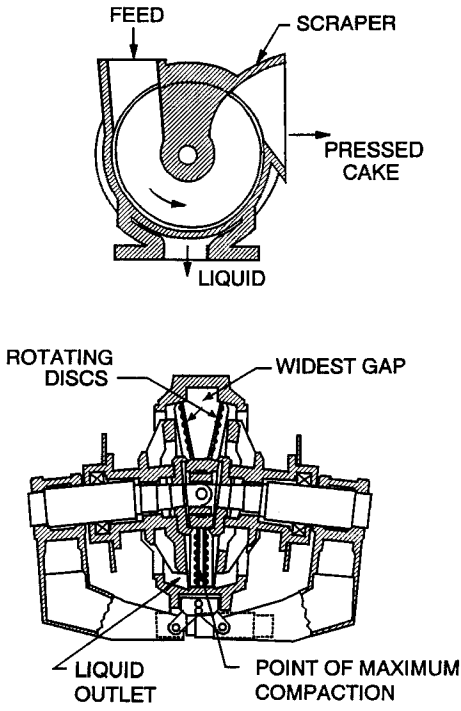

FIGURE 19 Disc press (Davenport Machinery and Foundry Co.)

similar press with a horizontal axis is used to press oil from oilseeds[21]. A solid, inner roller with a grooved surface rotates inside a shallow cylindrical case containing outflow slits around its curved surface. Oil seed feeds are fed into a wide space between the roll and the case by an auger. Clearance between the stationary, curved outflow surface and the rotating roll progressively decreases until a nip is reached, compacting the cake and expelling oil through the outflow slits. Pressed cake passes through the nip and is discharged.

Disc Presses: Solids are pressed in the nip between individually driven, rotating, shallow, conical perforated discs in disc mills (see fig. 19). Disc presses are used for dewatering spent brewer's grains and bleached paper pulp.

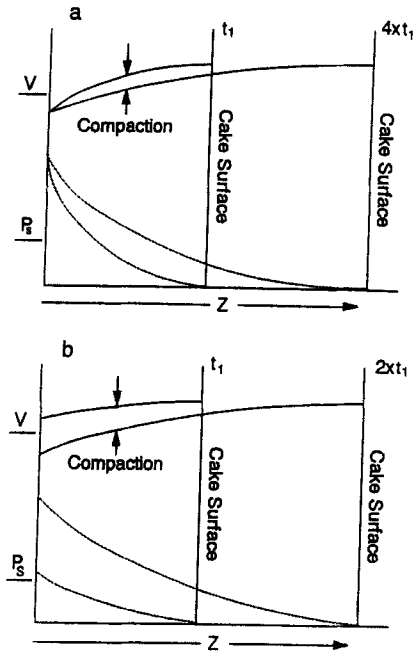

FIGURE 20 Cake compression during filtration: a) for constant-pressure filtration; b) for constant-rate filtration

Drag-Induced Expression: Drag forces due to flow cause filter cakes to consolidate slightly during filtration, as shown in fig. 20a for constant-pressure filtration. Fig. 20b is for constant-rate filtration, where slightly more consolidation occurs than for constant-pressure filtration.

Diaphragm Presses: Filter chambers are sometimes fitted with diaphragms to which hydraulic or pneumatic pressure is applied after filter cake deposition is complete. The pressure forces the diaphragm against the cake, pressing fluid out of it. Fig. 21 depicts operation of a plate and frame filter press in which diaphragms are placed over alternate plates[22]. Automatic means of opening the press and discharging the cake can be provided. In some units, (see fig.

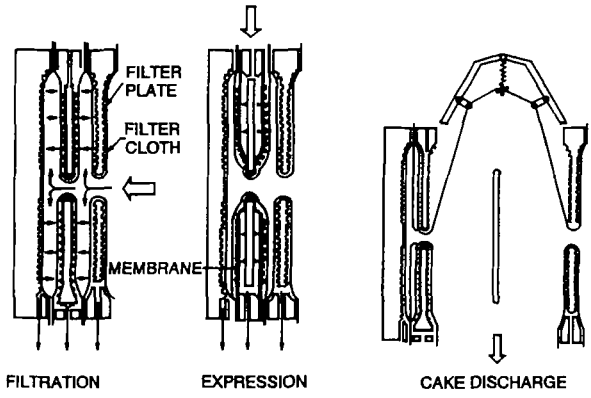

FIGURE 21 Pressing cycle for plate-and-frame filter press containing inflatable diaphragms over every other plate. (Shirato et al.[22] Reprinted from *Filtration, Principles and Practices*, p. 372 by courtesy of Marcel Dekker, Inc.)

22) a continuous belt of filter cloth passes over rolls placed at the ends of each plate-frame assembly[23]. Up to twenty frames, stacked in a vertical array providing 31.5 m^2 of outflow area, are used. After filtration and pressing end, the frames and upper plates are lifted, the belt advances and passes over a roll, dumping the cake. Doctor blades help provide clean removal of cake from the cloth and rolls. The cloth is washed after it leaves the final plate-frame assembly; then returns to the first assembly. Large rolls of disposable filter paper may be used instead of continuous cloth belts. In other units, separate belts are used for each frame.

Expanding Tube Presses: Presses based on use of an inflatable tube are inexpensive and can be very efficient when pressing soft fruits[11]. Ground or milled fruit is loaded through an open, hinged door in a long perforated stainless steel cylinder (fig. 23). The door is closed. Then a rubber tube inside the cylinder is inflated, compressing the fruit between the tube and the cylinder wall, and forcing liquid out through the perforated wall. Sometimes solid walled cylinders are used, and the liquid is forced into V-shaped perforated

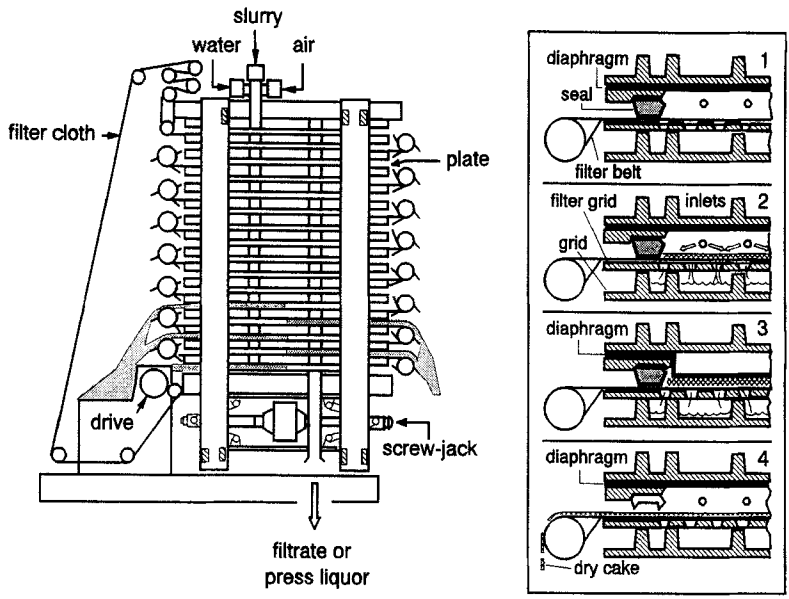

FIGURE 22 Multi-chamber, vertical, plate-and-frame filter press fitted with expandable pressing diaphragms in each frame and a motor-driven continuous filter cloth belt to provide automatic cake discharge (Larox Inc.[23])

drainage channels attached to the inside of the cylinder. Pressure is often released from time to time while the cylinder is rotated to break up the cake. This reduces outflow surface blinding. After pressing, the cylinder is rotated and opened to dump the pressed cake. Labor requirements are lower than for rack and cloth presses but greater than for screw presses. The presses are inexpensive and produce juice of good quality, but the inflatable tube wears out and has to be replaced fairly frequently.

Fig. 24, shows a cylindrical tank whose wall has V-shaped perforated juice-drainage channels attached to it on one side[24]. A semi-cylindrical, food-grade polyurethane diaphragm is attached at its edges to the channel-free half of the wall and initially lies close to that half of the wall. Milled fruit is loaded through

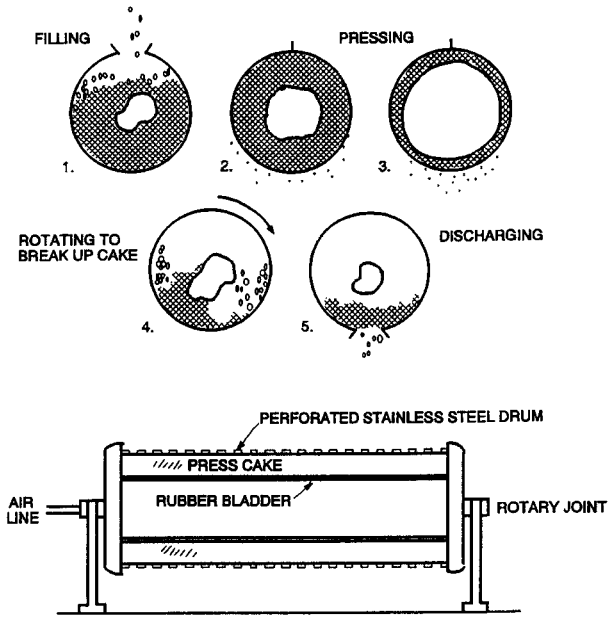

FIGURE 23 Expanding-tube press (Wilmes press)

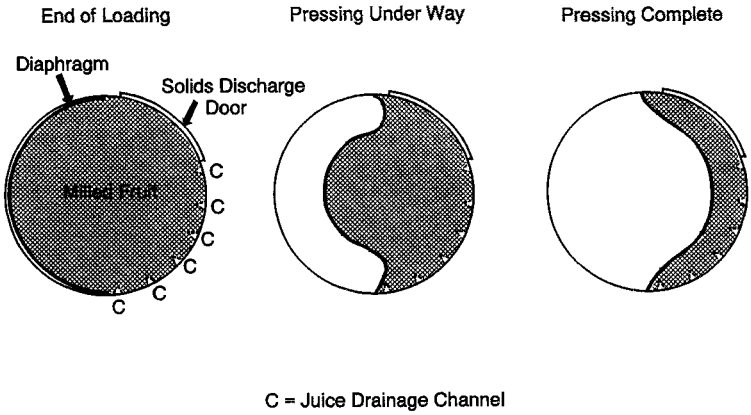

FIGURE 24 Tank press fitted with a hemi-cylindrical inflatable diaphragm (CMMC[24])

a door in the channel-lined side or is pumped in through a line attached to one end of the cylinders axis. Then the door or line is closed. Compressed air is injected between the channel-free wall and diaphragm, pushing the diaphragm towards the channel-lined wall, compressing the fruit and pressing juice out through the perforated channels. Successively higher pressures are applied in three steps. For apples, 200 kPa is used in the final step. To reduce expression of tannins, only 130 kPa is used when pressing crushed grapes for wine making. The operating cycle is similar to that used with expanding tube presses. The diaphragm changes little in length or area during the pressing cycle. Therefore it wears out less frequently than tubes do in inflated tube presses. When the tank is ready to be unloaded, the diaphragm is pulled back against the channel-free wall by vacuum, and the door is opened. During unloading the tank rotates, and spiral flights in the channel-free wall convey spent mash to the discharge door.

Belt Presses: Feeds are pressed between pairs of moving, polyester cloth belts that simultaneously serve as conveyors, filter cloths and pressing elements[25-27]. Moist feed, e.g. milled fruit, waste treatment sludge, is deposited on the lower belt in a free-drainage section. After enough fluid drains through the cloth, a pressable cake forms, and the top belt moves down against the cake. The belts are pressed together, expelling fluid from the cake as they travel. Then they separate and pass around rolls to start on return paths. The bottom belt turns downward and the cake drops off. Both belts are cleaned with high pressure sprays before returning to the press feed zone. Data for dewatering of waste-treatment sludge by belt presses are provided by Dick and Ball[28], Andreasen and Nielsen[29] and Roest et al.[30].

Paired-Roll Belt Presses: In paired-roll presses, the belts are pressed closer and closer together by a series of pairs of opposed rollers (see fig. 25). Paired-roll belt presses with belts up to 3.6-m wide are available. Most are used to dewater waste-treatment sludges; much smaller numbers are used to press juice out of milled fruit[26,31].

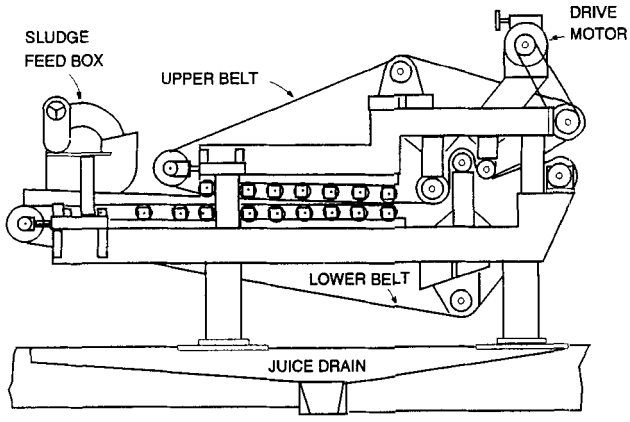

FIGURE 25 Continuous belt press with paired opposing rolls (Andritz-Ruthner Inc.[25])

Impermeable Belts: In some belt presses one belt is permeable and the other is not. In the unit shown in fig. 26, a food-grade, fiber-reinforced impermeable rubber belt is used to press wash water out of cottage cheese curds carried on a woven polyester belt passing over a perforated drum[32]. Pressure on the curds is regulated by adjusting the tension applied to the rubber belt. Wine grapes are sometimes dejuiced in systems where crushed grapes carried on a perforated belt moves over a long, slightly curved grid of stainless steel slats with drainage gaps between them[33]. An impermeable upper belt presses the grapes against the slat-supported lower belt, expelling juice. Again, pressure is controlled by adjusting roll-applied tension in the upper belt. In other belt presses used for wine grapes, the solid belt is pressed against a perforated lower belt by loaded rollers. Very light pressure is usually used for both cottage cheese and wine grape pressing. Several pressing and juice collection zones are used in some belt presses for grapes. Progressively greater pressure is applied as the crushed grapes move through the system[11]. Juices collected from different zones may be used for different purposes.

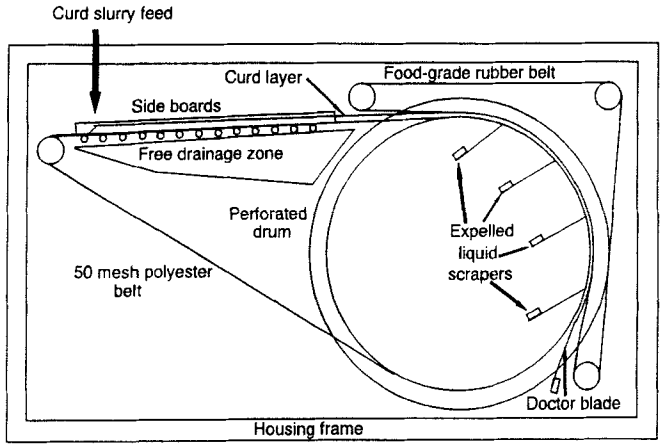

FIGURE 26 Belt press fitted with a single perforated cylinder (Stoelting[32])

Serpentine Belt Presses: Well over 2,000 serpentine belt presses are in use. In these presses, the pair of belts passes back and forth over rolls in a zigzag path[25,26,34-36]. Pressure is controlled by adjusting belt tension. In some presses, the rolls are of the same size; in others, rolls of progressively smaller diameter are used. Belt presses containing combinations of paired rolls and rolls mounted in a serpentine array are also used. Ten rolls of progressively smaller diameter are used in the unit shown in fig. 27. The first three press rolls in the unit are perforated; all the others are solid. Presses with belts up to 2.7-m wide are available. A press with a 2.2-m wide belt requiring 5.1 Kw of power to operate can press 5.6 kg/s of apples ($2x10^4$ kg/hr) and provide 83% juice yield[26]. Serpentine presses for pressing wine grapes have similar capacities. Serpentine presses have been used to obtain dry solids contents up to 50% for spent sugar beets[8]. Holdup times of solids in such presses are three to five minutes.

Belt presses are sometimes used in series to improve juice recovery. Cake discharged from the first press is first washed with press juice from a second press, and then with water on the belt-filter section of the second press. The

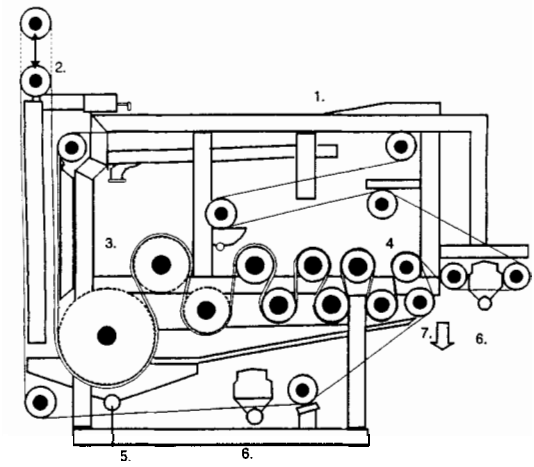

FIGURE 27 Serpentine belt press (Gebr. Bellmer GmbH and Co.[26])

filtrate obtained from the first washing is combined with juice from the first press. Dilute juice expelled in the serpentine section of the second press is used for the first washing. Up to 92% juice yield is obtained.

Large numbers of belt presses are used to dewater waste-treatment sludges. Dewatered waste treatment sludges in Germany will soon have to have dry solids contents $\geq$ 35% to be deposited in landfills. Since freshly treated sludges often contain less than 3% solids, they are usually first passed over high capacity drainage belts or drum filters to provide pressable feed for the belt press. Presses that can handle up to 21 kg/s (7.6×10^4 kg/hr) of pre-concentrated sludge are available. Sludges containing up to 30% solids are obtainable with serpentine presses; up to 50% solids can be obtained when non-biological materials are pressed. Sludges from belt presses fitted with paired rolls contain up to 24% solids. Multi-unit belt pressing systems operate 24 hours a day, 365 days a year are used in many municipal waste treatment plants: e.g. twenty-four serpentine presses handle waste treatment sludge for Milwaukee; 10 are used in Akron. Belt presses are also used to dewater harbor

and waterway dredging sludges, waste-paper-treatment sludges, paper-mill pulps, slaughterhouse and feed-lot wastes, fine coal slurries and soil treatment intermediates.

Waste-treatment sludges are usually mixed with soluble polymeric agents to flocculate them before being pressed on belt presses. If insufficient polymer is used (e.g. < 8 to 10 g/kg sludge), the fluid effluent will contain too much solids and the cake will drain slowly. There should be less than 500 mg solids per liter of discharged liquor. If insufficient polymer is added, there may be 2,300 mg solids per liter of discharge. Excess polymer does not further reduce solids in the effluent or further improve drainage rates[37]. Effectiveness of polymer addition depends on how it is mixed with sludge. Required mixing times are inversely proportional to the shear rate provided by the mixer; but excessive shear rates cause flocs to break down and reduce filtration and pressing effectiveness and rates[37].

The solids content of sludges discharged from belt presses can be increased, e.g. from 28.1% to 32.4%, by pretreatment with 2.5 to 5 ppm of an enzyme mixture having carbohydrase, lipase and protease activity[38]. Dewatering benefits decrease and ultimately disappear when higher enzyme doses are used.

Pressures between 35 kPa and 140 kPa are used in belt presses operating with polymer-treated sludges. Cake dryness generally does not increase as pressure increases. Solids contents of sludges discharged from such belt-presses can be predicted by tests carried out in a 10-cm square cell fitted with drainage belt cloth on its bottom. A 30-mm deep layer of sludge is deposited and allowed to drain for one minute, and is then pressed for two minutes at the pressure to be used on the belt[37].

The solids content of polymer-treated sludge initially containing 6% solids may increase to 8% in the free drainage zone of a belt press, and then increase to 15% to 17% in the pressing section. Final solids contents usually increase as belt speed decreases, e.g. go from 15.5% at a belt speed of 1.45 m/min to 16.9% at a speed of 1.25 m/min. In some cases, however, solids contents of discharged sludge shows slight maxima at intermediate belt speeds[37].

Multi-Layer Belt Presses: 20- to 30-mm thick layers of feed are deposited on each of 20 parallel, moving cloth belts in large presses developed for pressing spent sugar-beet pulp[39,40]. After loading, the belts and feed come to rest between a 23-m long battery of hydraulic presses, which apply 10 MPa pressure for 15 minutes on the parallel belt-load array. After pressing the belts pass over rollers that cause spent cake to discharge.

Cylindrical multi-layer arrangements have also been used[41]. Spent sugar-beet pulp is deposited on a 1.3-m wide, 300-m long moving cloth belt which winds around a mandrel. After loading is completed, the rolled assembly is placed inside a cylinder lined with an elastomeric membrane. Water is pumped into the space between the cylinder and membrane, applying 5.3 MPa pressure to the roll to for 10 to 15 minutes. The roll is removed from the cylinder and unwound causing the cake to fall off.

In both cases, expelled fluid flows out transversely through the cloth. Press-cake dry-matter contents of 50% have been obtained with the parallel belt arrangement, 53% with the cylindrical arrangement.

Citrus Juice Expression: Most citrus fruit have thick, tough skins that contains highly flavored oils. If pressed juice from these fruits contains too much of these oils, its quality and storage stability are impaired. Therefore equipment that expresses juice while limiting expression of skin oil is usually used.

FMC Extractors: FMC extractors are used to press juice from oranges or grapefruit separated according to size[42]. Individual fruits drop into an upward-facing, open, ribbed S.S. cage that fits the fruit. A mating downward-facing, upper cage with ribs that interdigitate with the ribs in the lower cage is pressed against the fruit (see fig. 28) forcing it downward against the sharp, circular knife-edge of a 25-mm diameter "prefinisher' tube that protrudes slightly upward through a hole in the base of the bottom cage. This cuts a round hole ("coin") in the fruit's peel. The top cage is pushed down, forcing juicy fruit flesh down the prefinisher tube and ultimately shreds the peel. The shredded peel extrudes through the top cage, is washed by sprays to recover expelled

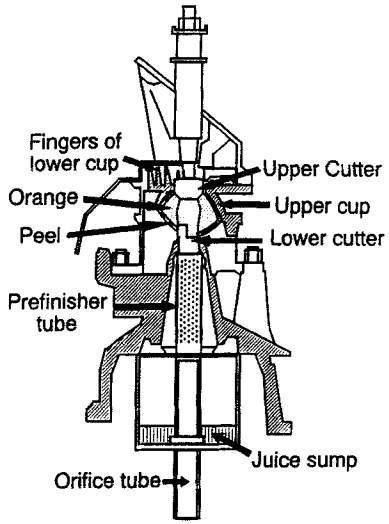

FIGURE 28 FMC citrus juice extractor (FMC corporation[42])

peel oil and is then blown away by an air blast. Juice expelled from the flesh forced down the prefinisher tube drains through a grid of fine holes in the side of the tube. A sharp-edged "orifice" tube is pressed upward inside the prefinisher, severing juice cells that remain stuck in drainage holes. This also forces pressed flesh into the orifice tube, displacing flesh already there and forces spent flesh out of an opening near the tube's bottom. Extractors have four to six pressing heads and can handle 300 to 700 pieces of fruit a minute.

Reamers: Reamers rotate inside halves of cut citrus fruit seated in cups in extractors[43] made by Brown International (see fig. 29). The cups prevent the fruit from turning. The reamers and cups pass through processing stations on apposed moving belts or conveyor. The fruit half enters the cup cut face up. The reamer and cup come together. The reamer rotates inside the fruit while the cup, fruit and reamer pass over a juice collection trough. Then the reamer and cup separate and the fruit's skin drops out of the cup. Such "extractors"

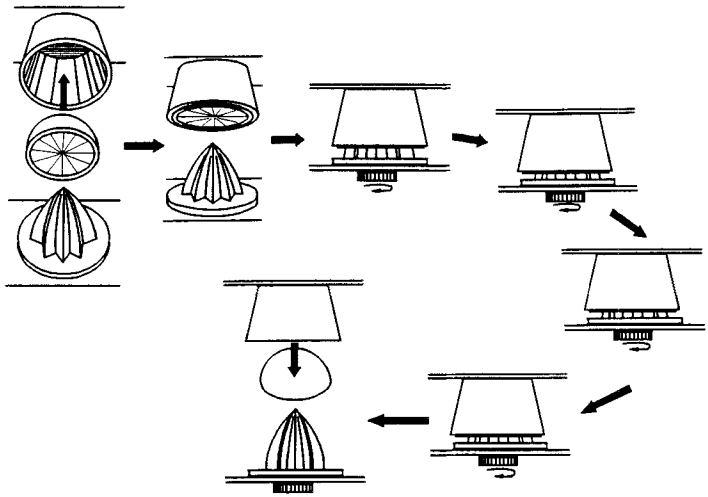

FIGURE 29 Operation of multi-head reamer system for expressing juice from citrus fruit (Brown International[43])

use multiple pressing heads and process 300 to 700 fruit per minute. Single head reamers are used for citrus-juice extraction in bars and homes.

Decanter Centrifuges: Decanter centrifuges contain a scroll inside a rapidly rotating shell, containing a cylindrical section and a truncated conical section (see fig. 30). Centrifugal force causes the solids in slurry fed into the cylindrical section to deposit on its inside wall and compact, forcing fluid out of them. The scroll rotates at a slightly different speed than the centrifuge and conveys the solids towards a solids discharge port at the narrow end of the conical section. The solids emerge from the liquid and compact further as they move through the cone. Scroll centrifuges are sometimes used to gently press juice out of crushed wine grapes. They are used to press juice out of other fruits[44] and widely used to expel mixed fruit water and olive oil out of olive pulp. Olive pulp is mixed with water to increase expressed fluid yield when centrifugal expression is used.

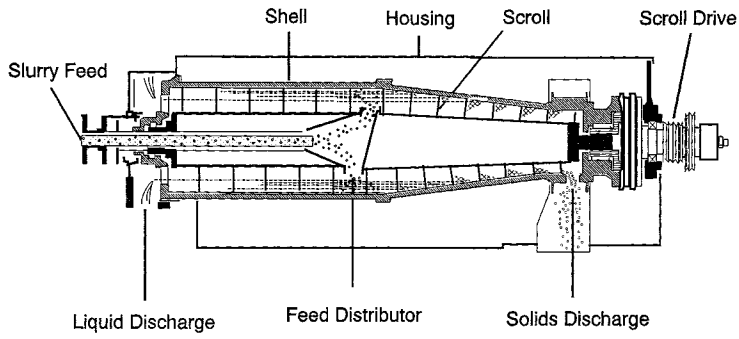

FIGURE 30 Decanter centrifuge (Alfa-Laval Sharples[46])

Decanter centrifuges are extensively used to compact and expel water from waste-treatment sludges. Discharged sludge from conventional decanter centrifuges contains about 25% solids. Waste-treatment-sludge dewatering data for decanter centrifuges are provided by Dick and Ball[28], Andreasen and Nielsen[29] and Roest et al.[30]. Sludge is now dewatered in units with smaller solids discharge ports and scrolls with heavy-duty drives that force solids into the narrow end of the cone, pressing added liquid out of them. Such units can process 50 m^3/hr of digested sludge and provide discharged sludge containing 30 to 35% solids[45].

Decanter centrifuges providing up to 10,000 g's and having shallow liquid pond depths and long scrolls are used to separate and express fluid-rich microbial debris and cells in biotechnological applications[46]. Cake drynesses up to 89% have been obtained with *e. coli* cell debris in a small-scale, 8100-g unit operating at a low conveyer speed and a feed rate of 0.06 m^3/hr. Units requiring 45 to 90 kW of power that are capable of handling 15 m^3/hr of feed are available. In some units, computer-based systems automatically control the fluid content of discharged solids when feed solids content varies[47]. The power used to drive the scroll is sensed. Scroll speed automatically decreases when power-use drops because discharged solids are too dilute and increases when power-use rises because discharged solids are too concentrated.

Other Centrifuges: Expression occurs when sediments consolidate to form dense plugs in clinical and laboratory centrifuges. Expression has been carried out in perforated basket centrifuges, which were used to dewater waste-treatment sludge as early as 1902[48]

Lowe et al.[49] used a batch, perforated-basket centrifuge with 0.5-mm holes to recover juice from milled apples in a two-stage system. A screw press served as the second stage. Cakes of partly pressed mash were periodically plowed out of the centrifuge and fed into the screw press, which worked more efficiently because of the centrifugal dejuicing. 60% to 75% of the available juice was recovered in the centrifuge. The centrifuge initially rotated just fast enough (e.g. 100 rpm for a 0.9-m diameter basket) to hold mash against the basket wall. Feed was fed in to form a 75-mm to 150-mm thick cake, which was lightly compacted using slow rotation for another 15 to 60 seconds. Then speed was progressively increased to full speed (e.g. 200 rpm) and held there until a desired level of juice recovery was obtained. This typically took two minutes. When prolonged holding was used, the residual cake weight dropped to 35% of the original feed weight; centrifugation was stopped well before this point. Juice produced in the centrifuge was much clearer than juice produced in the press; combining the two juice streams provided juice of acceptable clarity. Overall juice yields of about 82% were obtained.

Mercone centrifuges, i.e. centrifuges in which a vertical, conical scroll rotates in perforated, vertical, conical shell, are used to continuously press juice from hammer-milled apples[50]. The scroll rotates at a slightly different speed than the shell and conveys apple mash pumped into the narrow top end of the unit downward through the shell to its wide, bottom-discharge end. Typically, 75 gallons of mash per minute are fed into a unit, 50 gallons/min of fluid are expelled and 25 gallons of presscake discharges per minute. Three centrifuges are used in series to provide countercurrent expression. Water is mixed with the presscake leaving the second centrifuge to provide feed for the third centrifuge; and weak juice expelled in the third centrifuge is mixed with presscake leaving the first centrifuge to provide feed for the second centrifuge. Juices from the first and second centrifuge are combined as product. 85% of the juice solids in the apples are recovered. Presscake discharged from the

third centrifuge is mixed with water again and pressed in a fourth Mercone, yielding weak juice used for production of vinegar.

4. TECHNICAL BACKGROUND

Definitions: Special definitions and abbreviations will be used to facilitate discussion, e.g. CBS frequently will be used as an abbreviation for cellular biological solids. Porous outflow surfaces or combinations of such surfaces and filter papers, cloths or screens that cover them will be called "media". Insoluble solids that cannot pass through media are called "fixed solids", sometimes abbreviated as FS. Fluid, the material that can pass through the media, often contains dissolved solids and may contain fine solids not retained by the media. These fines would be retained by other media with smaller openings or might be partly trapped in a cake by depth filtration. Therefore, whether fines are part of the fixed solids or part of the fluid depends on the nature of the media and any depth filtration that occurs. Unwanted fines carried through the media by fluid are called "dregs". Solids that extrude through the media are called "foots".

When cake compositions are expressed on an as-is weight fraction basis, Y_w is the as-is weight fraction of water in a cake, and Y_S is the as-is weight fraction of dry fixed solids. Water contents of cakes are also often expressed on a dry-fixed-solids basis, designated by the symbol X, whose units are kg water/kg FS. "Non-expressible water" is water so strongly bound to or so strongly entrapped in a cake that it cannot be expressed at all. It can be removed by drying. X_{ne} is a cake's content of non-expressible water. Cell walls often strongly adsorb roughly 0.25 to 0.35 kg water/kg FS. Based on residual X at very high pressures, X_{ne} for separated but otherwise-unaltered, hollow wood fiber cells $\approx$ 0.40 kg water/kg FS[51]. Removal of lignin and hemicellulose by pulping causes X_{ne} for wood fiber cells to increase to 0.65 to 1.2 kg water/kg FS depending on the method of pulping used. Therefore X_{ne} for cell walls may depend on its lignin content.

ε, the porosity, is the fraction of cake volume occupied by pores, i.e. not occupied by fixed solids, and (1 - ε), the solidosity, is the fraction occupied by

fixed solids. Presscakes frequently contain air or other gases. The fraction of the cake volume occupied by air or gas is $(1 - s) \cdot \varepsilon$, where s is the fractional saturation of the pores.

Cellular biological solids contain many internal pores. Ψ indicates the fraction of cake volume occupied by pores inside particles, and ε' indicates the fraction of cake volume occupied by pores outside the particles. The solidosity of cakes containing porous solids, is $1 - \varepsilon' - \Psi$; the total porosity, $\varepsilon = \varepsilon' + \Psi$. The "apparent solidosity" of cakes containing particles with closed pores is $(1 - \varepsilon')$.

Compaction and Flow Paths: Liquid may move in the direction of compaction or in other directions when cakes are pressed. When a cake is confined between a moving, flat, impermeable ram and a parallel porous outflow surface, compaction and flow occur in the direction of ram movement. When a cake is compacted between parallel porous plates, there is a "neutral-plane" where the relative velocity between the fixed solids and the fluid is zero. Compaction and flow on either side of this plane occurs towards the apposing porous plate, and the neutral plane effectively acts like a ram. Both of these types of expression involve uniaxial compaction and flow, and both can be analyzed in the same way.

Cakes are sometimes pressed between expanding or contracting imperforate cylindrical surface and a concentric perforated surface. Fluid moves radially outward or inward away from the expanding or contracting surface and towards the perforated surface; compaction occurs in the same direction.

In screw presses where screws with a diminishing pitch are used and/or where solids outflow is restricted, compaction primarily occurs in the axial direction and flow primarily occurs in the radial direction. Axial compaction and radial flow also occur in curb presses, where cakes are compacted between solid end plates coming together in perforated cylindrical barrels. In each of these cases, drag due to flow causes additional compaction in the radial direction.

Solids follow spiral flow paths as they compact and pressure builds up in screw presses, generating a pressure gradient along the spiral path. The built-

up pressure causes radial outflow; the fluid pressure gradient along the spiral path forces some fluid backward. This fluid discharges through barrel perforations in regions where the cake is less compacted. Based on observed rates of solid or fluid discharge and nominal conveying rates for screws, some slippage or local back-movement of solids occurs in screws. Part of that back-movement may be caused by drag exerted by backflowing fluid.

Compaction is mainly axial in cases where perforated plates move together inside perforated frames. Mixed axial and transverse flow occur. The transverse flow causes transverse compaction.

In roll mills, fixed solids move forward through the nip between pairs of rolls; expelled fluid does not. Some of the expelled fluid moves backward through the advancing solids and some moves into grooves on the roll surfaces and then flows backward. Compaction primarily occurs roughly at right angles to the direction of solids flow. The fluid flowing directly backward passes through progressively less compacted cake and sooner or later turns away from the solid flow path and drains out of the advancing bed[17]. The greatest applied pressure occurs slightly upstream of the nip. This generates a fluid pressure gradient that pumps some fluid through the nip.

Solid Stress and Fluid Pressure: Particles deform when saturated cakes are compressed, and fluid flows in pores between the particles. Consequently stress increase, ΔP_S, develops in the particles, and a flow-induced pressure increase, ΔP_F, develops in the fluid in the pores. Fig. 31, adapted from Terzaghi and Peck[52], provides a way of visualizing how ΔP_S and ΔP_F behave during uniaxial compression and flow. It depicts a layer of saturated soil or presscake as a series of plates separated by liquid layers containing many parallel springs. Fine channels pass through each plate. The springs represent mechanical resistance to consolidation, the factor generating ΔP_S; the fine openings in the plates represent the filtration resistance of the bed, the factor causing P_F to rise. When pressure increase, ΔP_T, is applied, liquid flows through the openings in the plates and out of the bed, generating a flow-induced rise in P_F. Initially, counterpressure provided by the springs does not

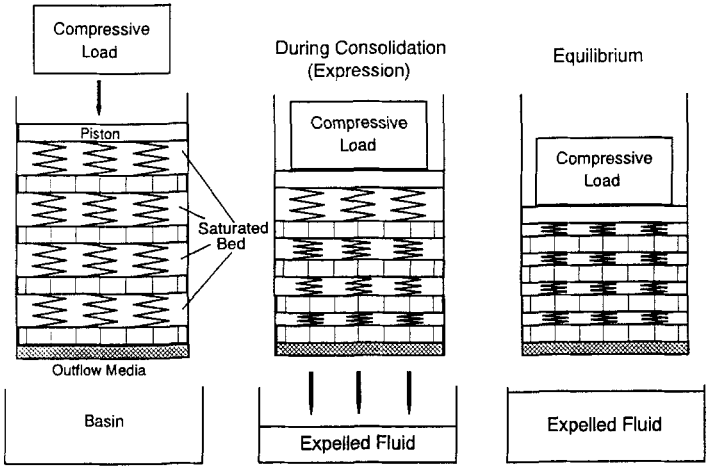

FIGURE 31 Terzaghi-Peck model for consolidation of saturated soils[52]

increase. Therefore, ΔP_F initially = ΔP_T. Then the springs compress in regions where fluid has flowed out of spaces between plates, generating stress increase, ΔP_S, which partially counterbalances ΔP_T. Therefore, flow progressively slows down; and ΔP_F progressively decays and ultimately approaches 0. ΔP_S = 0 initially, but progressively increases and gradually approaches ΔP_T. In unsaturated cakes ΔP_F = 0, not ΔP_T, when compaction starts.

$\Delta P_S + \Delta P_F = \Delta P_T$ in all parts of saturated cakes; but local P_S and P_F change as local outflow and compaction occur. A similar equation applies for P_S, P_F and P_T, i.e. for cases where $P_T \neq 0$ prior to pressing, or for changes in P_T in cakes that are already undergoing deformation. ΔP_T, ΔP_S, and ΔP_F, the respective changes in P_T, P_S and P_F caused by the change in load, are simply added to the P_T, P_S and P_F that existed before load changed and $P_T = P_S + P_F$.

Cakes effectively contain an infinite series of differentially small rheological elements. Therefore cake compaction can be described in terms of a partial differential equation (PDE) and associated initial and boundary conditions (IC

and BC). Solutions of such PDE often satisfactorily describe initial stages of moist soil consolidation and expression of fluid from filter cakes[53-56].

Nature of P_S: Fluids transmit pressure equally in all directions; so P_F acts uniformly on all exterior surfaces of particles at given levels in a cake. Solid stresses do not act uniformly in all directions. P_S is the axial component of solid stress. The corresponding transverse component is P_h. $B \equiv P_h/P_S$. B, an analog of Poisson's ratio, often appears to remain constant as P_S changes.

By definition, $P_S \equiv P_T - P_F$. Thus P_S measures by how much total axial force per unit area exceeds P_F, i.e. it is the local excess axial stress acting on particles averaged over the whole area. Particles only occupy $(1 - \varepsilon')$ of that area. Therefore the true mean excess axial stress in particles $= P_S/(1 - \varepsilon')$. The local excess stress varies from point to point. It is greater than $P_S/(1 - \varepsilon')$ where particle surfaces press on one another.

Bulk Specific Volumes and Porosity Ratios: Volumes and heights or thicknesses of presscakes change during pressing. The volume or mass of dry fixed solids remains constant and can provide a convenient frame of reference for describing volume changes during pressing. V is the local bulk volume per unit mass of dry fixed solids, (in S.I. units, m^3/kg FS). The porosity ratio, $e \equiv \varepsilon/(1 - \varepsilon)$, is the pore volume per unit volume of fixed solids. V_o is the value of V at the start of pressing and V_f is its final value. e_o and e_f are the corresponding values of e.

e is useful for dealing with cakes containing non-biological solids where particle volume does not change during pressing. Cellular biological solids (CBS) deform much more than non-biological solids and contain relatively closed pores. Curds and flocs of biological origin also deform readily and contain very fine open pores. Ψ and ε are often difficult to determine for such solids, and flows within such solids behave quite differently than flows in spaces between particles. V can be more readily determined than e for presscake containing CBS. Therefore expression involving CBS will often be analyzed in terms of V instead of e. Conversions between e, ε and V involving use of ρ_S, the intrinsic density of fixed solids, are listed in Table II.

TABLE II Conversions between variables

(Entries provide variable listed at top in terms of variable listed at left.)

Variable	ε	e	V
ε	-	$\varepsilon/(1 - \varepsilon)$	$1/[(1 - \varepsilon)\rho_s]$
e	$e/(1 + e)$	-	$(1 + e)/\rho_s$
V	$(V\rho_s - 1)/V\rho_s$	$V\rho_s - 1$	-

To determine V, a measured volume, Q_C, of cake is sampled, leached to remove soluble solids, and then dried to constant weight, M_d. $V = Q_C/M_d$. V_S, the specific volume of the fixed solids $= 1/\rho_S$. $V_S \approx 0.67 \times 10^{-3}$ m^3/kg FS for CBS; for soils it ranges from 0.33×10^{-3} to 0.5×10^{-3} m^3/kg FS, and $\approx 0.4 \times 10^{-3}$ m^3/kg FS on the average.

V and e Ranges: V_o and e_o and typical e_f and V_f for different classes of materials are listed in Table III.

V_P, the initial V for fluid-filled particles by themselves $= V_o \cdot (1 - \varepsilon')$ at the start of pressing. V_P/V_S for moisture-rich CBS usually lies between 11 and 49, but sometimes is as low as 4. V_C is the V at which a cake becomes completely saturated when all gas is cleanly expelled. V_C depends on s, the fractional saturation. V_C equals V_P when $s = 0$ and it equals V_o when $s = 1$. Fluid clings to particles in drained cakes. Therefore V_C is always greater than V_P and usually less than V_o for drained cakes.

Non Expressible Water: Moist cakes contain non-expressible water. Therefore V_f for such cakes is always somewhat greater than V_U, the bulk specific volume of the fixed solids and non-expressible water they contain. $V_U = V_S(1 + X_{ne} \cdot V_w)$ where V_w is the specific volume of water, (i.e. $\approx 1 \times 10^{-3}$ m^3/kg). Some V_U are listed in Table III.

Table III Typical V and e for different types of cakes
(Units of listed V are $1x10^{-3}$ m^3/kg FS)

Material	e_o	V_o	e_f	V_f	V_U
Fruit	28 to 90	19 to 60	1.5 to 15	1.7 to 11	1.1 to 1.25 est.
Oil seeds	4 to 8	3.3 to 6	0.06 to 0.16	0.74 to 0.83	0.74
Sugar Cane	15 to 17	10 to 11.3	4.7	3.8	
Waste Treatment sludge	13 to 23	9 to 16	3.5 to 6	3 to 5.3	
Kraft Pulp	5 to 5.5	4 to 4.3	2.25	2.17	1.07 to 1.27
Other Pulps	6 to 13	4.7 to 9.3	2.4 to 2.7	2.3 to 2.5	1.07 to 1.85
Hard Particles	0.54 to 0.82		0.25 to 0.33		
Most soils	0.7 to 1.3	0.68 to 0.92	0.25 to 0.5	0.5 to 0.6	0.5
Swellable Clays	1.7 to 5	1.1 to 2.4	0.45 to 2.3	0.58 to 1.32	

5. SOLID STRESS

P_S Correlations: It usually is assumed that P_S only depends on e during compression. Function $P_S(e)$ provides P_S when e is specified. An inverse function $e(P_S)$ provides e when P_S is specified. V varies linearly as e varies. Therefore $P_S(e)$ can readily be converted into function $P_S(V)$, which provides P_S when V is specified. $V(P_S)$ provides V when P_S is specified.

P_S *usually does not increase linearly as e or V decreases; and* $P_S(e)$ *and* $P_S(V)$ are usually non-linear functions that depend on the nature of the material being compressed. For many soils[54,55].

$$\frac{e_{ref} - e}{C_C} = \ln\left[\frac{P_S}{P_{ref}}\right] \quad (1)$$

for $P_S > P_{ref}$. $e = e_{ref}$ when $P_S = P_{ref}$. C_C is known as the coefficient of compressibility. Eq (1) is frequently used in expression literature. For sandy soils, C_C = 0.02 to 0.2; for clays, C_C = 0.04 to 1.1. Most C_C fall between 0.04 and 0.4, but are higher for clays with high initial moisture contents. For foods that obey Eq (1), C_C range between 1 and 5.6.

$P_S(V)$ are more convenient to use for CBS than $P_S(e)$. For materials that obey Eq (1):

$$\ln\left[\frac{P_S}{P_{ref}}\right] = K \cdot (V_{ref} - V) \quad (2)$$

$V = V_{ref}$ when $P_S = P_{ref}$. $K = \rho_S/C_C$. In addition to working well for many soils, Eqs (1) and (2) also work well over some P_S and V ranges for spent coffee grounds[56], alfalfa[57], protein curds[58], solka-floc[59] and sugar beets[60].

Eqs (1) and (2) probably have a mechanistic basis. P_N, the normal stress acting on interfaces between particles is proportional to P_S. f_p is the coefficient of friction between particles and A_c is the contact area between particles. The frictional force acting on adjacent particles moving relative to one another during compaction is $P_N \cdot f_p \cdot A_c$, i.e. and therefore is proportional to $P_S \cdot f_p \cdot A_c$. A_c increases because particle surfaces overlap each other more and more as compaction proceeds. dA_c is proportional to - dV during uniaxial compaction of a confined bed of particles. P_S must increase to overcome friction between particles for compaction to proceed. Therefore dP_S is proportional to $P_S \cdot f_p \cdot dA_c$ and $-P_S \cdot f_p \cdot dV$. If f_p and all other proportionality constants are combined in a single constant, K, $dP_S = -K \cdot P_S \cdot dV$, which when integrated yields Eq (2).

Eqs (1) and (2) do not apply over the whole pressing range. As V approaches V_U, P_S increases more rapidly than described by Eq (1) or Eq (2). For initially uncompacted cakes $P_S \rightarrow 0$ as $V \rightarrow V_o$. Since Eq (2) does not satisfy this condition, it is not valid at V close to V_o. Fig. 32 depicts how $\log(P_S)$ probably varies as V changes between V_o and V_U, when Eq (2) applies

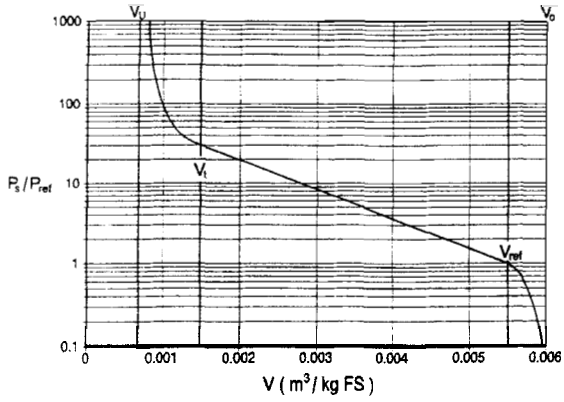

FIGURE 32 Log P_S versus V including non-linear ranges for materials that obey Eq (2) over much of their potential consolidation range

between V_{ref} and V_t. Below V_t, P_S turns up sharply as V decreases; and above V_{ref}, P_S probably increases linearly V decreases. Eqs (1) and (2) apply between 1 Mpa to 10 Mpa for sandy soils[54], 0.1 Mpa to 200 MP_a for clays, 0.1 Mpa to 1.2 Mpa for spent coffee grounds; and 4 Kpa to 100 Kpa for protein curds.

Compressive Stress-Strain Maps: The P_S behavior versus V behavior depicted in fig. 32 is in some ways similar to that shown in maps of P_S versus compressive strain developed for porous solids by Ashby[61,62]. A modified Ashby map is shown in fig. 33. It shows steep P_S versus $(V_o - V)/V_o$ behavior at $(V_o - V)/V_o$ close to 0 and near $(V_o - V_U)/V_o$. The intermediate region in Ashby maps is usually flatter than shown in fig, 33, but for biological solids, P_S often rises more steeply than usually depicted for that region[61,63,64]. Densification and the rapid P_S rises that accompany it start at lower $(V_o - V)/V_o$ when cell walls are thick, i.e. V_S/V_o is large. P_S also is larger prior to densification when cell walls are thick. Ashby[61] shows that strength and deformation properties of cellular porous solids depend strongly on V_S/V_o. Properties such as the elastic modulus, various types of yield stresses and fracture toughness tend to be

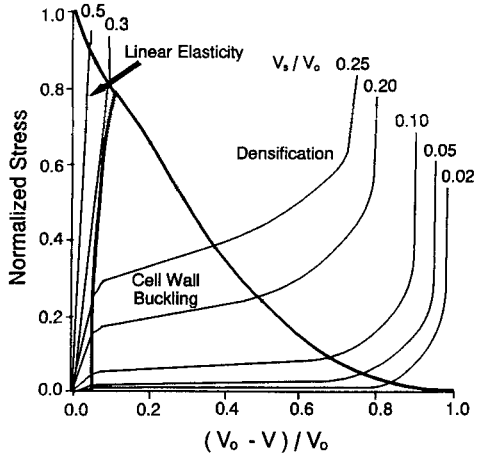

FIGURE 33 Modified Ashby compressive stress-strain map for porous solids[61]

proportional to $(V_S/V_o)^m$. m depends on the property in question and usually lies between 1.5 and 2 for foams with open cells and between 2 and 3 for foams with closed cells. Ashby's strength versus V_S/V_o relationships provide bases for estimating how the deformation properties of cellular tissue will change as cell wall thicknesses change during growth and ripening.

Irreversibility: Consolidation is not reversible. As shown in fig. 34, P_S decreases extremely rapidly when V or e is allowed to increase following compaction[52,56,57]. P_S drops to 0 after slight increases in V or e and rises very rapidly if pressing is resumed. After a small decrease in V, P_S follows the $P_S(V)$ curve that would have applied if pressing had not been interrupted. Thus the initial part of a P_S versus V curve for a previously pressed material would be different from that for an unpressed material of the same type. Consequently $P_S(V)$ often depend on past compression history. Friction between particles opposes both compaction and expansion. Therefore it probably contributes to P_S irreversibility.

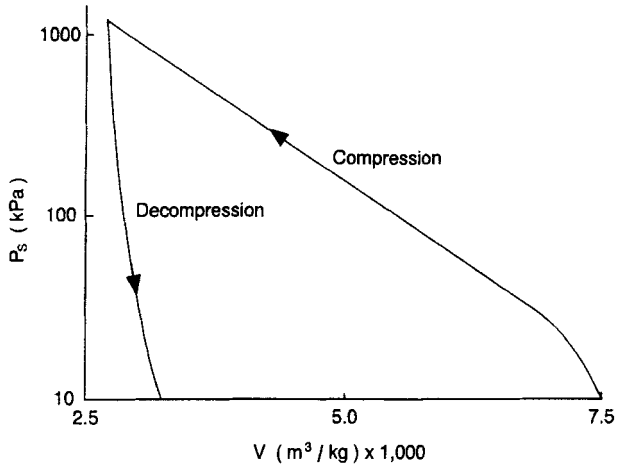

FIGURE 34 Irreversibility of P_S versus V behavior during compaction and expansion

Because of irreversibility, $P_S(V)$ used for compaction cannot be used as-is for expansion. Even if Eq (2) applies for expansion, K will be much larger for expansion than for compression.

Other $P_S(e)$: P_S for waste-treatment sludges[65] and clays has been correlated by

$$P_S / P_{ref} = E_o [e_{ref}/e]^n \quad (3)$$

Leonhard[65,67] found n were between 1.4 and 10 for waste-treatment sludges. Another equation used for sludges and clays[65] is

$$\frac{e - e_\infty}{e_o - e_\infty} = \exp[-\lambda P_S] \quad (4)$$

with λ ranging from 0.09 to 0.53/Pa for waste-treatment sludges and from 0.007 to 0.02/Pa for concentrated clays. The following relationship is frequently used for filter cakes[68]

$$\frac{1 - \varepsilon}{1 - \varepsilon_o} = \left[1 + \frac{P_S}{P_{ref}}\right]^b \quad (5)$$

Leu[69] indicates that b ≈ 0.05 for slightly compressible filter cakes, 0.15 for moderately compressible cakes and 0.30 for very compressible cakes.

Other $P_S(V)$: Many other types of non-linear P_S versus V correlations have been reported for CBS. Several are presented below. The constants used are indicated by E with a subscript. n is used as an exponent for V terms and b is used as an exponent for P_S terms. For sugar cane and bagasse:[70-72]

$$P_S = \frac{E_1}{V^n} \quad (6)$$

Different n have to be used for different pressure ranges[70], e.g. n = 5 when P_S is between 5MPa and 82 MPa (an important P_S range in sugar mills) and n = 2.5 for P_S between 7 kPa and 390 kPa[70]. Murry and Holt[17] found that $P_S = E_2[(V_C/V - E_3]^2$ for sugar cane and bagasse at low P_S, E_2 markedly increases and E_3 slightly increases as the coarseness of the shredded cane or bagasse increases. E_2 is much higher for bagasse (23 to 53 MPa) than for cane (0.28 to 0.9 MPa). E_3 ranges between 0.24 and 0.28 for cane and 0.0235 and 0.028 for bagasse.

For paper pulp at P_S between 4 kPa and 2.0 MPa[73,74] and for talc, polystyrene latex, metal powders, metal oxides and sulfides, $CaCO_3$, activated carbon, iron blue pigment, solka floc and diatomaceous earth[59] at P_S between 7 to 70 kPa and P_S = 7 MPa.

$$\frac{dP_s}{dV} = -E_4 \cdot P^b \quad (7)$$

which when integrated for b ≠ 1 yields

$$\frac{1}{V} = E_4 P_s^{(b-1)} \quad (8)$$

b ranges between 0.65 and 1.35, and frequently is reasonably close to 1 at high P_S; e.g. b = 1 for solka floc and grade SF carbonyl iron, 1.035 for polystyrene latex, and 1.07 for tungsten powder. If b = 1, Eq (2) is obtained when Eq (7) is integrated.

Eq (9) has been used for dry, and oil- and water-saturated absorbent cotton, wool felt and asbestos[75,76] at P_S between 1.7 MPa and 138 MPa, dry paper pulp, pulp moistened with various different liquids, wool fibers and sawdust[77] at P_S between 27.5 MPa and 138 MPa; and dry polymer granules[78] at $P_S > 14$ MPa.

$$\ln(P_S) = E_5 + \frac{E_6}{V} \qquad (9)$$

For apple pulp[79] at P_S between 400 kPa and 1.8 MPa

$$P_s = 3.3 \times 10^6 \left[\frac{V_c - V}{V_c}\right]^5 \qquad (10)$$

The units of P_S in Eq (10) are Pascals.

$V(P_S)$ Dependence on Time: In tests used to measure P_S versus V behavior, P_T is maintained constant while V equilibrates. At equilibrium, $P_T = P_S$ and $V = V(P_S)$. Relatively long times may be required for equilibration. Waits of a day or more are used when determining $P_S(e)$ for soils; and it is recognized that true equilibrium is not reached even then. One-day tests apparently yield true values for C_C; and time-induced changes in $P_S(e)$ apparently can be accounted for by allowing e_{ref} to decrease slightly as time increases.

In pressing tests with other materials, P_T was maintained constant until no more liquid was expelled. Often, only 2 to 15 minutes was allowed for equilibration. The time allowed for equilibration is not given in many cases. Equilibrium was not reached even after 2 hrs for milled apples[79], nor was it reached after 4 hrs for oil seeds[80,81].

Kormendy[79] and Mrema[82] noted that after a while $\log[V - V(P_S)]$ decreased linearly as holding time, t_p, increased, which agrees with pressing equations

based on the model in Fig. 31. Kormendy used this observation to determine $V(P_S)$.

Wilder[83] noted that for paper pulp E_1 in Eq (6) increases linearly as $\log(t_p)$ increases. This relationship can only apply over a limited time range, otherwise V would ultimately approach 0.

Koo[80,81] used Eq (11) for t_p between 0.5 and 4 hr for oilseeds pressed in a curb press.

$$\frac{(V_P - V)\,\rho_F}{V_P \cdot \rho_P} = E_7\, P_T^{1/2}\, t_p^{1/6} \left[\frac{\rho_F}{\mu}\right]^m \qquad \textbf{(11)}$$

ρ_P is the particle density prior to pressing, ρ_F the oil density and μ its viscosity. E_7 varied with the type of seed used and was higher for seeds with high oil content. The exponent m also varied; e.g. it was 1/4 for soybeans and cottonseed, 1/6 for rapeseed, peanut and tung and 1/12 for sesame seed and castor beans. Similar equations with different constants have been reported[80]. These relationships cause V to ultimately become negative at large t_p. Therefore they cannot be true at very large t_p.

Effect of Pressing Rate on P_S: As rates of pressing increase ram pressure, P_T, at equal V increases[55,72,79,84]. It is usually assumed that this occurs solely because P_F increases as flow rates increases. Both P_T and P_F were measured during constant speed pressing of spent coffee grounds[85] and used to calculate P_S. $P_S = P_T - P_F$. It was found that P_S depended on pressing speed as well as on V.

Secondary Consolidation: Primary consolidation in soils is often followed by slower secondary consolidation of smaller extent caused by "plastic creep"[86]. The model in fig. 31 is modified in fig. 35a to account for such creep by placing a Kelvin-Voigt element (a spring and dashpot in parallel) in series with each original spring. If the added element represents part of the rheological behavior of solid particles in a cake, P_S should be time dependent.

Compactions of cellular biological particles causes outflow from particles. This outflow causes much more cake volume reduction for CBS than secondary

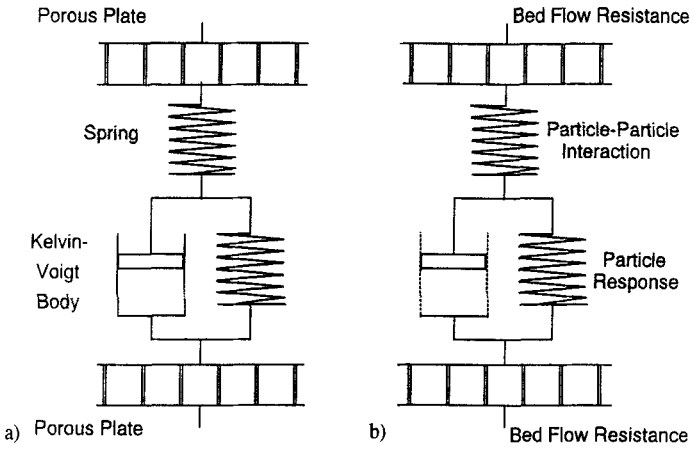

FIGURE 35 Kelvin-Voigt modifications of Terzaghi-Peck model; a) use of a solid dashpot to model creep; b) use of a perforated dashpot to model outflow from particles of cellular biological solids

consolidation does for soils. The dashpot in 35a is replaced by a perforated one in 35b to depict pressing of fluid out of particles into spaces between particles.

Internal Pressure: Excess pressure P_E builds up in fluid inside CBS particles during pressing, and sooner or later forces fluid out of particles. Particles of CBS usually contain many cells separated by walls with small pores. Thus individual particles may act like miniature presscakes. Therefore, as shown in fig. 36, miniature versions of the array shown in fig. 31 may be used instead of Kelvin-Voigt elements to model pressing responses of CBS particles in cakes.

Exudation rates are probably proportional to P_E, the available flow area and the hydraulic conductivity of cells walls involved, and are inversely proportional to flow path length. Hydraulic conductivities have been measured for some cell walls[87-92], but usually are not known. P_F can be measured during pressing; P_E is hard to measure, and is usually treated as part of P_S. Since P_E usually depends on the pressing rate or local rate of compaction, local P_S for CBS

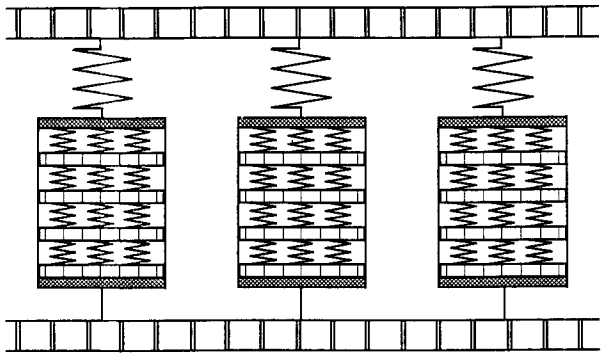

FIGURE 36 Use of Terzaghi-Peck sub-elements in Terzaghi-Peck model to account for deformation and flow inside of particles of cellular biological solids

should also be a function of pressing rate or of local $\partial V/\partial t$ as well as being a function of V or e.

6. CELL AND TISSUE STRUCTURE

Cells: Cell properties can greatly affect the pressing behavior of plant material. Therefore, plant cell structure will be discussed in some detail. Plant cells are encased in a selectively permeable lipoprotein membrane, the plasma membrane, surrounded by a relatively rigid wall made of cellulose fibers imbedded in a matrix containing hemicelluloses, pectins and small amounts of glycoproteins (see fig. 37) all linked together mainly by hydrogen bonds[93]. Acidic pectins in the matrix are also cross-linked by Ca^{++} ions. Large amounts of lignin, an amorphous polyphenol, are found in many plant cell walls. Lignin cements cells together in wood, which contains 20% to 35% lignin by weight. Fruit and vegetable cells are cemented together by protopectin, an insoluble form of pectin; the junction region is called the middle lamella.

Some plant cell walls are only 0.1 μm thick, others are many micrometers thick, e.g. some wood cell walls are 7 μm thick. The wall supports the cell and provides a base for bonding it to other cells. Most animal cells have walls that

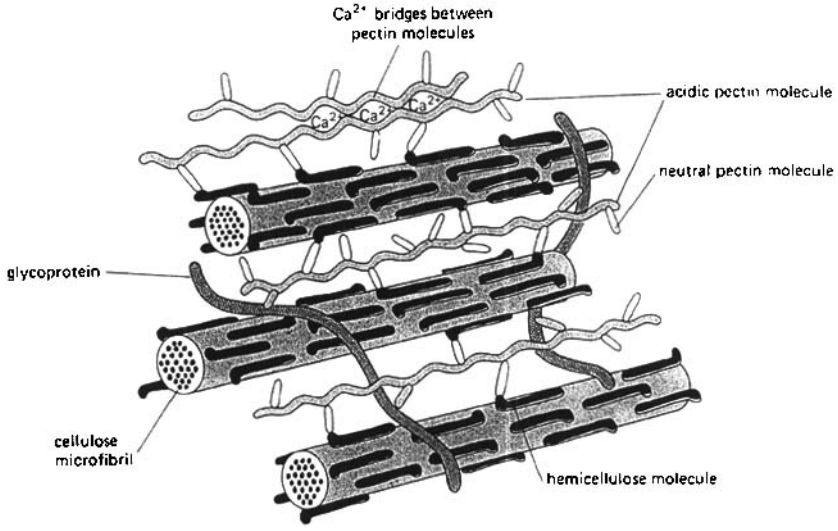

FIGURE 37 Model of cell-wall structure (Alberts et al.[93] From *Molecular Biology of the Cell*, Garland Publishing, Inc.)

performs similar functions; but they consist of fibrous proteins, e.g. collagen, embedded in a hydrated polysaccharide gel.

Cells contain an internal, fluid-filled compartment, the vacuole, surrounded by a second membrane, the tonoplast. Vacuoles usually occupy most of the interior of cells of juicy plant materials. The cytoplasm, the cell region between the tonoplast and the plasma membrane, contains the cell nucleus, organelles and other physiologically active units. It may also contain grains of starch and oil droplets. Active cells take in water and expel wastes. Most of the resistance to passage of water and small molecules occurs in the plasma membrane; less than 10% occurs in the wall. Therefore resistance to expulsion of juices or diffusion of water or solutes out of cells can be greatly reduced by denaturing or rupturing the plasma membrane.

Typical plant cells diameters range between 20 μm and 130 μm. Wood cells are 1 mm to 7 mm long, but only 16 μm to 44 μm wide[94]. Cell diameters

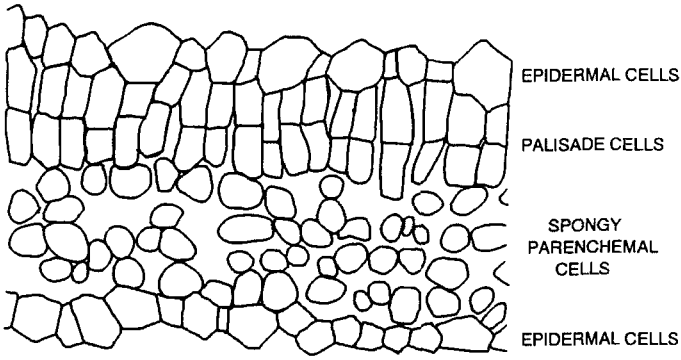

FIGURE 38 Cross section of a young alfalfa leaf. The highly porous mid-section occupied by spongy parenchymal cells is more completely filled when the leaf matures.

vary with time and position in the plant. The average diameter of apple cells three weeks prior to full ripeness is roughly 100 μm; at full ripeness it is roughly 130 μm[95]. Thicknesses of apple cell walls vary between 0.5 μm and 1.0 μm. In late stages of growth, wall thickness decreases as cell diameter expands. Sugar beets cells have an average diameter of roughly 40 μm and a wall thickness of roughly 0.8 μm; individual cell diameters range from 20 μm to 60 μm[96,97].

Some cells have a great deal of intercellular space between them, e.g. intercellular space occupies roughly 25% of the volume of apple tissue and roughly 30% of the volume in sugar beets. On the other hand, cells in most seeds, are tightly packed. Fig. 38, a sketch of a young alfalfa leaf, shows a case where both tightly packed and loosely packed cells are present[98]. Expelled fluid encounters very little in-particle resistance to flow after leaving a cell when the amount of intercellular space is large. Unfortunately, intercellular space often collapses quickly during pressing[96,99]. Vascular systems of plants may also facilitate flow of expelled juice. In sugar beets, part of the vascular system (fine, highly lignified tubes, "tracheary" elements, 20 to 40 μm in

diameter) remains open during pressing[96,99]. Expelled fluid has to travel through many cell walls in series when material made of densely packed cells is pressed. Therefore in-particle flow resistance for such materials will be large.

Most cell walls have pores with diameters ranging between 3.5 and 4.2 nm[93]. Pores in cells with thick walls may have effective diameters as small as 1 nm[100]. Large molecules cannot pass through such pores. Comparisons of solute diffusion coefficients in water and in spent coffee grounds, a CBS with completely denatured plasma membranes, indicate that pores occupy roughly 4 to 5% of cell wall area. Exterior surfaces of cells located on the outside of plants are covered by a waxy cuticle that greatly reduces transfer of any sort. Solid components in the wall hydrogen-bond with one another instead of with water when plant tissue is completely dried, and cell wall pores effectively close. Plant cell walls and epidermal cells have to be ruptured in order to express organelles and high molecular weight solutes.

Turgor: *Excess internal pressure, "turgor", develops inside biologically active* plant cells due to osmotic imbalances between intracellular and extracellular fluid. Turgor pressure provides much of the structural strength of plant cells. It ranges from 50 kPa (0.5 atm) in some large single-celled algae to 5 MPa (50 atm) in some stomatal guard cells (cells that regulate gas exchange in leaves)[93]. Plasma membranes and cell walls in living plants are under tension because of turgor. Most of the strength of plasma-membrane cell-wall combinations is provided by the wall. Tension in the wall counterbalances tension in the membrane. Plant cell walls are very strong in tension, but buckle easily when turgor pressure is relieved. Cells that have their walls removed and are placed in water rapidly swell, and their plasma membranes burst.

If plasma membranes are denatured, e.g. by heating plant tissue to 50° to 70°C or by chemical treatment[101], turgor disappears and cells deform much more readily. Heating above 70°C causes pectin to dissolve. This allows cells to break apart fairly readily when subjected to stress. Pectin also breaks down slowly as fruits age after harvest; consequently fruits soften as they age. These changes greatly affect the pressability of fruit.

Growing cells have only a primary wall containing randomly oriented, highly hydrated cellulose fibers. Water and dissolved solutes make up roughly 60% of the weight of primary walls in biologically active cells[87]. Turgor pressure causes primary walls to stretch as cells grow. Therefore cell walls often become thinner as fruits ripen.

Secondary walls are laid down inside the primary wall after cells stop growing. Secondary walls often consist of several layers[102]. Cellulose fibers in some of these layers lie largely parallel to each other; in other layers there may be a cross-weave pattern. Such fiber arrangements greatly strengthen wood cells, which remain strong in the absence of turgor.

Plasmodesmata: Interiors of adjacent cells connect through fine membrane-lined channels, "plasmodesmata", that interconnect neighboring plasma membranes and pass through cell walls at "pits", round depressions in the wall. In some cells, the pits is only 10 to 20% as thick as the rest of the wall[103]. Therefore pits are weak points in walls. Plasmodesmata are usually 20 to 40 nm in diameter[93]; diameters of 80 to 120 nm have been reported for oilseeds[82]. There may be as few as 0.008 plasmodesmata per μm^2 of cell surface, and as many as 140 per μm^2 on nectar-secreting cell surfaces. Often there are less than 1 plasmodesmata/μm^2. There would be roughly 7850 plasmodesmata in the wall of a 50 μm diameter cell containing 1 plasmodesmata/μm^2, but the plasmodesmata would cover less than 0.13% of the wall area. Therefore in cells with denatured membranes, plasmodesmata provide much less area for transport of small molecules than cell wall pores do. Plasmodesmata also seal when cell membranes are denatured by heating[99].

Intact plasmodesmata allow molecules to pass directly from cell to cell. Flow within the symplast, i.e. the space bounded by interconnected plasma membranes, is called symplasmic flow[89]. Flow that takes place in dead vascular cells (xylem) and in extracellular parts of plant tissue, including flow in pores between cells and in hydrated cell walls is called apoplasmic flow.

Plant tissue is far from homogeneous in structure. Cell size varies with radial position in apples and from the top of an apple to its bottom. Alfalfa

leaves contain several different types of cells, and leaf characteristics vary from the top of an alfalfa plant to its bottom[104]. Sugar cane, a very frequently pressed material, has a core (pith) that contains fine-walled sugar-rich cells, and a rind made up of hard, woody cells that contain less sugar[105]. Straight sections of sugar cane are also separated by woodier nodes. In wood, cells that form in the spring are small and their walls are thin. Wood cells that form in the summer are larger and their walls are thick[94]. The alternation in cell wall thickness and cell size is responsible for annual rings in wood. In spite of such non-uniformity, pressed materials are usually treated as if they are homogeneous in nature when expression is analyzed. In industrial scale pressing, initial inhomogeneity is partly averaged out by mixing of feeds and by processes that convert tissue into particles; but errors due to inhomogeneity can easily occur when small test samples of material are pressed.

7. COMPACTION AND FLOW

Uniaxial Compaction and Flow: To illustrate how compaction and flow in presscakes are described mathematically, let us examine uniaxial compaction and flow in a cake pressed between an impermeable flat ram and a flat outflow surface in a cylinder with impermeable walls. See fig. 39.

The cake height is Z and it contains mass W of fixed solids per unit of cross sectional area. As shown, Z and heights of local bits of fixed solids decrease during pressing. To provide coordinates whose positions do not change with time during pressing (see fig. 40), axial coordinates based on w, the mass of fixed solids between the ram surface (w = 0) and positions in the cake will be used. Such coordinates are called material coordinates or reference-substance coordinates. It is assumed that fixed solids initially present at any w/W remain there during pressing.

In the literature, w is usually measured from the outflow surface, i.e. w = 0 at the outflow surfaces. To provide positive flows in the direction of increasing w, the opposite convention is used here. This affects the sign of some terms in equations, but does not affect basic results significantly.

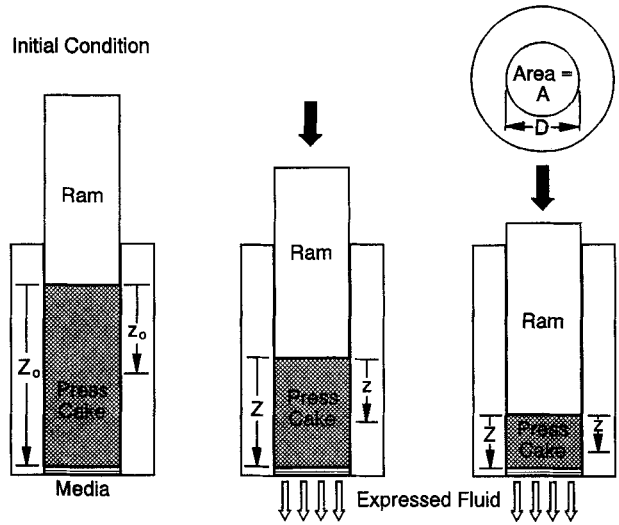

FIGURE 39 Ram, cake and outflow media setup during uniaxial expression

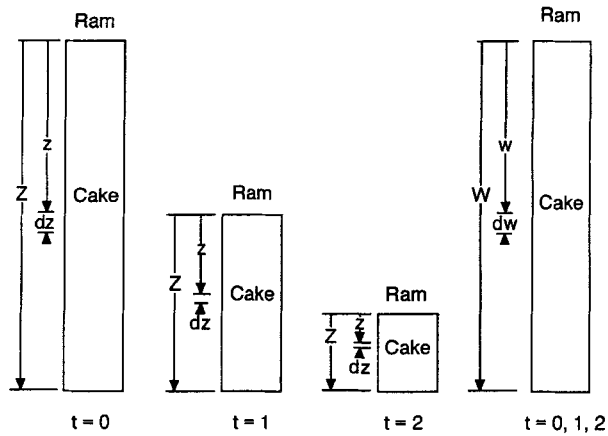

FIGURE 40 Changes in Z-based and (w/W)-based coordinates during uniaxial compression

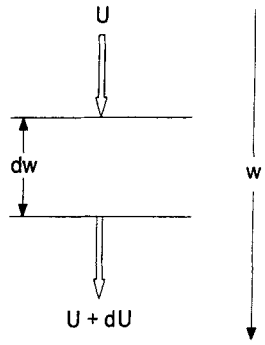

Net volume outflow rate = AdU =

Volume reduction rate = - dw(dV/dt)A

Therefore dU/dw = - dV/dt

FIGURE 41 Balance between net outflow and volume changes for a dw thick slice during uniaxial compression

$$Z = V_a \cdot W = \int_0^W V\,dw \qquad (12)$$

V_a, the average value of V, = Z/W. The cake may contain air. If so interparticle flow of fluid will occur between w_1 and w_2 when

$$\frac{1}{(w_2 - w_1)} \int_{w_1}^{w_2} V\,dw \leq V_c \qquad (13)$$

V_c is the value of V when all air has just been expelled, i.e. the largest V at which cake contains only fluid and solids. If all air initially present is cleanly displaced during pressing, outflow occurs when $V_a \leq V_c$.

U is the local superficial fluid velocity relative to the fixed solids. Since the fixed solids and fluid move together at the ram surface, U = 0 at w = 0. Fig. 41 shows flow into and out of a slice of unit area and thickness dw during compaction. The net rate of outflow = $(\partial U/\partial w) \cdot dw$. If the fluid and fixed

solids are incompressible and the cake does not contain air or other compressible gas, the net rate of outflow equals $-(\partial V/\partial t) \cdot dw$, the rate of volume contraction in the slice. Therefore

$$\frac{\partial U}{\partial w} = -\frac{\partial V}{\partial t} \tag{14}$$

U at w is given by

$$U = -\int_0^w \left(\frac{\partial V}{\partial t}\right) dw \tag{15}$$

P_S versus w/W: It will be assumed that P_F, and P_S in w/W planes do not vary with lateral position during pressing. This assumption, used by most workers in the field, is supported by measurements by Sawamoto[106], but contradicted by equilibrium P_S measured by Tiller and Lu[107] in tests where wall friction was quite large. Therefore, whether or not P_S is uniform across w/W planes may depend on the relative magnitudes of wall friction and shear forces produced by friction between particles during pressing.

Flow Friction: If field forces, i.e, gravity and centrifugal force, are negligibly small, dP_F/dw will be governed by Eq (16) for flow through filter cakes[59,108]

$$\frac{dP_F}{dw} = -\alpha \mu U \tag{16}$$

α is the local specific filtration resistances and μ is the viscosity of the fluid. Alternative expressions[48,109] based on Darcy's permeability law are often used: e.g. Eq (17) is used in soil mechanics

$$k' \frac{dh}{dz} = U \tag{17}$$

h is the fluid pressure drop expressed in terms of liquid head and k' is the Darcy's law permeability. This become

$$\frac{dP_F}{dw} = - \frac{g \rho_F V U}{k'} \qquad (18)$$

where the pressure gradient driving flow is dP_F/dw. Note: $\alpha = (g\rho_F V)/(k' \mu)$. Eqs (16), (17) and (18) are equivalent and all lead to equivalent results in analyzing expression. When field forces and friction between the cake and the side wall of the pressing device are negligible, $dP_S = - dP_F$. Hence Eq (16) becomes

$$\frac{dP_S}{dw} = \alpha \mu U \qquad (19)$$

Eq (19), rearranged and partially differentiated with respect to w, becomes

$$\frac{\partial U}{\partial w} = \frac{1}{\mu} \frac{\partial}{\partial w} \left[\frac{1}{\alpha} \frac{\partial P_S}{\partial w} \right] \qquad (20)$$

8. PARTIAL DIFFERENTIAL EQUATIONS

Using Eq (14) and substituting $-\partial V/\partial t$ for $\partial U/\partial w$, one obtains

$$\frac{\partial V}{\partial t} = - \frac{\partial}{\partial w} \left[\frac{1}{\alpha \mu} \left(\frac{\partial P_S}{\partial w} \right) \right] \qquad (21)$$

If, as previous workers in the field[52,53] have assumed, P_S is solely a function of V, Eq (21) can be converted into

$$\frac{\partial V}{\partial t} = - \frac{\partial}{\partial w} \left[\frac{1}{\mu \alpha} \left(\frac{dP_S}{dV} \right) \frac{\partial V}{\partial w} \right] = \frac{\partial}{\partial w} \left[C \frac{\partial V}{\partial w} \right] \qquad (22)$$

where $C = - (1/\mu \alpha)(dP_S/dV)$. Kormendy[110] derived an equivalent equation. Similar equations in terms of ε or e instead of V and sometimes in terms of k' instead of α are often used in soil mechanics and work on expression [22,52,54]. Kormendy[110] showed that they all are equivalent. C is often treated as a constant, or a mean effective C is used, causing Eq (22) to reduce to

$$\frac{\partial V}{\partial t} = C \frac{\partial^2 V}{\partial w^2} \qquad (23)$$

An analogous, frequently used equation in terms of e is [22]

$$\frac{\partial e}{\partial t} = C_e \frac{\partial^2 e}{\partial \omega^2} \qquad (24)$$

ω is the volume of dry fixed solids per unit area between levels in the cake and the ram. $C_e = -(dP_S/de)/(\mu\alpha\rho_S)$. Since ω has the dimensions of length, C_e, like diffusivity and thermal diffusivity, has the dimensions m^2/s in the SI system. By contrast, the SI dimension for C are (kg $FS^2/m^4 \cdot s$). C_e is converted into C by multiplying it by $\rho_S{}^2$.

PDE in terms of e and z instead of e and ω are used in soil mechanics, where relative deformations are small. Use of z as a variable instead of ω or w can cause computational difficulty when deformations are large.

Use of a constant C in solving Eq (23) or of a constant C_e in Eq (24) often works fairly well for soil consolidation and for pressing tests carried out with non-biological cake at constant ram pressure, P_T. V and cake properties change greatly for milled fruit or waste-treatment sludges pressed at constant P_T. Therefore C or C_e cannot be treated as constant for such materials[110-112]. 20- to 50-fold variations in C_e occur during constant-rate pressing of casein curds, halved cranberries and spent sugar beet pulp[113]. C_e for such materials may also vary with pressing rate. Thus Eqs (23) or (24) cannot be used with a constant C for many biological materials.

P_S based PDE: Eq (21) can be converted to one solely in terms of P_S, i.e.

$$\frac{\partial P_s}{\partial t} = -\frac{dP_s}{dV}\frac{\partial}{\partial w}\left[\frac{1}{\alpha\mu}\left(\frac{\partial P_s}{\partial w}\right)\right] \qquad (25)$$

which is equivalent to

$$\frac{\partial P_s}{\partial t} = C\left[\frac{\partial^2 P_s}{\partial w^2} - \frac{1}{\alpha}\left(\frac{d\alpha}{dP_s}\right)\left(\frac{\partial P_s}{\partial w}\right)^2\right] \qquad (26)$$

Again, it is often assumed[52,53] that a suitable mean value of C can be found and that Eq (27) can be used instead of Eq (26)

$$\frac{\partial P_S}{\partial t} = C\frac{\partial^2 P_S}{\partial w^2} \qquad (27)$$

A similar equation can be written with ω used instead w and C_e instead of C.

Analogous PDE: Eqs (22) and (23) can be written in terms of the dimensionless variables $(V - V_\infty)/(V_o - V_\infty)$, w/W and $C_{ref}t/W^2$. Eq (27) can be made dimensionless by using $(P - P_\infty)/(P_o - P_\infty)$, w/W and $C_{ref}t/W^2$ as variables. The subscripts o and ∞ respectively indicate initial value and equilibrium value. Kormendy[110] showed that if media resistance was negligibly small, juice yields were functions of t/W^2 during pressing of milled apples at constant P_T. Dimensionless forms of Eqs (23), (24) and (27) are formally identical to dimensionless PDE describing conductive heat transfer and diffusive mass transfer in solids. Therefore PDE solutions for such transfer can be adapted to solve Eqs (23), (24) and (27). If C and factors involved in relevant BC are constant, available solutions of analogs of Eq (23) can be used to treat cases where media resistance (R_m) is important[115,116] or cases where constant rate compaction is used[117,118]. Appropriate replacements of dimensionless variables have to be used, e.g. Ct/W^2 in place of the Fourier number or Fick's number and $R_m/\alpha W$ in place of the heat-transfer or mass-transfer Biot number.

Some Standard Solutions If C is constant, media resistance is negligible, V is initially uniform and less than V_C, and constant-pressure expression is used

$$\frac{V_o - V_a}{V_o - V_\infty} = 1 - \sum_{j=1}^{\infty} \frac{8}{\pi^2(2j-1)^2} \exp\left[\frac{(2j-1)^2\pi^2 Ct}{4W^2}\right] \qquad (28)$$

If two parallel outflow surfaces are used, there is a surface between them where U = 0. This surface, the "neutral surface" effectively acts like a ram. In such cases W is based on half the cake load. It can be shown that $(Z_o - Z)/(Z_o - Z_\infty)$ can be used in place of $(V_o - V_a)/(V_o - V_\infty)$ in the left-hand side of Eq (28). When $(V_o - V_a)/(V_o - V_\infty) > 0.415$ or $Ct/W^2 > 0.135$, the first term in the series can be used alone with less than 1% error.

Large numbers of terms are needed if Eq (28) is used when t is small. Eq (29) can be used then instead of Eq (28). Use of Eq (29) causes less than 1% errors when $(V_o - V_a)/(V_o - V_\infty) < 0.62$ or $Ct/W^2 < 0.31$.

$$\frac{Z_o - Z}{Z_o - Z_\infty} = \frac{V_o - V}{V_o - V_\infty} = 2 \cdot \left[\frac{Ct}{\pi W^2}\right]^{1/2} \qquad (29)$$

When cakes obtained from constant-pressure filtration are pressed at the same pressure as soon as filtration ends, V at the start of pressing $\approx V_\infty + (\pi/2) \cdot (V_o - V_\infty) \cdot \cos(\pi w/2W)$. In such cases, Eq (30) can be used to predict pressed cake thickness if C is constant[22].

$$\frac{V_o - V_a}{V_o - V_\infty} = \frac{Z_o - Z}{Z_o - Z_\infty} = 1 - \exp\left[-\frac{\pi^2}{4}\left(\frac{Ct}{W^2}\right)\right] \qquad (30)$$

If desired, $C_e t/\Omega^2$ can be used in place of Ct/W^2 in Eqs (28) to (30). Ω is the value of ω at the outflow surface.

Wall Friction: To obtain high pressures, expression tests are sometimes carried out in small-diameter tests cells where wall friction cannot be neglected. Shirato[119] assumed that the local frictional force per unit of wall area between the cake and cylinder wall $= f_w \cdot P_h$, where f_w is the coefficient of friction between the cake and the wall. $B \equiv P_h/P_S$. Therefore, the local friction force per unit area $= B \cdot f_w \cdot P_S$. For pressing tests carried out in a cylinder of bore diameter D when $dP_F/dw = 0$, a force balance yields

$$\frac{\partial P_S}{\partial w} = -\frac{4 B f_w P_S V}{D} \qquad (31)$$

When interparticle flow occurs and $dP_F/dw \neq 0$

$$\frac{\partial P_S}{\partial w} = -\frac{4 B f_w P_S V}{D} - \frac{\partial P_F}{\partial w} \qquad (32)$$

Substituting Eq (16) in Eq (32) one obtains

$$U = \frac{1}{\alpha \mu}\left[\frac{dP_S}{dw} + HVP_S\right] \quad (33)$$

where $H = 4Bf_w/D$. Differentiating Eq (33) with respect to w and substituting for $\partial U/\partial w$ from Eq (14), one obtains

$$\frac{\partial U}{\partial w} = -\frac{\partial V}{\partial t} = \frac{\partial}{\partial w}\left[\frac{1}{\alpha \mu}\left(\frac{\partial P_S}{\partial w} + HVP_S\right)\right] \quad (34)$$

Field Forces: While gravity and centrifugal force can be neglected in most cases of expression, gravity is important when sediments compact and expel fluid in settling tanks, and centrifugal force is important when cakes compact in centrifuges. In such cases

$$\frac{dP_F}{dw} - V\rho\Theta = -\alpha \mu U \quad (35)$$

Θ depends on the nature and direction of the field force. $\Theta = g$ when gravity is the only important field force and acts in the direction of flow; $\Theta = -g$ if gravity acts in the opposite direction. Similarly, when centrifugal force is the only important field force, $\Theta = \omega^2 r$ when centrifugal force acts in the direction of flow; and $\Theta = -\omega^2 r$ when centrifugal force acts in the opposite direction. In the present instance ω means angular velocity. When wall friction is negligible, use of a force balance and accounting for buoyancy effects, yields

$$\frac{dP_S}{dw} = \alpha \mu U + [1 - V_S \rho_F]\Theta \quad (36)$$

Manipulation like that used in obtaining Eq (21) yields

$$\frac{\partial V}{\partial t} = -\frac{1}{\mu}\frac{\partial}{\partial w}\left[\frac{1}{\alpha}\frac{\partial P_S}{\partial w} - \frac{(1 - V_S \rho_F)\Theta}{\alpha}\right] \quad (37)$$

$V_S\rho_F$ also equals ρ_F/ρ_S. In this review, we will only deal with cases where field forces are negligible.

Need for Numerical Approach: R_m and cake properties for cellular biological solids vary strongly during pressing. Wall friction complicates PDE describing expression in small-diameter test equipment. Therefore numerical solution of Eq (21) or (34) often have to be used to analyze pressing behavior.

Boundary Conditions: One boundary condition (BC) for Eq (21) or (34) is:

$$U = 0 \qquad \text{at } w = 0 \tag{38}$$

Consequently

$$\frac{dP_S}{dw} = -HVP_S \qquad \text{at } w = 0 \tag{39}$$

If wall friction is negligible, $H = 0$ and $\partial P_S/\partial w = 0$ at $w = 0$. Further

$$U = -\frac{dZ}{dt} \qquad \text{at } w = W \tag{40}$$

Fixed-Rate Expression: Eq. 41 provides a useful boundary condition when ram speed, -dZ/dt, is constant or a known function of time, i.e.

$$-\frac{dZ}{dt} = \frac{1}{\alpha\mu}\left[\frac{dP_S}{dw} + HVP_S\right] \qquad \text{at } w = W \tag{41}$$

When wall friction is negligible this reduces to

$$-\frac{dZ}{dt} = \frac{1}{\alpha\mu}\left(\frac{dP_S}{dw}\right) \qquad \text{at } w = W \tag{42}$$

Expression at Constant Pressure: If a constant ram pressure, P_T, is used and media resistance, R_m, is negligible

$$P_S = P_T \qquad \text{at } w = W \tag{43}$$

When media resistance is significant, flow pressure ΔP_m occurs across the medium, and

$$P_S = P_T - \Delta P_m = P_T - \mu R_m\left(-\frac{dZ}{dt}\right) \qquad \text{at } w = W \qquad (44)$$

Since -dZ/dt is not specified when constant P_T are used, it must be determined by other means.

Initial Conditions: If V is initially uniform, the initial condition is

$$V = V_o \qquad \text{at all w when } t = 0 \qquad (45)$$

and, if P_S is solely a function of V,

$$P_S = P_S(V_o) \qquad \text{at all w when } t = 0 \qquad (46)$$

If pressing occurs after filtration, the P_S, P_F and V versus w profiles at the start of expression and the end of filtration are the same. Saturated mixtures of milled fruit and juice liberated from ruptured cells are often used as press feeds. If the free-juice content is large, expression may effectively be preceded by a period of ram-driven filtration. If so, the initial conditions for ram-driven solids compaction will be the conditions at the end of filtration. If the cake is saturated and solids compaction starts immediately, $V = V_o = V_C$ at all w. If the cake is not saturated, $V = V_o > V_C$. Numerical methods for determining V versus w when $V_o > V_C$ are described later.

9. NUMERICAL METHODS

One can readily solve Eq (21) or Eq (34) by finite-difference methods if appropriate BC and IC are known and P_S and α are solely functions of V, i.e. local P_S can be obtained from $P_S(V)$ and local α can be obtained from $\alpha(V)$ once local V are known. This section describes how this can be done for cases where: a) the cake is saturated; b) a known pressing rate is used; c) wall friction has to be accounted for; and d) V versus w is initially known. The pressing rate (-dZ/dt) may be constant or a prescribed function of time.

N nodes, equally spaced in terms of Δw, are used. Node 1 is at the ram surface and node N at the outflow surface. Nodes 2 to (N - 1) are at the

centers of Δw-thick slices. Node 1 is at the inner surface of the first slice, which is Δw/2 thick; and node N at the outer surface of the last slice, which is also Δw/2 thick. Index I or subscript I is used to indicate that a variable is evaluated at the Ith node. Thus V(I) and $[\Delta V/\Delta t]_I$ respectively represent V and ΔV/Δt for the Ith slice. Based on V(I) and $[\partial V/\partial t]_I$ determined from prior steps and application of $P_S(V)$ and $\alpha(V)$, V(I), $P_S(I)$ and $\alpha(I)$ are known at all I. If U(I) is the velocity leaving slice I, the velocity entering slice I, = U(I - 1). Therefore, in general

$$\left(\frac{\partial V}{\partial t}\right)_I = \frac{U(I-1) - U(I)}{\Delta w} \qquad (47)$$

and, based on Eq (33)

$$\left(\frac{\partial V}{\partial t}\right)_I = \frac{1}{\mu (\Delta W)^2} [A_I + B_I] \qquad (48)$$

where for slices 2 to (N - 1)

$$A_I = \left[\frac{P_S(I) - P_S(I+1)}{\alpha(I+1/2)} + \frac{P_S(I) - P_S(I-1)}{\alpha(I-1/2)}\right] \qquad (49)$$

and

$$B_I = H(\Delta w)\left[\frac{P_S(I-1/2)V(I-1/2)}{\alpha(I-1/2)} - \frac{P(I+1/2)V(I+1/2)}{\alpha(I+1/2)}\right] \qquad (50)$$

where V(I+1/2) = [V(I) + V(I+1)]/2 and V(I-1/2) = [V(I) + V(I - 1)]/2. $\alpha(I+1/2)$ and $\alpha(I - 1/2)$ and $P_S(I+1/2)$ and $P_S(I - 1/2)$ are respectively evaluated at V(I+1/2) and V(I - 1/2).

Surface Nodes: Since the slice thickness is only Δw/2 and U_{in} = 0 at I = 1

$$A_1 = 2\left[\frac{P_S(1) - P_S(2)}{\alpha(1.5)}\right] \qquad (51)$$

and

$$B_1 = -2H\Delta w\left[\frac{P_S(1.5)\,V(1.5)}{\alpha(1.5)}\right] \qquad (52)$$

At I = N the slice thickness is also Δw/2, but U_{out} = -dZ/dt, the pressing rate. Therefore

$$A_N = \frac{2\,[P_S(N) - P_S(N-1)\,]}{\alpha(N-1/2)} + 2\,(\Delta w)\,\mu\,(dZ/dt) \qquad (53)$$

and

$$B_N = H\,(\Delta w)\left[\frac{P_S(N-1.2)\,V(N-1/2)}{\alpha(N-1/2)}\right] \qquad (54)$$

When $V_a \leq V_c$ and w = W, $U_{out} = U_o$. Eq (15) can be expressed in finite difference form and summed from I = 1 to n to obtain U_n, the fluid velocity leaving slice n. Noting that $U_{in}(1) = 0$, one obtains

$$\sum_{I=1}^{n}\,[U(I) - U(I-1)\,] = U_n = -\frac{\Delta w}{2}\sum_{I=2}^{n}\left[\left(\frac{\partial V}{\partial t}\right)_I + \left(\frac{\partial V}{\partial t}\right)_{I-1}\right] \qquad (55)$$

If I = N is used as the upper limit in Eq (55), one obtains U(N), which should equal - dZ/dt. Agreement between U(N) and -dZ/dt provides a test of computational correctness when prescribed -dZ/dt are used.

ΔP_m, the fluid pressure drop across the media is given by

$$\Delta P_m = R_m\,\mu\left[-\frac{dZ}{dt}\right] \qquad (56)$$

R_m usually varies during pressing and may be a function of V or P_S at the outflow surface of the cake, i.e. of V(N) or P_S(N). R_m appears to be a function of V_a for some cakes. This may occur because the amount of sediment deposited on a unit area of media is proportional to the amount of fluid that has passed through that area, i.e. $W\cdot(V_C - V_a)$. In any case, R_m has to be correlated in terms of the most appropriate variable or variables.

P_F(N), the fluid pressure at the outflow surface of the cake, = ΔP_m. P_F(I), the fluid pressure at node I is given by

$$P_F(I) = \Delta P_m + \Delta w \sum_{I=N-1}^{I} \left(\frac{\alpha(I) + \alpha(I+1)}{2}\right)\cdot\left(\frac{U(I) + U(I+1)}{2\mu}\right) \quad (57)$$

$P_F(1)$ is the fluid pressure at the ram surface. $P_S(I)$ are obtained by substituting the V(I) in $P_s(V)$. The ram pressure, $P_T = P_S(1) + P_F(1)$.

New V(I) are obtained using

$$V(I,J) = V(I,J-1) + [\partial V/\partial t(I,J-1)] \cdot \Delta t \quad (58)$$

where Δt is a small time step. J, a time-step index, usually does not have to be expressed specifically.

Δt must be small enough to prevent computational instability. Criteria for stable Δt were obtained from a modified form of Eq (34) in which P_S is the dependent variable

$$\frac{\partial P_S}{\partial t} = = -\left(\frac{dP_S}{dV}\right)\frac{\partial}{\partial w}\left[\frac{1}{\alpha\mu}\left(\frac{\partial P_S}{\partial w} + HVP_S\right)\right] \quad (59)$$

Stability: Eq (59) is converted into a finite-difference equation that provides $(\Delta P_S/\Delta t)_I \equiv [P_S(I)_{J+1} - P_S(I)_J]/\Delta t$ in terms of $P_S(I)$, $P_S(I-1)$ and $P_S(I+1)$, dP_S/dV at I and values of $V(I+1/2)$, $V(I-1/2)$ and α and P_S at $V(I-1/2)$ and $V(I+1/2)$, all evaluated at time step J. Both sides of the equation are multiplied by Δt. To provide stability, the coefficients of the $P_S(I)_J$ terms on the right-hand side of these equations must be less than 1 at all (I). For this to be true, Δt has to satisfy the most rigorous of the following three criteria based on values of variables at time step J

$$\Delta t \leq -\frac{\mu(\Delta w)^2\,\alpha(I-1/2)\,\alpha(I+1/2)}{2\,(dP_s/dV)_I\,[\alpha(I+1/2) + \alpha(I-1/2) + E]} \quad (60)$$

where

$$E = \frac{H(\Delta w)}{2}\,[V(I-1/2)\,\alpha(I+1/2) - V(I+1/2)\,\alpha(I-1/2)] \quad (61)$$

$$\Delta t \leq \frac{-\mu(\Delta w)^2\,\alpha(1.5)}{(dP_S/dV)_1\,[2 - H(\Delta w)\,V(1.5)]} \quad (62)$$

and

$$\Delta t \leq \frac{-\mu\,(\Delta w)^2\,\alpha\,(N-1/2)}{(dP_S/dV)_N\,[2 + H\,(\Delta w)\,V\,(N-1/2)]} \qquad (63)$$

New sets of V(I) are obtained by using in Eq (58) the smallest Δt obtained from Eqs (60) to (63). The new t, $t_{J+1} = t_J + \Delta t$. The new V(I) are substituted in $P_S(V)$ and $\alpha(V)$ to obtain new $P_S(I)$, $\alpha(I)$ and $(dP_S/dV)_I$. Eqs (48) to (58) and (60) to (63) are used over and over again to generate V(I), $P_S(I)$, U(I), $P_F(I)$ and P_T versus t and V_a. The process is allowed to continue until P_T reaches a maximum tolerable value, P_{max}. To prevent computed P_T from overshooting P_{max} by too much, Δt should be reduced as P_t approached P_{max}. Larger Δt reductions should be used for conditions that tend to produce greater P_T overshoot, i.e. rapid ram movement and large W.

P_S that were functions of both $\partial V/\partial t$ and V invariably caused instability when used in numerically solving Eq (34) or Eq (48) . Stable solutions were obtained when $\partial V_a/\partial t$ was used instead of local $(\partial V/\partial t)$ in such P_S functions. Attempts to provide stability criteria that account for the influence of local $\partial V/\partial t$ have thus far been unsuccessful. Since $\partial P_S/\partial w$ will depend on $\partial V/\partial t$ in ways other than described by Eqs (34) or (48) if P_S is intrinsically a function of $\partial V/\partial t$, the problem may not really be one of computational stability at all.

After P_T Reaches P_{max}: In cases where ram pressure P_T remains at P_{max} once it reaches that value, computations can be continued using most of the same equations. In such cases, the dZ/dt used in Eq (53) changes with time and is obtained from Eq (64)

$$\frac{dZ}{dt} = -U(N) = -\frac{\Delta P_m}{\mu R_m} = -\frac{P_F(N)}{\mu R_m} = \frac{P_T - \Delta P_w - P_S(N)}{\mu R_m} \qquad (64)$$

where P_T remains set at P_{max}. ΔP_w in Eq (64) is the decrease in $(P_S + P_F)$ due to friction between the cell wall and the cake, and is given by

$$\Delta P_w = \frac{(\Delta w)\,H}{4} \sum_{I=2}^{N} [P_S(I) + P_S(I-1)]\,[V(I) + V(I-1)] \qquad (65)$$

-dZ/dt obtained from Eq (64) are used in Eq (53) when Eqs (48) to (58) are solved to determine how Z, V_a, juice yield and cake properties change as hold time, t_p, increases at constant P_T. The same approach can be used when pressing at constant P_T is used without prior constant-rate pressing.

The situation is more complicated when cakes are maintained at constant volume by stopping the ram when P_T reaches P_{max}. Setting dZ/dt at zero in Eq (53) automatically provides zero volume change, but use of dZ/dt = 0 in Eq (64), which should still be valid, causes $P_F(N)$ to instantaneously fall to zero, which does not occur experimentally. The -dZ/dt used in Eq (53) should still be obtainable from Eq (64) after allowing for decreases of P_T caused by outflow; Use of Eq (64) in Eq (53) would cause the cake volume to shrink, which does not occur because cake volume is held constant. This contradiction can be resolved if decreases in P_S and P_F caused by outflow and relaxation cause local expansions that counterbalance any volume reduction due to outflow. Solids and liquids in cakes are not truly incompressible. For example, when P_F decreases by 8 MPa, the specific volume of water will increase roughly 0.3%. Similarly, when P_F decreases by 8 MPa the volume of cellulosic solids surrounded by fluid will increase by roughly 1%. Much more substantial expansion will occur if air or other gases are trapped in a cake.

A method for roughly accounting for such expansion might be to add a volume expansion contribution, $(\partial V/\partial t)_{exp}$, to $(\partial V/\partial t)_j$ computed by solving Eqs (48) to (58) and (64). $(\partial V/\partial t)_{exp}$ is the rate of volume change that occurs because of the intrinsic compressibility of the materials involved, as opposed to volume changes caused by local U gradients. If we assume that $(\partial V/\partial t)_{exp}$ is the same at all I, it will counteract any volume contraction due to outflow if

$$\left(\frac{\partial V}{\partial t}\right)_{exp} = \frac{U(N)}{W} \qquad (66)$$

where U(N) is obtained from Eq (64). Eq (66) must be used in conjunction with other equations that determine how P_S and P_F change when the fluid and solids in the cake expand. For V changes of equal magnitude, P_S drops very much

more rapidly during expansion than it rises in compaction; i.e. $-dP_S/dV$ for expansion is much greater than for compaction. Much less is known about $P_S(V)$ for expansion than $P_S(V)$ for compaction. $-dP_F/dV$ probably is the same for expansion and compaction. Drops in $P_F(N)$ caused by outflow will cause U(N) to decrease. Therefore ΔP_m, as experimentally observed, should decrease gradually rather than precipitously dropping to zero as soon as the ram stops.

Other factors influence P_S after a ram stops. Cell walls and other barriers that limit fluid escape rates in particles distend during pressing. This causes fluid compaction inside particles, thereby giving rise to excess internal fluid pressure, P_E, a major component of P_S. As fluid escapes from particles, flow barrier distension decreases, causing P_E and P_S to drop. For materials where P_S is large compared to P_F, decreases in P_S and P_E due to relaxation of flow-barrier distension may well be greater than decreases caused by outflow from the system after the ram stops. P_S changes due to relaxation of cell-wall distension have been modeled by using functions $P_S(V,t_r)$, that describe how P_S depends on V and t_r, the relaxation time at constant volume. Different $P_S(V,t_r)$ have been tested in calculations relating to cakes maintained at constant total volume after constant-rate pressing. In most of these calculations, -dZ/dt was set equal to 0 in Eq (53). Computations based on this approach have been used with some success to predict how P_T changes with relaxation time, t_r; but they do not adequately describe how ΔP_m changes as t_r increases.

Uses of Computation: When $P_S(V)$ and $\alpha(V)$ are known functions of V alone, programs based on previously described approaches can be used to determine pressing and relaxation histories, juice yields and juice production rates for various choices of W, P_{max}, -dZ/dt and t_r. η_J, the juice yield based on the amount of available juice initially present, is

$$\eta_J = \frac{V_C - V_{af}}{V_C - V_S} \qquad (67)$$

where V_{af} is the final V_a and V_S is the specific volume of the fixed solids. η_S, the juice yield based on the total amount of feed, is

$$\eta_S = Y_S \cdot \rho_F \cdot (V_C - V_{af}) \quad (68)$$

The juice production rate = $\rho_F \cdot W \cdot A(V_C - V_{af})/(t + t_p + t_u)$, where A is the ram area, t_p is the time the cake is held at constant pressure and t_u is the turnaround time, i.e. the time required to load and unload a press.

Such programs can also be used to evaluate the suitability of alternative functional forms for $P_S(V)$ and $\alpha(V)$ and to determine suitable values of parameters in those functions.

Alternative Numerical Method: Eq (59) was also solved numerically instead of Eq (34). These calculations provided $(P_s/\partial t)_I$ instead of $(\partial V/\partial t)_I$. The $(\partial P_s/\partial t)_I$ were divided by $(dP_s/dV)_I$ to obtain $(\partial V/\partial t)_I$. U(N) calculated from such $(\partial V/\partial t)_I$ by means of Eq (55) agreed with -dZ/dt near the start of pressing, but deviated further and further from -dZ/dt as pressing progressed. Thus computations based on use of Eq (59) instead of Eq (34) or Eq (48) lead to volume-material-balance errors. Stable numerical solutions of Eq (34) or (48) always provided $(\partial V/\partial t)_I$ that produced U(N) that equaled -dZ/dt.

Initial V(I): Eqs (48) to (64) and associated BC can be used immediately when the initial V(I) = $V_o = V_C$. If pressing is immediately preceded by filtration, P_S versus w at the end of filtration often can be determined reasonably accurately from filtration pressure drop equations. Since P_S at the end of filtration = P_S at the start of pressing, $P_S(I)$ can be determined at all I when pressing starts. V(I) at t = 0 can be obtained from $V(P_S)$.

The following method has been used for constant-rate pressing when $V_o > V_C$. V(1) was decreased in a series of small steps, $\Delta V(1)$, i.e. $V(1) = V(1)_{old} - \Delta V(1)$, where, for example $\Delta V(1) = (V_o - V_C)/50$. $P_S(1)$ was obtained from $P_S(V_I)$ at each step. V(1) and $P_S(1)$ were then substituted in a finite-difference form of Eq (31) to obtain $P_S(2)$, which, in turn, was used to obtain V(2) from $V[P_S(2)]$. The process was repeated until V(I) and $P_S(I)$ at all I were obtained for the current value of V(1). Then the V(I) were used in a summation form of Eq (12) to determine V_a. The pressing time, t, = $W(V_o - V_a)/(-dZ/dt)$, and $\Delta t = W[(V_a)_J - (V_a)_{J-1}]/(-dZ/dt)$, where J is the number of V(1) steps taken.

Internal flow starts when V(1) reaches V_C. A different computational procedure was used from that point on. Eq (31) was used to obtain a tentative V(I). Then, a summation form of Eq (13) was used with $w_1 = 0$ and $w_2 = (I - 1)\Delta w$ to evaluate the average V (between I = 0 and the current I). If the average V for the range $\leq V_C$, U(I), the estimated local fluid velocity at I, was calculated from Eq (55), using $\Delta V_I/\Delta t = (\partial V/\partial t)_J$, where $\Delta V_I = (V_I)_J - (V_I)_{J-1}$, and Δt was that calculated for the previous V_a decrease. The tentative V(I) were used to determine $\alpha(I)$. Then Eq (19) was used to find ΔP_F between I and (I -1), i.e. $\Delta P_F(I) = (\Delta w\mu/4)[U(I) + U(I\text{-}1)][\alpha(I) + \alpha(I\text{-}1)]$. $\Sigma(\Delta P_F(n)$ from n = 1 to I was added to the tentative $P_S(I)$ to obtain a revised $P_S(I)$, which was then used to revise V(I). $\alpha(I)$ and U(I) were not revised to obtain better estimated V(I) and $P_S(I)$. When the average V between I = 0 and the current I was greater than V_C, the $P_S(I)$ and V(I) obtained by using Eq (31) and $V[P_S]$ were not revised. After all the V(I) were obtained, they were used to obtain V_a, t and Δt as before. The process was repeated until $V_a = V_C$, after which Eqs (47) through (63) were used to continue the numerical solution.

Extension to Filtration: Though treatment of filtration is beyond the scope of this review, Eq (21) also applies for filter cakes during filtration. Special boundary conditions apply at the moving interface between the cake and slurry, where $w = w_c$ during filtration. If sedimentation does not occur:

$$P_S = 0 \qquad V = V_c \qquad \text{at } w = w^+ \tag{69}$$

and

$$P_S = 0 \quad V = V_c = V(P_S = 0) \qquad \text{at } w = w_c^- \tag{70}$$

where w_c^+ indicates just outside the cake and w_c^- indicates just inside the cake. V_c is the value of V for the feed slurry. U = 0 at w_c^+.

$$U \text{ at } w_c^- = U_c = \frac{1}{\mu\,\alpha\,(V_c)}\,\frac{dP_S}{dw} \tag{71}$$

and

$$-\frac{dw_c}{dt} = \frac{U_c}{V_c - V_o} \qquad (72)$$

Equations like Eq (21) or similar equations based on e or ε and ω have been used to predict changes in e or ε for different types of filtration[111,120-124]. Similar equations in Z-based coordinates have also been used[125,126]. Tiller and Hsyung[127] present a unified scheme for describing filtration, sedimentation and expression.

10. FILTRATION RESISTANCE

$\alpha(V)$ must be known to solve PDE describing expression. α is usually measured using modifications of procedures described by Ruth[128] and Grace[59]. The apparatus used, a compression permeability cell, consists of a hollow, thick-walled cylinder with a bore of diameter D and cross-sectional area A. A perforated, media-covered plate, drain basin and outflow channel are located at the bottom of the bore (see fig. 42). The cylinder is placed on a press stand. A sample of cake containing a measured weight, M_d, of fixed solids is placed in the bore of the cell and saturated with liquid. Alternatively, the bore is filled with a slurry containing weight M of fixed solids. A close-fitting piston fitted with a porous tip and flow channel is inserted into the bore and pushed downward until it rests on the top of the cake. Liquid supplied by a constant head source is fed into the piston, flows out through its porous tip, passes through the cake, and flows out of the cell through the media, perforated plate and outflow channel. "O" rings are used on the piston and other junctions to prevent leakage.

Q, the volume of permeate, is measured versus time, t, until $\Delta Q/\Delta t$ becomes constant.

$$\alpha_a = \frac{\Delta P_F/(U\mu) - R_m}{W} = \frac{h \cdot \rho_F \cdot g \cdot \Delta t \cdot A^2}{M_d \cdot \mu \cdot \Delta Q} - \frac{R_m \cdot A}{M_d} \qquad (73)$$

α_a is the mean α for the cake, h the liquid-head difference driving flow, ρ_F the fluid density and g gravitational acceleration. SI units for α are m/kg, and for R_m

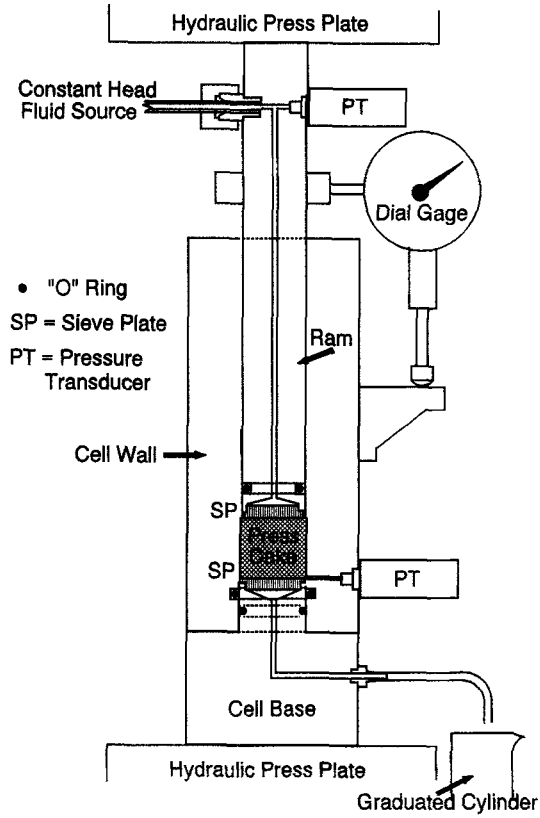

FIGURE 42 Pressing cell for measuring filtration resistance, R_m as well as α

they are 1/m. Relatively small heads are usually used, e.g. 0.5 m of water. Gas pressurization of the liquid feed is used to provide higher ΔP_F when α is very large. In such cases, ΔP_F is in place of $\Delta h \cdot \rho_F \cdot g$ in Eq (73). R_m is often measured by a similar test carried out without a cake.

$$R_m = \frac{\Delta P_F}{\mu U_m} = \frac{h \cdot \rho_F \cdot g \cdot A \cdot \Delta t}{\mu \cdot \Delta Q_m} \qquad (74)$$

where U_m is the flow rate without cake present and Q_m the corresponding volume of permeate. However, because of cake-media interactions it is

preferable to determine R_m by directly measuring ΔP_m using as pressure transducer, as shown in fig. 42.

The cake is slowly compressed, usually at speeds < 5 mm/min, then allowed to equilibrate either at constant P_T or constant cake height, Z. Z is accurately measured by using a dial gauge or other means to permit accurate determination of V, ε and e. Liquid from the constant head source is again passed through the cake until $\Delta Q/\Delta t$ becomes constant. α_a for the new equilibrium condition is again calculated by applying Eq (73). It is assumed that $P_T = P_S$ and that α_a is the same as the true α at P_S or at $V = Z \cdot A/M_d$ if small cake thicknesses are used. $Z/D < 0.6$ are recommended[59]; . The process is repeated at a series of successively higher P_S or lower V until the P_S or V range of interest is completely covered. It is usually assumed that R_m is a function of P_S. Therefore it is independently measured over the P_S range covered so as to provide appropriate R_m values for use in Eq (73). Typical R_m for two sheets of filter paper are 1.3×10^9/m to 4×10^9/m at low P_s to 2×10^{10}/m and 6×10^{10}/m at P_S = 200 MPa. Usually, $R_m << \alpha \cdot W$ for non-biological solids.

Filter Cakes: α is usually correlated versus P_S for use in filtration calculations. Typical α versus P_S variation patterns are shown in fig. 43. Grace[59] noted that frequently

$$\ln\left[\frac{\alpha}{\alpha_{ref}}\right] = C_\alpha(\varepsilon_{ref} - \varepsilon) \qquad (75)$$

where C_α is constant over much of the compaction range. α_{ref} and ε_{ref} are respective reference values of α and ε. Examples of such behavior are shown in fig. 44.

Another frequently used correlation[68] is

$$\alpha = \alpha_o\left[1 + \frac{P_S}{P_{ref}}\right]^n \qquad (76)$$

Leu[69] suggested that n is approximately 0.2 for slightly compressible cakes, 0.6 for moderately compressible cakes and 1.2 for highly compressible cakes;

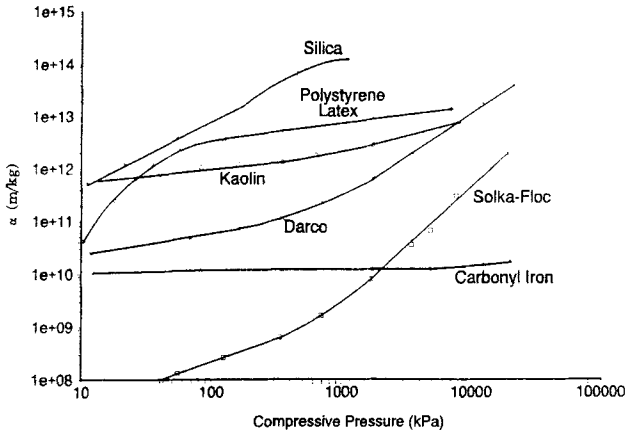

FIGURE 43 α versus P_S behavior for several filter cakes (Grace[59]. Reproduced with permission of the American Institute of Chemical Engineers. Copyright © 1953)

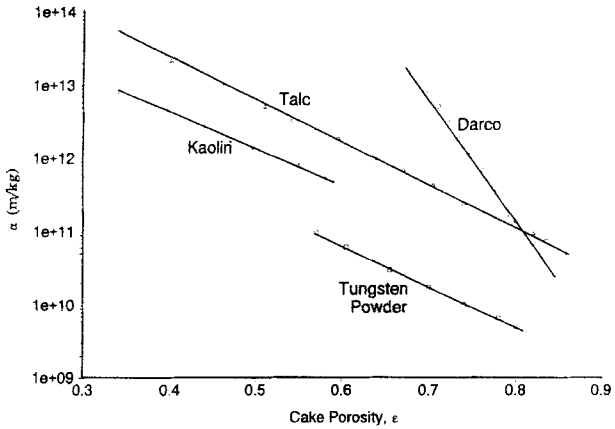

FIGURE 44 Straight log(α) versus ε plots obtained for certain filter cakes (Grace[59]. Reproduced with permission of the American Institute of Chemical Engineers. Copyright © 1953)

but Sorenson and Hansen[112] showed that for waste treatment sludges, n is likely to be 5 or greater. The following correlation[129] is also frequently used

$$\alpha = \alpha_{ref} P_s^n \quad (77)$$

The n in Eq (77) is different from that used in Eq (76).

Factors Affecting α: Theories dealing with effects of cake or bed structure on k and α are reviewed by Scheidegger[130]. The Kozeny-Carman equation[131] and other equations[132] used to predict flow pressure drop in fine porous media indicate that α is proportional to $(1 - \varepsilon)\xi^2/\varepsilon^3$ at flow rates usually encountered in filter cakes and presscakes. ξ is the external particle-surface area per unit of particle volume. The Kozeny-Carman equation usually works well for closely-packed, nearly spherical particles with normal size distributions[133]; but deviations occur for particle mixtures with bimodal size distributions. ξ is inversely proportional to particle diameter, d_p, for similarly shaped particles. Therefore α is often proportional to $(1 - \varepsilon)/(\varepsilon^3 \cdot d_p^2)$. For particles with closed pores, ε' should be used instead of ε in these expressions. Other models, e.g. the Happel unit-cell model[134,135], have been used to predict how α varies as the solidosity $(1 - \varepsilon)$ or apparent solidosity $(1 - \varepsilon')$ of a bed varies. These relationships provide a basis for predicting how α changes as consolidation proceeds, i.e. as ε or ε' decreases. While the Kozeny-Carman equation often works reasonably well for hard, non-porous, non-flocculated particles; it does not work well for highly porous particles or particles that flocculate, i.e. form cakes containing dense clusters separated by large voids. Because of the open structure of flocs, α is lower than expected. The effective d_p is close to that of the cluster rather than that of the individual particles. Particles smaller than 1 or 2 μm in diameter often form flocs. ε may be as high as 0.9 or greater for beds containing flocs.

Consolidation breaks down the open structure of flocs and causes large reductions in ε and large increases in α; the increases in α are 1.5 to four times greater than predicted for the corresponding ε change by the Kozeny-Carman equation. Apparent deviations from the Kozeny-Carman equation also occur

when particles break into smaller pieces, and for particles where large ξ are caused by the presence of open internal pores. α for beds containing flocs may increase up to 1000 fold when P_S increases from 7 kPa to 7 MPa. When hard non-flocculated particles are subjected to the same increase in P_S, the increase in α is often less than 10 fold. Typical α for filter cakes range from $5x10^9$ to $1x10^{14}$ m/kg; with the higher values occurring at high P_S or low V for particles with d_p in the 0.1 to 0.2 μm range.

k' *i.e.* $(g\rho_F V)/(\alpha\mu)$, *is sometimes used instead of* α *to calculate flow* pressure drops. SI units for k' are m/s. $\alpha \approx 6700/k'$ for most soils when the permeating fluid is water and α and k' are expressed in SI units. k' is usually correlated versus e. For many soils[109] it appears that

$$\ln\left[\frac{k}{k_{ref}}\right] = C_k \cdot (e - e_{ref}) \qquad \textbf{(78)}$$

where k'_{ref} and e_{ref} are the respective values of k' and e at a reference state.

Cellular Biological Solids: Compression permeability techniques have been used to determine α versus V for a limited number of cellular biological solids. Much of the available data[85] is presented in fig. 45. The slightly bowed curves in fig. 45 tend to become linear when $\log(\alpha)$ is plotted versus ε; the sharply bowed curves remain curved. Though the CBS particles involved were all greater than 1-mm in diameter, α almost always approached or exceeded 10^{13} m/kg at high levels of compaction. α often increases more than 1000 fold during compaction; million fold increases sometimes occur. Thus α for CBS are usually much greater than for non-cellular solids of comparable size and much more subject to increase during pressing. This probably occurs because CBS are plastic enough to deform in ways that completely block flow channels. Though ε' for unpressed water-rich cellular solids is often 0.5 or less, ε usually ranges between 0.92 and 0.97, but may be as small as 0.85 for particles with thick cell walls. At the end of pressing, ε for CBS usually range between 0.55 for particles with thick cell walls and 0.85 for particles with thin cell walls.

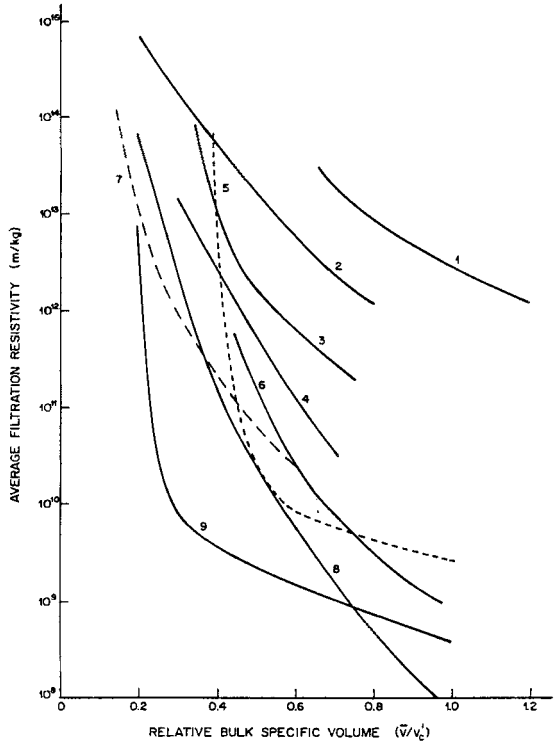

FIGURE 45 α versus V plots for cellular biological materials: 1) spent, drip-grind coffee; 2) Jonathan apples; 3) milled alfalfa; 4) spent sugar beet cossettes; 5) spent -16+30 mesh coffee; 6) spent -4+8 mesh coffee; 7) spent milled alfalfa; 8) shredded sugar cane; 9) Kehura apples (Schwartzberg[85]. Reprinted by permission of Van Nostrand Reinhold, copyright © 1983)

Effects of Media Resistance: Cakes of CBS strongly interact with media. Organelles and other fine matter expelled from cells often plug fine-pored media. Soft particles may wedge into and plug spaces in coarser media. Consequently R_m measured at given P_S without a cake present are often much smaller than R_m at the same P_S when a cake is present. Excessively low values of R_m may have been used in calculating some of the α in fig. 45. These α

consequently may be 10% to 30% too high. If a compression permeability cell that permits measuring ΔP_m, the pressure drop across the media[113,136] (as in fig. 42) is used, both α and R_m, can be determined more accurately, i.e.

$$\alpha = \frac{(\Delta P_F - \Delta P_m) A^2 \Delta t}{\Delta Q \mu M} \quad (79)$$

and

$$R_m = \frac{\Delta P_m A \Delta t}{\Delta Q \mu} \quad (80)$$

Effect of Time: $\Delta Q/\Delta t$ often progressively decreases during permeation tests carried out with cakes of CBS maintained at constant volume. The rate of decrease soon slows down, but decreases often persist for very long times. The decrease has usually been rationalized as an artifact. It has, for example, been attributed to progressive migration of fines or entrapment of migrating fines at the surface of the media. Reported α were usually calculated using $\Delta Q/\Delta t$ obtained after the initial rapid decrease has occurred. However α for CBS may indeed progressively change with time. Why $\Delta Q/\Delta t$ changes with time and whether such changes are due to true changes in α are worth determining.

Gels deform very readily and can reach equilibrium stages of compaction very slowly[137]. Therefore long times may be required before permeation rates through gels equilibrate. For example; it took roughly 1.5 hours for flow through a 2-mm thick slice of polyacrylamide gel to equilibrate. Apparent initial permeation rates can be quite high, but then progressively slow down and ultimately reach an equilibrium value. Thus apparent α increase with time. Gel slice compaction times are proportional Z^2, where Z is the gel slice thickness. Thus permeability and α measurements for gels are often carried out using very thin slices of gel.

Partial Particle Breakdown: Cakes are treated as locally uniform when analyzing expression and flow. This approach may not be valid when mixtures

of large and small particles are pressed or when particles partially break into smaller particles during pressing or when a cake contains two different types of particles, e.g. rind and pith in sugar cane. Effects of partial breakdown of apple particles into mash are discussed later in this review.

Oil Seeds: ε values for oil seeds include space occupied by oil inside particles. Initial ε for oil seeds usually lie between 0.5 and 0.65; final ε are as low as 0.12. Relevant data is only available for cashews[82], which are not frequently used for oil production. It indicates that: $\alpha \approx 6 \times 10^8$ m/kg FS when $\varepsilon = 0.58$ ($V = 1.7 \times 10^{-3}$ m^3/kg FS); $\alpha = 3 \times 10^9$ m/kg FS when $\varepsilon = 0.55$ ($V = 1.59 \times 10^{-3}$ m^3/kg FS) and $\alpha = 7 \times 10^{10}$ m/kg FS when $\varepsilon = 0.51$ ($V = 1.46 \times 10^{-3}$ m^3/kg FS).

Waste-Treatment Sludges: Waste-treatment sludges are complex mixtures of microorganisms formed by biological treatment of waste water, suspended solids found in that water, chemical precipitates formed by reactions with dissolved matter, and coagulants added to improve sludge dewatering[28]. Further information about waste-treatment sludges and sludge properties are provided by Dick and Ball[28] and Vesilind[139]. α_a, average α for such sludges, are usually measured by filtering a sample of sludge in a Buchner funnel while maintaining a $\Delta P_F \approx 50$ kPa by applying vacuum to the filtrate receiver. Q, the volume of filtrate is monitored versus time t; α_a is determined by applying Eq (81)

$$\alpha_a = \frac{2 b \Delta P_F A^2}{\mu C_f} \qquad (81)$$

where A is the funnel area, b is the slope of a plot of t/Q versus Q and C_f is the mass of fixed solids deposited in the cake per unit volume of filtrate. For unconditioned, raw sludges[28,140,141], α_a usually range between 0.4×10^{14} m/kg and 2×10^{14}. Activated sludges with pH between 3 and 8 have α_a between 0.1×10^{14}m/kg and 1.0×10^{14} m/kg, with lower α_a being obtained at low pH. Anaerobically digested sludges have higher α_a, e.g. 3×10^{14} to 1.7×10^{15} m/kg. α_a as high as 1.8×10^{17} m/kg have been observed[65]. Lower α_a are usually, but

not invariably, associated with larger particle sizes. Increased amounts of "supracolloidal" particles in the 1 μm to 100 μm size range usually greatly increases α_a. Relative α_a of raw, activated and anaerobically digested sludge largely depend on the amount of supracolloidal particles they contain: supracolloidal solids may make up 4% to 10% of the solids content of raw sludge, 1% of the solids content of activated sludge, and up to 30% of the solids content of anaerobically digested sludge[141].

Flocculation ("conditioning") of sludges by treatment with aluminum or iron salts, lime and/or polyelectrolytes, decreases supracolloidal particle levels[141], increases sludge mean particle size[140,142] and can decrease α_a almost 1,000 fold[28,129]. α_a as low as 3×10^8 m/kg are sometimes obtained for conditioned sludges. $\alpha_a \leq 4 \times 10^{12}$ m/kg are thought necessary for efficient dewatering[143]. Therefore, conditioning is usually needed. At low flocculant doses, reductions in α_a tend to be proportional to flocculant dosage; at higher flocculant doses, α_a reductions level off and α_a asymptotically approach a lower limit or even increases slightly. α_a reductions are greatest when flocculation is accompanied by a minimum of shearing[129]; high shearing rates or prolonged mixing breaks up flocs and largely counteract α_a reductions initially produced by flocculation. Friedrich et al.[144] claim that filtration rates can be maximized by correctly proportioning amounts of small and large particles in flocculated sludges.

For moderate ΔP_F, e.g. 6 to 60 kPa, α_a for compressed sludges obeys a modified version of Eq (77) in which ΔP_F replaces P_S. For raw sludges, n may range from 0.4 to 0.6; n for anaerobic and activated sludges range between 0.7 and 1.0; for conditioned sludges[129], n is often close to 1.0. If n = 1, dewatering rates do not increase when ΔP_F increases. This occurs because α increases markedly as P_S increases[112]. α_a versus ΔP_F behavior is a very poor indicator of α versus P_S behavior. The permeability, k, of sludges and clays has been correlated[67,145] in terms of e

$$k = \frac{k_{ref}\, e^{n}}{1 + e} \qquad (82)$$

n typically ranging between 3 and 5 for sludges, indicating that k decreases very sharply and α increases very sharply as e and V decreases.

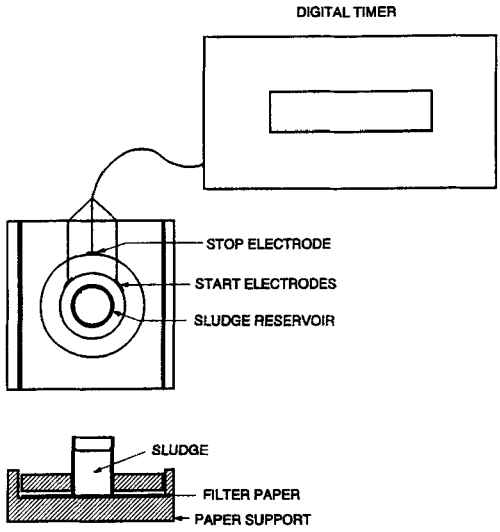

FIGURE 46 Capillary-suction test cell

Capillary-Suction Time: An empirical test, measurement of capillary-suction time (CST), developed by Baskerville and Gale[146] in 1967, is frequently used to evaluate the dewaterability of waste-treatment sludges. In CST test units (see fig. 46), a plastic block with stainless steel well in its middle is placed on top of a piece of filter paper which in turn sits on another plastic block. The upper block contains electrical contacts, 8 mm and 18 mm from the well's edge. A measured sample of sludge is poured into the well; and capillary action of the filter paper draws water from the sludge into the paper. An electrical timer starts when the advancing water reaches the inner electrical contact and stops when the water reaches the outer contact. The elapsed times, t_c is the capillary suction time.

Capillary suction tests are widely used, probably because they can be carried out very quickly; and t_c are widely cited in literature dealing with waste-treatment sludges[37,38,129,140,142,147,148]. While results of CST tests have very little fundamental significance, they are often used to qualitatively determine

how different types and levels of sludge treatment, e.g. polyelectrolyte addition levels, affect dewaterability. Unno at al.[149] and Vesilind[150] have attempted to relate t_c measurements to more fundamental properties such as α; but, at best, have only been partly successful. Vesilind[150] indicates that a parameter, χ, defined below, provides a more fundamental measure of dewaterability than t_c.

$$\chi = \left[(D_o^2 - D_i^2)\left(\frac{\pi d_f}{A Z_c}\right)\right] \cdot \left[\frac{\mu Y_S}{t_c}\right] \qquad (83)$$

D_o and D_i are the respective diameters at the outer and inner electrical contacts, A is the cross sectional area of the well, d_f, the thickness of the filter paper, Z_c is the capillary rise height (usually roughly 100 mm) produced by the filter paper used, Y_S is the weight fraction of fixed solids in the sludge and μ is filtrate viscosity. For specific sludges, $1/\chi$ is clearly proportional to α; but it is not known whether $1/\chi$ values for different sludges can be used to determine relative values of α for those sludges.

Protein Gels: α for casein gels produced from renneted skim-milk gels (i.e. gels like those used to produce cheese) depend on pH, gel solids concentration, temperature and time[151]. $\alpha = 4\times10^{12}$ m/kg FS for a 0.5 hr old, pH 6.68 renneted gel for which $\varepsilon = 0.91$ (V = .008 m^3/kg FS). α for a similar gel formed at pH 5.35 = 8.9×10^{12} m/kg FS. α decreases with time; and the decrease is more rapid at low pH. Thus α for the pH 5.35 gel is 4.7×10^{12} m/kg FS at one hour; whereas for the pH 6.68 gel, $\alpha = 2.3\times10^{12}$ at three hours. α experiences a 3.5-fold decrease when temperature increases from 20°C to 35°C, and a 30-fold increase when ε decreases to 0.84 (V decreases to 0.004 m^3/kg FS). Skim milk gels act somewhat like highly flocculated polystyrene latexes. The solids are flocculated chain-like arrays of roughly spherical casein micelles 0.05 to 0.3 μm in diameter.

α is only moderately large for rennet-treated casein, because the tendency towards high resistance due to low d_p is counterbalanced by a large ε and a high degree of flocculation. As time passes more bonds form between chains, producing denser solid clusters with larger pores between them; consequently α

decreases. Higher temperatures both speed up and increase bond formation. The marked increases in α due to compaction is largely due to breakdown of the open flocculated structure and formation of a structure with more uniform smaller pores. Effects of other factors on α are largely explained by how they affect rates and extents of bond formation and cluster densification. Bond formation leads to gel contraction that causes expulsion of interstitial fluid (whey) when the casein gels are cut into cubes. This contraction leads to higher α as fluid expulsion (i.e. syneresis) proceeds.

Relatively dense compact casein curds are made when direct acidification is used instead of renneting[152]. Such curds form unconsolidated cakes with ε ranging between 0.55 (at 45°C) and 0.62 (at 11°C). α for such cakes $\approx$ 1×10^{10} m/kg, which is roughly 100 times smaller than α for cakes of curds formed by renneting. α for acid casein increase rapidly during consolidation and depending on temperature approaches 4×10^{12} m/kg at ε between 0.32 (at 45°C) and 0.52 (at 11°C). Cakes made of acid casein initially act like a bed of distinct, impermeable particles, which fuse together only at relatively high pressures. Before the particles fuse together, flow occurs in spaces between the particles, where resistance is low. On the other hand, particles of renneted casein fuse together at relatively low pressures, and flow takes place through very fine pores within the particles. Therefore α is very high for only slightly consolidated cakes of renneted casein curds.

Fibrous Beds Gels may be regarded as a three dimensional solid network immersed in liquid, or as liquid trapped in a three dimensional solid network. Solid contents in such network often are quite small, e.g. $(1 - \varepsilon)$ may be as low as 0.01. Many gel solids are fibrous, i.e. their lengths are very much greater than their diameter. Because of this, permeability relationships for fibrous porous media have important implications for gels.

Jackson and James[153] analyzed permeability measurements and correlations for fibrous media with fiber diameters ranging in size from 10 mm (for heat-exchanger tube arrays) to 0.65 nm (for fibers in gels), for cases where slip flow does not occur and $Re_p = d_p \mu U/\rho < 10$, i.e. for fibers where flow is

in the Stokes law range. The data was analyzed in terms of permeability, k, defined by

$$k = \frac{\mu U Z}{\Delta P_F} \qquad (84)$$

where Z is the fiber bed thickness. Note, $\alpha = V/k$. k for such fibers tends to be inversely proportional to a^2, where a is the fiber radius. k/a^2 is dimensionless. Jackson and James examined the experimental and theoretical dependence of k/a^2 on $(1 - \varepsilon)$. They showed that experimental k/a^2 data from a great many studies all fell within a single band when plotted versus $(1 - \varepsilon)$, (see fig. 47). Differences within the band are partly due to differences in: a) fiber orientation and aspect with respect to the direction of flow, b) cross-sectional shape, c) size uniformity, and d) the uniformity of packing.

Jackson and James reviewed unit-cell approaches that have been used to predict k/a^2 as function of $(1 - \varepsilon)$ for uniformly spaced and oriented arrays of fibers[154-156]. For fibers oriented parallel to the direction of flow, most k/a^2 versus $(1 - \varepsilon)$ relationships resemble[157]

$$\frac{k}{a^2} = \frac{1}{4(1-\varepsilon)}\left[-\ln(1-\varepsilon) - A_k + 2(1-\varepsilon) - \frac{(1-\varepsilon)^2}{2}\right] \qquad (85)$$

a form originally developed for circular unit-cells by Langmuir[154] and Happel[155]. A_k depends on the type of unit-cell used. A_k is 1.5 for circular cells, 1.476 for square arrays, 1.498 for equilateral triangular arrays, 1.354 for hexagonal arrays and 1.130 for two-by-one rectangular arrays. An extra term proportional to a higher power of $(1 - \varepsilon)$ has to be used for non-circular unit cells; but its effects are negligible when $(1 - \varepsilon) < 0.3$. For $(1 - \varepsilon) > 0.005$, plots of these functions fall near the high side of the k/a^2 versus $(1 - \varepsilon)$ band shown in fig. 47. For $(1 - \varepsilon) < 0.005$, predicted k/a^2 fall slightly above the data in fig. 47.

Similar equations for k/a^2 have been derived for unit cells containing regular arrays with fibers oriented perpendicular to the flow[155,158-164]. In these equations, the lead coefficient on the right-hand-side is $0.125/(1 - \varepsilon)$ instead of $0.25/(1 - \varepsilon)$, as in Eq (85). Therefore k for fibers lying perpendicular to the

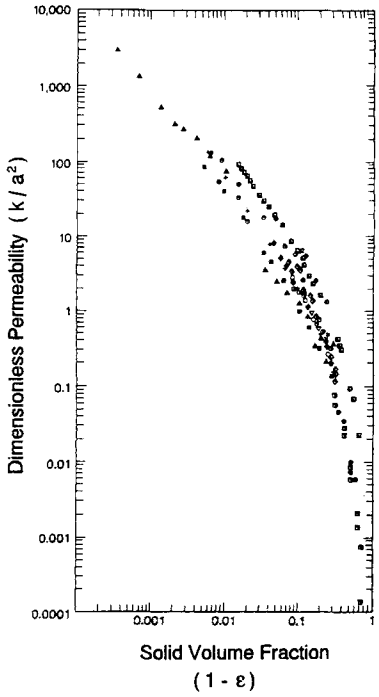

FIGURE 47 Plot of dimensionless permeability, k/a^2, versus $(1 - \varepsilon)$ (Jackson and James[153]

flow are roughly only half as great as for fiber lying parallel to the flow. In many cases, the terms following the lead term for fibers lying perpendicular to the flow are similar to the terms following $1/[4(1 - \varepsilon)]$ in eq (85), e.g.

$$\frac{k}{a^2} = \frac{0.125}{(1-\varepsilon)}\left[-\ln(1-\varepsilon) - A_k + 2(1-\varepsilon) - O(1-\varepsilon)^2\right] \qquad \textbf{(86)}$$

where $O(1 - \varepsilon)^2$ is a term whose magnitude is close to $(1 - \varepsilon)^2$. In most cases, $A_k \approx 1.48$ for perpendicular fibers. Plots of k/a^2 versus $(1 - \varepsilon)$ based on Eq (86) fall in the mid- to low-mid range of the k/a^2 versus $(1 - \varepsilon)$ data band in fig 47 when $(1 - \varepsilon) > 0.001$. For $(1 - \varepsilon) < 0.001$, the experimental data fall

slightly above the Eq (86) plot. Effects of fiber cross-sectional shape and packing non-uniformity are also reviewed by Jackson and James[153], whose article should be consulted for further details. Spacing inhomogeneity may increase k by as much as 50%. Jackson and James propose the following equation for three-dimensional cubical lattices

$$\frac{k}{a^2} = \frac{0.15}{1-\varepsilon}[-\ln(1-\varepsilon) - 0.931 + O\{\ln(1-\varepsilon)^{-1}\}] \quad \textbf{(87)}$$

where $O\{\ln(1 - \varepsilon)^{-1}\}$ is a term whose magnitude is close to $\ln[1/(1 - \varepsilon)]$. Eq (87) predicts k/a^2 that fall in the mid range of experimental values.

For gels, a is very small, e.g. close to 1 nm. Therefore k for gels are very small, even though ε is often > 0.9. Table IV lists available k and $(1 - \varepsilon)$ range data for different types of gels. The smallest k are for the largest $(1 - \varepsilon)$. For the listed gels, $V \approx 0.00071/(1 - \varepsilon)$ and $\alpha = V/k \approx 0.00071/[k \cdot (1 - \varepsilon)]$. α ranges calculated on this basis are also listed in Table IV.

k measurements for gels do not appears to be very reproducible; reported k for the same class of gel differ by as much as a factor of 20. α for gels varies significantly less than k varies when $(1 - \varepsilon)$ changes. α for gels are sometimes as much as 10^7 as large as typical α for filter cakes; the most permeable gels have α near the upper end of the high α range for filter cakes. Thus when dealing with cakes made up of gel particles, flow resistances within particles will greatly exceed flow resistances in spaces between particles.

α versus $(1 - \varepsilon)$ relationships that differ from Eq (87) have been reported. White[161] found that log(k) decreased linearly as $(1 - \varepsilon)$ increased; Tokita and Tanaka[137] found k was proportional to $(1 - \varepsilon)^{-1.5}$; and Johnson and Dean[164] found that k was proportional to $(1 - \varepsilon)^{-2.45}$.

Effects of pH: The filterability of proteins and other materials with surfaces charges can be strongly affected by pH and electrokinetic effects. Apparent filtration resistances for proteins passing through beds of filter-aid tends to be greatest at their isoelectric point, where their solubility tends to be smallest and their viscosity greatest. In some cases marked decreases in α occur in certain

Table IV - Permeability, α and Solidosity Ranges for Gels

Gel Type	k range (nm^2)	(1 - e) range	α range (10^{15} m/kg)
Polyacrylamide[153]	0.021 - 0.38	0.035 - 0.245	53 - 138
Polyacrylamide[161]	0.42 - 6.7	0.021 - 0.157	5 - 11
Poly-Hyaluronic Acid[153]	18 - 720	0.00035 - 0.014	2.8
Collagen[153,163]	2.1 - 75.9	0.0875 - 0.27	0.11 - 1.25
Collagen[153,162,163]	2.8 - 6.1	0.107 - 0.235	1.1 - 1.7
Agarose[164]	18 - 350	0.019 - 0.072	0.11 - 0.55
Casein[151]	37 - 1,800	0.09 - 0.16	0.01 - 0.12

pH ranges above the isoelectric point; e.g. relative values of α for chloroplastic alfalfa protein filtered through diatomaceous earth[165] were 1 at pH 6, 0.06 at pH 8 and 0.39 at pH 10. Different pH effects are observed with clays[166] where the apparent α for bentonite increases roughly eight-fold as pH increases from 3.8 to 7.5. Such changes in pH are usually associated with changes in the zeta potential of retained particles[166]. It is difficult to tell whether apparent changes are due to true changes in α or are caused by electrokinetic effects that alter driving force for flow through cakes. Amounts of supracolloidal particle in activated, waste-treatment sludge increase as pH increases. Consequently α increases. Increases in supracolloidal particle contents and α are particularly large at pH 11. This may be due to lysing of cells at that pH.

11. EXPERIMENTAL RESULTS: CONSTANT-PRESSURE TESTS

Soils: Constant-pressure consolidation tests for soils are often carried out in cells where a sample is placed in a snugly fitting metal ring of standard diameter (108 mm) and height (31.8 mm) and placed on a hard, porous base[86]. The sample is trimmed to level its top with the top of the ring and covered with

a hard, porous disc. A flat piston is placed on top of the porous cover disc and wrapped with a rubber jacket that seals the space between the piston and ring. Then, a weight or a fast-acting pneumatic or hydraulic ram capable of generating desired pressure, P_T, is caused to act on the piston. The pressure causes the piston to move down, consolidating the sample, forcing water out through the porous cover and base. Piston displacement, ΔZ, or sample height, Z, measured with the aid of a dial gauge, is recorded versus time, t.

Consolidation: If: a) Eq (23) or (24) apply, b) P_T and C are constant and c) V is initially uniform, Eq (29) should describe sample height behavior during the early stages of consolidation; and $\zeta \equiv (Z_o - Z)/(Z_o - Z_\infty)$ should increase linearly as $t^{1/2}$ increases for $\zeta < 0.62$. Consequently, $(Z_o - Z)$ or ζ are often plotted versus $t^{1/2}$ when pressing test results are depicted. ζ scales are usually arranged with 0 at their top and 1.0 at their bottom. Departures from linearity frequently occur at both low and high ζ. Departures from linearity at low ζ are attributed to expulsion of entrapped air.

Plastic Creep: Departures from non-linearity at high ζ may be caused by "plastic" creep[86], extra-slow "secondary" consolidation which occurs because of: a) plastic deformation of particles, b) friction between particles, c) expulsion of fluid from particles or d) combinations of these effects. One method for characterizing creep is shown in fig. 48, where $(Z_o - Z)$ is plotted versus log(t). For $t > 100$ min, $(Z_o - Z)$ increases linearly, but slowly, as log(t) increases. In such cases, changes in e due to creep $= C_S \cdot \ln(t/t_s)$, where C_S is the creep coefficient and t_s is the time at which creep starts; and ΔV, ΔZ and changes in $(1 - \zeta)$ during creep are also be proportional to $\ln(t/t_s)$, i.e.

$$1 - \zeta = \sum_{j=1}^{\infty} \frac{8}{\pi^2 (2j-1)^2} \exp\left[\frac{(2j-1)^2 \pi^2 \tau}{4}\right] - \frac{C_S \ln(t/t_s)}{Z_o - Z_\infty} \quad \textbf{(88)}$$

Z_∞ and t_s on plots of $(Z_o - Z)$ versus log t are located at the intersection of extensions of straight line sections on the creep curve and the normal

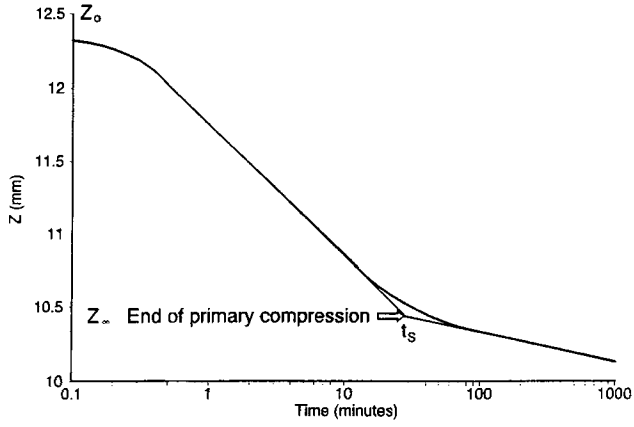

FIGURE 48 Method of using Z versus log t plot to determine where secondary creep starts (Taylor[86])

consolidation curve, i.e. at point A in fig. 48. $\tau = Ct/W^2$ or $C_e t/\Omega^2$. W is the mass of fixed solids per unit area of outflow surface. Therefore, when two outflow surfaces are used, W is half the mass of fixed solids per unit of cross-sectional area.

For soils C_S appears to depend on C_C[109]. Creep rates are high for highly organic soils and peats. Wilder[83] noted that V for paper pulp decreases linearly as $\ln(t_p)$ increases.

Changes in e or V for the Kelvin-Voigt element in fig. 35a are often used to model creep[167,168]. Eq (89), based on such a model, is used frequently in analyzing constant-pressure expression test results. It applies when V is initially uniform and less than V_C when expression starts

$$1-\zeta = (1-f)\left[\sum_{j=1}^{\infty} \frac{8\exp[-(2j-1)^2\pi^2\tau/4]}{\pi^2(2j-1)^2}\right] + f\exp(-\Lambda t) \quad \textbf{(89)}$$

f is the fraction of $(Z_o - Z_\infty)$ attributable to creep and Λ is the creep rate coefficient. Eqs (88) and (89) are not compatible. Since Eq (88) causes $(1 - \zeta)$ to become smaller than zero at very large t, it cannot be correct at such t.

Exp[-Λt] is also used to correct for creep in Eq (90), which is used when expression occurs immediately after constant pressure filtration[22].

$$\zeta = (1 - f)\left[1 - \exp\left(-\frac{\pi^2 \tau}{4}\right)\right] + f\,[1 - \exp(-\Lambda t) \quad \textbf{(90)}$$

Eqs (89) and (90) theoretically apply only when $\Lambda << \pi^2 C/4W^2$. More complex equations[53] are used when this condition is not satisfied. Shirato and coworkers[172-177] and Rebouillat[178,179] have used Eqs (89) and (90) to describe Z versus t behavior for constant-pressure expression tests for clays and other non-biological materials. For one clay, Shirato found that f initially decreased as P_T increased and then asymptotically approached a constant value at $P_T >$ 0.6 Mpa[182].

Shirato and coworkers[22,53,116,118,119,172-177,180-182] carried out many constant-pressure tests with non-biological materials: clays, diatomaceous earths, sands, glass beads, and precipitated $CaSO_4$. Rebouillat[178,179] later carried out similar tests with digested municipal-waste-treatment sludge, sugar beet pulp, ground alfalfa and ground black currants in addition to tests with kaolin. Cells similar to the one shown in fig. 49 were used, but the rams were mechanically rather than pneumatically driven. Shirato's group used a hollow ram with a porous tip, so outflow occurred in two directions.

Rebouillat used a 85-mm diameter 225-mm high cell fitted with a solid ram, so outflow occurred in one direction. Millipore membranes with 4 μm pores were used as media. Their flow resistance, R_m, was less than 0.01% of $\alpha_a \cdot W$, the flow resistance of the loads tested. His results can be used to compare pressing properties of cellular biological solids with those of non-biological solids. His data for aqueous slurries containing 20% kaolin by weight illustrate typical pressing characteristics of very fine non-biological solids. Methods developed by Shirato and co-workers[22,53] were used to analyze this data. $(1 - \varepsilon) = 0.088$ initially, so the feed slurry was fairly fluid.

Filtration: When highly fluid slurries are pressed, a filter cake forms and grows in thickness, as shown in fig. 50. Expression starts when the ram reached the surface of the cake, i.e. when cake fills the whole chamber. α_a for filter cakes

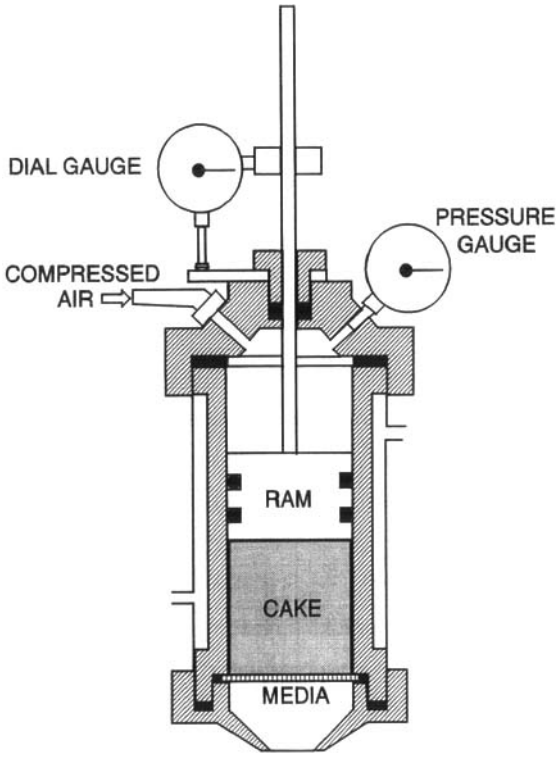

FIGURE 49 Test cell for carrying out expression at constant pressure[114]

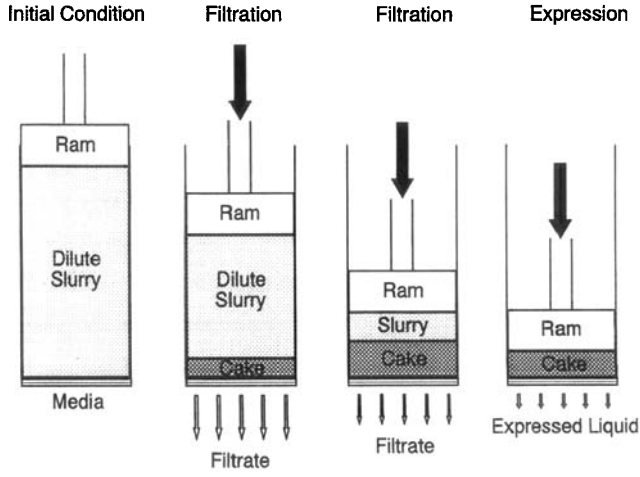

FIGURE 50 Pressing sequence for slurry showing ram-induced filtration followed by consolidation

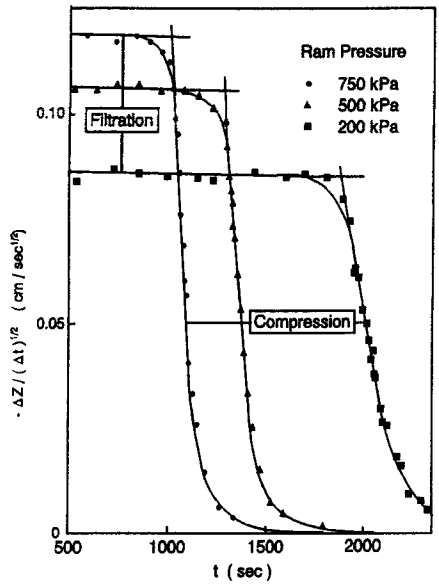

FIGURE 51 Plots of $\Delta Z/t^{1/2}$ versus t for pressing of slurries containing 20% kaolin at three constant pressures. $\Delta Z/t^{1/2}$ remains constant while constant-pressure filtration is occurring and then decreases rapidly once expression starts. (Rebouillat[178])

usually remains constant during constant-pressure filtration[183]. If so, $-dZ/d(t + t_m)^{1/2}$ also remains as t changes constant during filtration. t_m is a time correction that compensates for media resistance[22]. But, as Shirato et al.[22,53] showed and fig. 51 illustrates, sharp changes in slopes of $-\Delta Z/\Delta(t^{1/2})$ versus t plots occur when filtration ends and expression starts, particularly when $t_m << t$. Fig. 51 is for pressing of 20% kaolin slurries containing roughly 72 grams of kaolin; most of the Z change occurred during filtration; only 7% occurred during expression. Plots of $-\Delta Z/(t^{1/2})$ versus t for dilute biological solids exhibit similar sharp changes in slope when filtration ends; but when semi-solid slurries are pressed breaks in slope are much less sharp[22].

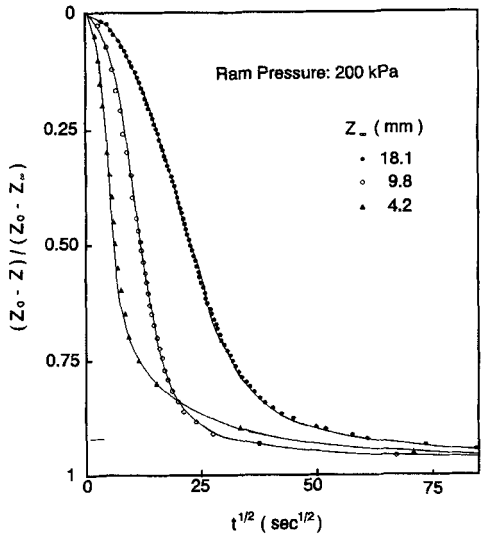

FIGURE 52 ζ versus $t^{1/2}$ for three different loads of kaolin while subjected to consolidation at a constant pressure of 200 kPa after filtration at the same pressure (Rebouillat[178])

Expression After Filtration: ζ is plotted versus $t^{1/2}$ in fig. 52 for expression from three kaolin cakes formed by filtration. t is measured from the end of filtration; Z_o is the cake height at the end of filtration. P_T = 0.2 Mpa in all cases, but different solids loads were used: 21.2 kg/m^2, 12.7 kg/m^2, and 5.0 kg/m^2. Compaction during expression was slight; $Z_\infty/Z_o \approx 0.81$.

Eq (29) indicates that if e is initially uniform ζ should initially increase linearly as $t^{1/2}$ increases. The plots in fig. 52 are curved instead of linear at small $t^{1/2}$ because e is not uniform in compressible filter cakes. Eq (30) often applies when prior filtration is used. It fits the data in fig. 52 quite well at $\zeta <$ 0.5; but deviates at larger ζ. Part of the deviation is due to creep. Eq (90) provided good agreement between experimental and predicted results over the entire ζ range when best fit values of C, f and Λ were used; but f differed for each load weight. Fig. 53 shows how f and C can be determined[178,179].

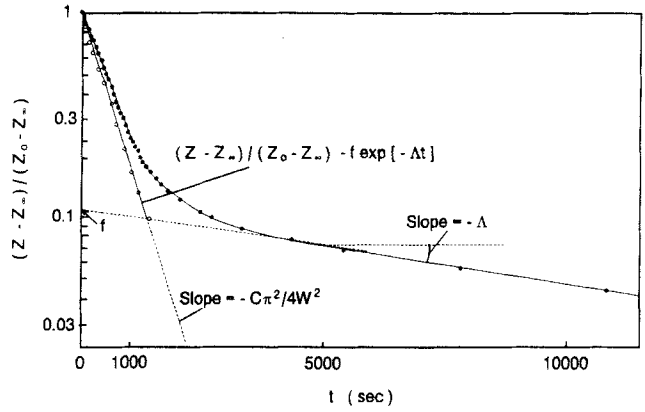

FIGURE 53 Method for determining of C and f for a case where primary consolidation is followed by secondary consolidation, e.g. for kaolin consolidated at a constant pressure of 200 kPa (Rebouillat[178])

Determining C: When C is constant, $C = \text{slope}^2 \cdot \pi W^2/4$ for ζ versus $t^{1/2}$ plots that are linear. Eq (90) is used to determine C when prior filtration is used and creep occurs. Calculated C sometimes have been based on t/W^2 at a single point, such as t_{90}, the time at which $\zeta - (1 - f) \cdot \exp[-\Lambda t] = 0.90$[178,179]. In such cases[177], the calculated $C = 0.848 \cdot W^2/t_{90}$, or $C_e = 0.933\Omega^2/t_{90}$. C_e obtained this way may not agree with its defined value, $-(dP_S/de)/(\mu\alpha\rho_S)$. In one case, Rebouillat's data for kaolin show that $-(dP_S/de)/(\mu\alpha\rho_S) = 4.1 \times 10^{-7}$ m^2/s, and that $0.848\Omega^2/t_{90} = 2.8 \times 10^{-8}$ m^2/s.

Effect of Flocculants: Use of flocculants causes the fraction of Z change due to expression to increase and linear range of Z versus $t^{1/2}$ plots for consolidation to increase.

Penetration-Type Behavior: ζ will be proportional to $t^{1/2}/W$ initially even when C varies, if: a) V is initially uniform; b) R_m is negligible; c) C is a function of V alone; d) t and w can be converted into a single variable $(W - w)/t^{1/2}$ by means of a Boltzman transformation; and e) significant changes in V do not occur at

the ram or neutral surface. In such cases, V will be a function of $t^{1/2}/(W - w)$ and changes in V will be confined to a "penetration" zone whose depth is proportional to $t^{1/2}$, i.e $-\Delta Z/t^{1/2}$ will remain constant. The Boltzman transformation can no longer be used after the penetration zone's leading edge reaches the ram surface or neutral plane. When this occurs $-\Delta Z/t^{1/2}$ decreases instead of remaining constant.

If C varies, $\zeta/t^{1/2}$ and $-\Delta Z/t^{1/2}$ usually will remain constant for longer or shorter periods than when C is constant. Thus, unusually long linear regions in the ζ versus $t^{1/2}$ plot for flocculated kaolin may be due to variation in C. In analogous situations in heat transfer[184] and mass transfer[185], the mass or heat lost or gained is proportional to $t^{1/2}$ even though mass or thermal diffusivity changes with concentration or temperature. Methods used in analogous mass-transfer cases[185] can be used to predict effective C for use in Eq (29) when C varies as local e and V change.

Since ζ is usually linearly proportional to $t^{1/2}$ during constant-pressure filtration, such filtration can be analyzed using a penetration approach; and Smiles[120], Smiles and Kirby[121], Wu[122] and Haight[186] have done so by using appropriate Boltzman transformations. For filtration, $-\Delta Z/t^{1/2}$ drops very sharply at the end of the penetration period; $-\Delta Z/t^{1/2}$ drops more gradually at the end of penetration periods in expression.

Porosity Profiles: Electrical resistance[187-189], X ray attenuation[190,191], nuclear magnetic resonance[124,192], mechanical sectioning[122,192], and the movement of colored bands of cake[193] have been used to measure profiles of solids concentration (Y), ε or e versus distance in cakes during constant-pressure filtration and subsequent constant-pressure expression. These techniques can be used to determine Y, ε, e or V profiles for different types of expression.

When appropriate cake property data is available and $R_m = 0$, profiles of ε, e or V versus distance from the outflow surface, (Z - z), can be computed at a series of t by numerically solving PDE describing constant-pressure filtration and expression. Fig. 54 shows how ε versus (Z - z) profiles theoretically should change as t increases. t increases in going from the top profile to the bottom profile. In regions where expression occurs, the maximum values of ε

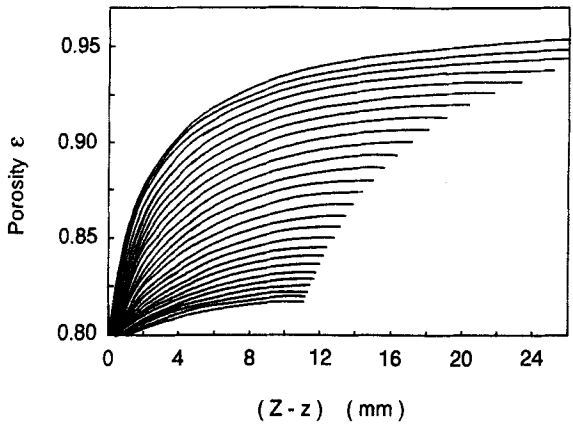

FIGURE 54 Theoretically-based ε versus (Z - z) profiles at times 320 s apart during constant-pressure filtration and expression (La Heij at al.[124]. Reproduced with permission of the American Institute of Chemical Engineers. Copyright © 1996)

and (Z - z) decrease and profiles progressively flatten as t increases. During filtration, ε is theoretically a function of $w/t^{1/2}$. Further, $w_c/t^{1/2}$ and $Z/t^{1/2}$ theoretically remain constant. w_c is the mass of fixed solids deposited per unit area and Z is the cake thickness. In some experimental profiles, e.g. those obtained for clays by Horsfield et al.[192] and by Bierck at al.[190], ε was a smooth function of $w/t^{1/2}$ at most t and essentially behaved as theoretically predicted. Deviations occurred at very small t, because R_m was not truly negligible then. Profiles obtained with different experimental methods differed slightly, e.g. ε calculated from NMR measurement were slightly lower than ε obtained by mechanical sectioning[192].

The NMR-based ε profiles of La Heij et al[124] (for flocculated waste-treatment sludge pressed at 100 Kpa) deviated significantly from predicted behavior. Fig. 55 shows their ε versus z profiles for a series of times, 160 s apart. The bottom profile is for the largest t. The curves resemble those in fig. 54, but, because of media resistance, ε at the outflow decreased fairly slowly rather than immediately falling to its equilibrium value. More importantly, ε at

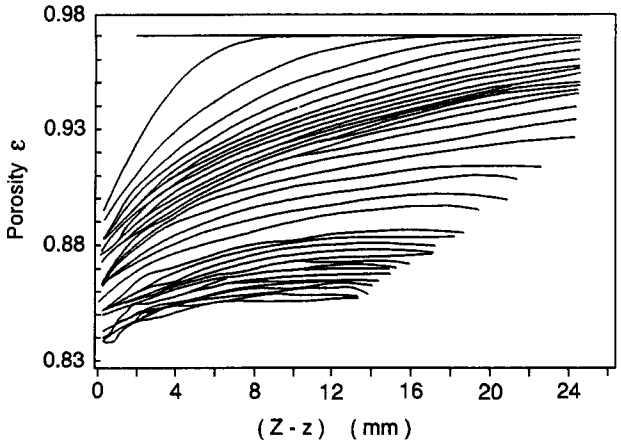

FIGURE 55 ε versus z profiles for flocculated waste-treatment sludge pressed at 100 kPa and measured by La Heij et al.[124] at a sequence of times, 160 s apart. Reproduced with permission of the American Institute of Chemical Engineers. Copyright © 1996.

fixed z decreased irregularly as time increased (see fig. 56). ε at the outflow surface also decreased irregularly. This may have been caused by intermittent extrusion of cake through the media. Such extrusion may also have caused the irregular ε versus t behavior observed higher in the cake. Extrusion has often been observed during expression tests with soft materials. The applied pressure affected profiles mainly through its effect on ε_∞, the equilibrium ε. At 100 Kpa, ε_∞ was 0.834; at 50 Kpa, ε_∞ was 0.841.

Particles segregate according to size and density, and abnormal porosity profiles develop if sedimentation accompanies filtration[126]. Sedimentation's relative importance increases as filter cakes thicken and flow rates through cakes decrease. Particle segregation and abnormal porosity profiles caused by sedimentation will affect subsequent expression.

Empirical Equations; Shirato[194] proposed that Eq (91), a modification of an equation developed by Sivaram and Swamee[195], could be used to empirically

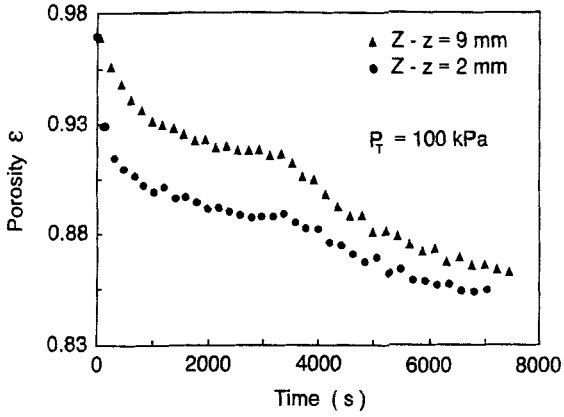

FIGURE 56 Plots of ε versus t at fixed z for waste-treatment sludge flocculated by addition of iron chloride and lime and pressed at 100 kPa. (La Heij et al.[124]. Reproduced with permission of the American Institute of Chemical Engineers. Copyright © 1996)

deal with plastic creep and deviations from Eq (29) at large t.

$$\frac{Z_o - Z}{Z_o - Z_\infty} = \left\{ \frac{4Ct/\pi W^2}{[1 + (4Ct/\pi W^2)^{\upsilon}]^{1/\upsilon}} \right\}^{1/2} \qquad (91)$$

Eq (91) approaches Eq (29) as $\tau^{1/2}$ approaches 0. Therefore it predicts penetration-type behavior at the start of the pressing. Plots of ζ versus $\tau^{1/2}$ obtained from Eq (91) for various values of υ are shown in fig. 57. To provide good agreement between Eq (91) and Eq (28) at both small and large τ, Sivaram and Swamee use 2.8 for υ. An empirical constant, K_e, is sometimes used in Eq (91) in place of $4C/\pi$. Rebouillat[178,179] used K_e-based versions on Eq (91) to fit ζ versus τ data for constant-pressure expression of cellular biological solids; in other cases, better fits were obtained by use of Eq (92).

$$\zeta = 1 - \exp[-\beta t^{\gamma}] \qquad (92)$$

Eqs (91) and (92) provide compact ways of describing ζ versus τ behavior, but have little physical significance. C and υ and β and γ are empirical constants

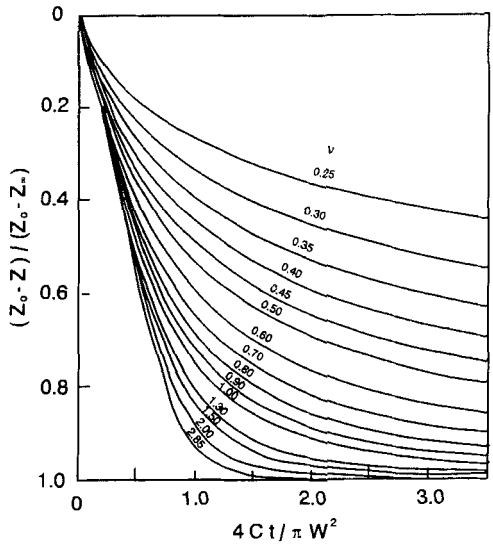

FIGURE 57 Shirato's modification[22] of the constant-pressure ζ versus $t^{1/2}$ plot of Sivaram and Swamee[195]. Reprinted from *Filtration, Principles and Practices*, p. 365 by courtesy of Marcel Dekker, Inc.

whose values are obtained by best-fit procedures for particular cases. Consequently such values have limited utility.

Biological Materials: $-\Delta Z/\Delta(t^{1/2})$ versus t behavior similar to that shown in fig. 51 has been observed for highly flocculated soy protein curds[196], but the change from constant to decreasing $-\Delta Z/\Delta(t^{1/2})$ occurred gradually. This gradual change was attributed to the end of filtration[197]; but some other type of penetration behavior may have occurred. The combination of "filtration" and expression, was well correlated by use of Eq (92)[188].

Fig. 58 shows ζ versus $t^{1/2}$ curves for 3.0 kg FS/m^2, 4.5 kg FS/m^2 and 5.66 kg FS/m^2 of sugar beet pulp pressed at 0.8 Mpa. Penetration-type behavior occurred at small t, but at larger t, ζ data could not be fitted by Eqs (88), (89) and (90). This and other ζ data for sugar beet pulp were well fitted by Eq (91) with υ between 0.65 and 0.75 and by Eq (92) with γ between 0.36

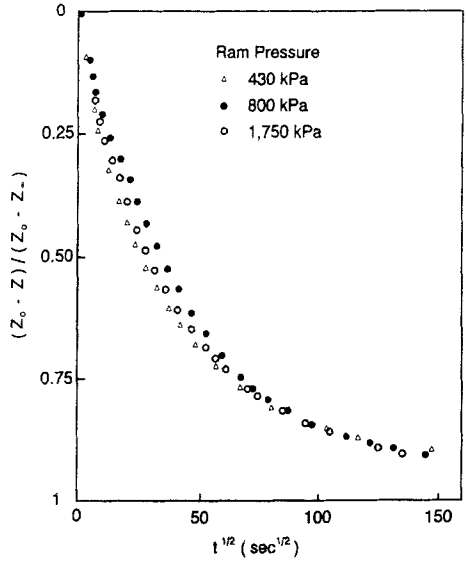

FIGURE 58 ζ versus $t^{1/2}$ plot for pressing of sugar beet pulps at three different constant pressures (Rebouillat[178])

and 0.45. Rebouillat[178,179] provides correlations for these parameters.

$Z_\infty/Z_o \approx 0.19$ for beet pulp from one factory, 0.11 for pulp from another, and was greater for old pulp than for fresh pulp. Addition of $CaSO_4$, which causes cross-linking of pectin, promoted faster pressing.

ζ versus $t^{1/2}$ curves similar to those obtained for sugar beets were obtained for drained, digested waste-treatment sludge[178,179], peat and apple pulp[114] pressed at a constant P_T. Eq (91) fitted the sludge data, with υ ranging between 0.6 and 0.7. Initial slopes in ζ versus $t^{1/2}$ curves for sludge were inversely proportional to W or Ω. Z_∞/Z_o decreased when higher P_T were used.

When unsaturated cakes were used, e.g. ground alfalfa, rapid initial compression occurred due to expulsion of air; then primary expression followed by creep occurred. ζ versus $t^{1/2}$ data for alfalfa for the latter two periods were fitted moderately well by use of Eq (92) with γ between 0.19 and 0.24 and $Z_\infty/Z_o = 0.386$.

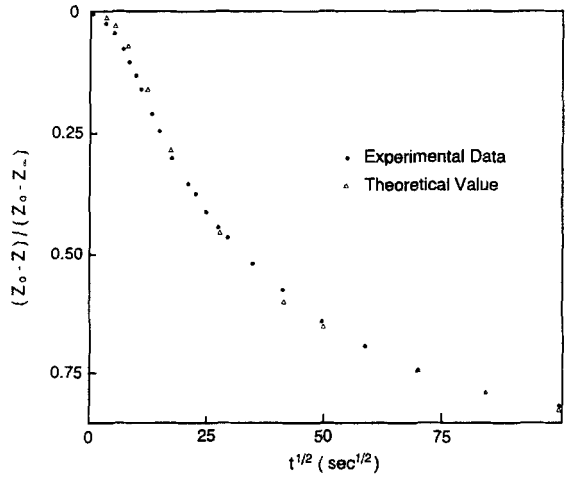

FIGURE 59 ζ versus $t^{1/2}$ data for pressing of ground black currants at a constant pressure of 1,000 kPa (Rebouillat[178])

Filtration occurred initially in pressing tests carried out with ground black currants[178,179]; but the filtration period was relatively short. Fig. 59 shows ζ versus $t^{1/2}$ for the expression period. Eq (90) fitted the data fairly well, but f was much larger than for non-biological materials.

Buttersack's Approach: Buttersack[197] assumed that pressed cakes of sugar beet strips contain a compacted zone adjacent to the outflow media and that the rest of the cake is not compacted. During pressing, the compacted zone becomes thicker, as with filter cakes, and the uncompacted zone becomes thinner. Buttersack assumed that P_S is proportional to $P_T \cdot (V_o - V)$ in the compacted zone and that R_T (R_m plus the cake flow resistance) is given by

$$R_T = R_m + r \cdot \ln\left[\frac{V_\infty - V_o}{V_\infty - V}\right] \qquad (93)$$

Eq (93) causes R_T to become infinite when $V = V_\infty$, which is unrealistic. Buttersack derived an equation covering both filtration and expression.

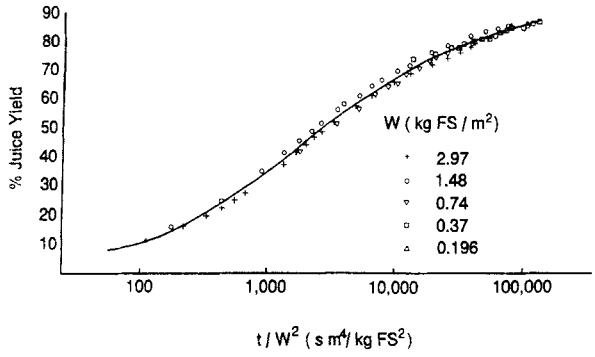

FIGURE 60 Percent yield of juice versus t/W^2 for pressing of milled apples at different values of W at a constant pressure of 980 kPa (Kormendy[114]. Reproduced with permission of the Institute of Food Technologists)

Converted into notation used in this review, it is

$$\ln\left[\frac{V_\infty - V_a}{V_\infty - V_o}\right] = \ln\left[\frac{Z_\infty - Z}{Z_\infty - Z_o}\right] = \frac{R_m}{r} - \left[\frac{R_m^2}{r^2} + \frac{2P_T t}{r\mu W (V_o - V_\infty)}\right]^{1/2} \quad (94)$$

R_m and r are empirically determined. If one expands the left-hand side of Eq (94) using a Taylor series, and retains only the first term for small t, one obtains an equation formally, but not literally, identical to one used by Shirato[22] for constant-pressure filtration. Since R_m and V_∞ depend on P_T, effects of P_T on expression rate are not well defined. At large t, Eq (94) reduces to a special case of Eq (92) where $\beta = [2P_T/r\mu(V_o - V_\infty)]^{1/2}$ and $\gamma = 1/2$.

t/W^2 or $t^{1/2}/W$ as Variables: Eq. (29) indicates that ζ should be a function of t/W^2 or its square root, $t^{1/2}/W$. Eq (88) to (91) indicate that ζ should be a function of t/W^2 or of $t^{1/2}/W$ over all or part of the ζ range. When ζ versus $t^{1/2}$ curves obtained at different W for both biological and non-biological materials were analyzed, $t^{1/2}/W$ at equal ζ varied by less than 10 to 15% for each case when ζ was less than 0.8; in some cases, this was true up to $\zeta = 0.9$. Since juice yield is proportional to $(Z_o - Z)$, juice yield also should be a function of t/W^2 during constant-pressure expression when R_m is negligibly small. Fig. 60,

a replot of a similar figure by Kormendy[114], clearly shows that juice yields for expression of juice from core- and peel-free apple pulp at a constant pressure of 0.98 Mpa are a single function of t/W^2 over a 15-fold range of variation in W. Kormendy did not specify the fixed-solids content of the apples used; fig. 60 is based on an assumed fixed-solids content of 5% by weight. Juice yields for apple pulp that contained cores and peels and for grated apples similarly fell on single curves of yield versus t/W^2 when W varied. Yields at equal values of t/W^2 were markedly lower for grated apples and for pulp that contained cores and peels than for core- and peel-free apple pulp. Cores and peels reduced juice yields for apple pulp; they scarcely affected yield at all for grated apples.

Oil Seeds: Koo[80,81] pressed different types of oil seeds at constant P_T in a curb press, and found that $(Z_o - Z)$ was proportional to $t^{1/6}$.

Mrema and McNulty[82,198-200] carried out uniaxial, oil-expression tests with cashew containing 43.7% oil and 4.3% moisture and with rapeseed containing 41.7% oil and 3.9% moisture. P_T was raised at a steady rate of 62.9 Kpa/s, 94.3 Kpa/s, 188 Kpa/s or 377 Kpa/S until P_T = 56.6 Mpa and held there until t = 2,000 s. P_F was measured 8 mm, 18 mm, and 28 mm above the media during these runs. The media was a fine wire-mesh screen, supported on a perforated steel plate that provided 0.26%, 0.64%, 1.85%, 3.6%, 5.7% or 8.3% open area. Oil yield depended strongly on percentage open area and peaked sharply at 0.64% open area (see fig. 61 for rapeseed).

As shown in fig 62, when 0.64% open area was used, roughly 80% of rapeseed's oil content was expressed at 30 min regardless of the initial rate of P_T increase. Fig. 63 shows that P_F measured 8 mm, 18 mm, and 28 mm above the media were very small compared to P_T when cashew was pressed. A maximum P_T of 67.9 Mpa and a plate with 8.25% open area were used. The maximum P_F was only 0.18% of P_T during the constant P_T period. P_F at all levels declined very slowly when P_T was maintained constant. Slightly higher P_F/P_T were observed when P_T increased more rapidly and when smaller open drainage areas were used. $\text{Log}(P_F)$ for rapeseed decreased linearly as t_p increased; $\text{log}(P_F)$ for cashew did not.

P_T and P_F were measured while P_T increased at a constant rate in tests

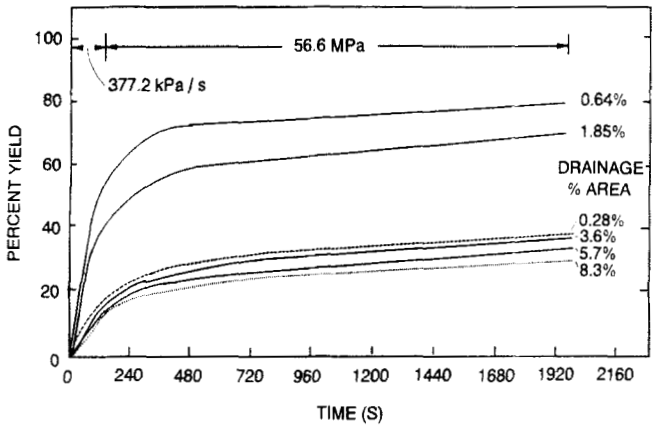

FIGURE 61 Oil yield versus t for pressing of rapeseed using outflow plates with different percentages of open area (Mrema[82])

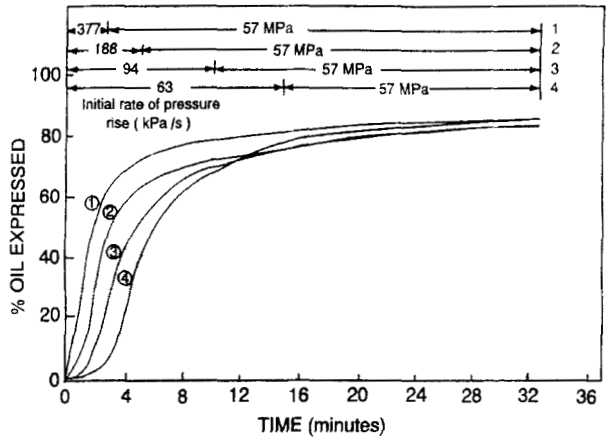

FIGURE 62 Oil yield versus t for different initial rates of pressure increase during pressing of rapeseed while using an outflow plate with 0.64% open area (Mrema[82])

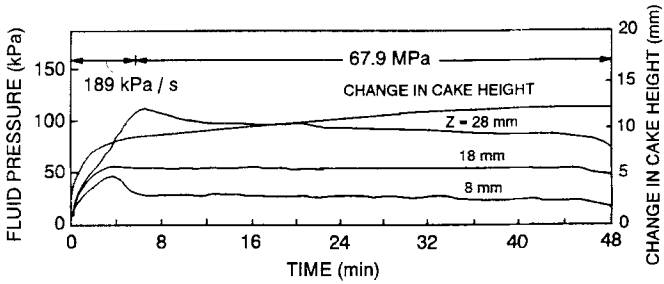

FIGURE 63 Fluid pressures measured at different heights above the media during the pressing of cashew at specified pattern of pressure rise and pressure maintenance (Mrema[82])

carried out with a plate that had no holes. Results for rapeseed are depicted in fig. 64. P_T rose linearly. P_F also initially rose linearly, but much less rapidly than P_T. When $P_T \approx 28.5$ MP_a, P_F rose suddenly and reached P_T. Pressing was stopped shortly thereafter, and both P_T and P_F fell to 0. Similar behavior occurred for rapeseed; but the P_T at which P_F rose was higher, 39 Mpa. Since $P_S = P_T - P_F$, P_S fell to zero when P_F rose. This indicates that virtually all of P_S for these oilseeds was caused by excess, internal hydraulic pressure, P_E.

Electron micrographs of cells in the seeds before and after pressing showed that cell walls remained intact during normal pressing, but were completely disrupted after P_F suddenly increased when using the plate without holes. Why cell wall rupture occurred is not clear; but it led to greater yields during subsequent pressing in which an open plate was used. Fig. 65 shows second-pressing yield versus time data for seeds that had undergone such treatment. A plate with 1.85% open area was used. Fig. 65 also shows that grinding untreated seeds to powder, greatly reduced yield. Peaking of yield when outflow area is low may occur because low areas cause more cell wall rupture, but too low an area excessively interferes with outflow.

Mrema proposed that oil flows out of normally pressed seeds by passing through plasmodesmata in series of cell walls. Using electron micrographs, he

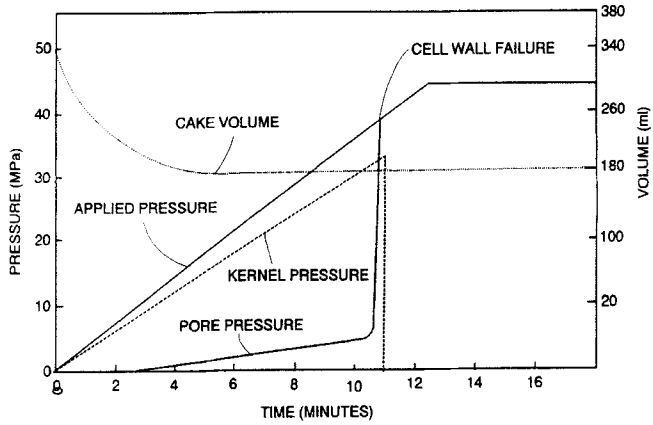

FIGURE 64 Behavior of ram pressure, P_T, and fluid pressure, P_F, for rapeseed pressed using an outflow plate with no holes (Mrema[82])

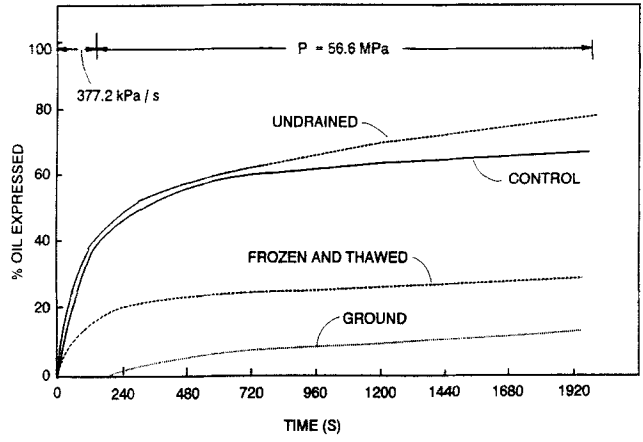

FIGURE 65 Oil yield versus time plot for pressing of rapeseed using a plate with 1.85% drainage area. Samples include: rapeseed previously pressed using a plate with no holes; intact rapeseed; ground rapeseed; and frozen-and-thawed rapeseed (Mrema[82])

Table V - Microstructure Data for Rapeseed and Cashew

	Rapeseed	Cashew
Plasmodesmata diameter (nm)	87.1 ± 3.5	126 ± 7
Cell wall thickness (nm)	913 ± 49	496 ± 23
Cell diameter (μm)	22.3 ± 1.77	20.2 ± 0.55
Number of plasmodesmata/cell	244	181
Number of plasmodesmata/μm^2	0.156	0.137
% Open area in cell wall	0.093	0.171

measured cell diameters (d_c), cell wall thickness (d_w), the diameter (d_{op}) of plasmodesmata and how many plasmodesmata occurred per unit area of cell wall. Results[82,199] of these measurements are tabulated in Table V.
These data, rapeseed oil's viscosity and the number of cell walls encountered by oil flowing out of a seed were used in conjunction with the Hagen-Poiseulle equation to calculate oil outflow rates per seed when $\Delta P = P_T - P_F$. The outflow rates per seed were multiplied by the calculated number of seeds in the load to estimate the overall oil outflow rate. The estimated outflow rate was roughly compatible with the experimental outflow rate near the start of pressing when P_T was low. The experimental rate decreased as P_T rose, while the predicted rate increased. The predicted rate was 10 times as large as the experimental rate when P_T reached 56.6 Mpa. Though plasmodesmata provide only small flow area, they clearly can accommodate the rates of expression encountered in Mrema's tests.

Volume Reduction Contributions: Lanoiselle et al.[201] carried out constant pressure-expression tests with rapeseed. They analyzed their results by accounting for volume diminutions in: a) spaces between particles, b) symplasmic spaces within particles, c) extracellular (apoplasmic) spaces within particles, and d) fixed solids volume due to creep. Their approach is one of the few attempts to analyze expression from biological materials in terms of flow

processes within particles. Lanoiselle at al. assumed that: a) oil flows from symplasmic space to apoplasmic space, then to interparticle space and out through the media, whose resistance was neglected; b) flow rates between adjacent spaces are proportional to the (constant) hydraulic conductivities of intervening barriers and to the pressure differences between spaces and ; c) flow rates within spaces obey Darcy's law, i.e. are proportional to P_F gradients and permeabilities characterizing the spaces and d) volume reductions in individual liquid-filled spaces are due to the net outflow from those spaces.

Based on simplifying assumptions, they summed the volume-reduction contributions for the spaces using four terms, each of which exponentially decays with time, i.e.

$$\xi = \sum_{i=1}^{4} G_i [1 - \exp(-\lambda_i t)] \qquad (95)$$

G_i and λ_i are based on the hydraulic characteristics of the spaces involved and on the conductivities of barriers between spaces. Using the method of residues, they empirically found G_i and λ_i that provided a very close fit between Eq (95) and experimental ξ versus t data. G_i and λ_i were not independently measured. Oilseeds contain very little apoplasmic space; and outflow from such seeds probably depends on passage through cell walls in series rather than on passage from apoplasmic to symplasmic space. The good agreement between Eq (95) and experimental data may depend solely on the inherent ability of such equations to empirically fit many time-decay processes quite well.

Rheological Model: Eq (96) applies for constant-pressure deformation behavior for the system shown in fig. 35a when $\ln(P_i/P_{ref}) = k_i(V_{ref} - V_i)$ governs the stress versus V behavior of spring-analog i and $\ln(P/P_{ref}) = \eta_K d(V_{ref} - V_i)/dt$ governs the deformation rate behavior of the dashpot-like element. i is 1 for the in-series spring and 2 for the spring in the Kelvin-Voigt element.

$$V_{ref} - V = \ln\left[\frac{P_s}{P_{ref}}\right] \cdot \left[\frac{1}{k_1} + \frac{1 - \exp(-k_2 t/\eta_K)}{k_2}\right] \qquad (96)$$

Eq (96) shows that $-dP_S/dV$ decreases as time increases. Therefore $C = (-dP_S/dV)/\mu\alpha$ also decreases as time decreases. If k_2/η_K is $<< C/W^2$ initially, the decrease in C will be negligibly small until consolidation is nearly complete, and Eq (89) or (90) will apply. However if k_2/η_K is comparable to the initial value of C/W^2, C will steadily decrease during expression, and expression rates will decrease slower than predicted by Eqs (89) or (90). Changes in C will be large when k_2/k_1 is small, as is likely to be the case for highly deformable biological solids. It appears likely that apparently anomalous consolidation in biological solids can be modelled by use of rheological models like those in fig. 35.

Summary - Constant Pressure Expression of Biological Feeds: Deformations during compaction at constant P_T are much larger for biological presscakes than for non-biological cakes and follow different patterns with respect to time. Very rapid initial compaction occurs when biological presscakes initially contain air. Media outflow area affects expression from oilseeds in ways that are not wholly understood.

Eqs (88) to (90) do a fairly good job of describing constant pressure compaction of non-biological solids, but usually cannot be used for biological solids. Even when they can be used for biological solids, changes in ζ due to secondary consolidation will be large. ζ increases linearly as $t^{1/2}$ increases only for $\zeta < 0.2$ for many biological materials; compared to ζ up to 0.5 to 0.65 for non-biological solids. Solutions of Eqs (23) and (24) based on use of constant C do not adequately account for the pressing behavior of biological materials, and the deviant behavior of biological solids cannot be simply attributed to changes in C as V or e change.

Expulsion of fluid from particles probably causes many of the differences between the pressing behavior of cellular biological solids and non-biological solids. Excess internal hydraulic pressure, P_E, provides the driving force for fluid expulsion from particles. P_E increases P_S and reduces P_F when P_T is fixed. This slows down flow in pores between particles and thereby reduces cake compaction rates. Consolidation behavior for cellular biological solids often

depends on factors affecting flows inside particles. Rheological systems such as shown in figs. 35 and 36 probably can be used to model such flows.

12. FLOW WITHIN PARTICLES

Sooner or later, fluid is expelled out of particles when moist particulate biological materials are pressed. Pressure drops driving that expulsion will be proportional to the flow-path length, $d_p/2$, and to the rate of particle compaction, $-d(d_p)/dt$. The particle compaction rate will be roughly proportional to the overall cake compaction rate; i.e. $-d(d_p)/dt \approx (d_p/Z)(-dZ/dt)$. Therefore, P_E will be roughly proportional to $(d_p^2/2Z)(-dZ/dt)$ times the internal flow resistance of particles. Thus, P_E should be smaller when d_p is smaller. On the other hand, α tends to be proportional to $1/d_p^2$; and ΔP_F will increase as d_p decreases. Consequently, there will be an optimum d_p which minimizes the sum of d_p's effects of P_E and ΔP_F. That optimum will depend on the relative magnitude of flow resistance within particles and flow resistance in the cake. Rupturing cell walls will decrease internal flow resistance and reduce P_E, but may permit particles to collapse in ways that block flow channels in cakes and cause α and ΔP_F to increase. Thus, there may be an optimum extent of cell wall rupture. Therefore, more knowledge about the nature of flow resistance and flow within cells is desirable. Treatment of internal flow by Mrema[82,199] and Lanoiselle et al.[201] have already been covered.

Compaction at Constant Pressure: Buttersack and Basler[87] used a heavily loaded, porous-tipped piston to express juice from cylinders of denatured sugar beet tissue placed in a tight-fitting glass tube sealed at its bottom. The beet's cell membranes were destroyed by prior heating or chemical treatment. Overall and local compaction were measured versus time during pressing at P_T = 0.7 Mpa. Fig. 66 shows the test setup used and progress of an experiment. Changes in height of local sections of tissue in the cylinder are depicted in fig. 67. First, the top section of the cylinder compacted. After it almost finished compacting, the section below it started to compact. Section-by-section

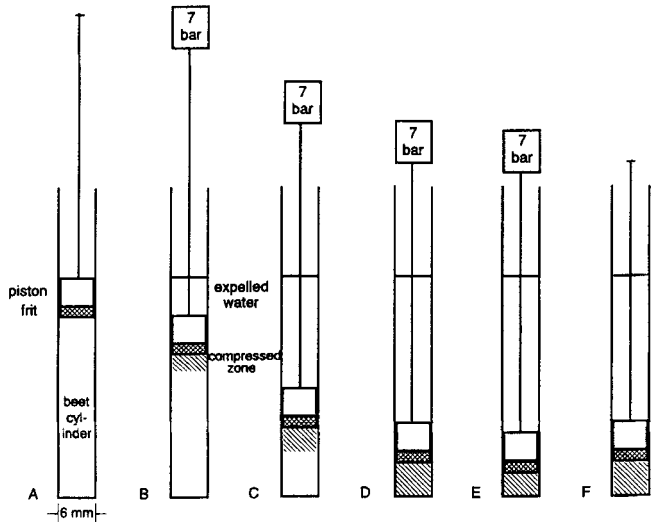

FIGURE 66 Setup for pressing cylinders of denatured beet tissue, and progress of a constant-pressure cylinder compaction test (Buttersack and Basler[87]. Reprinted with permission from Plant Science.)

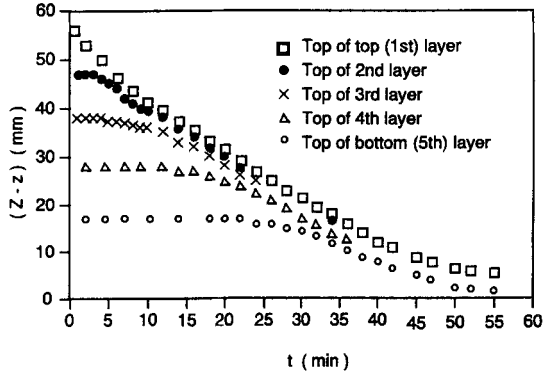

FIGURE 67 Change in height of local section of beet cylinder during compaction at constant pressure (Buttersack and Basler[87]. Reprinted with permission from Plant Science.)

compaction continued until the lowest section compacted. As compaction proceeded, lower sections started to compact more and more before the end of compaction in the section above. If particles behave in a similar way during constant-pressure expression, they will compact layer by layer inward, and except when flow starts in the outermost layer, internal flows will occur mainly across previously compacted layers.

In contrast to denatured beets, cylinders of undenatured beets whose cell membranes were intact scarcely compacted at all when similarly loaded; i.e. little expression occurred. Cell wall-membrane combinations in laterally-confined, undenatured sugar beet tissue apparently can withstand at least 0.7 Mpa of axially applied pressure without bursting.

Cell walls are very strong in tension, but buckle easily if fluid can flow out of tissue. Therefore, if cell membranes are denatured, cells can undergo a great deal of compaction before generating much solid stress. Ultimately, solid stress will build up; but fluid pressure drops and solid stress gradients will still occur across layers of compacted cells.

For denatured beet cylinders, ζ was proportional to $t^{1/2}$ until $\zeta \approx 0.58$, which occurred when $t = t_i \approx 2$ min. Shortly afterward, $\ln(1 - \zeta)$ increased linearly as $(t - t_i)^{1/2}$ increased. Because of the initial proportionality between ζ and $t^{1/2}$, Buttersack and Basler concluded that cell wall pairs through which flow occurs act like a filter cake growing in thickness. Based on that conclusion and measured rates of compaction, they calculated L_p, the hydraulic conductivity of cell wall pairs in the cake-like region. These L_p ranged from 0.55×10^{-6} to 4.7×10^{-6} m/Pa·s, and were greater for chemically denatured beets than for beets thermally denatured at 72°C. L_p may appear smaller for thermally denatured beets because thermal denaturation converted some solid protopectin to viscous dissolved pectin and the associated increase in viscosity was not accounted for. L_p increased when longer test cylinders were used. This effect is not explained by theory.

If fluid pressure drop across a presscake is negligibly small, P_S should be the same in all parts of the cake; and each particle should compact in ways similar to those described for beet cylinders. Directions of particle compaction would

differ from site to site, but the overall effect would probably be the same, i.e. compacted zones would form and move inward in particles. Thus Eq (94) may characterize a process based on compacted and uncompacted zones within particles, instead of a process based on similar zone within the cake as a whole.

Single-Particle Tests: Akkerman, Fox and Walstra[202] pressed individual 8-mm or 10-mm cubes of renneted cheese between a glass slide and a transparent surface at a series of different normal pressures, P_N, ranging between 0.05 and 4.5 Kpa. The cubes were submerged in fluid in a transparent vessel. Akkerman et al. measured cube heights versus time and cube volumes as the cubes deformed. The surrounding fluid was isosmotic with respect to the fluid inside the cubes; and the volumes of unpressed cubes placed in the liquid did not change. At the start of pressing, cube heights almost immediately decreased 30% to 45%, depending on the pressure used and the fixed solids content of the cube; but the cubes regained their initial shape if the applied load was removed in a few seconds. Thus the initial deformation was elastic. No elastic recovery was observed after fifteen minutes of pressing. The cubes expanded laterally when pressed; e.g. their final width was 1.6 times their initial width when P_N was 3 Kpa.

Cube volume decreased at a progressively decreasing rate during pressing. Since virtually no fixed solids left the cube, volume shrinkage was due to fluid outflow from the cube. Since the top and bottom surface were sealed by the slide and tank bottom, outflow occurred from vertical sides of the cube. Cube volume shrinkage increased as P_N increased but levelled off at $P_N > 2$ Kpa. After 15 minutes of pressing, $V_a/V_o \approx 0.25$ for P_N between 2 and 4.5 Kpa.

Akkerman et al. assumed several values of k_{int} (permeability within the cube) and tried to determine how large P_E would have to be to produce flows consistent with the observed rate of volume reduction. They concluded that k_{int} had to be greater than 3×10^{-14} m^2 initially for P_E to be less than P_N. When dV/dt decreased later in pressing, P_E would not exceed P_N even if k_{int} was 1×10^{-14} m^2 or smaller. Therefore, Akkerman et al. concluded that P_E was only a very small fraction of P_N during the last stages of pressing and that P_N

depended solely on internal solid stress at the end of pressing. Except for the initial elastic deformation, volume reductions in single pressed cubes of cheese curd appear to roughly follow the Terzaghi model.

Fluid Expulsion from Particles: Abularach[203] determined extents of fluid expulsion from particle during constant-rate pressing. Saturated cakes containing either coffee or apple particles mixed with dextran-blue solution were pressed at ram speeds of 20 or 50 mm/min. Pressing was stopped when P_T = 6 Mpa. The dextran blue (M.W. $6x10^6$) could not diffuse into cells with intact walls. Amounts of fluid expelled from the particles were determined by optically measuring how much the expelled fluid diluted the dextran blue. A similar technique was used by Laivins and Scallan[51] to measure expulsion of fluid from wood cell walls.

Fig. 68 depicts results obtained for spent drip-grind coffee grounds pressed at 50 mm/min. Y_e, the volume fraction in outflow of fluid expelled from particles, is plotted versus V_a/V_{po}. V_{po} is the initial fixed-solids-based specific volume of the particles; V_p is the corresponding specific volume during pressing. In all cases Y_e was very small at the start of pressing, but rapidly increased once V_a/V_{po} fell below a certain value. Based on a volume balance.

$$\frac{dV_p}{dV_a} = \left[\frac{2Y_e}{1 + Y_e}\right] + \frac{V_a - V_p}{1 + Y_e}\frac{dY_e}{dV_a} \qquad (97)$$

Calculations based on Eq (97) show that dV_p/dV_a progressively increased as soon as Y_e started to increase rapidly. Thus, at late stages of pressing, shrinkage of particles caused progressively greater portions of cake volume decrease and significantly exceeded the volume reduction contribution due to shrinkage of spaces between particles. Because particle volume reduction dominated at late stages of pressing, ε' actually increased then. For spent, drip-grind coffee, Y_e started to increase when $V_a/V_{po} \approx 1.3$; for apples, it started when $V_a/V_{po} \approx 2$; and for spent grounds whose cell walls had been rendered more permeable by high temperature hydrolysis, the rise started when $V_a/V_p \approx 1.5$. Thus fluid expulsion from particles starts earlier when cell walls are highly permeable or easily ruptured.

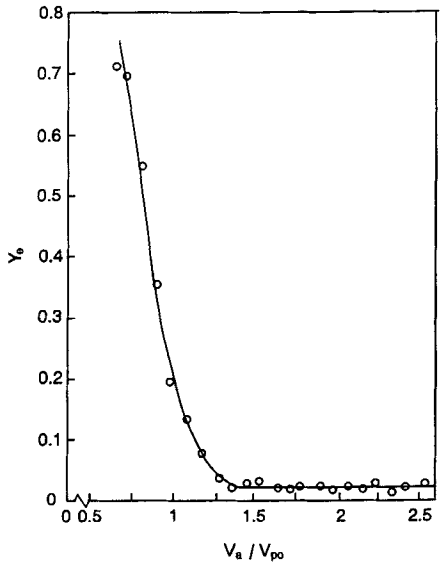

FIGURE 68 Fraction of fluid expressed from particles in fluid outflow during constant-rate compaction of a saturated bed of spent coffee grounds (Abularach[203])

If increases in P_E causes P_T to increase and reach P_{max} more quickly, less overall compaction will occur when P_E rises rapidly than when it rises slowly. For material with open or readily rupturable pores, i.e. apples and hydrolyzed spent grounds, Y_e reached 0.92 when P_T = 6 Mpa. Y_e at P_T = 6 Mpa was lower for untreated spent grounds with intact cell walls: 0.63 when -dZ/dt = 50 mm/min, and 0.71 when -dZ/dt = 20 mm/min. For grounds that had been soaked in 50% sucrose solution, Y_e rose very rapidly, but only reached 0.50 when P_T = 6 Mpa. Thus, high viscosity tends to reduce rates of fluid expulsion from particles.

Fluid pressed out of spent coffee grounds contains fine colloidal particles, which can be removed by filtration using membranes with 0.45 μm pores, but not by membranes with coarser pores. Since molecules with molecular weights

larger than 1960 normally do not pass through cell walls in spent coffee grounds[100], pressing must have ruptured cell walls to some extent for the colloidal particles to have escaped.

13. CONSTANT-RATE PRESSING BEHAVIOR

Soil Consolidation: Constant-rate consolidation tests have been used in soil mechanics since 1959[204]. They provide continuous P_s versus e (or V) curves and permit evaluation of the influence of pressing rate on test results[205]. Two media surfaces are used, but one is usually blocked, and P_F is measured at that surface. If media resistance is negligibly small, P_F at the blocked surface equals ΔP_F across the cake.

If the initial V is V_o at all w and C and -dZ/dt are constant, the solution of Eq (23) is

$$V_o - V = -\frac{dZ}{dt}\frac{W}{C}\left[\frac{Ct}{W^2} + \frac{3w^2 - W^2}{6W^2} - \Phi\right] \qquad (98)$$

where

$$\Phi = \frac{2}{\pi^2}\sum_{j=1}^{\infty}\frac{(-1)^j}{j^2}\exp\left[-\frac{j^2\pi^2 Ct}{W^2}\right]\cos\left(\frac{j\pi w}{W}\right) \qquad (99)$$

Φ approaches zero quickly as time increases and usually can be neglected in analyzing consolidation test data. The product of -(dZ/dt)W/C and the first term in the brackets in Eq (98) is -(dZ/dt)·t/W, which equals $(Z_o - Z)/W$, which in turn equals $(V_o - V_a)$. If Φ is negligible, and we evaluate Eq (98) at w = 0, where V = V(0), we get

$$[V_o - V(0)] = [V_o - V_a] + \frac{dZ}{dt}\frac{W}{6C} \qquad (100)$$

and at w = W, where V = V(W), we get

$$[V_o - V(W)] = [V_o - V_a] - \frac{dZ}{dt}\frac{W}{3C} \qquad (101)$$

Table VI - Effect of Pressing Rate on $\Delta P_F/P_S(V_a)$

-(dZ/dt)(W/KC)	0	0.25	0.5	1	2
$P_T/P_S(V_a)$	1	1.087	1.181	1.396	1.948
$\Delta P_F/P_S(V_a)$	0	0.128	0.247	0.549	1.231
$\Delta P_F/P_T$	0	0.118	0.221	0.393	0.632

If P_S is a function of V alone, V(0) and V(W) can be used to obtain $P_S(0)$ and $P_S(W)$, i.e. P_S at w = 0 and W respectively. $P_S(W) = P_T$ if wall friction is negligible.

Therefore, if P_S obeys Eq (2)

$$\ln\left[\frac{P_T}{P_S(V_a)}\right] = -\frac{dZ}{dt}\,\frac{KW}{3C} \qquad \textbf{(102)}$$

where $P_S(V_a)$ is the value P_S at V_a. From Eq (2) and Eq (100), $\ln[P_S(0)/P_S(V_a)]$ = (dZ/dt)·K·W/6C. When wall friction is negligible, $[P_S(W) - P_S(0)] = \Delta P_F$, the fluid pressure drop across the cake. Therefore

$$\Delta P_F = P_S(V_a)\,\exp\left(-\frac{dZ}{dt}\,\frac{WK}{3C}\right)\left[1 - \exp\left(\frac{dZ}{dt}\,\frac{WK}{2C}\right)\right] \qquad \textbf{(103)}$$

$P_S(V_a) = P_S(V_o)_{ref})\exp[K(V_o - V_a)]$. If C and -dZ/dt are constant and Eq (2) applies, $\Delta P_F/P_T$, $P_T/P_S(V_a)$ and $\Delta P_F/P_S(V_a)$ will remain constant as V_a decreases; and both - $d\ln(P_T)/dVa$ and - $d\ln(\Delta P_F)/dV_a$ will equal - $d\ln[\Delta P_S(V_a)]/dV_a$ which, in turn, equals the constant, K, in Eq (2). Eqs (102) and (103) can be used together to numerically determine -(dZ/dt)(W/KC) from P_F and ΔP_T values measured during pressing. Values of $\Delta P_F/P_T$, $P_T/P_S(V_a)$, $\Delta P_F/P_S(V_a)$ obtained by applying Eq (102) and (103) at chosen -(dZ/dt)(W/KC) are listed in Table 6. W and -dZ/dt are known, and -[(dZ/dt)(W/KC)] and K can be found. Therefore, C can be determined, i.e. C = W(dZ/dt)/K[(dZ/dt)(W/KC)].

If $\Delta P_F/P_T$ is known and remains constant, -(dZ/dt)(W/KC) can be determined and substituted in Eq (102) or (103) to determine values of $P_S(V_a)$ from either P_T or ΔP_F. Constants, P_{ref} and V_{ref} used in Eq (2), can be found by

simultaneously solving Eq (2) for two $P_S(V_a)$, V_a pairs. Thus all constants needed to correlate $P_S(V)$ in terms of Eq (2) can be found.

If $\Delta P_F/P_T$ changes as V_a decreases during pressing and Eq (2) applies, C varies instead of remaining constant. Other ways of interpreting constant-rate tests are used[206] if this occurs or if Eq (2) does not apply at V_o. Transients caused by changes in C soon decay, and for practical purposes, current values of C can be used in Eqs (100) to (103) with little error when C changes slowly as V_a decreases and -dZ/dt is small. If C changes slowly, $\Delta P_F/P_T$ measured at different V_a and fixed -dZ/dt can still be used to find $P_T/P_S(V_a$ and $\Delta P_F/P_S(V_a)$. These ratios can be used to convert P_T or P_F versus V_a data into P_S versus V_a data, which in turn can be used to generate a $\log(P_S)$ versus V_a plot. K can be determined from the slope of that plot, and then can be used in conjunction with W and -dZ/dt, as previously described, to determine C at chosen V_a from $\Delta P_F/P_T$ at those V_a.

Fig. 69 contains a plot of $\log[P_S(V_a)]$ and plots of $\log(\Delta P_F)$ versus V_a at different pressing speeds for calcium montmorillonite[206]. The $\log(\Delta P_F)$ versus V_a plots are parallel where Eq (2) applies, but are not parallel to the $\log[P_S(V_a)]$ plot. Therefore C is not constant. The slope of the $\log[P_S(V_a)]$ versus V_a curve $= -K/2.303$. $\Delta P_F/P_S(V_a)$ can be used in Eq (103) to find $-(dZ/dt)(W/KC)$ values, which in turn can be used in conjunction with K, W and -dZ/dt to find C at different extents of compaction. C can also be determined by another method, described by Smith and Wahls[206]. Both computational methods show how C changes during the course of pressing. Smith and Wahls found that ΔP_F versus ΔZ data for the two lower speeds could be used to calculate K reasonably accurately, but calculated K were 31% to 33% too high when ΔP_F data for higher pressing speeds was used. Therefore use of low $-(dZ/dt) \cdot W$ is recommended when constant-rate pressing tests are used to determine K.

Shirato[118] successfully used an e-based version of Eq (104) for cases where constant-rate consolidation followed constant-rate filtration.

$$\ln\left[\frac{P_T}{P_o}\right] = \frac{\rho_S(-dZ/dt)\,t}{C_C W} = K_T(V_o - V_a) \qquad \textbf{(104)}$$

P_o and V_o are the values of P_T and V_a at the start of expression, and t is the

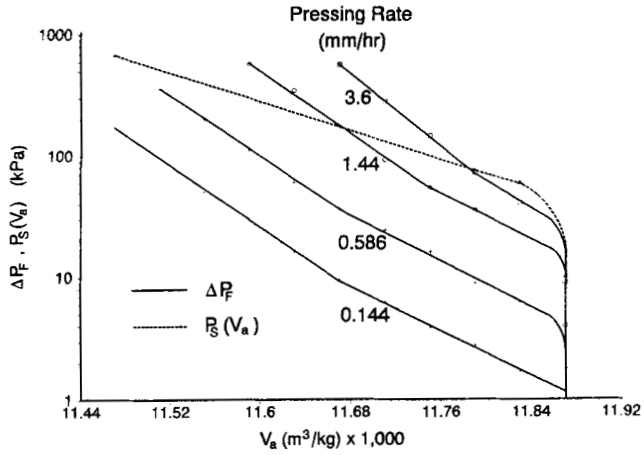

FIGURE 69 $\log(\Delta P_F)$ versus V_a and $\log[P_S(V_a)]$ versus V_a behavior during constant-rate consolidations of calcium montmorillonite (Smith and Wahls[206])

expression time. The alternative right-hand side results from substituting $(V_o - V_a)$ for $-(dZ/dt) \cdot t/W$ and replacing ρ_S/C_C by a single constant K_T.

Tests with Cellular Biological Solids: Many constant-rate pressing tests have been carried out with biological solids at the University of Massachusetts. Presscake properties and many different types of pressing responses were measured over wide ranges of pressing speeds for spent coffee grounds, different varieties of apples, chopped alfalfa, fresh extracted and cooked sugar beets, prepressed sugar beet pulp, halved cranberries, casein curds, alfalfa protein curds and sponges. Information about the pressing behavior of cellular biological solids was obtained by analyzing results from these tests and constant-rate pressing data obtained elsewhere. These results were also used to evaluate the suitability of computational methods dealing with pressing.

Equipment: Many tests were carried using the cell depicted in fig. 70. A ram with a relatively small diameter, 25.4 mm, was used to permit attaining P_T up to 8 MPa. The ram was driven in compression mode by an Instron Universal

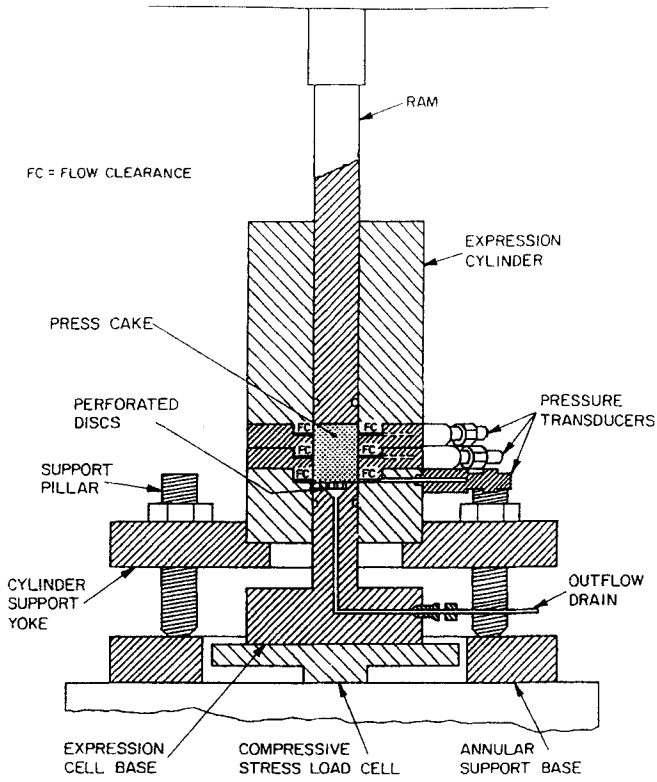

FIGURE 70 25-mm expression test cell fitted for measurement of P_F, ΔP_m and ΔP_w (Schwartzberg[85]. Reprinted by permission of Van Nostrand Reinhold, copyright © 1983)

Test Machine capable of providing compressive forces up to 4450 N. Constant pressing speeds ranging from 0.5 mm/min to 200 mm/min were used. Pressure transducers mounted on the cell wall were used to measure ΔP_m, the fluid pressure drop across the outflow media, and P_F 1 and 2 cm above the media[85]. F_w, the force transmitted to the wall by friction was measured by means of a load cell attached to a yoke supporting the wall. F_B, the force acting on the bottom of the cell, was measured instead of ram force, F_T, when the wall support yoke was used. $F_T = F_w + F_B$

A similar cell with a 133.4-mm bore was used in a system that provided F_T up to 22.4 kN (P_T up to 1.6 Mpa) and pressing speeds of 2.54, 7.62 or 25.4 mm/min[208]. This cell contained two fluid pressure transducers, one to measure P_F at the ram face and one to measure ΔP_m. Because of its larger diameter, wall friction was much smaller in this cell than in the 25.4-mm cell.

In some work, a simpler 25.4-mm diameter cell that only permitted measurement of F_T versus cake height, Z, and relaxation time, t_r, was used.

In all cases, a close-fitting ram was driven downward in a cake-filled bore at a fixed speed (-dZ/dt). Test-machine instruments recorded F_T or F_B versus Z and t. The ram automatically stopped when F_T or F_B reached a maximum tolerable value, F_{max}, whereupon F_T decreased, first rapidly, then more and more slowly. F_T ultimately asymptotically approached a much-lower fully relaxed value, F_R. F_T or F_B and Z were converted into corresponding values of P_T or P_B versus V_a during ram motion and into P_T or P_B versus t_r after the ram stopped.

Ram-Force Pressing Records: Typical F_T versus Z records are shown for pressing of spent coffee grounds (fig. 71) and red delicious apples (fig. 72)[56]. These figures also depict F_T versus t_r during relaxation, i.e. after the ram automatically stopped at $F_T = F_{max}$. The curve for spent grounds rises smoothly during ram motion and drops fairly quickly once the ram stops. For spent grounds $F_R/F_{max} = 0.11$, where F_R is the fully relaxed value of F_T. The F_{max} used for apples is 1/4 to 1/5 as large as for spent grounds; $F_R/F_{max} = 0.25$. For apples, F_T passes through a jagged slightly-rising plateau before rising rapidly to its peak value. Pressing curves for diced or sliced fruits or vegetables often exhibit similar plateaus, which are probably caused by repeated mechanical breakdown and/or cell rupture at critical values of stress. The plateau's jaggedness is due to repeated buildup and relief of stress. Such behavior is sometimes called "bioyield". Jaggedness decreases when larger diameter test cells are used and effects of stress buildup and relief average out over a larger area. F_T versus Z plateaus do not occur when milled fruit is pressed. During pressing, diced apples progressively change into a mash that resembles apple sauce. The dices probably break down because of mechanical failure at weak middle lamellae between cells. Intact dices are often found imbedded in the mash.

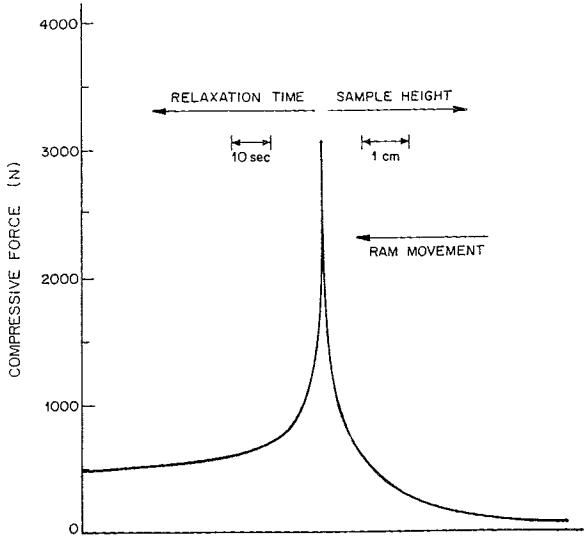

FIGURE 71 F_T versus Z and t_r for spent drip-grind coffee grounds pressed at a constant speed of 50 mm/min (Schwartzberg et al,[56]. Reproduced with permission of the American Institute of Chemical Engineers. Copyright © 1977)

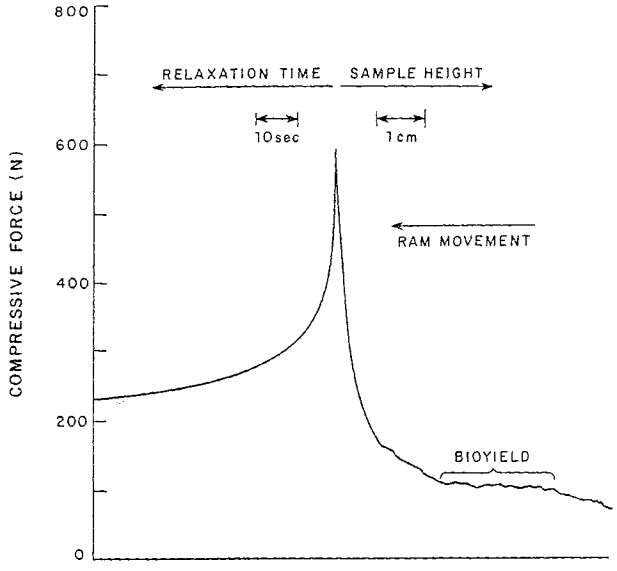

FIGURE 72 F_T versus Z and t_r for red delicious apples pressed at a constant speed of 50 mm/min (Schwartzberg et al.[56] Reproduced with permission of the American Institute of Chemical Engineers. Copyright © 1977)

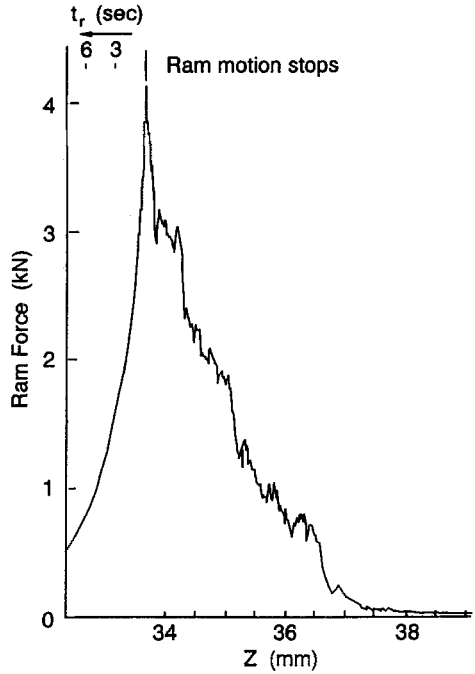

FIGURE 73 F_T versus Z record for sugar beets extracted at 100°C for two hours and then pressed at a constant speed of 10 mm/min. (Huang[60])

Fig. 73 is a F_T versus Z record for pressing extracted sugar beets[60] at a ram speed of 10 mm/min. The beets had been cooked at 100°C, a treatment that breaks down protopectin. Almost all regions of the curve are jagged. Jagged pressing curves are also obtained when diced or milled fruits and vegetables are pressed at ram speeds higher than 10 or 20 mm/min. Pressing tests for fruit and vegetable often are carried out mainly at pressing speeds $\leq$ 10 mm/min so as to obtain smooth F_T versus Z records. Pressing curves for extracted beets that had not been cooked at 100°C were less jagged. The extreme jaggedness encountered with beets cooked at 100°C probably was caused by weakening of bonds between cells in the beets. Pressed extracted beets that were repressed exhibited pressing curves that were only jagged at

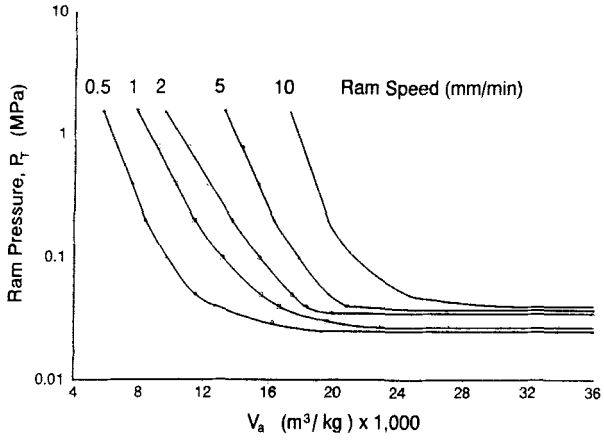

FIGURE 74 $\log(P_T)$ versus V for constant-rate pressing of Granny Smith apples with pressing speed as a parameter. (Vallon et al.[138])

high pressures. This probably occurred because mechanical failures that ordinarily cause jaggedness at low pressures during pressing had already occurred.

Ram Pressure: F_T, F_B, and F_w versus Z data were respectively converted into records of P_T, P_B and ΔP_w versus V_a. P_T is the ram pressure, P_B is the pressure at the base of the cake, and ΔP_w is the pressure drop due to wall friction. $P_T = F_T/A$ or $(F_B + F_w)/A$, $P_B = F_B/A$, $\Delta P_w = F_w/A$, $P_{max} = F_{max}/A$ and $V_a = Z/W$. P_T, P_B and ΔP_w versus t, data were similarly obtained. Figs. 74 and 75 respectively contain $\log P_T$ versus V_a plots for diced Granny Smith apples[138] and extracted sugar beet strips[60]. The bioyield plateau is fairly flat in fig. 74, which is for a batch of Granny Smith apples with very thin cell walls. For most diced apples (including other batches of Granny Smith apples that had thick-walled cells), P_T increases slightly as V_a decreases in the bioyield region.

$\text{Log}(P_T)$ versus V_a curves for olive paste[209] are similar to those for apples and those for milled alfalfa[57] are similar to those for extracted sugar beets. These constant-rate curves behave very differently than constant-rate $\log(P_T)$

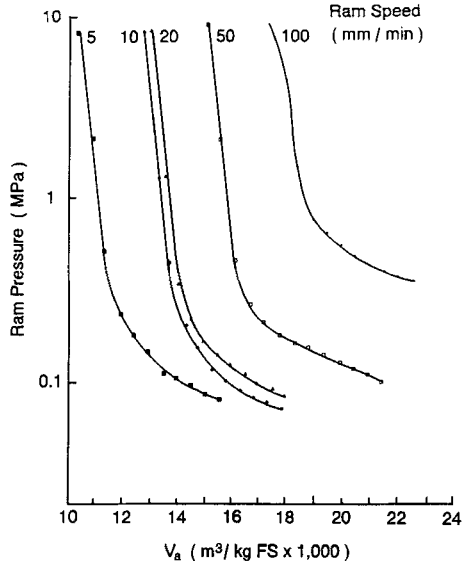

FIGURE 75 $\log(P_T)$ versus V for 25 gram samples of extracted sugar beets pressed at different constant speeds (Huang[60])

versus V_a curves for non-biological materials. As -dZ/dt increases, $\log(P_T)$ versus V_a curves for these biological materials primarily shift to higher V_a values without changing shape, rather than shifting upward to higher P_T values, as happens with non-biological materials. The curves have two branches: a flat or moderately sloped branch at high V_a and a branch at lower V_a where $\log(P_T)$ rises very rapidly.

Fig. 76 contains plots of $\log(P_T)$ versus V_a for spent, roasted coffee grounds at different pressing speeds[85,207]. Over a large part of the pressing range

$$\ln\left[\frac{P_T}{P_{ref}}\right] = K_T \cdot (V_{ref} - V_a) \qquad \textbf{(105)}$$

Once P_F starts to rise, P_T become larger than indicated by Eq (105). Eq (105) is similar to Eqs (2) and (104) which respectively describe major portions of log (P_S) versus V and $\log(P_T)$ versus V_a curves for non-biological solids; but for

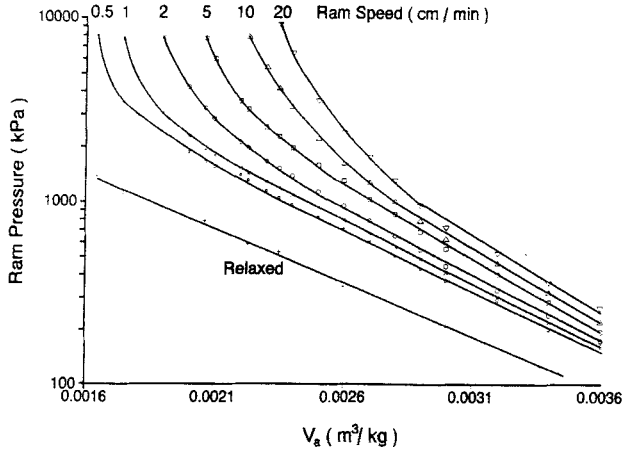

FIGURE 76 $\log(P_T)$ versus V for constant-rate pressing of spent coffee grounds at different pressing speeds (Huang[207])

coffee grounds $K_T \equiv -d[\log(P_T)]/dV_a$ increases as -dZ/dt increases, whereas for non-biological solids $-d[\log(P_T)]/dV_a$ remains constant when -dZ/dt increases. Moreover, $\log(P_T)$ versus V_a curves for non-biological solids do not curve upward sharply once P_F rises. $\text{Log}(P_T)$ versus V_a curves for coffee grounds exhibit less radical increases in $-d[\log(P_T)/dV_a$ near the end of pressing than $\log(P_T)$ versus V_a plots for softer cellular biological solids.

Cell and tissue structure for biological materials no doubt strongly influence the nature of their $\log(P_T)$ versus V_a curves. In roasted coffee, there is virtually no intercellular space between cells, cells contain no plasma membrane and are roughly 25 μm in diameter, and their walls are roughly 2.5 μm thick. The other materials tested have thinner walls or ruptured walls, plasma membranes, much smaller ratios of cell wall thickness to cell diameter; and, except for milled olive paste, contain large amounts of intercellular space. Structural properties of apples, alfalfa and sugar beets have previously been described (see Section 6). Olive paste is a moderately fluid mixture of ruptured cell walls (2% by weight), olive oil (20.5% by weight), aqueous juice (49% by weight), and 1.5- to 2-mm diameter pit fragments (28% by weight)[209].

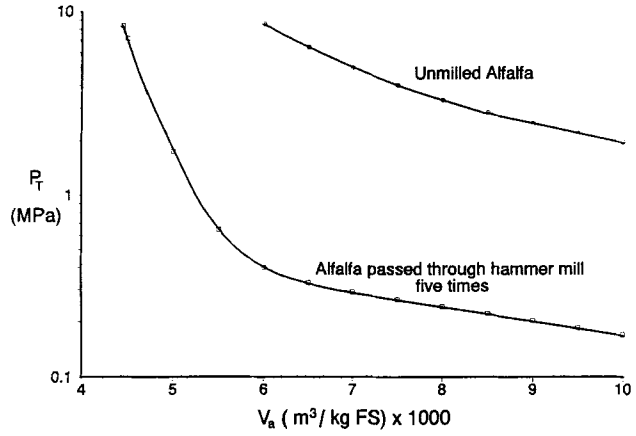

FIGURE 77 $\log(P_T)$ versus V for 25-gram samples of thoroughly milled and unmilled alfalfa, each pressed at a constant speed of 50 mm/min (Schwartzberg et al.[57])

Fig. 77, a $\log(P_T)$ versus V_a plot for compaction of thoroughly milled alfalfa and unmilled alfalfa[57], shows that: a) cell rupture is needed to obtain high pressed juice yields; b) simple compaction is a poor way to achieve cell rupture; and c) the shape of $\log(P_T)$ versus V_a curves is greatly affected by the presence or absence of cell rupture. Shearing and impact rupture alfalfa cells more efficiently than pressing[98,104,210]. The shapes of $\log(P_T)$ versus V_a plots for spent coffee grounds and unmilled alfalfa probably differ from those for apples, olive paste, sugar beets and milled alfalfa because most cell walls in coffee and unmilled alfalfa are only slightly permeable, intact, and resist rupture, whereas cells in the other materials cited are more permeable, ruptured or rupture easily. Fig. 78 depicts a $\log(P_T)$ versus V_a curve for pressing of oil out of cashew[82], a material with cell walls that remain intact during pressing. Its shape resembles that for spent grounds and unmilled alfalfa.

Figs. 79, 80 and 81 are $\log(P_T)$ versus V_a curves for spent coffee grounds pressed at room temperature using a ram speed of 50 mm/min. Fig 79 is for four different loads of grounds of similar size. Eq (102) indicates P_T should

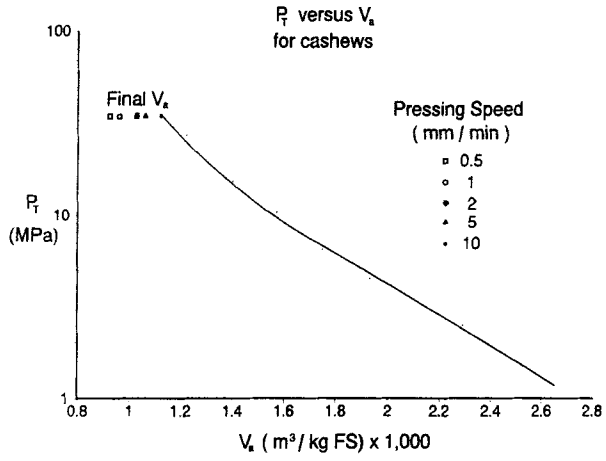

FIGURE 78 $\log(P_T)$ versus V for constant-rate pressing of cashew (Mrema[82]). Final V_a are indicated for different pressing speeds.

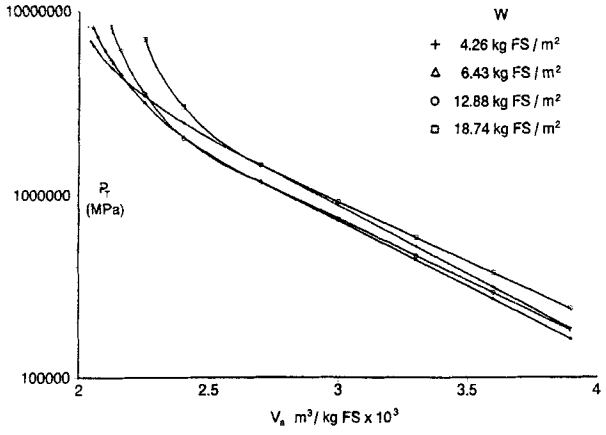

FIGURE 79 $\log(P_T)$ versus V for different loads of spent coffee grounds, each pressed at constant rate of 50 mm/min. (Schwartzberg et al.[56] Reproduced with permission of the American Institute of Chemical Engineers. Copyright © 1977)

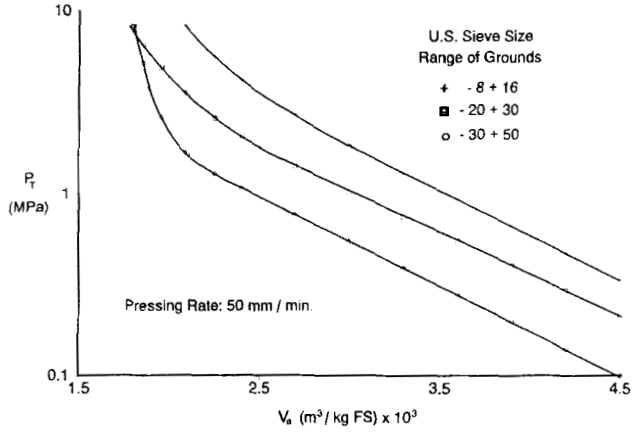

FIGURE 80 log(P_T) versus V for 26.2-gram samples of spent coffee grounds of different d_p pressed at a constant rate of 50 mm/min. (Schwartzberg et al.[56] Reproduced with permission of the American Institute of Chemical Engineers. Copyright © 1977)

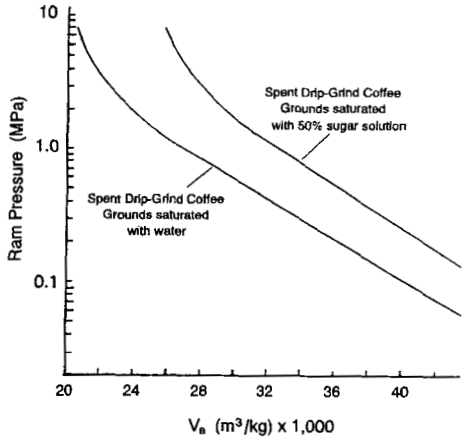

FIGURE 81 log(P_T) versus V for 26.2-gram samples of spent coffee grounds containing either water or 50% sugar solution, each pressed at a constant-rate of 50 mm/min. (Schwartzberg et al.[56] Reproduced with permission of the American Institute of Chemical Engineers. Copyright © 1977)

increase as W increases. Even though W varied by a factor of 4, the data roughly fall on a single curve except near the very end of pressing. Fig. 80 is for nearly constant loads of grounds of different size[56]. P_T is larger for the larger particles except near the end of pressing. Fig. 81 is for two samples of drip-grind grounds, one containing water and the other 50% aqueous sugar solution. The ratio of P_T for grounds containing sugar solution to P_T for grounds containing water is 2.5:1 over most of the pressing range. Near the end of pressing it increases to 6:1. The viscosity of 50% sugar solution is roughly 15 times that of water at room temperature.

If P_T for spent grounds was significantly affected by flow pressure drop, ΔP_F, it would have increased when W increased and when particle size decreased. W had little effect on P_T and smaller particle sizes caused P_T to decrease except near the end of pressing. Therefore ΔP_F has little effect on the pressing of spent grounds except near the end of pressing. This can be reconciled with the large effect of viscosity on P_T, if part of P_S is caused by P_E, the excess hydraulic pressure inside the grounds. Larger P_E are required to force fluid out of grounds particles when viscosity is greater. Based on arguments advanced in Section 12, P_E should also be larger for larger grounds. Since larger P_T were caused by factors that increase P_E, pressing of spent coffee grounds is strongly affected by P_E and flow resistance inside particles. The increase in K_T caused by increases in -dZ/dt is probably partly caused by effects of -dZ/dt on internal flow and P_E. Increases in K_T as -dZ/dt increases have also been observed for spent sugar beet pulp and cranberries[113].

Like $\log(P_T)$, $\log(P_B)$ for spent grounds increases linearly as V_a decreases when P_F is small. $K_B \equiv -d\ln(P_B)/dV_a$ in the linear range of $\log(P_B)$ versus V_a plots. K_B for spent grounds are significantly larger than K_T and similarly increases as pressing speed (-dZ/dt) increases. The rapid final rise in both $\log(P_T)$ and $\log(P_B)$ occurs earlier, i.e at larger V_a, when larger -dZ/dt are used.

Final V_a: Table VII list V_a/V_C at $P_T = P_{max} = 11$ MPa, i.e. at the end of pressing, for spent grounds of different size and different pressing speeds[207].

Table VIII lists V_a/V_C when $P_T = P_{max} = 1.55$ MPa versus pressing speed for 3-mm cubes of Granny Smith Apples[138]. Though Granny Smith apples are

Table VII V_a/V_C at P_{max} = 11 MPa Versus Pressing Rate For Spent Coffee Grounds: $V_C = 2.65 \times 10^{-3}$ m^3/kg

Type of Coffee Feed	Pressing Speed (mm/min)						
	0.5	5	10	20	50	100	200
	V_a/V_C						
As-Is Drip Grind*	0.50	0.55 0.59	0.58 0.63	0.65 0.67	0.70 0.70	0.74 0.77	0.77 0.79
+16 mesh					0.69		
-16/+20 mesh		0.50	0.53 0.53	0.57	0.61 0.64	0.65	0.70
-20/+30 mesh					0.60		

* Mesh-based particle size distribution: +8, 1.1%; -8+16, 42.7%; -16+20, 32.1%; -20+30, 10%; -30+50, 7%; -50, 7.3%.

Table VIII - V_a/V_C at P_T = 1.55 MPa for Pressing of 3-mm cubes of Granny Smith Apples at Different Ram Speeds (Load: 40 grams)

Ram Speed mm/min	No. of Points	V_a/V_C $m^3/kg \times 1000$	$\sigma/(V_a/V_C)$
0.5	5	0.14	0.10
1	7	0.19	0.22
2	9	0.24	0.33
5	19	0.33	0.29
10	11	0.43	0.38
20	5	0.55	0.10
50	2	0.65	0.08
100	3	0.59	0.13
200	1	0.68	-

σ is the standard deviation for V_a/V_C at the given pressing speed.

usually rather firm, for this batch, Y_s was only 0.0235 kg FS/kg apple. Therefore their cell walls probably were very thin. $V_C = 40.22 \times 10^{-3}$ m^3/kg FS. The apples were diced by cutting them into 3-mm thick slices and pressing the slices through a screen with 3-mm square openings. Probably many cell walls ruptured and bonds between cells broke in the latter step.

Table VIII shows that V_a/V_C often vary substantially from run to run in sets of tests carried out at the same pressing speed. V_a/V_C for the Granny Smith apples are much smaller than V_a/V_C for spent grounds at the same pressing speed, but for apples, ratios of V_a to V_S, the specific volume of the fixed solids, are much larger than V_a/V_S for spent coffee grounds.

Values of V_a/V_C for some other materials[56,113,138,211] at $P_T = 1.1$ MPa and different pressing speeds are listed in Table IX. For comparison purposes Table IX also contains values obtained by interpolation from runs used to obtain data listed in Table VIII.

Note: $V_a/V_C = 0.62$ at 1.55 MPa and $-dZ/dt = 2.54$ mm/min for Granny Smith apples for which $Y_S = 0.064$ and which had been sliced into 10-mm square, 2-mm thick slabs using a very sharp rotating slicer[208]; V_a/V_C was much lower for diced Granny Smith apples that had thinner and more extensively ruptured cell walls. Since juice yield increases as V_a/V_C decreases, this V_a/V_C difference illustrates the importance of cell wall rupture or rupturability.

The differences between the two sets of results for sugar beets indicates that media resistance can significantly affect V_a/V_C and juice yield.

Relaxation: P_T falls rapidly after the ram stops at $P_T = P_{max}$, but P_T's rate of fall progressively decreases as t, increases, and P_T ultimately asymptotically approaches a fully relaxed value, P_{TR}. $\boldsymbol{P} = (P_T - P_{TR})/(P_{max} - P_{TR})$ is the normalized pressure change during relaxation. Fig. 82 contains plots of $\log(\boldsymbol{P})$ versus $t_r^{1/3}$ for spent grounds. After small time lags, $\log(\boldsymbol{P})$ decreases linearly as $t_r^{1/3}$ increases. Similar $\log(\boldsymbol{P})$ versus $t_r^{1/3}$ behavior is observed with other cellular biological materials, e.g. apples, alfalfa, olive paste. For spent grounds, $-d[\log(\boldsymbol{P})]/dt_r^{1/3}$ is roughly inversely proportional to $(V_o - V_a)$, and is smaller for larger sized grounds and for grounds that contain 50% sucrose solution instead of water.

Table IX - V_a/V_C at P_T = 1.1 MPa for Pressing of Various Feeds at Different Ram Speeds

Material	Y_S	-dZ/dt mm/min	2.54	7.62	25.4	76.2
		Media	V_a/V_C			
Casein curds	0.35	NC	0.40	0.44	0.53	
Sugar Beets	0.133	NC	0.26	0.41	0.60	0.64
Sugar Beets	0.10	FP		0.57*	0.64*	
Cranberries	0.105	NC	0.30	0.34	0.56	
Red Delicious Apples	0.055	NC	0.42	0.49	0.55	
Granny Smith Apples	0.024	FC	0.25*	0.38*	0.57*	0.65*
Granny Smith Apples	0.064	NC	0.62			
McIntosh Apples	0.045	NC	0.34			
Golden Delic. Apples	0.056	NC	0.67			

* Interpolated using V_a/V_C obtained at slightly different -dZ/dt

NC = Monofilament nylon with 0.5 mm openings,

FP = Whatman No. 4 Filter paper, FC = Fine mesh filter cloth

As P_T relaxes, P_F in some parts of cakes of spent grounds sometimes rises initially, then declines slowly[207]. ΔP_m decays gradually, even though outflow apparently stops as soon as the ram stops moving. If the ram is restarted during relaxation, P_T rises rapidly and returns to P_{max} after a very small decrease in V_a.

Even though the shape of $\log(P_T)$ versus V_a curves differed widely during ram movement for spent coffee grounds, apples and sugar beets, $\log(P_{TR})$ for each of these materials obeyed the following equation.

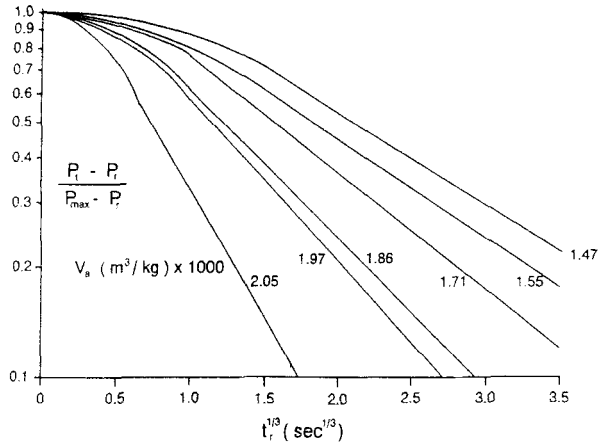

FIGURE 82 log(*P*) versus $t^{1/3}$ for spent coffee grounds at different final V_a (Schwartzberg[85]. Reprinted by permission of Van Nostrand Reinhold, copyright © 1983)

$$\ln\left[\frac{P_{TR}}{P_{ref}}\right] = K_R(V_{ref} - V_a) \qquad \textbf{(106)}$$

This occurred even in plateau regions of log(P_T) versus V_a plots for apples.

Pressure Components: Fig. 83 depicts semi-log plots of P_T, P_B and ΔP_m versus V_a for spent drip-grind coffee grounds at -dZ/dt of 5 mm/min and 200 mm/min. The particle-size distribution of the grounds is given at the bottom of Table VII. Data are shown only at V_a where ΔP_m were significant. Similar curves were obtained at other -dZ/dt. $(\Delta P_F)_C$, the total fluid pressure drop across the cake $= P_F(0) - P_F(W)$. At high -dZ/dt, $(\Delta P_F)_C/\Delta P_m \approx 0.1$ when P_T reached P_{max}; $(\Delta P_F)_C/\Delta P_m \approx 0$ at low -dZ/dt. Therefore for these spent grounds, the total fluid pressure drop, $P_F(0)$, was only slightly greater than ΔP_m. $P_F(0)/P_T$ increased markedly as the end of pressing approached. At the end of pressing, $P_F(0)/P_T \approx 0.32$ when -dZ/dt = 5 mm/min. $P_F(0)/P_T \approx 0.50$ when -dZ/dt = 200 mm/min. In both cases, almost all the fluid pressure drop was across the media and not across the cake. Use of -16 + 20 mesh spent grounds instead of

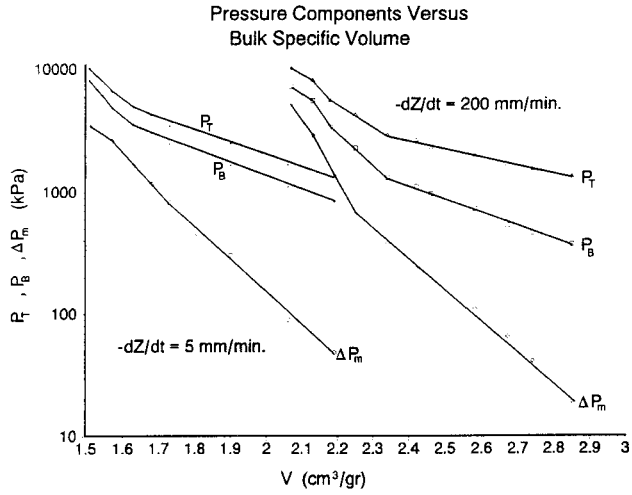

FIGURE 83 $\log(P_T)$, $\log(P_B)$ and $\log(\Delta P_m)$ versus V_a for constant-rate pressing of spent coffee grounds at 5 mm/min and 200 mm/min (Schwartzberg et al.[136])

as-is spent drip-grind coffee reduced both $P_F(0)$ and ΔP_m 60% at -dZ/dt = 200 mm/min, and reduced them 90% at -dZ/dt = 5 mm/min. When -20+30 mesh spent grounds were pressed at 50 mm/min, $P_F(0)$ and ΔP_m were 97% lower than $P_F(0)$ and ΔP_m for as-is spent drip-grind coffee pressed at the same speed.

It will be shown later that measured ΔP_m for apples probably include parts of sharp P_F rises that occur near outflow media. Therefore measured ΔP_m for apples will be called apparent ΔP_m or $(\Delta P_m)_{app}$. Fig. 84 depicts a semi-log plot of P_T, $(\Delta P_m)_{app}$ and $P_F(Z - 2)$ versus V_a for Granny Smith Apples at -dZ/dt = 50 mm/min. $P_F(Z - 2)$ is P_F at 2 cm above the media. Since these apples extruded through the media at $P_T > 1.55$ MPa, P_{max} was set at 1.55 MPa. At the end of pressing, $P_F(Z - 2) \approx P_T$ and $(\Delta P_m)_{app} \approx 0.8 \cdot P_F(Z-2)$; further $P_F(Z - 2) \approx P_T$ over much of the region of sharp P_T rise. P_F at 1 cm above the media was only very slightly greater than $(\Delta P_m)_{app}$. Therefore $P_F(Z - 2) \approx P_F(0)$, i.e. P_F at the ram. $P_F(0)$ was measured directly for constant-rate pressing of several types of apples[208], cranberries, casein curds and sugar beet pulp[113]. For these

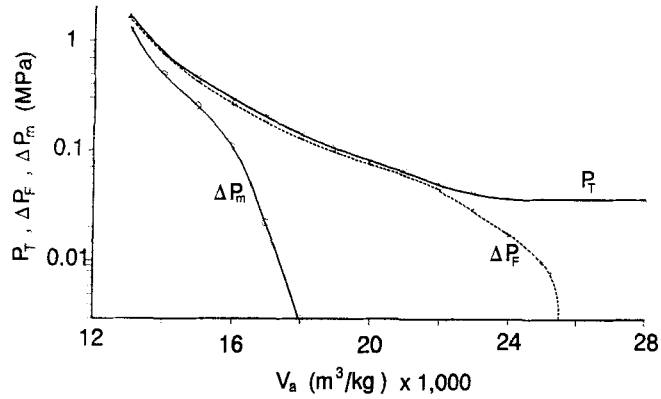

FIGURE 84 $\log(P_T)$, $\log(\Delta P_F)$ and $\log(\Delta P_m)$ versus V_a for pressing of a 40-gram sample of 3-mm Granny Smith apple cubes at a constant-rate of 5 mm/min (Schwartzberg et al.[214])

materials, $P_F(0)/P_T$ at the end of pressing ranged between 0.72 and 0.98. Once $(\Delta P_m)_{app}$ for these materials started to rise, $(\Delta P_m)_{app}/P_F(0)$ increased as V_a decreased. Therefore, $(\Delta P_m)_{app}$ are much more important for these materials than ΔP_m is for spent coffee grounds, particularly grounds that do not contain fines.

While apparent $(\Delta P_m)_{app}$ are often large at the end of pressing for fruit- and vegetable-based presscakes, ΔP_m were negligibly small for sugar beet strips that had been simply extracted at 55°C and for certain apples with very thick cell walls. At the end of pressing, $P_F(0)/P_T \approx 0.2$ for sugar beets that had been simply extracted at 55°C, and $P_F(0)/P_T \approx 0.1$ for diced apples with very thick cell walls. While $P_F(0)/P_T$ at the end of pressing was small and $(\Delta P_m)_{app}$ was negligible for sugar beet strips extracted at 55°C; for similar strips that had been cooked at 100°C, $P_F(0)/P_T$ at the end of pressing ≈ 0.8, and 90% of the fluid pressure drop apparently occurred across the outflow media. Cooking at 100°C converts protopectin that bonds cells together into soluble pectin which has little or no bonding power. Therefore susceptibility to high $(\Delta P_m)_{app}$ may depend on the weakness of bonding between cells.

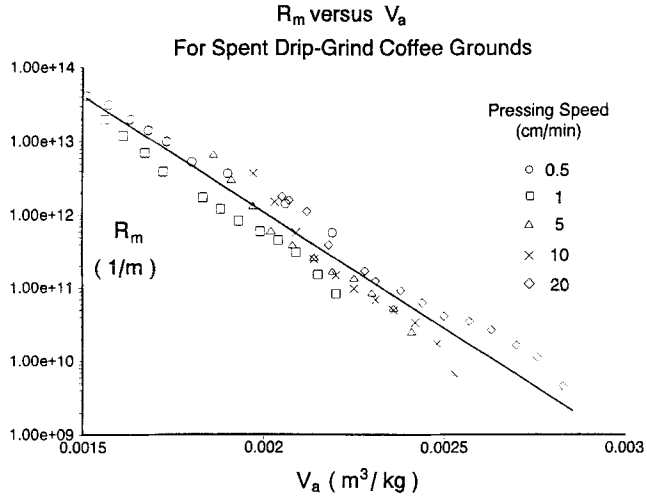

FIGURE 85 Log R_m versus V_a during constant-rate pressing of spent coffee grounds at different speeds (Schwartzberg et al.[136])

Media Resistance - Spent Grounds: $R_m = \Delta P_m/[\mu \cdot (-dZ/dt)]$ during pressing. Measured ΔP_m at series of V_a were used to calculate R_m for spent drip-grind coffee at each -dZ/dt tested. Whatman No. 4 filter paper was used as the media. Log(R_m) is plotted versus V_a in fig. 85 for these -dZ/dt. The data all fall roughly on a single straight line and are correlated in terms of V_a by

$$R_m = 1.38 \times 10^{18} \cdot \exp[-7,016 \cdot V_a] \qquad \textbf{(107)}$$

where the units are m^3/kg for V_a and 1/m for R_m. Correlation of R_m in terms of P_s(W) can be ruled out, because very different R_m were obtained at equal values of P_s(W). Local compaction data show that V(W) was proportional to V_a. Therefore R_m might truly depend on V(W) instead of V_a.

By changing numerical factors, the exponent in Eq (107) can be written in terms of (V_c - V_a) instead of V_a. $W \cdot (V_c - V_a)$ = the volume of outflow per unit of media area. Therefore for spent coffee grounds pressed over filter paper, R_m may be a function of the volume of fluid expelled unit area, or of the amount of sediment deposited on the media by expelled fluid. Log(R_m) often increases

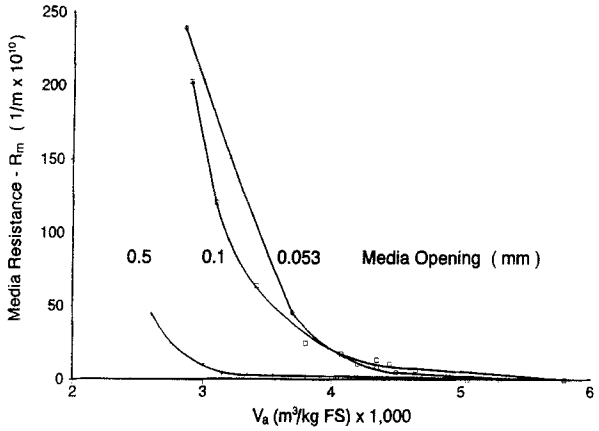

FIGURE 86 R_m versus V_a for cranberries pressed over media with three different pore sizes; pressing speed: 2.54 mm/min. (Rebouillat[213])

linearly as filtrate volume increases during pad filtration of wines[212]. The filter paper used when pressing spent grounds may have behaved like such pad filters. If so, R_m may depend on the amount of migratable fines expelled from spent grounds and on how effectively a press cake filters out such fines. Variation in migratable fines content and efficiency of fines removal by cakes may be reasons why R_m for spent coffee grounds varied with particle size and particle-size distribution.

Media Resistance - Media Pore Size: R_m for cloths can depend strongly on cloth pore size. Fig. 86 depicts R_m versus V_a for cranberries pressed at 2.54 mm/min using as media monofilament nylon cloths with opening sizes of either 0.053 mm, 0.1 mm or 0.5 mm[213]. Use of the greatest opening size greatly reduced R_m. $P_F(0)/P_T \approx 0.7$ at the end of pressing when the cloth with 0.5 mm opening was used, but only 2% of the fluid pressure drop occurred across the media.

Apparent Media Resistance - Apples: As previously noted, $(\Delta P_m)_{app}$ for apples probably are much larger than actual ΔP_m. The $(R_m)_{app}$ discussed in this section are based on measured $(\Delta P_m)_{app}$, and probably are often larger than true R_m.

For diced apples pressed at different constant speeds over nylon cloth with 0.5-mm openings, $(R_m)_{app}$ were negligible until $P_S(W)$ reached a critical value P_c, but rose very rapidly once P_c was reached[208,214]. P_c for any given type of apple appears to be independent of pressing speed, but is different for each type of apple. P_c also depends on cell wall thickness, tissue strength and method of dice preparation. For Granny Smith apples with thin walls, $P_c \approx$ 200 kPa; for Red Delicious apples with thick walls, $P_c \approx 460$ kPa; and for Granny Smith Apples with thick cell walls, $P_c > 1550$ kPa.

As $P_S(W)$ approaches P_c, $P_S(W)$ often almost equals $(\Delta P_F)_C$ the fluid pressure drop across the cake. $(\Delta P_F)_C$ tends to be proportional to -dZ/dt. Therefore P_c is reached earlier and V_b, the value of V_a at which $P_S(W) = P_c$, increases as -dZ/dt increases.

For some very firm apples with thick cell walls, R_m remained negligibly small during the entire course of pressing; but for most apples, after an initial period of slow increase, $(R_m)_{app}$ increased linearly as $(V_b - V_a)$ increased. Sugar beets and cranberries exhibited similar behavior. Based on relatively limited data, $(R_m)_{app}$ for most apples was reasonably well correlated by Eq (108) over the entire range of $(R_m)_{app}$ increase.

$$(R_m)_{app} = R_a \exp [K_r (V_b - V_a)] - R_b \quad \text{for } V_a < V_r \quad \textbf{(108)}$$

R_b, R_a and K_r are properties of the cake and media involved. As $(\Delta P_m)_{app}$ and $(R_m)_{app}$ for apples increased, apparent fluid pressure drops, $(\Delta P_F)_C$, across apple press cakes levelled off or rose at a progressively decreasing rate. $(\Delta P_F)_C$ levelled off very rapidly at high pressing speeds, and progressively less rapidly as pressing speed decreased[208,214].

Extrusion: Materials for which $(\Delta P_m)_{app}$ was large often extruded at some critical value of P_T or ΔP_m when large-pored media were used. When media with 0.5 mm pores was used[208], McIntosh apples extruded when $P_T = 545$ kPa, Red Delicious apples extruded at 752 kPa and Golden Delicious at 1090 kPa. ΔP_m was negligible for Granny Smith apples with thick walls; and they did not extrude at $P_T = 1550$ kPa. The deformability modulus, compressive yield strength and juice viscosity of these apples were examined to see which related

most strongly with extrudability. In most cases, but not all, extrudability increased as yield strength went down. In all cases, extrudability increased as juice viscosity went up. High viscosity in apple juice is usually caused by conversion of protopectin to soluble pectin. Such conversion weakens bonds between adjacent cell walls. This suggests that cakes extrude more readily when bonding between cells is weak.

Wall Friction: ΔP_w, the decrease in P_S due to wall friction, $= (P_T - P_B)$. For spent coffee grounds pressed by a 25 mm ram, $\Delta P_w \approx 0.8 \cdot P_T$ near the start of pressing; at the end of pressing $\Delta P_w \approx 0.22$ to $0.30 \cdot P_T$. ΔP_w steadily increased as V_a decreased, but P_B and P_T increased more rapidly. When P_F was negligible for spent grounds, $\ln(P_T/P_B)$ obeyed an integrated form of Eq (31)

$$\ln\left[\frac{P_T}{P_B}\right] = \ln\left[\frac{P_S(W) + \Delta P_w}{P_S(W)}\right] = \frac{4Bf_w}{D}\int_0^W V\,dw = \frac{4Bf_wZ}{D} \quad \textbf{(109)}$$

or

$$\Delta P_w = P_B\left[\exp\left(\frac{4Bf_wZ}{D}\right) - 1\right] = P_T\left[1 - \exp\left(-\frac{4Bf_wZ}{D}\right)\right] \quad \textbf{(110)}$$

For spent grounds, $B \cdot f_w$ remained constant as Z decreased at any given pressing speed, but increases as speed increased and was correlated by Eq (111).

$$B \cdot f_w \approx 0.1048 + 0.679\,(-dZ/dt)^{1/2} \quad \textbf{(111)}$$

ΔP_w was significant only at the start of pressing for apples.

Local V: Local V were measured by photographing sections of cake during pressing tests carried out in a transparent cell[85,207]. The sections were separated by thin, highly reflective perforated aluminum sieve plates, as shown in fig. 87. Heights $(\Delta z)_i$ of cake section i on time-lapse photographs were determined by measuring distances between the plate surfaces bounding section i. V_i, the specific volume in section i, $= (\Delta z)_i/(\Delta w)_i$, where $(\Delta w)_i$ was the w increment in section i. All $(\Delta w)_i$ were equal. Fig. 88 depicts V_i/V_o in

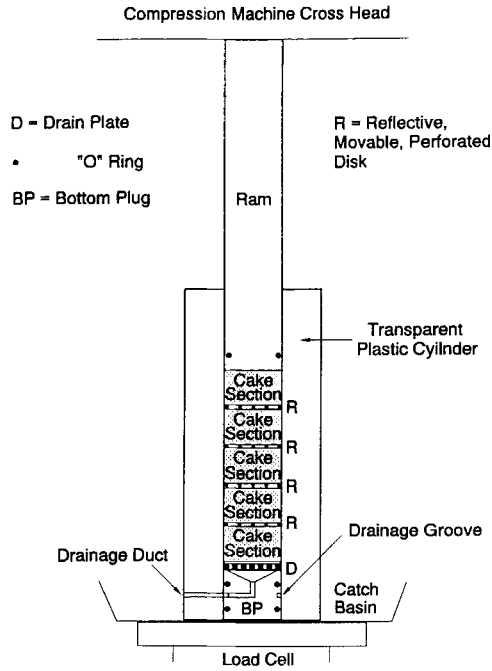

FIGURE 87 Cell for measuring local V (Schwartzberg[85]. Reprinted by permission of Van Nostrand Reinhold, copyright © 1983)

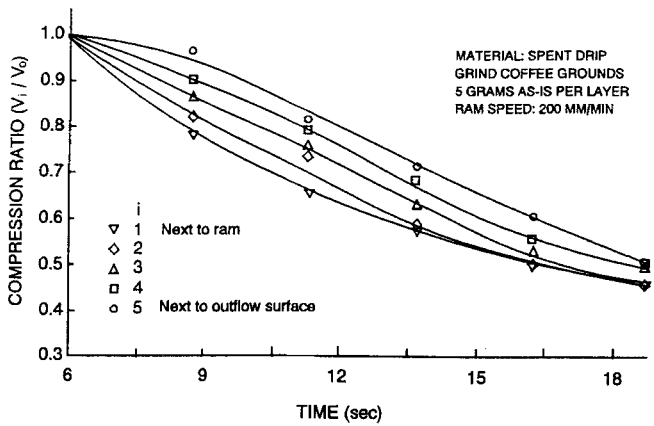

FIGURE 88 V/V_o versus t during constant rate pressing of spent coffee grounds at 200 mm/min (Huang[207])

five, equal Δw layers of spent grounds during pressing at -dZ/dt = 200 mm/min. i = 1 at the ram surface; and i = 5 is at the outflow surface. After startup transients died out, V_i/V_o for spent grounds decreased in roughly parallel fashion in all layers as pressing proceeded. V_i/V_o was smallest at i = 1 and progressively increased as i and w/W increased. Near the end of pressing, the V_i/V_o converged slightly when -dZ/dt = 200 mm/min. Similar plots were obtained at lower -dZ/dt; but at -dZ/dt < 200 mm/min, the V_i/V_o remained parallel until the end of pressing. V_i/V_o did not change detectably as P_T relaxed after the ram stopped. Further, cakes of spent grounds expanded only slightly when pushed out of a test cylinder. $V_5 \approx V(W)$ near the end of pressing. V_5 was approximately 0.0004 m^3/kg larger than V_a at all -dZ/dt, whereas numerical solutions of Eq (21) indicate that V(W) should have been 0.00023 m^3/kg larger than V_a. Differences between computed and experimental $[V(W) - V_a]$ may be due to f_w being larger in the plastic cell where V(W) were measured than in the metal cell where ΔP_w were measured.

Fig. 89 is a V_i/V_o plot for Granny Smith apple cubes[138]. Initially V_1 decreased most rapidly and was smaller than all other V_i. The situation changed soon, and V_5 became the smallest V_i. This occurred because effects of wall friction dominated at the start of pressing, but $(\Delta P_F)_C$ soon rose, causing P_S rises and greater cake compaction near the outflow surface.

Local U: U_i, U at the downflow surface of slice i is

$$U_i = (\Delta w) \cdot \sum_{j=1}^{i} \left[\frac{\partial V_j}{\partial t} \right] \qquad \textbf{(112)}$$

$\partial V_i/\partial t$ obtained from time-lapse data used to prepare fig. 88 and similar figures for other -dZ/dt were used to compute U versus w. U versus w/W curves for spent grounds during outflow are plotted in fig. 90 for the tested -dZ/dt. At -dZ/dt < 100 mm/min, U increased linearly as w/W increased; but at higher -dZ/dt, U curved upward slightly at w/W close to 1.0 . Local U versus w/W behavior for Granny Smith apples was similar to that for spent grounds; but for Granny Smith apples, U versus w/W curves started to curve upward at -dZ/dt $\geq$ 20 mm/min.

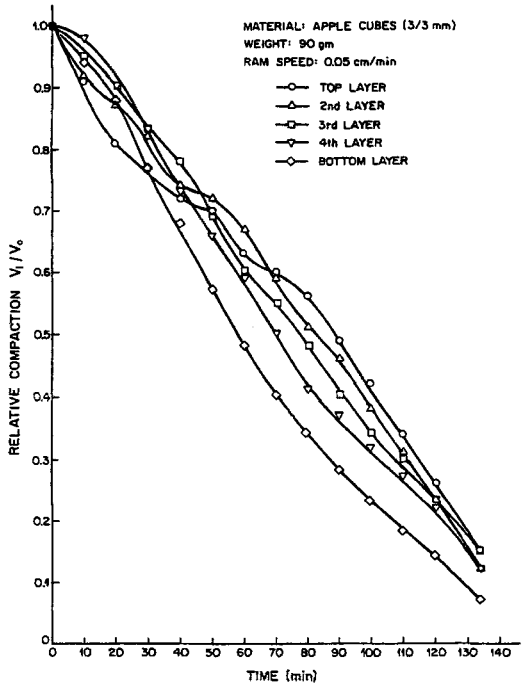

FIGURE 89 V/V_0 versus t during constant-rate pressing of Granny Smith apples at 0.5 mm/min (Vallon et al.[138])

Filtration Resistance: Pollak[215] used standard, compression-permeability techniques[59] to measure α_a versus V_a for spent grounds. Fig. 91 is a semi-log plot of his α_a versus V_a data. Pollak assumed that R_m was the same as R_m measured without cake present. However R_m increases markedly during pressing when cake is present. Therefore the original α_a in fig. 91 were corrected. $\alpha_{corr} = \alpha_a - R_m/W$. The correction is significant only at small V_a. Assuming that local α versus V behavior is the same as corrected α_a versus V_a behavior

$$\alpha = 8.0 \times 10^9 + 2.0 \times 10^{13} \cdot \exp[-2300 \cdot V] \qquad \textbf{(113)}$$

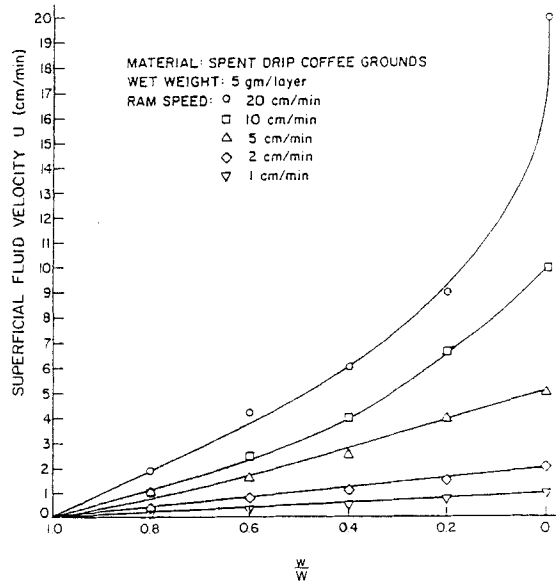

FIGURE 90 U versus w/W during constant rate pressing of spent coffee grounds at different speeds (Huang[207])

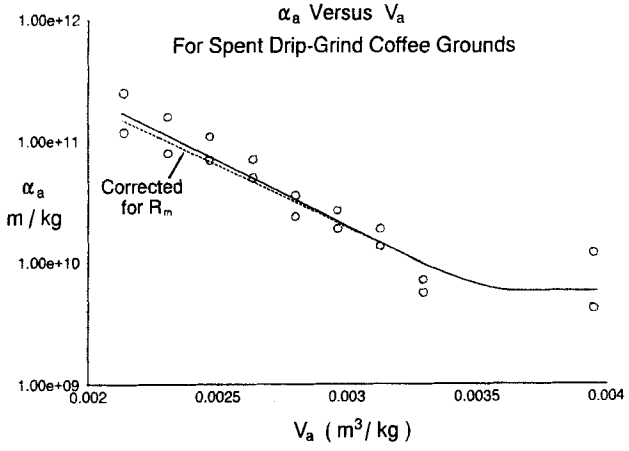

FIGURE 91 Log α versus V plot for spent, drip-grind coffee grounds based on Pollack's data (Pollack[215], Schwartzberg et al.[136])

Huang[207] using the same experimental method and similar spent grounds obtained significantly higher values of α_a at low V_a.

α for a number of cellular biological solids were correlated by Eq (114).

$$\alpha = \alpha_o \exp\left[\frac{B_C}{V^n}\right] + \alpha_b \qquad (114)$$

For example, compression permeability data for diced Granny Smith apples with thin cell walls[138] appeared to be reasonably well fitted by using $\alpha_o = 4\times10^9$ m/kg, $\alpha_b = -2\times10^{10}$ m/kg, n = 1.4 and $B_c = 0.005$ $(m^3/kg)^{1.4}$.

Summary: Log(P_T) and log(ΔP_f) versus V_a plots for constant-rate pressing of non-biological solids are often straight over much of the V_a range involved; and in the straight-line range, plots obtained at different pressing speed are usually parallel. P_T and ΔP_F are simply higher at higher pressing speeds. Even though the plots are straight and parallel, C for these materials often does not remain constant as V changes.

Log (P_T) and log(ΔP_f) versus V_a plots for constant-rate pressing of biological solids behave very differently from those of non-biological solids. If nearly straight plots are obtained, their slopes change as pressing speed increases. Plots for biological materials may also have two branches: one at high V_a, where log(P_T) rises relatively slowly as V_a decreases, and one at smaller V_a, where log(P_T) rises very rapidly. Such curves shift to larger values of V_a when pressing speed increases. The first type of curve, i.e. nearly straight log(P_T) versus V_a plots, occurs for materials like spent coffee grounds, with cells with thick, strong walls. For such materials, ΔP_F across presscakes is often small during constant-rate pressing and P_S is the dominant factor affecting P_T. P_S depends on excess internal fluid pressure, P_E, which, in turn, is strongly affected by pressing rate.

Two-branched curves are obtained for materials with ruptured cell walls (e.g. milled apples, and olive paste), cell walls that rupture easily or which have a tissue structure that provides low flow resistance (e.g. diced apples with thin cell walls). For such materials, P_F is relatively large, particularly during the late stages of constant-rate pressing. P_S becomes large near the outflow surface

because fluid pressure drop across the cake acts to increases solid stress there. Effects of P_E on P_S are more difficult to detect for such materials and may be negligibly small at the end of pressing. Intermediate types of behavior occur. Whether a material behaves more like coffee grounds or more like milled apples depends on the strength and intactness of its cell walls. Materials that behave more like coffee grounds can be converted into materials which behave more like milled apples by treatments that rupture of weaken cell walls.

A third type of behavior occurs when curds are pressed at constant rate. P_E and ΔP_F across the cake are small when pressing starts, but rise rapidly. Particles fuse together as pressing proceeds. Interparticle pores progressively disappear after this happens. Finally, flow occurs within a continuous fine-pored matrix, and P_E and P_F become indistinguishable. Sometimes $\Delta P_F = 0.98P_T$ at late stages of pressing. $P_S(0)$ rises near the end of pressing. Therefore $\Delta P_F/P_T$ may then fall somewhat near the end of pressing[152], even though ΔP_F continues to rise.

Pressure drop across media and media resistance, R_m, apparently increase markedly during pressing and exert more influence on pressing behavior and ram pressure than is usually acknowledged. Two types of R_m behavior have been observed; other types may well occur. In one of the observed types, fine-pored media are plugged by fines expelled from cake particles. In the other type, coarse-pored media may be partially plugged by pressing of soft cake particles into media pores. Partial plugging or apparent plugging is followed by less well-defined events that cause apparent media resistance to increase rapidly. The second type of behavior is often associated with extrusion of cake at high pressures and two-branched $\log(P_T)$ versus V_a curves; and may be largely responsible for the rapid increases in P_T in the steep branch.

Wall friction greatly affects the pressing behavior of some materials and has to be adequately accounted for in analyzing pressing test results.

14. ANALYSIS: CONSTANT-RATE PRESSING

Apples and spent coffee grounds provide polar examples of types of pressing behavior encountered with cellular biological solids. Therefore,

constant-rate pressing of these materials will be analyzed in depth in this section. Constant-rate pressing for olive paste will also be discussed.

14A. CONSTANT RATE PRESSING OF APPLES

Apple cells usually have thin walls, large amounts of space between them, and separate from one another fairly readily. Therefore fluid can escape from apple tissue quite easily, and only small excess internal hydraulic pressures, P_E, develop during pressing. Therefore analysis of constant-rate pressing of apples should provide information about factors underlying the pressing behavior of cellular biological materials from which fluid escapes fairly readily.

Eq (48) to (54) were numerically solved[214] for constant-rate pressing of 0.3-mm Granny Smith apple cubes using candidate $P_S(V)$ and $\alpha(V)$ functions and different methods of accounting for R_m. Since the apples in question contained only 0.0235 kg FS/kg apple, their cell walls were very thin. Further, the cubes were formed by methods that caused considerable cell wall rupture. Because $B \cdot f$ was small, a constant $B \cdot f$ was assumed; initially $B \cdot f = 0.05$, was used. $\mu \approx 3$ cps.

Initial Modelling of R_m: Eq (108) was initially used to correlate R_m. For the Granny Smith apples in question it appeared that $R_b \approx 1 \times 10^{10}$/m and that $R_a \approx 3.7 \times 10^{10}$/m; but to fit experimental $(\Delta P_m)_{app}$ well with Eq (108), a K_r that decreased as pressing speed increased had to be used. There is no satisfactory reason for why K_r should decrease this way. As noted before, Eq (108) may be unreliable because steep P_F gradients near outflow surfaces make it difficult to measure ΔP_m correctly for apples.

Modelling $P_S(V)$: The curves in Fig. 74, which depicts $\log(P_T)$ versus V_a behavior at different -dZ/dt for the Granny Smith apples being considered, contain: a) a plateau region at large V_a, where P_T has a low, almost constant value, P_L; and b) a region at lower V_a where P_T rises very sharply as V_a decreases. There is also a third region, not shown, at V_a close to V_o, where $P_F = 0$ and P_T rises fairly sharply from 0 to P_L. To account for this initial rise in

P_T, it was assumed that: $P_S = P_L(V_o - V)/(0.19V_o)$ for $V > V_i = 0.81V_o$. Use of this assumption does not effect predicted conditions at the middle and end of pressing.

P_L is higher at higher -dZ/dt, even though $P_F = 0$ in that region. The measured variation of P_T with -dZ/dt in the plateau region was fairly well accounted for by assuming $P_L = 25{,}000 + 1.2\text{x}10^6(\text{-dZ/dt})^{0.5}$.

It is difficult to determine stable time steps for numerical computation when $dP_S/dV = 0$, i.e. when P_S remains absolutely flat as V decreases. Further, V cannot be determined precisely from P_S in such cases. To circumvent these difficulties, $P_S(V)$ were used that provided slight increases in P_S as V decreased in the plateau region[214], i.e. $P_S = P_L + 500{,}000(V_i - V)$ for $V_T < V < V_i$. P_S increases slightly as V decreases in the plateau region for firmer apples, and the rate of increase increases slightly as -dZ/dt increases.

Behavior of P_T at very low pressing speeds was used to infer how P_S behaved as V changed. The P_T versus V_a curve for pressing at -dZ/dt = 0.5 mm/min showed that P_S remained quite small and scarcely rose until V_a reached a critical value, V_T, ≈ 0.012 m^3/kg; then P_S rose quite rapidly. To provide for continuity in P_S at V_T and rapid rises in P_S as V decreased below V_T, it was assumed that: $P_S = P_L + 500{,}000(V_i - V_T)\cdot\exp[K(V_T - V)]$ for $V < V_T$. K ranging between 400 and 650 kg/m^3, were used in numerically solving Eqs (48) to (54).

Initial Modelling of $\alpha(V)$: Initially, $\alpha(V)$ was based on $(\Delta P_F)_C$ and V_a measured just before $(\Delta P_m)_{app}$ started to rise. These $(\Delta P_F)_C$ versus V_a data appeared to be well fitted by

$$\alpha = \alpha_b + \alpha_o \exp(-GV) \qquad (115)$$

where $\alpha_o \approx 2\text{x}10^{13}$ m/kg, $\alpha_b \approx 4\text{x}10^9$ m/kg and $G \approx 400$ kg/m^3.

Initial Results: Eqs (48) to (54) were numerically solved using the cited B•f, $\alpha(V)$, $P_S(V)$ and function for R_m. Eleven, equally-spaced nodes between w = 0 (node 1) and w = W (node N) were used. Solutions provided $\partial V/\partial t$ at each node. The values of $\partial V/\partial t$ were used in Eq (55) and Eq (58) respectively to

determine U and V at each node. The V at the nodes were suitably averaged to obtain V_a. P_S at each node was obtained from $P_S(V)$, i.e. P_S at node I = $P_S(V_I)$. α_m, mean α in gaps between nodes, were obtained by substituting the average of V for adjacent nodes in $\alpha(V)$. $P_F(N) = \Delta P_m = \mu R_m(-dZ/dt)$. P_F at the other nodes were calculated by using Eq (57). The ram pressure, P_T, = $P_S(1) + P_F(1)$. Different, but previously described, computational procedures were used at the start of pressing when the cake was not yet fully saturated and juice outflow did not occur.

Predicted V_a at P_T = 1.55 MPa were computed for each of the -dZ/dt listed in Table VIII. Deviations between these V_a and the experimental V_a listed in Table VIII were used to determine σ_{ov} the overall, root-mean-square percent deviation between experimental and predicted V_a. The parameters affecting $\alpha(V)$, $P_S(V)$ and R_m were then adjusted so as to minimize σ_{ov}. The best fit (σ_{ov} = 8.3%) in terms of the chosen function was obtained when $\alpha_o = 2.1 \times 10^{13}$ m/kg, $\alpha_b = 4 \times 10^9$ m/kg and G = 240 kg/m^3 and Eq (108) was used with the previously listed R_a and R_b and K_r = 2546 - 762,000(-dZ/dt); but the computed ΔP_m were less than the experimental $(\Delta P_m)_{app}$. However, the sum of the computed ΔP_m and ΔP_F for the internodal space adjacent to the outflow surface, i.e. $\Delta P_m + [P_F(N-1) - P_F(N)]$, roughly equaled $(\Delta P_m)_{app}$. Based on Δw and V at w = W at the end of pressing, the internodal space next to W was roughly 1 mm wide, which is roughly equal to the diameter of the pressure port used to measure ΔP_m. Therefore it appeared likely that $(\Delta P_m)_{app}$ might include all or part of ΔP_F across the layer of press cake immediately adjacent to the outflow surface.

Revised Modelling: To determine whether large P_F gradients close to the outflow surface could completely account for $(\Delta P_m)_{app}$, other calculations were carried out in which R_m was assumed to be zero. Use of Eq (115) for α did not provide good V_a agreement when R_m = 0. $\alpha(V)$ based on Eq (114) were used and provided better agreement.

Trial-and-error solutions of Eqs (48) to (54) were used to find best-fit parameter values for $P_S(V)$ and for Eq (114). Parameters were selected not

Table X Predicted and Experimental Final V_a at P_T = 1.55 MPa for 0.3-mm Granny Smith Apple Cubes that contain 0.0235 kg FS/kg apples

-dZ/dt (mm/min)	0.5	1	2	5	10	20	50	200
No. Data Points	5	7	9	19	11	5	2	1
$V_a m^3/kg \times 1000$	5.7	7.8	9.6	13.2	17.2	22.1	26.0	27.3
σ_V/V_a	0.1	0.2	0.3	0.3	0.4	0.1	0.1	-
Predicted V_a	6.5	7.4	9.1	13.7	17.2	21.1	25.0	28.4

only to minimize σ_{ov}, but also to provide log(P_T) versus V_a curves of proper shape. The latter objective was satisfied by obtaining differences between predicted V_a values at P_T = 200 kPa and 1.55 kP_a that averaged 0.003 m^3/kg, the corresponding average experimental V_a difference. At the best fit found by trial and error: σ_{ov} = 6.4%, $a_o = 4.8 \times 10^8$ m/kg, $a_b = 8.24 \times 10^9$ m/kg, n = 0.59, B_c = 0.553, V_T = 0.0119 m^3/kg, B·f = 0.046 and K = 610 kg/m^3. V_a computed using these parameters and corresponding experimental V_a for P_T = 1.55 MPa are compared in Table X and for the full range of -dZ/dt tested.

Agreement between experimental and predicted V_a is very good except for the slowest pressing speeds tested, where fair agreement is obtained. Fig. 92 shows log(P_T) versus V_a plots based on the calculated data. It compares favorably with the corresponding experimental plot, fig. 74. Fig. 93, plots of P_F versus w and z at the end of pressing, shows how rapidly P_F rises near the outflow surface. Fig. 94 shows that sharp changes in V and α also occur near the outflow surface.

Parameters that minimized σ_{ov} could be obtained when larger n were used in Eq (114), but these produced greater differences between the predicted and experimental shapes of curve log(P_T) versus V_a curves, i.e. the ΔV_a criterion was not satisfied. The ΔV_a criterion also was not satisfied when Eq (108) was

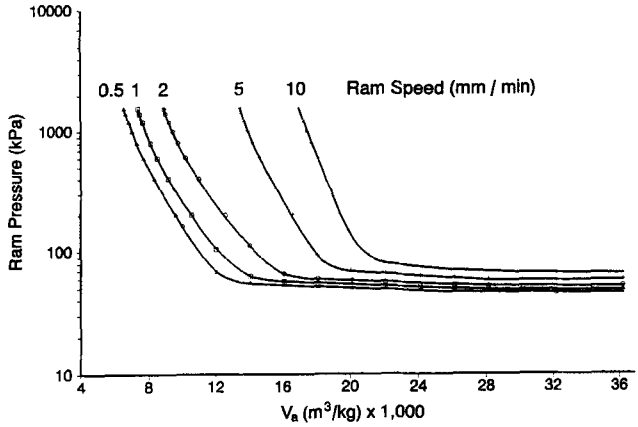

FIGURE 92 Computed plots of log(P_T) versus V_a at different -dZ/dt for Granny Smith apples containing 2.35 % fixed solids (Schwartzberg et al.[214])

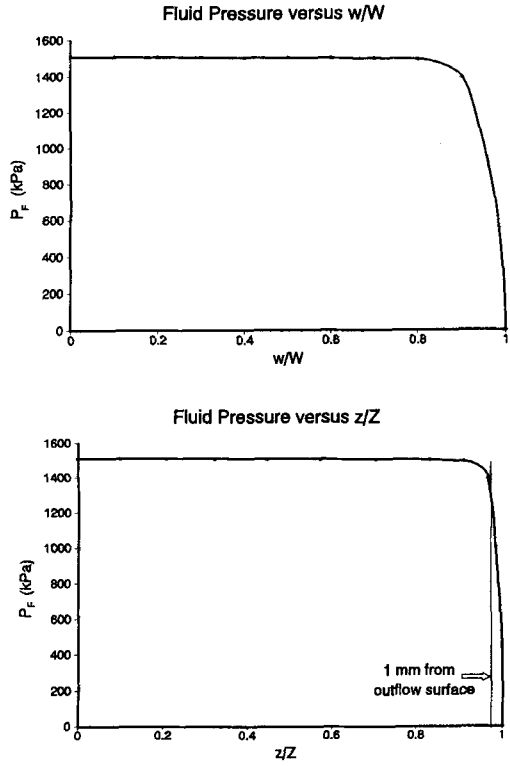

FIGURE 93 P_F versus w/W and z/Z at the end of constant-rate pressing of Granny Smith apples; pressing speed: 0.5 mm/min (Schwartzberg et al.[214])

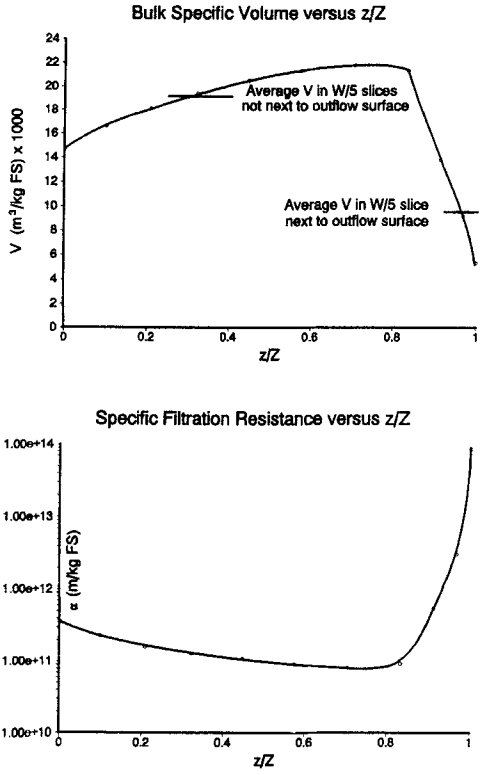

FIGURE 94 V and α versus z/Z at the end of constant-rate pressing of Granny Smith apples; pressing speed: 0.5 mm/min (Schwartzberg et al.[214])

used to obtain R_m and Eq (115) was used to provide α. Use of R_m = 0 and n = 0.59 not only provided curves of correct shape, it also provided the lowest σ_{ov} found.

Predicted $(\Delta P_F)_C$ and ΔP_m: As previously noted, at and near the end of pressing, the Nth Δw slice is roughly as thick as the pressure sensing port. Therefore $(\Delta P_m)_{app}$ may well be approximately equal to $\Delta P_m + [P_F(N-1) - P_F(N)]$, where $P_F(N)$ and $P_F(N-1)$ respectively are the P_F at nodes N and N-1. When the true $\Delta P_m = 0$, $(\Delta P_m)_{app}$ should equal $[P_F(N-1) - P_F(N)]$. If so, $(\Delta P_F)_C$, the

apparent ΔP_F across the rest of the cake, should = $[P_F(1) - P_F(N-1)]$. Predicted values of $[P_F(N-1) - P_F(N)]$ decreased as V_a increased and thus behaved like experimentally measured $(\Delta P_m)_{app}$. Moreover, starting from the V_a where $[P_F(N-1) - P_F(N)]$ began to rise rapidly, $-d[P_F(N-1) - P_F(N)]/dV_a$ were roughly the same at all -dZ/dt, which again agrees with experimental $(\Delta P_m)_{app}$ behavior. This $(\Delta P_m)_{app}$ behavior causes $(R_m)_{app}$ decreases as -dZ/dt increases, the effect obtained by using $K_r = 2546 - 762{,}000(-dZ/dt)$ in Eq (108).

Predicted $[P_F(1) - P_F(N-1)]$ also behaved similarly to experimental apparent $(\Delta P_F)_C$. Thus $[P_F(1) - P_F(N-1)]$ levelled off rapidly as V_a decreased when -dZ/dt was large and leveled off progressively more slowly as -dZ/dt decreased. Predicted values of V close to the media were also more in line with experimental V next to the media when R_m was assumed to be negligibly small. Thus, use of best-fit parameters for $\alpha(V)$ and $P_S(V)$ when $R_m = 0$ not only provided suitably shaped P_T versus V_a curves and low σ_{ov}, it also provided much better agreement between predicted and experimental behavior for $(\Delta P_m)_{app}$, V and apparent $(\Delta P_F)_C$.

$(R_m)_{app}$ for cranberries depend very much on media pore size (see fig. 86), an effect that would not be produced if $(R_m)_{app}$ depended solely on high $-dP_F/dw$ near $w = W$. Therefore true R_m may not be wholly negligible for the apples and may increase significantly towards the end of pressing; but one cannot presently determine how much of $(\Delta P_m)_{app}$ is due to R_m proper.

It is noteworthy that final V_a at comparable pressing conditions were larger, i.e. pressing yields were smaller, when 7-mm cubes made from the same Granny Smith apples were used instead of 3-mm cubes. Some cubes remained intact in both cases, and flow took place in the mash surrounding them. This reduced areas available for flow, effectively increasing α and ΔP_F. When the larger cubes were used, flow area reduction was greater; consequently α was greater. Compression permeability measurements also showed that α was much larger for 7-mm cubes than for 3-mm cubes.

The assumed B•F provided predicted ΔP_w and V that respectively agreed reasonably well with experimentally measured ΔP_w and V at the start of pressing. At the end of pressing, the calculated ΔP_w were too large. Therefore B•f may decrease as pressing proceeds. This may occur because B decreases

as cells rupture during pressing. Trial computations showed that $B \cdot f$ significantly affected computed P_T, final V_a and predicted juice yields. Higher yields were computed when larger $B \cdot f$ were assumed and lower yields when smaller $B \cdot f$ were assumed. This occurred because wall friction acts to reduce P_S increases near the outflow surface. This, in turn, produced larger V and much smaller α and P_F gradients near that surface, thereby delaying the time at which P_T equalled P_{max}.

Buttersack and Blecher[216] recently reported constant-rate P_T versus V_a plots for constant-rate pressing of sugar beet pulp at -dZ/dt between 0.01 and 30 mm/min. These curves and similar curves obtained by Huang[60] resemble those obtained for apples. It is very likely that still other soft CBS will exhibit the constant-rate pressing behavior similar to that for apples, and that their pressing behavior can be analyzed by means similar to those just described.

14B. CONSTANT-RATE PRESSING OF OLIVE PASTE

Olive paste is a complex material. It contains drops of highly viscous olive oil dispersed in much-less viscous fruit water. It also contains: a) pit fragments, that provide little filtration resistance but ultimately generate high P_S, and b) fine pulp, which is responsible for virtually all of olive paste's filtration resistance, but has very little direct effect on P_S. One cannot be sure that the solid components do not move relative to one another during pressing. Therefore, these two components may not be treatable as a single fixed solid. Differential wetting and adhesion of each liquid phase to fixed solids may also cause one liquid phase to move faster than the other during pressing. Effective viscosities for liquid flow in olive paste presscakes are difficult to predict. Thus pressing of olive paste potentially may be difficult to analyze.

P_T versus V_a curves for pressing of olive paste are similar in shape to corresponding curves for apples. In spite of previously mentioned potential problems, very good agreement between predicted and experimental curve shapes and final V_a were obtained[217] when the constant-pressing rate behavior of olive paste at -dZ/dt of 0.5 mm/min and 2-mm/min was analyzed by methods similar to those used for apples. Since the effective viscosity of the

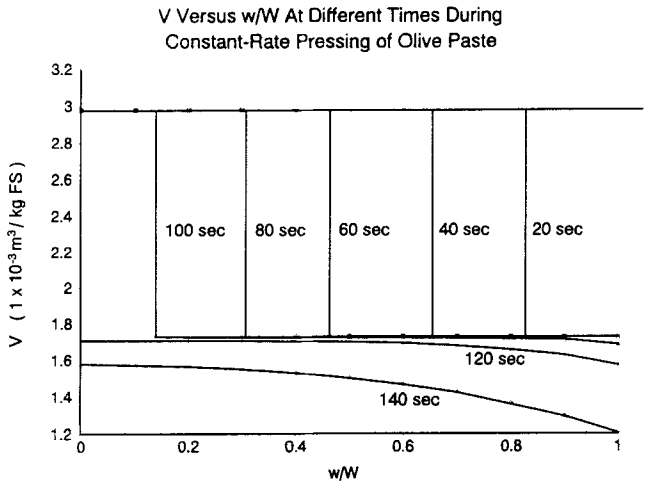

FIGURE 95 V versus w/W during at different times during pressing of olive paste (Schwartzberg et al.[217])

fluid in the cake is not known, modelling was based on determining a best-fit correlation for $\mu \cdot \alpha$ instead of using a known μ and correlating α alone. Thus in the pressing rate range tested, olive paste cakes can be treated as if they contain homogeneous fixed solids and a single fluid.

Olive paste acts as a fairly dilute slurry. Therefore filtration occurs and a filter cake deposits above the outflow surface. As shown in fig. 95, V changes sharply at the upper surface of the cake; and w_c/W, at the w/W boundary of the cake zone, where V is low, progressively decreases until $w_c/W = 0$. After this, the cake consolidates and V varies smoothly with w/W.

Predicted P_F versus w/W and z/Z profiles during consolidation of olive paste are shown in fig. 96. These profiles change much more gradually than similar profiles for apples. i.e, predicted P_F for olive paste do not increase sharply near the outflow surface. This probably occurs because friction provided by hard ground pit fragments in olive paste retards compaction of flow-resisting pulp near the outflow media. This prevents α from increasing excessively near the

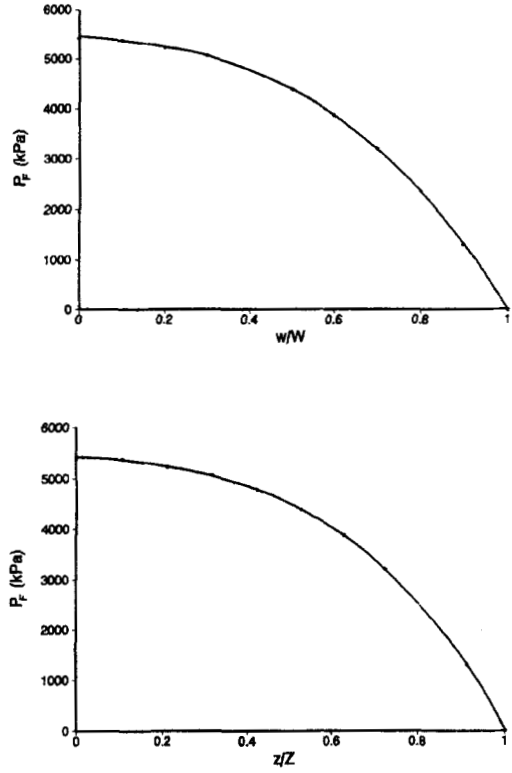

FIGURE 96 P_F versus w/W and z/Z for olive paste at the end of constant-rate pressing at 2 mm/min (Schwartzberg et al.[217])

media. Higher expressed fluid yields have been obtained by increasing the amount of pit fragments in olive paste[209].

14C. CONSTANT-RATE PRESSING OF SPENT COFFEE GROUNDS

Unlike apples which have weak cell walls, and olive paste, whose cell walls have largely been ruptured, spent coffee grounds have thick cell walls that are difficult to rupture, and there is virtually no space between cells in coffee grounds.

$P_s(V)$ for Spent Grounds: Experimental pressing behavior for spent grounds was analyzed[136] to determine $P_S(V)$ and $\alpha(V)$. Except for V_a close to V_o, both $\log(P_T)$ and $\log(P_B)$ for spent grounds increase linearly as V_a decreases when P_F is negligibly small. Eq (2) describes similar $\ln(P_S)$ versus V behavior.

$$\ln\left[\frac{P_S}{P_{ref}}\right] = K \cdot (V_{ref} - V) \qquad (2)$$

When P_F is negligibly small, local V and P_S are strongly affected by wall friction. If P_S obeys Eq (2)

$$V(w) = V(0)\exp[Hw/K] \qquad (116)$$

where V(0) is V at w = 0, and V(w) is V at w = w. Further

$$V_a = \frac{V(0)K}{HW}\left[\exp\left(\frac{HW}{K}\right) - 1\right] \qquad (117)$$

V_a decreases linearly with time during constant-rate pressing. Since both V_a and V(w) are proportional to V(0) when $P_F = 0$, V(w) should decrease linearly with time. Fig. 88 shows that over most of the compaction range V(w) increases as w increases as predicted by Eq (116). Deviations from linearity near the end of compaction are due to fluid-pressure drop.

As noted in Section 5, Eq (2) does not apply at V very close to V_o. Most likely

$$P_S = K_o \cdot (V_o - V) \qquad (118)$$

at V close to V_o. If one uses Eq (118) between V_o and V_L, a transition V, and Eq (2) for $V < V_L$, one can provide continuity for P_S and dP_S/dV at $V = V_L$ by letting $V_L = (V_o - 1/K)$ and $K_o = K \cdot P_L$, where P_L is the value of P_S obtained from Eq (2) at $V = V_L$. When this was done and Eq (34) was numerically solved, good agreement between predicted and experimental local V was obtained both at small V_a and V_a close to V_L.

When $P_F = 0$ and Eq (2) applies, $P_T = P_S(0) = P_{ref} \cdot \exp[K(V_{ref} - V(0)]$. Therefore

$$\ln\left[\frac{P_T}{P_{ref}}\right] = \ln\left[\frac{P_S(0)}{P_{ref}}\right] = K\left[V_{ref} - \frac{V_a HW}{K[\exp(HW/K) - 1]}\right] \quad \textbf{(119)}$$

Similarly, $P_B = P_S(W) = P_{ref} \cdot \exp(K(V_{ref} - V(W)$, and

$$\ln\left[\frac{P_B}{P_{ref}}\right] = \ln\left[\frac{P_S(W)}{P_{ref}}\right] = K\left[V_{ref} - \frac{V_a HW}{K[1 - \exp(-HW/K)]}\right] \quad \textbf{(120)}$$

$K_T \equiv -d\ln(P_T)/dV_a$. Based on Eq (119)

$$K = \frac{HW}{\ln[1 + HW/K_T]} \approx \frac{K_T}{1 - HW/2K_T} \quad \textbf{(121)}$$

The second right-hand side is obtained by expanding $\ln[1 + HW/K_T]$ as a Taylor series. It can only be used when HW/K_T is fairly small. Similarly from Eq (120)

$$K = -\frac{HW}{\ln[1 - HW/K_B]} \approx \frac{K_B}{1 + HW/2K_B} \quad \textbf{(122)}$$

Again, the second right hand side can only be used when HW/K_B is fairly small. Eqs (121) and (122) show that $K_B > K_T$, which agrees with experimental observations.

Eqs (121) or (122) can be used to obtain K. K also $\approx (K_T + K_B)/2$. K_T and K_B increase as -dZ/dt increases. Therefore, K also increases as pressing speed increases, and P_S is not a function of V alone. Functions that possibly might account for how P_S is affected by pressing speed were evaluated by using them when solving Eq (34). For example

$$K = 1{,}629 + 8{,}950 \cdot \left[-\frac{dZ}{dt}\right]^{0.33} \quad \textbf{(123)}$$

provided K that moderately well agreed with experimental K for spent grounds. The units used are: kg/m^3 for K, and m/s for -dZ/dt.

P_{TR} are much smaller than P_T both when P_F is large and when $P_F \approx 0$. Therefore P_S decreases during relaxation. $P_S(V)$ should account for how P_S

changes during relaxation. If $P_S = P_R + P_E$, where P_R is the relaxed value of P_S and P_E is the mean, excess fluid pressure inside particles, P_E and P_S will decrease as fluid exudes from particles during relaxation. How P_E varies as V, -dV/dt and t change might be used to explain relaxation behavior and to explain why K increases as -dZ/dt increases. Functions for P_E that satisfied these purposes for spent grounds were evaluated.

The most successful function tested was based on models depicted in fig. 35. Eq (124), an analog of the equation for creep in a Kelvin-Voigt body in series with a spring, provides P_S that decrease as relaxation time, t_r, increases.

$$\ln\left[\frac{P_S}{P_{ref}}\right] = \frac{V_{ref} - V}{G_I + G_i \cdot [1 - \exp(-t_r/\tau_r)]} \qquad \textbf{(124)}$$

Spring behavior in the model on which Eq (124) is based is governed by Eq (2) instead of Hooke's law. As $t_r \rightarrow \infty$ during relaxation, Eq (124) causes P_S to approach $P_R = P_{ref} \cdot \exp[(V_{ref} - V)]/(G_r + G_i)$. Thus $K_R \equiv -d\ln(P_R)/dV = 1/(G_r + G_i)$. Further, based on numerical evaluation, Eq (124) causes $\ln(P)$ to decrease linearly as $t_r^{1/3}$ increases. $\tau_o \cdot (V_o - V)$ can be substituted for τ_r to account for relaxation slowing down as $(V_o - V_a)$ increases.

Equations employing the sum of several $\exp(-t_r/\tau_r)$ terms have been used to characterize P_T relaxation following constant rate pressing[218,219]. If Eq (124) is applied at constant P_S, V decreases linearly as $\exp[-t_p/\tau]$ decreases, which is the kind of secondary consolidation behavior observed during constant-pressure expression from clay filter cakes[22,174-177], apples[79] and black currants[178,179].

Eq (124) is an analog of an equation for creep after sudden imposition of a load. It is used here for a different process, i.e. stress relaxation after constant-rate deformation, which is actually described by a different equation for the systems shown in fig. 35. Nevertheless, Eq (124) worked quite well for constant-rate pressing of spent coffee grounds.

Elements of the model in fig. 35b may have physical significance. Behavior of the in-series spring may correspond to interactions between particles. Flow out of the perforated dashpot corresponds to exudation of fluid from particles; the pressure acting on the dashpot corresponds to P_E, the pressure driving exudation. The parallel spring corresponds to stresses generated in cell walls in

particles and/or relief of tension in such walls as fluid leaves cells. Relaxation is slower at smaller V or larger (V_o - V). This probably occurs because particle surfaces block one another more when V is small. It may also occur because fluid leaves from cells near the particle surface during early stages of pressing and from cells deeper inside particles during late stages of pressing. Thus fluid expelled from particles during relaxation may have to traverse more cell walls when V_a is very small.

Delays in escape of fluid from particles prevents local P_S equilibrium from being reached during constant-rate pressing. This lag in equilibration can be described in terms of an effective relaxation time. If the relaxation time is proportional to pressing time, i.e. $W(V_o - V_a)/(-dZ/dt)$, and τ during pressing is proportional to $\eta(V_o - V_a)$, one obtains an analog of Eq (124) that can used to correlate how -dZ/dt affects K.

$$\ln\left[\frac{P_s}{P_{ref}}\right] = \frac{V_{ref} - V}{G_r + G_i \cdot \{1 - \exp[-W/\eta(-dZ/dt)]\}} \qquad \textbf{(125)}$$

η in Eq (125) is proportional to the in-particle flow resistance, which increases as (V_o - V_a). As -dZ/dt becomes large, K approaches $1/G_r$ and when -dZ/dt → 0, K → $1/(G_r + G_i) = K_R$. K (i.e. $(K_T + K_B)/2$) and K_R were used to determine best fit values for G_r, G_i and η. These were: G_r = 0.000461 m^3/kg, G_i = 0.000146 m^3/kg and η = 9.505×10^4 $kg \cdot s/m^3$. Overall, Eq (125) provided a better fit for experimental K than Eq (123) did.

For uniform compaction, Eq (125) becomes

$$-\frac{d\ln(P_S)}{dV} = K = \frac{1}{G_r + G_i \cdot \left(1 - \exp\left[\frac{1}{\eta(dV/dt)}\right]\right)} \qquad \textbf{(126)}$$

Eq (126) depends on local -dV/dt rather than on -dZ/dt. As noted in section 9, use of Eq (126) or other equations in which P_S depended both on local dV/dt as well as local V caused instability when used in attempts to numerically solve Eq (34). Therefore Eq (125) rather than Eq (126) was used to numerically solve Eq (34). Experimentally determined -dV/dt were roughly the same at all w except at the beginning and end of pressing (see fig. 88). Therefore use of

$(dZ/dt)/W = dV_a/dt$ instead of local dV/dt in computations should not cause much error.

Eq (125) applies during ram motion. Elements of Eqs (124) and (125) were combined to provide an equation that also applies during relaxation, i.e.

$$\ln\left[\frac{P_S}{P_{ref}}\right] = \frac{V_{ref} - V}{G_r + G_i\{1 - \exp[-W/\eta\,(-dZ/dt) - t_r/\tau_r]\}} \qquad \textbf{(127)}$$

Eq (127) provides P_S that can agree with P_S at the end of pressing, when $t_r = 0$, and still causes P_S to approach P_R when t_r becomes large. Since $t_r = 0$ during ram movement, Eq (127) reduces to Eq (125) during ram movement.

Experimental P_T for all -dZ/dt relaxed to P_{TR} on a single $\ln(P_{TR})$ versus V_a curve. Eq (127) provides such behavior if P_{ref} and V_{ref} are the same at all -dZ/dt including -dZ/dt = 0. Values of P_{ref} and V_{ref} that provided computed P_S versus V_a values that fitted all experimental data well in the linear $\ln(P_T)$ versus V_a range were sought by trial and error. The smallest mean square differences between experimental and computed P_T was obtained when $V_{ref} = 0.00465$ and $P_{ref} = 12.88$ kPa. Experimental and computed P_T at $V_a = 0.0032$ m^3/kg (i.e. in the linear $\ln(P_S)$ versus V_a range are listed in Table XI for the selected P_{ref} and V_{ref}.

Though the fit between experimental and computed P_T is fairly good at -dZ/dt $\geq$ 10 mm/min, it is quite poor at -dZ/dt $\leq$ 5 mm/min. A markedly better fit is obtained when the data for -dZ/dt = 0 is left out and different P_{ref} and V_{ref} are used. Nevertheless, Eq (127) was usually used with $P_{ref} = 12.88$ kPa and $V_{ref} = 0.00465$ when solving Eq (34) for spent grounds.

Since fluid pressure drops across cakes of coffee grounds are small, $(P_T - \Delta P_m) \approx P_S(0)$ and $(P_B - \Delta P_m) \approx P_S(W)$. Both $\log(P_T - \Delta P_m)$ versus V_a and $\log(P_B - \Delta P_m)$ versus V_a plots remain linear until V_a became small, then turn upward more sharply as V_a decreases. This behavior is similar to log P_S versus V behavior shown between V_t and V_u in fig. 32. To account for this behavior, Eq (127) was empirically modified as follows

ξ is a function designed to account for increases in ln (P_S) versus V curvature at

$$\ln\left[\frac{P_S}{P_{ref}}\right] = \frac{V_{ref} - V}{G_r + G_i\{1 - \exp[-W/\eta\,(-dZ/dt) - t_r/\tau_r + \xi]\}} \qquad \textbf{(128)}$$

Table XI - Computed and Experimental P_T versus -dZ/dt for Spent Grounds at V_a = 0.0032 m^3/kg

-dZ/dt (mm/min)	0	5	10	20	50	100	200
	P_T (kPa)						
Calc.	217	239	279	338	419	471	517
Exper.	160	290	300	330	405	465	530

small V. As in Eq (127), t_r = 0 during ram movement. Eq (128) allows P_S to relax to the same value of P_R that applied before ξ was introduced. Various ξ were tested. The one that provided the smallest root-mean-square difference between predicted and experimental final V_a was ξ = 0 for $V > V_t$ and $\xi = 3[(V_t - V)/V]^2$ for $V < V_t$; V_t = 0.0019. The root-mean-square percentage difference between experimental and calculated final V_a was 1.88%.

Computed ΔP_F: Eqs (48) to (54) were numerically solved using P_S given by Eq (128), α given by Eq (113), R_m given by Eq (107) and B•f given by Eq (111). Computed ΔP_F across the cake were found to be much larger than experimental ΔP_F, which were almost negligibly small. Therefore α during pressing were much smaller than predicted by Eq (113). Suitably low ΔP_F for spent grounds were obtained only after α predicted by Eq (113) had been reduced roughly by a factor of 20. Incorrect α may have been obtained because of use of improper experimental methods during compression permeability tests, e.g. use of beds that were too deep. Far more liquid passes through a cake during compression permeability testing than is expressed during compaction. Permeation rates often progressively decreased during compression permeability testing. Therefore percolation during testing may have carried sediment to the surface of the media causing increases in R_m that were computed as increases in α.

However, there may be other, more profound reasons for the apparent disparity in α. Flow profiles in interparticle pores during pressing are very different from flow profiles during percolation; and frictional pressure drops in permeable channels are strongly effected by rates of permeation out of or into the channels[220]. Peristaltic pumping caused by progressive constriction of interparticle channels may have helped cause unusually low ΔP_F during pressing. If local peristaltic pumping counterbalances local fluid pressure drop due to flow friction, α would appear to be unusually low. Local pumping has not been considered before in dealing with fluid flow during pressing. P_F profiles measured when pressing -16+20 mesh spent grounds tend to suggest that such pumping takes place. Fig. 97 shows an example of such profiles. P_F goes through a maximum as w increases. This disagrees with Eq (16) which shows that P_F should monotonically decrease as w increases. Though such P_F behavior could be caused by local pumping, it could also be due to leakage of fluid past the ram "O" ring. Such leakage would cause outflow from both ends of the cake and given rise to a P_F maximum in the middle of the cake. Leakage may well have caused the P_F maxima, but local pumping cannot be ruled out as a cause at present.

Computed P_T: After predicted α were reduced by a factor of 20, numerical solution of the Eqs (48) to (54) using Eq (128) with best-fit values of G_r, G_i, P_{ref} and V_{ref} yielded $\log(P_T)$ versus V_a curves of suitable shape. Moreover predicted final V_a agreed with experimental V_a fairly well, but the final ΔP_m values were too low. R_m at the end of pressing were significantly higher than R_m along the trend line in fig. 86. Therefore Eq (107) was modified to better fit values of R_m at the end of pressing

$$R_m = 1.97 \times 10^{17} \exp[-5520 V_a] \qquad \textbf{(129)}$$

After this was done, computed final ΔP_m and experimental ΔP_m agreed reasonably well and agreement between computed and experimental final V_a greatly improved. Resulting computed and experimental final V_a are listed in Table XII.

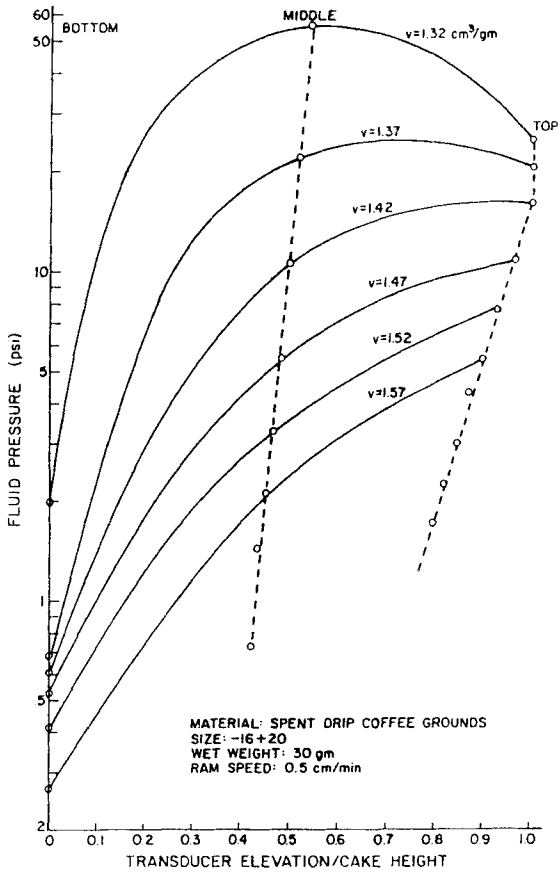

FIGURE 97 P_F versus z/Z during constant-rate pressing of spent, -16 +20 mesh coffee grounds; Pressing speed: 5 mm/min (Huang[207])

Table XII Experimental and Calculated V_a at $P_t = P_{max} = 11$ MPa

-dZ/dt (cm/min)	0.5	1	2	5	10	20
Conditions	Final V_a (m^3/kg) x 1000					
Experimental (Ave)	1.49	1.62	1.75	1.86	2.01	2.07
Calculated	1.49	1.62	1.74	1.87	1.98	2.09

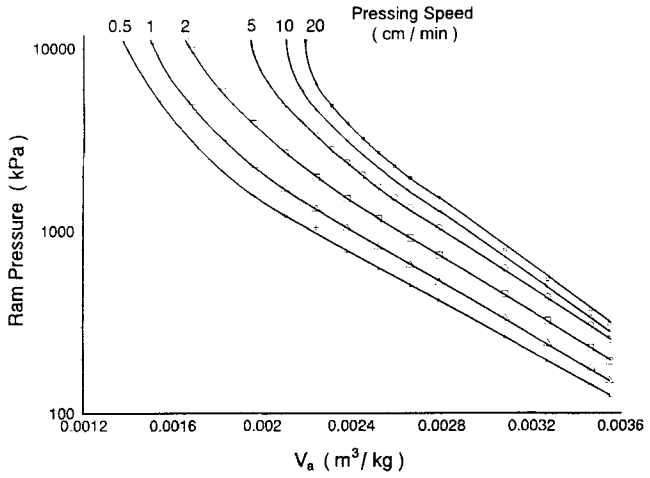

FIGURE 98 Computed plots of log(P_T) versus V_a at different -dZ/dt for spent coffee grounds (Schwartzberg et al.[136])

Agreement between the experimental and empirically corrected computed final V_a is excellent. Fig. 98 depicts log(P_T) versus V_a curves based on the numerical solution. They are very similar to the curves depicted in fig. 76; but the low V_a portions of experimental plots for low -dZ/dt curve upward slightly more sharply than the computed ones do. That is probably due to use of an imperfect ξ in Eq (128).

Relaxation: Fig. 99 contains computed plots of log(P) versus $t_r^{1/3}$ for spent coffee grounds[136]. While similar to fig. 82, the linear range log(P) versus $t_r^{1/3}$ range is larger for the experimental data than it is for the computed data. This difference is due to failures in accounting for how ΔP_m decrease as t_r increases. Even though outflow nominally stopped when the ram stopped, ΔP_m did not drop to zero at that time; it decreased slowly and only gradually approached 0. To account for that decrease in solving Eq (48) for the relaxation period, (ΔP_m) at $P_T = P_{max}$ was arbitrarily multiplied by exp(-t_r/τ). Not enough ΔP_m versus t_r data is available to provide better correlation. An alternative method of

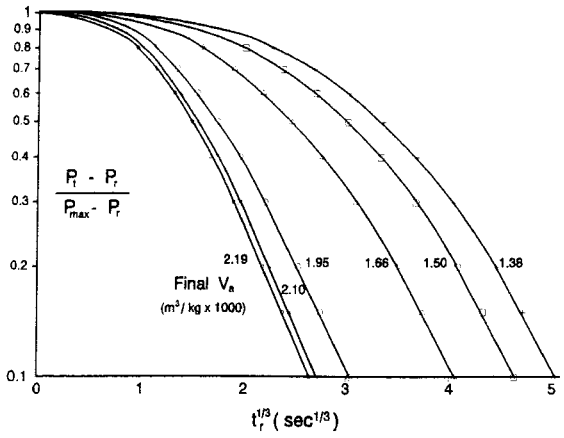

FIGURE 99 Computed plots of log(*P*) versus $t_r^{1/3}$ at different final V_a for spent coffee grounds (Schwartzberg et al.[136])

accounting for how ΔP_m and P_F decay was presented in Section 9, but effectiveness of its use has not yet been evaluated.

The P_{TR} provided by using Eq (128) are too high. Perhaps that is because P_S relaxation has only been accounted for in terms of P_E reduction. Stress also relaxes in the fixed solid. This solid relaxation might be accounted for by introducing an added term $G_S[1 - \exp(-t_r/\tau_S)]$ in the denominator of Eq (128)

V and U versus w: Experimental and computed V versus w profiles for spent grounds were qualitatively similar. Calculated and experimental U versus w profiles were virtually identical as long as suitably small α were used in solving Eqs (48).

14D. CONCLUSIONS - CONSTANT-RATE PRESSING

Most aspects of constant-rate pressing behavior for cellular biological solids (CBS) can be successfully predicted by using appropriate values or functions and parameters for $P_S(V)$, $\alpha(V)$, R_m and B•f and numerically solving Eq (34).

Comparisons between numerically predicted and experimental pressing data can be used to help select $P_S(V)$, $\alpha(V)$, R_m and $B \cdot f$ and associated parameters.

P_S often depends on $-dZ/dt$ or on $-dV_a/dt$ in addition to being a function of V. Effects of $-dZ/dt$ on P_S are small for CBS whose cells have ruptured or easily rupturable walls and which contain large amounts of space between cells. For such materials, effects of $-dZ/dt$ on P_S are significant mainly at large V, and apparently diminish as cell walls rupture or particles break down into mashes during pressing.

$(\Delta P_F)_C$ are large for soft CBS at late stages of pressing. This causes sharp reductions in V and sharp increases in α and P_F near outflow surfaces. $(\Delta P_F)_C$ increase as $-dZ/dt$ increases, causing P_T versus V_a curves for soft CBS to shift with little change in shape toward larger V_a. Thus, for such solids, final V_a increase markedly and juice yields decrease markedly as $-dZ/dt$ increases. Hard pressing aids, such as pit fragments or rice hulls, can reduce sharp increases in α and P_F near outflow surfaces and thereby improve juice yields. Similar benefits can be obtained by breaking up and mixing presscakes between repeated pressing steps, as is done in several types of pressing equipment for soft fruit.

Effects of $-dZ/dt$ on P_S are large and persist even at low V for CBS that have tightly packed cells with thick walls. $-dZ/dt$ affects P_S in such materials largely by affecting P_E, excess hydraulic pressures within particles. P_E drives fluid exudation from particles and has a large effect on P_S when spent coffee grounds and oil seeds are pressed. P_E decreases fairly slowly after ram movement stops, causing P_T to relax relatively slowly for such particles once ram movement stops. Equations based in part on the rheological model in fig. 35b provide ways to interpret P_E and P_S behavior during pressing and relaxation. P_T relaxation is also affected by stress relaxation in cake solids and by fluid outflow caused by fluid and solid expansion that occurs when P_F and P_S drop.

$(\Delta P_F)_C$ are quite small for spent coffee grounds. Therefore, effective $\alpha(V)$ are small for such grounds, much smaller than α measured in static compression permeability tests. Causes for the lower-than-anticipated $(\Delta P_F)_C$ and α are not yet clear, but may involve local pumping caused by pore contraction.

15. MULTI-DIMENSIONAL PROBLEMS

Expression involving flows in several directions and/or conveyed solids requires use of more complex equations. The first mathematical description of the problem was provided by Biot[221], who derived equations suitable for saturated porous solids that: 1) are isotropic, 2) have reversible, linear stress-stain relations at equilibrium condition, 3) are subject to small strains, and 4) contain incompressible fluid subject to flows governed by Darcy's law. The second and third assumption are not valid for most press cakes. Other researchers [110,222-225] have modified Biot's approach to account for stress-strain non-linearity or to deal with bodies that are unsaturated. Kormendy[110] derived the following equation to describe three-dimensional expression from moving, saturated solids without restriction as to stress-strain linearity or smallness of compaction.

$$\nabla \cdot \left[\frac{k}{\mu} \nabla (P_F) \right] = \frac{1}{1 - \varepsilon} \frac{de}{dt} \qquad (130)$$

When expanded, the left-hand side is

$$\frac{\partial}{\partial x}\left[\frac{k_x}{\mu} \frac{\partial P_F}{\partial x} \right] + \frac{\partial}{\partial y}\left[\frac{k_y}{\mu} \frac{\partial P_F}{\partial y} \right] + \frac{\partial}{\partial z}\left[\frac{k_z}{\mu} \frac{\partial P_F}{\partial z} \right] \qquad (131)$$

k_x, k_y and k_z are the permeabilities in the x, y and z direction. The right-hand side is

$$\frac{1}{1 - \varepsilon}\left[\frac{\partial e}{\partial t} + u_x \frac{\partial e}{\partial x} + u_y \frac{\partial e}{\partial y} + u_z \frac{\partial e}{\partial z} \right] \qquad (132)$$

where u_x, u_y and u_z respectively represent the local solid velocity in the x, y and z direction. P_F is related to solids stress components by

$$\begin{aligned} -\frac{\partial P_{Sx}}{\partial x} + \frac{\partial \tau_{xy}}{\partial y} + \frac{\partial \tau_{xz}}{\partial z} &= \frac{\partial P_F}{\partial x} \\ \frac{\partial \tau_{yx}}{\partial x} - \frac{\partial P_{Sy}}{\partial y} + \frac{\partial \tau_{yz}}{\partial z} &= \frac{\partial P_F}{\partial y} \\ \frac{\partial \tau_{zx}}{\partial x} + \frac{\partial \tau_{zy}}{\partial y} - \frac{\partial P_{Sz}}{\partial z} &= \frac{\partial P_f}{\partial z} \end{aligned} \qquad (133)$$

where the subscripts x, y, z respectively indicate the direction in which normal stress P_S is acting and τ_{ji} indicates a shear stress acting in direction j on the solid at a plane normal to direction i. To solve these equations one must know how k or k_x, k_y and k_z vary as e changes and how the P_S and τ_{ji} components vary as e, e gradients and possibly $\partial e/\partial t$ change, i.e. have an appropriate constitutive equation for the cake[225]. One must also know how u_x, u_y, and u_z depend on the surface motion and tractive stresses provided by conveying or pressing devices.

Most of the data required is not available, therefore solutions have been usually limited to one-dimensional cases, like those previously considered. Radical simplifications are sometimes used: a) neglecting the τ_{ji}, b) assuming $k_x = k_y = k_z = k$, c) letting P_{Sz} and $P_{Sy} = B \cdot P_{Sx}$, where x is the direction in which external pressure is applied; d) assuming that only one directional component of P_S affects flow; and/or e) assuming that solids conveying occurs in one directions only.

16. PROCESS ANALYSIS

Batch Equipment: Unidirectional axial compaction is provided in some batch equipment, e.g. pot presses, box presses, rack-and-cloth presses and some cheese presses. Expression in such equipment can be analyzed readily by methods previously presented in this review if suitable $P_S(V)$, $\alpha(V)$ are known or can be determined.

Radial Compaction and Flow: Certain batch equipment contain concentric cylindrical surfaces, one perforated and immobile, and the other imperforate and capable of expanding or contracting. An example is the Wilmes press, where an expanding cylindrical rubber tube forces liquid out of a cake through an outer, concentric, perforated, cylindrical surface. Equations involving use of coordinates based on m, the mass of fixed solids per unit length between the inner cylinder and a concentric surface in the bed can be used to describe expression in such equipment. Other variables are P_{Sr} the solid stress in the radial direction, and P_F. If $dP_{Sr} = -dP_F$, the governing partial differential equation is:

$$\frac{\partial V}{\partial t} = -\frac{\partial}{\partial m}\left[\frac{A_z}{\mu\alpha}\frac{\partial P_{Sr}}{\partial (m/A_z)}\right] \qquad (134)$$

where A_z, the radial flow area at m per unit length of the cylinder, is

$$A_z = 2\left[(\pi r_i)^2 + \pi\int_0^m V\,dm\right]^{1/2} \qquad (135)$$

where r_i is the diameter of the inner cylinder, where m = 0. M_z is the load of fixed solids per unit length of cylinder. In presses where the inner cylinder expands, $dP_{Sr}/d(m/A_z) = 0$ at r_i, where m = 0; and at r_o, where $m = M_z$, $dP_{Sr}/d(m/A_z) = (1/\mu\alpha)(r_i/r_o)(dr_i/dt)$. If v_i, the volume of the inner cylinder per unit length expands at a constant rate, dv_i/dt, $dP_{Sr}/d(m/A_z) = (dv_i/dt)/\mu\alpha 2\pi r_o$ at $m = M_z$. If $R_m = 0$, at M_Z, $P_{Sr} = P_T$, the pressure acting on the inner cylinder. This can be used as a boundary condition for constant-pressure expression.

Eqs (134) and (135) still apply when an outer cylinder contracts and outflow occurs through an immobile, perforated inner cylindrical surface, but the previously given boundary conditions for r_i are used at r_o and vice-versa.

Bucher-Guyer presses (see fig. 10) contain outflow tubes that contort during pressing. Nevertheless, as a reasonable approximation, one can effectively divide the load space around each tube into cylindrical unit-cells whose outer boundaries act as neutral surfaces that contract at rates compatible with the volume-reduction rate produced by piston advance in the cylindrical casing of the press. Based on a volume-reduction balance

$$D_u = \left[D_{uo}^2 - (D_C^2 - N_T D_T^2)\left(\frac{Z_o - Z}{N_T Z_o}\right)\right]^{1/2} \qquad (136)$$

where D_C, D_T and D_u (or $2r_o$) respectively are the diameters of the press case, tubes and unit-cells, N_T is the number of tubes and Z is the distance between the ram and head of the case. When o is used as a second subscript, it indicates an initial value. M_Z for each cell = M_d/N_t $D_{uo} = D_C/N_T^{1/2}$, and

$$\frac{dD_u}{dt} = \frac{D_C^2 - N_T D_T^2}{4 Z_o N_T D_u}\frac{dZ}{dt} \qquad (137)$$

The outflow velocity at each tube surface is

$$U_s = \frac{D_C^2 - N_T D_T^2}{4 Z_o N_T D_T} \left(-\frac{dZ}{dt}\right) \quad \textbf{(138)}$$

At r_i, where m = 0, P_{Sr} equals the applied pressure and $dP_{Sr}/(dm/A_z) = U_o/\mu\alpha$ if $R_m = 0$. $dP_{Sr}/(dm/A_z) = 0$ at r_o, where $m = M_Z$. If one uses these relationships and the unit-cell approach, one can apply Eqs (134) and (135) to analyze the operation of Bucher-Guyer presses.

Murase et al.[226,227] present a method of dealing with constant-pressure radial squeezing, i.e. expression caused by contraction of impermeable cylindrical surface surrounding a load and a concentric, stationary, perforated cylindrical surface. The method involves correcting Eq (28) or other equations for uniaxial compaction at constant C by applying a factor (J) based on ratio of the mean effective flow area to the outflow area. J is obtained from the ratio of respective first terms in analytical solutions for $d\zeta/dr$ for uniaxial expression and squeezing. For $r_o/r_i < 3$, $J \approx 0.703 + 0.297(r_o/r_i)$. If at a given ζ for uniaxial expression, $\tau = \tau_1$, at the same ζ, τ for squeezing $= \tau_1/J^2$. When creep occurs, Eq (93) can be used for radial squeezing by using $J^2\tau$ instead of τ. Predicted results matched experimental results for two clays well for $r_o/r_i \leq 3$, $\tau > 0.2$ and fractional volume reductions up to 0.35.

Axial Compaction - Radial Flow: Axial compaction and radial flow occur in curb presses and spindle presses. In such presses, W, the fixed-solids load per unit of outflow area, increases with time because outflow area progressively decreases. Therefore, it is preferable to use length-based radial coordinates, which do not change with time in such cases. If friction between the cake and ram surface and base can be neglected and $dP_{Sr} + dP_F = 0$,

$$\frac{\partial e}{\partial t} = \frac{1 + e}{r} \frac{\partial}{\partial r}\left[\frac{r k}{\mu}\left(\frac{\partial P_{Sr}}{\partial r}\right)\right] \quad \textbf{(139)}$$

If R is the radius of the press cylinder and Z is the current cake length, U_o the fluid velocity at the outflow surface is given by

$$U_o = -\frac{R}{2Z}\frac{dZ}{dt} \quad \textbf{(140)}$$

-dZ/dt, the rate of ram advance, if not prescribed, can be found from

$$\frac{dZ}{dt} = \frac{2\int_0^R \frac{r\,(de/dt)}{(1+e)^2}\,dr}{R^2 - 2\int_0^R \frac{er}{1+e}\,dr} \qquad (141)$$

F_T, the force acting on the ram in the axial (z) direction, if not prescribed, and if wall friction can be neglected, can be obtained from

$$F_T = 2\pi \int_0^R [\,(P_{Sr}/B) + P_F\,]\, r\, dr \qquad (142)$$

where $B = P_{Sr}/P_{Sz}$. Since P_{Sr} at the outflow surface cannot be evaluated directly from F_T, it is easier to analyze constant-rate pressing than to analyze pressing at constant F_T for this type of expression. Boundary conditions for constant-rate pressing are $dP_{Sr}/dr = 0$ at $r = 0$ and $dP_{Sr}/dr = \mu U_o/k$ at $r = R$.

Continuous Equipment - Belt Presses: It is reasonable to assume that fixed solids move at belt speed in belt presses and that W, the fixed solids load per unit area of belt, does not change during movement. In serpentine belt presses, as a first approximation, expression from a unit of fixed solids can be treated as uniaxial expression by following the cake, and evaluating V changes caused by flow normal to the direction of solid movement. P_T, the effective ram pressure acting on the solids, $= T/D_R$ where T is the tension per unit of belt width and D_R is the diameter of the roller over which the solids are currently passing. The time the pressure is applied is $\Theta_c D_R/S_b$, where S_b is the belt speed and Θ_c is the angle of contact between the belt and roller. D_R usually decreases as the cake moves from roll to roll. Therefore P_T usually increases in step-wise fashion, falling to 0 in regions where the belts lose contact with rolls and D_R effectively becomes infinite. W and the initial V can be determined from the slurry deposition rate and the slurry's composition. Since P_T can be calculated as a function of time, extents and rates of expression can be readily calculated by methods used to solve PDE describing

uniaxial expression at series of prescribed pressures. In later stages of pressing, the direction of pressing changes as the cake moves from roll to roll; and in early stages, where perforated rolls are used, outflow occurs at both the inner belt and outer belt. Therefore, as the cake moves from roll to roll, boundary conditions have to be altered to account for these changes.

There are a number of other complicating factors: cake may tend to be expelled at the side of the belt; rolls may deflect slightly at their middle; and the outer belt travels significantly faster than the inner belt when the pair passes over small diameter rolls. It is felt that the latter effect produces shearing that helps to open up the cake and reduce blinding. No method of theoretically accounting for this effect has been developed. Though P_T on any given roll remains constant, P_S and P_F gradients develop both in the direction of movement and transverse to that direction. Because the length of contact on the roll and width of the roll are large relative to the cake thickness, flows produced by transverse gradient and gradients in the direction of movement are neglected. This may not be warranted for very compactable cakes that are subject to blinding near the belt surface, particularly for small diameter rolls encountered near the end of pressing.

Steady-State Approach: Except for brief start-up and shut-down intervals continuous processing equipment usually operates at steady-state. At steady state, e, and positions of local coordinates do not change with time. Therefore $\partial e/\partial t = 0$ at all points in the equipment. This facilitates use of Eq (130), particularly for cases, where solids flow occurs primarily in one direction (x) and liquid flow occurs primarily in a single direction, z, which is perpendicular to the plane of solid flow.. The fraction of the initial liquid content that is expressed $= (e_o - e_f)/e_o = \Sigma(\partial e/\partial x)\Delta x$, where e_o and e_f respectively are the initial and final values of e. Solution of Eq (130) is used to determine the $(\partial e/\partial x)$ in this summation.

Expression on serpentine belt presses can be analyzed using this approach. Even though the direction of solids flow changes as belts move over rollers, the current direction of belt movement is used as x, and the direction perpendicular

to the current direction of solids movement is used as z. Since $S_b = u_x$, the $\partial e/\partial x$ used in the summation are obtained by using

$$\frac{\partial e}{\partial x} = \frac{1 - \varepsilon}{S_b} \frac{\partial}{\partial z}\left[\frac{k}{\mu}\frac{\partial P_F}{\partial z}\right] = -\frac{1 - \varepsilon}{S_b} \frac{\partial}{\partial z}\left[\frac{k}{\mu}\frac{\partial P_S}{\partial z}\right] \quad \textbf{(143)}$$

P_S is set equal to T/D_R at the current outflow surface or surfaces of the belt. Z and z change as the cake moves in the x direction and complex procedures have to be used to account for such changes. Therefore it is preferable to convert Eq (143) into an equation in mixed coordinates, i.e.

$$\frac{\partial V}{\partial x} = -\frac{1}{S_b} \frac{\partial}{\partial w}\left[\frac{1}{\alpha \mu}\frac{\partial P_S}{\partial w}\right] \quad \textbf{(144)}$$

where w is the mass of fixed solids per unit of belt area between the neutral plane or impermeable surface and z. Eq (144) essentially is the same as the uniaxial approach previously described for belt presses.

One can account for effects of P_S gradients that tend to produces flow in the x and y direction by adding $-(\partial/\partial x)[(k/\mu)(B\partial P_S/\partial x)]\}$ and $-(\partial/\partial y)[(k/\mu)(B\partial P_S/\partial y)]\}$ to the right hand side of Eq (143). Because computation time and difficulty greatly increase as added dimensions are accounted for, use of Eq (144) usually will be preferred.

Roll Mills: Roll mills have been analyzed by treating flows and pressures in a bed of presscake passing between a pair of rolls[17]. Let x be the coordinate in the main direction of flow of the bed through the rolls, z be the coordinate perpendicular to the main flow and S_R be the surface speed of the roll. Θ is the angle on the roll between a position being examined on either roll and the nip between rolls, and Z_Θ is the bed height at Θ. Based on the system's geometry

$$Z_\Theta = D_R\left[1 + \frac{Z_n}{D_R} - \cos(\Theta)\right] \quad \textbf{(145)}$$

where D_R is the roll diameter and Z_n is the height of the bed at the nip. In

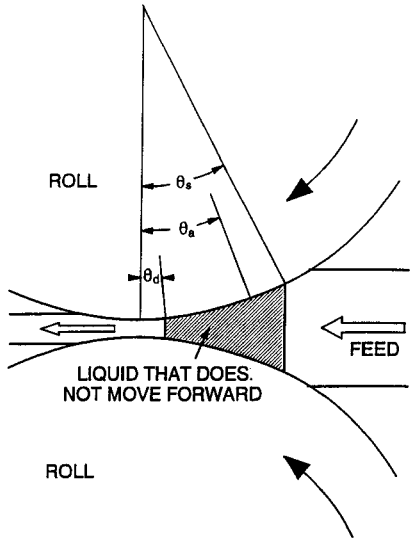

FIGURE 100 Passage of solids through stagnant pool of press liquor in two-roll mill (Murry and Holt[17])

sugar mills, Z_n is called the "work opening". Expelled liquid does not move forward through the rolls. Therefore Murry and Holt[17] viewed the process as one in which there is a stationary pool of liquid, through which "bulk fiber" move towards the discharge end of the roll, as depicted in fig. 100. Fixed solids are called "fiber" by sugar technologists. Bulk fiber is the fixed solids plus the occluded liquid they contain. The volume fraction occupied by bulk fiber is $(1 - \varepsilon')$, not $(1 - \varepsilon)$. At Θ, the compression ratio, C_R, $= Z_a/Z_\Theta$, where $Z_a = \dot{Q}_c/[S_R \cdot \cos(\Theta_a)]$, $\dot{Q}_c$ is the air-free, volume-feed-rate of juice-laden cane per unit length of roll and Θ_a is the angle at which $Z_\Theta = Z_a$. Solving for $\cos(\Theta_a)$ and then using it to find Z_a, one obtains

$$Z_a = \frac{2\dot{Q}_c}{S_R\left[1 + Z_n/D_R + \sqrt{(1 + Z_n/D_R)^2 - 4\dot{Q}_c/S_R D_R}\right]} \qquad \textbf{(146)}$$

$\dot{Q}_c = \dot{M}_c/\rho_c$, where $\dot{M}_c$ is the mass-feed-rate of juice-laden cane per unit length of roll, and ρ_c is the density of air-free, juice-laden cane (approximately 1130 kg/m^3). $C_R = 1$ at Θ_a. Because of juice expression, the bed of cane first becomes completely saturated at a larger angle, Θ_s, where $C_R \approx 0.6$ to 0.7. The overall compression ratio, C_o, $= Z_a/Z_n$.

Murry and Holt[17] assumed that only bulk fiber leaves from the discharge side of the rolls, i.e. $1 - \varepsilon' = 1$ and $\varepsilon' = 0$ in the discharge stream. $\dot{Q}_d$ is the air-free volume-discharge rate per unit length of roll. $\dot{Q}_d/S_R Z_n \equiv E_R$, the "reabsorption factor". E_R depends on S_R, C_o and the fineness of the shredded cane. At fixed S_R, $(E_R - 1) \propto (C_o - 1)$; and at $C_o = 3.0$ for finely shredded cane, $E_R = 1.06 + 0.0052 \cdot S_R$, where S_R is in ft/min. Thus $E_R > 1.0$, and usually is between 1.1 and 1.3.

It was further assumed[17] that u_x, the mean velocity of fiber in the x direction $= S_R \cdot \cos(\Theta)$ in regions where $Z_\Theta \cdot S_R \cdot \cos(\Theta) \geq \dot{Q}_d$. In those regions the volume-flow rate of bulk fiber per unit length of roll $= Z_\Theta \cdot S_R \cdot \cos(\Theta)(1 - \varepsilon')$. The region is bounded by Θ_d, where $Z_{\Theta d} \cdot S_R \cdot \cos(\Theta_d) = \dot{Q}_d = E_R \cdot S_R \cdot Z_n$. Thus $Z_{\Theta d} \cdot \cos(\Theta_d) = E_R \cdot Z_n$. Substituting for $Z_{\Theta d}$ in terms of Eq (145) and solving for $\cos(\Theta_d)$, Murry and Holt obtained

$$\cos(\Theta_d) = \frac{1 + Z_n/D_R + \sqrt{(1 + Z_n/D_R)^2 - 4 E_R Z_n/D_R}}{2} \quad \textbf{(147)}$$

$(1 - \varepsilon')$ cannot be greater than 1. But for $\Theta < \Theta_d$, $Z_\Theta \cdot S_R \cdot \cos(\Theta)(1 - \varepsilon')$ is less than $\dot{Q}_d$, the volume discharge rate of bulk fiber. Since the volume-flow rate of bulk fiber should be the same between the discharge and Θ_d, Murry and Holt reasoned that $u_x > S_R \cdot \cos(\Theta)$ in this region, possibly because of extrusion. The linear velocity of fiber relative to the stationary liquid in the region between Θ_s and Θ_d is $S_R \cdot \cos(\Theta)$. Hence the superficial velocity of the fluid relative to the fiber is $\varepsilon' \cdot S_R \cdot \cos(\Theta)$, where ε' is evaluated at Θ.

Murry and Holt determined P_F from Darcy's law, i.e.

$$\frac{dP_F}{dx} = -\frac{\mu}{k} U = -\frac{S_R \mu \varepsilon'}{k} \cos(\Theta) \quad \textbf{(148)}$$

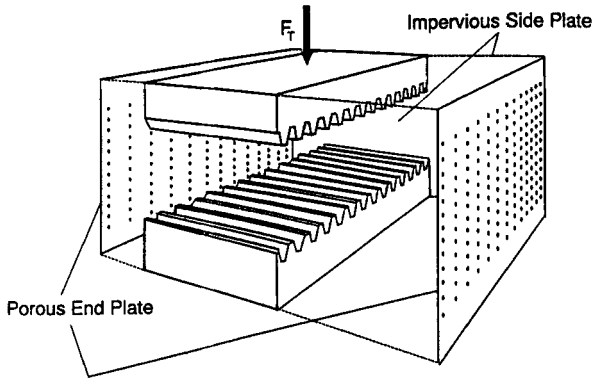

FIGURE 101 Pressing test cell for determining k_{eff} for expressing juice from shredded sugar cane in a roll mill (Loughran[228])

$dx = D_R \cdot \cos(\Theta) \cdot d\Theta/2$. Therefore

$$(P_F)_\Theta = \frac{D_R S_R \mu}{2} \int_{\Theta_s}^{\Theta} \frac{\varepsilon'}{k} \cos^2(\Theta)\, d\Theta \qquad \textbf{(149)}$$

ε' and k are functions of C_R, which, in turn, is a function of Θ, i.e.

$$C_R = \frac{Z_a / D_R}{1 + Z_n / D_R - \cos(\Theta)} \qquad \textbf{(150)}$$

Expulsion of fluid from bulk fiber during pressing causes its volume to decrease as C_R increases. Murry and Holt used an equation that probably is incorrect in accounting for how this decrease in volume affects ε', but effects of the error on calculated P_F probably are small.

Though the process was evaluated solely in terms of flows occurring in the x direction, fairly large amounts of fluid flow in the z or - z direction into vacant space at the base of the grooves on the rolls and then flow out the mill through the grooves. To account for this flow, Murry and Holt used k_{eff} in Eq (149) instead of the actual k. k_{eff} was determined by using the pressing cell shown in exploded form[228] in fig. 101. U = 0 at the mid-plane of the cell. Assuming

that U increases linearly from the mid-plane to the outflow surface, a volume balance shows that $U = -(x/2Z)(dZ/dt)$, where Z is the instantaneous height of the cake, -dZ/dt is the ram speed, and x is the distance from the mid plane of the cell. Assuming P_S is negligible and applying Darcy's law, Murry and Holt obtained

$$k = \frac{\mu(-dZ/dt)X^2}{12ZP_{Ta}} = \frac{\mu(-dZ/dt)X^3Y}{12Z\,F_T} \qquad (151)$$

where X is the length of the cell parallel to the assumed direction of flow, Y is its width and F_T is the force used to drive the grooved ram. In the cell they used, X = 102 mm and Y = 229 mm. P_{Ta}, the mean pressure corresponding to force F_T, $= F_T/XY$. $C_R = M_c/(\rho_c \cdot X \cdot Y \cdot Z)$, where M_c is the mass of cane used in the test and ρ_c is its density. Eq (151) was used in conjunction with measured F_T versus Z data to determine the k_{eff} versus C_R. For a sample of shredded cane with a bulk density of 40 lb/ft^3, $k_{eff} = 8\times10^{-11}\cdot C_R^{-3}$. Murry and Holt[17] indicated the actual $k = 9.33\times10^{-11}\cdot C_R^{-8.52}$. (Units were not specified in both cases, but probably are ft^2). Thus $k_{eff} \approx 370 \cdot k$ when $C_o = 3$. Using $k_{eff} = 8\times10^{-11}\cdot C_R^{-3}$ as k and their expression for ε' in Eq (149), Murry and Holt calculated a maximum P_F of 1675 psi (at $\Theta_d = 4.1°$) for $C_o = 3.0$, $S_R = 30$ ft/min, $Z_n = 0.466$ in. and $D_R = 26$ in.

Murry and Holt assumed that P_S is negligibly small and that P_n, the pressure acting normal to the roll surface, $= P_F$. Measured values of pressures at the crown of roll ridges versus Θ for the same S_R, D_R and fixed-solids content (12.8%) and various C_o are depicted in fig. 13 for very finely shredded cane. Experimental pressures at the crown were markedly higher than the calculated P_F at the same Θ and C_o and S_R. This occurred largely because pressures at the crown of ridges were significantly greater than the local mean pressure acting over the grooved surface as a whole.

Murry and Holt derived equations for F_R, the force applied per unit length of roll, and T_R, the torque applied per unit length of roll. These equations are

$$F_R = \frac{D}{2}\int_{\Theta_1}^{\Theta_2} P_n \sec(\Theta)\, d\Theta \qquad (152)$$

and

$$T_R = \frac{D^2}{4} \int_{\Theta_1}^{\Theta_2} P_n \tan(\Theta)\, d\Theta \qquad (153)$$

where P_n is the pressure acting normal to the roll surface and Θ_1 and Θ_2 respectively are the Θ at which cane contacts and leaves the roll surface. They assumed that $P_n = P_F$, i.e. neglected contributions of P_S to P_n.

Experiments[17] showed that: a) T_R is independent of S_R; b) F_R increases as C_o and cane coarseness increase and c) F_R slightly decreases or remains constant as S_R increases. Use of $P_n = P_F$ is inconsistent with these observations. Based on Eq (149), local P_F should increase linearly as S_R increases. Hence, if local P_n = local P_F, F_R should increase as S_R increases, instead of slightly decreasing or remaining constant. Further, T_R should increase as S_R increases instead of remaining constant. P_F should decrease as cane coarseness increases, because P_F is inversely proportional to k, and k should increase as cane coarseness increases. Deer[70] and Murry and Holt[17] showed that P_S increases markedly as coarseness increases. Therefore F_R probably increased as cane coarseness increased because P_S contributed significantly to P_n. The observed slight decrease in F_R as S_R increased is harder to explain. If P_n depended strongly on P_S and less strongly on P_F, F_R would tend to remain constant or increase slightly as S_R increases. Increases in S_R are accompanied by increases in E_R, which tend to reduce relative velocities of cane with respect to juice. This partly reduces the theoretically tendency of P_F to increase with S_R. In any case, it appears likely that P_S contributes significantly to P_n.

P_S versus C_R data calculated from measurements by Deer[70] indicate that even P_S for fine cane should contribute significantly to P_n. Murry and Holt accidentally may have partly compensated for neglecting P_S, by failing to account for its contributions to F_T when measuring k_{eff}. Measurement of k_{eff} involves other problems. Its value depends on the ratio of vertical and horizontal flow in the bed of cane. That ratio changes as compaction proceeds because the length of only one flow path changes. The ratio will be different

when different initial loads of cane are used. Probably, a standard load of cane is used, one that provides $Z = Z_n$ when $C = C_o$.

Loughran[229,230] found that for tests carried out in the cell shown in fig. 101 using cane of average fineness, $F_T = 112(C_R - 0.8)^2 + 3640\ (-dZ/dt)\ (C_R - 0.8)^2 - 186\ (-dZ/dt)$. F_T is in kN and $(-dZ/dt)$ is in m/s. F_T/XY for $-dZ/dt = 0$ probably can be used as a measure of the average P_S at different C_R. Based on Loughran's equation, $F_T/XY = 23.2$ MPa (3365 psi) at $C_R = 3.0$ when $-dZ/dt = 0$. Thus P_S apparently was very large in the tests that Loughran carried out, and corrected F_T should be used to determine k_{eff}. Presumably, the corrected $F_T = [3640\ (C_R - 0.8)^2 - 186]\ (-dZ/dt)$ for the shredded cane that Loughran tested.

Abularach[203] measured ε' during compaction of different types of plant matter, and, in all cases, found that ε' did not go to zero even at very high pressures and very high levels of compaction. Therefore it is very likely that discharged cane contains some free liquor in addition to bulk fiber. If so, net forward flow of free liquor occurs. The net forward flow of material per unit length of roll $E_R S_R Z_n = \dot{Q}_S + \dot{Q}_F$, where $\dot{Q}_S$ and $\dot{Q}_F$ respectively are the local net-forward volumetric flow rate of bulk fiber and free liquor. $\dot{Q}_S$ will go down as pressing proceeds, and $\dot{Q}_F$ will go up, but their sum will remain the same. If u_x for the bulk fiber $= S_R \cos(\Theta)$, the local $\varepsilon' = 1 - \dot{Q}_S/[Z_\Theta S_R \cos(\Theta)]$, where $\dot{Q}_S$ is a local value. U_F, the local velocity of the forward-moving free liquid $= \dot{Q}_F/(Z_\Theta \varepsilon')$; and the superficial relative velocity of the bulk solids with respect to the forward-moving free liquid, $U_r = \varepsilon'[S_R \cos(\Theta) - U_F] = S_R[\cos(\Theta) - E_R Z_n/Z_\Theta]$. U_r becomes 0 at $\Theta = \Theta_d$ and is negative at $\Theta < \Theta_d$, again goes to 0 as the cane leaves the rolls. If the approach just presented is valid, one does not have to account for changes in $\dot{Q}_S$ as pressing proceeds in order to determine U_r.

If U_r is negative in the region between Θ_d and Θ_e, where U_r again becomes 0, P_F should decrease as the cane goes from Θ_d to Θ_e. Murry and Holt observed that P_n remained fairly constant between Θ_d and $\Theta = 0$. Since C_R increases as Θ decreases in that region, P_S should also increase. $P_F = P_n - P_S \cdot \cos(\Theta)$. Therefore P_F decreases as cane moves from Θ_d to $\Theta = 0$; and existence of fairly constant P_n between Θ_d and $\Theta = 0$ is consistent with U_r being negative

there and with P_S contributing significantly to P_n. P_S versus C_R behavior is not reversible for compacted porous solids. Small decreases in C_R produce very large decreases in P_S. Since C_R decreases in going from $\Theta = 0$ to Θ_e, P_S drops very sharply then.

Only flows in the x direction have been considered up to now; flows towards the grooves in the rolls and effects of vertical components of solid velocity (u_z) and compaction non-uniformity also have to be considered. Use of k_{eff} in conjunction with total flow taken as occurring in the x direction is a crude and imprecise way of dealing with these complications. Use of Eqs (130) to (132) can provide a better way of dealing with them. It is difficult to numerically solve these equations by finite-difference methods for roll mills because of the complex geometry involved. Owen, Zhao and Loughran[230] resolved this difficulty by using finite-element methods to numerically solve equations similar to Eq (130) for conditions that apply for pressing of sugar cane in a two-roll mill and in the cell shown in fig. 101.

$P_F = 0$ was used as a boundary condition at both the grooved surfaces of the rolls and the cell shown in fig. 101. Owen et al. used an average bulk modulus, i.e. a linear approach, to account for how P_S changes during compaction. Thus, they do not appear to have adequately accounted for the highly non-linear and irreversible nature of P_S versus V behavior. Their computed P_F reach a maximum at $\Theta = 0$ or very much closer to it than Murry and Holt indicate; and, contrary to the experimental findings of Murry and Holt[17], they found that the peak P_F increased as S_R increased. Nevertheless, their approach represents a marked methodological improvement. The cited discrepancies between experimental and calculated results probably can be largely eliminated by use of better constitutive equations for the sugar cane.

Screw Expellers: Shirato and coworkers[174,231,232] systematically investigated screw expeller operation. They studied: a) distributions of normal pressure (P_n) along the length of the barrel, b) feed and discharge rates, and c) discharged solids dryness as functions of screw speed, solids concentration in the feed and feed pressurization. They used an expeller that had a screw with a gradually

decreasing channel height and a short throttling section at its discharge end. They viewed the process in terms of an effectively unwound, rectangular screw-channel that progressively diminished in height; and analyzed the process in terms of changes in e using an approach similar to that previously described for belt filters. However, as in Eq (24), they lumped effects caused dP_S/dV and α into an average consolidation coefficient, C_e.

For a 1:1 feed mix of a clay and a diatomaceous earth containing 42.3% solids by weight, they observed that: a) $\log(P_n)$ rose smoothly and progressively more rapidly as cake moved down the barrel, b) the maximum P_n occurred at the discharge end, and c) P_n at the discharge end rose and the percent solids in the discharge smoothly decreased as screw speed rose. For a more-fluid feed containing 30.7%-solids of the same composition, P_n did not rise smoothly at low screw-speeds; and the discharge rate increased and percent solids in the discharge gradually decreased as screw speed increased. However, at and above a critical speed; a) the percent solids in the discharge dropped radically, falling to close to the percent solids in the feed, b) the discharge rate rose radically, and c) P_n scarcely rose at all.

Effects produced by use of different throttling systems or dies and screws with different helix angles and channel depths were studied[232] using waste-treatment sludge and mixes of kaolin and diatomaceous earth or "sake cake". A die consisting of short, rotating, constant-pitch screw with a shallow channel of constant depth was particularly effective and provided high P_n and smooth discharge of cakes with high solids contents.

ACKNOWLEDGEMENTS

The National Science Foundation, the Agricultural Experiment Station of the University of Massachusetts, the Dipartimento di Scienze e Tecnologie Alimentari e Microbologiche at the Universita degli Studi di Milano and Special Project RAISA of the Consiglio Nazionale Delle Ricerche of Italy supported much of the work on which this review is based. I gratefully thank them for that support.

I also would like to acknowledge efforts by the following colleagues and co-workers at the University of Massachusetts, who shared in much of the work on which this review is based: Bor-Wen Huang, Serge Rebouillat, Victor Abularach, Joelle (Vallon) Humblot, Daniel Humblot, Naphtali Pollak, Tom Collyer, Shahed Zaman, Patrick Ngoddy, Gwen Richardson, Prasad Footrakul, Kong Hwan Kim, James Haight, John Rosenau and Lester Whitney. Other work of importance was done in cooperation with Prof. Claudio Peri, Bruno Zanoni, Laura Piazza, Cristina Rastelli, Maurizio Ghizzardi and Luciano Bernardi at the Universita degli Studi di Milano.

I would be remiss not to acknowledge the pioneering work of Karl Terzaghi, Mompei Shirato and Imre Kormendy, who provided scientific bases for studying expression and who helped shape or inform my thinking about expression.

17 NOMENCLATURE

A	cross sectional area of cake (m^2)
A_c	contact area between particles (m^2)
A_k	Constant, permeability correlations for fibrous beds [Eqs (85) and (86)]
A_I	term in Eq (48), (49), (51) and (53) (m^3/kg FS$\cdot$s)
A_z	local area for radial flow per unit length of cylinder (m)
a	fiber radius (m)
b	slope of t/Q versus Q plot for Buchner funnel filtration test (s/m^6)
b	exponent of P_S containing terms in $P_S(V)$ or $P_S(e)$ [Eqs (6), (7) and (10)]
B	P_h/P_S
B_I	term in Eq (48), (50), (52) and (54) (m^3/kg FS$\cdot$s)
B_C	coefficient in $\alpha(V)$ Eq (114)
c	exponent in $(1 - \varepsilon)$ versus P_S correlation [Eq (8)]
C	$-(1/\mu\alpha)(dP_S/dV)$ (kg FS^2/m$^4\cdot$s) [see Eqs (22), (24), (26) and (27)]
C_α	coefficient in Eq (75) (kg/m^3)
C_C	$de/d[\ln(P_S)]$ (dimensionless) [see Eq (1)]
C_e	$-1/[\mu\alpha\rho_S(de/dP_S)]$ (m^2/s) [see Eq (24)]
C_f	mass of retained solids per unit volume of filtrate (kg/m^3) Eq (81)

C_k constant used in Eq (78) (dimensionless)

C_o overall compression ratio in roll mill Z_a/Z_n

C_R compression ratio for sugar cane (Z_a/Z_Θ in roll mill; V_C/V_a in general)

C_S creep-term coefficient Eq (88)

D diameter of cake (m)

D_C diameter of a pressing system in which radial flow occurs or of Bucher-Guyer press (m)

D_i diameter at inner electrical contact in capillary suction test (m)

D_o diameter at outer electrical contact in capillary suction test (m)

D_R roll diameter (m)

D_T diameter of tubes in Bucher-Guyer press (m)

D_u diameter of unit cell (m)

d_c biological cell diameter (m)

d_{cp} plasmodesmata diameter (m)

d_f thickness of filter paper in capillary suction test (m)

d_p particle diameter (m)

d_w cell wall thickness

e porosity ratio, $\varepsilon/(1 - \varepsilon)$

E term defined by Eq (61)

E_o coefficient in Eq (3)

E_1 coefficient in Eq (6) $(m^3/kg\ FS)^n \cdot (kg/m \cdot s^2)$

E_2 coefficient in P_S versus V correlation of Murry and Holt (Pa)

E_3 constant in P_S versus V correlation of Murry and Holt

E_4 coefficient in Eq (7) and Eq (8) $(kg\ FS/m^3 \cdot Pa^{b-1})$

E_5 Constant used in Eq (9) (Pa)

E_6 Coefficient used in Eq (9) $(m^3/kg\ FS)$

E_R reabsorption factor in sugar-cane roll mill, $\dot{Q}_d/S_R Z_n$

F_B force acting on media (bottom of cell) (N)

F_{max} maximum value of F_T (N)

F_R relaxed value of F_T (N)

F_R force acting on unit length of roll in roll mill (N/m)

F_T ram force (N)

F_w axial force transmitted to cell wall by friction (N)

$F(I)$ $H(I) \cdot P_S(I) \cdot V(I)$ (m/s^2)

f_p coefficient of friction between particles

f_w coefficient of friction between cake and wall

f fraction of compaction due to secondary consolidation

g acceleration due to gravity (9.806 m/s^2)

G exponential coefficient in $\alpha(V)$ Eq (115) (kg/m^3)

G_1 $1/k_1$, compliance of in-series spring analog in rheological model

G_2 $1/k_2$, compliance of spring analog in Kelvin-Voigt element

G_i analog of compliance of spring-like element in Kelvin-Voigt body (m^3/kg)

G_i coefficient in Lanoiselle compaction equation Eq (95)

G_r analog of compliance of in-series spring-like element

H $4 \cdot B \cdot f/D$ (1/m) [see Eqs (33), (34) and (39)]

h drop in liquid head (m)

I position index

J time index

J Murase's correction factor for converting ζ for uniaxial consolidation into ζ for cylindrical squeezing

j term index in series [see Eq (28)]

k' Darcy's law permeability used in soil mechanics (m/s) [see Eq (17)]

k Darcy's law permeability (m^2)

k_{eff} effective value of k (m^2)

k_1 modulus for in-series spring analog in rheological model

k_2 modulus for spring analog in Kelvin-Voigt element

K $-d\ln(P_S)/dV$ (kg/m^3) [see Eq (2)]

K_B $-d\ln(P_B)/dV_a$ (kg/m^3)

K_e empirical constant used in place of $4C/\pi$ in Eq (93)

K_R $-d\ln(P_R)/dV$ (kg/m^3) Eq (106)

k_r $-d\ln(R_m)/dt$ in Eq (89) (1/t)

K_r $-d\ln(R_m)/dV$ in Eq (108) (kg/m^3)

K_T $-d\ln(P_T)/dV_a$ (kg/m^3) Eqs (104) and (105)

L_p hydraulic conductivity of cell walls ($m/Pa \cdot s$)

M initial mass of cake (kg)

M_c mass of sugar cane used in effective permeability cell (kg)

$\dot{M}_c$ mass feed rate of sugar cane per unit length of roll (kg cane/m • s)

M_d mass of dry fixed solids in cake sample or load, $M \cdot Y_S$ (kg)

M_z mass of fixed solids per unit length of cylinder (kg FS/m)

m exponent in Eq (11)

m mass of fixed solids per unit length between inner cylindrical surface and a cylindrical surface in cake (kg FS/m)

m exponent of (V_S/V_o) in Ashby's strength parameter correlations

N number of space nodes used in numerical solutions of PDE

N_T number of tubes in Bucher-Guyer press

n Value of I at which U is being computed [see Eq (49)]

n exponent of V in $P_S(V)$ [Eq (5)], (e_{ref}/e) in $P_S(e)$ [Eq (3)] or e in Eq (82)

n exponent in α versus P_S correlation [see Eqs (76) and (77)]

P_B axial pressure acting on media (Pa)

P_c value of $P_S(W)$ at which R_m starts to increases rapidly (Pa)

P_E P_S contribution due to excess fluid pressure inside particles (Pa)

P_F fluid pressure (Pa)

P_h horizontal component of superficial solid stress (Pa)

P_L P_S at which P_S stops increasing linearly as V decreases and starts to increase exponentially (Pa)

ΔP_m fluid pressure drop across media

P_{max} maximum allowed ram pressure (Pa)

P_N stress acting normal to contact area of particle (Pa)

P_n pressure acting normal to surface of roll or extruder wall (Pa)

P_R local P_S after completion of relaxation (Pa)

P_{ref} reference value of P_S in function $P_S(V)$ or $P_S(e)$

P_S axial component of superficial solid stress (Pa)

P_{Si} solid stress normal to i direction (Pa)

P_{Sr} solid stress in radial direction (Pa)

$P_S(e)$ function providing P_S when e is specified (Pa)

$P_S(V)$ function providing P_S when V is specified (Pa)

P_T ram pressure (Pa)

P_{Ta} average value of ram pressure in cell used to evaluate k_{eff} (Pa)

P_{TR} ram pressure after completion of relaxation (Pa)

ΔP_w decrease in P_S caused by wall friction (Pa)

P $(P_T - P_{rt})/(P_{max} - P_{rt})$

Q volume of permeate or filtrate (m^3)

Q_C volume of cake sample (m^3)

$\dot{Q}_d$ air-free volume rate of cake discharge per unit length of roll (m^2/s)

$\dot{Q}_F$ volume rate of forward free-fluid flow per unit length of roll (m^2/s)

Q_m volume of permeate collected with only media present (m^3)

$\dot{Q}_S$ volume rate of bulk fiber flow per unit length of roll (m^2/s)

R radius of curb press (m)

R_a constant in R_m correlations Eqs (88) and (89) (1/m)

R_b constant in R_m correlations Eq (108)) (1/m)

R_m media resistance (1/m)

R_o total flow resistance at the start of consolidation (1/m) Eq (91)

R_T total flow resistance (1/m) Eq (91)

r empirical constant used in Eqs (69) and (70) (1/m)

r radial distance (m)

r_i radius at inner cylindrical wall

r_o radius at outer cylindrical wall

S_b belt speed (m/s)

S_R surface velocity of roll (m/s)

s fractional saturation of interparticle pores (-)

T tension per unit width of belt (N/m)

T_R torque per unit length of roll in roll mill (N)

t time (s)

t_b t when $P_S(W) = P_c$ and media resistance starts to increase (s)

t_c time for water to move from D_i to D_o in capillary suction test (s)

t_m time correction used to account for media resistance during filtration at constant ΔP_F (s)

t_p time cake is maintained at constant pressure (s)

t_r relaxation time for cakes held at constant volume (s)

t_s time when creep induced compaction begins (s)

t_u loading and unloading time in pressing cycle (s)

t_{90} time at which 90% of primary consolidation is complete (s)

U local superficial velocity of fluid relative to fixed solids (m/s)

U_o U at outflow media (m/s)

U_c U at interface between filter cake and feed slurry (m/s)

U_F local absolute velocity of forward-flowing free fluid (m)

U_m flow rate in permeation test with only media present (m/s)

u_x fixed solids velocity in the x direction

u_y fixed solids velocity in the y direction

u_z fixed solids velocity in the z direction

V local bulk specific volume based on mass of fixed solids (m^3/kg FS)

V_a average value of V (m^3/kg FS)

V_{af} final value of V_a (m^3/kg FS)

V_b V_a when $P_S(W) = P_c$ and R_m increase starts (m^3/kg FS) Eq (108)

V_c V when $P_S = 0$; V at w_{c+} (m^3/kg)

V_C value of V at which cake becomes saturated (m^3/kg FS)

V_i average value of V in ith layer (m^3/kg FS)

V_L transition V for change from linear to exponential P_S versus V behavior (m^3/kg FS)

V_o V in feed slurry during filtration; initial value of V (m^3/kg FS)

V_p volume of particles in cake per unit mass of fixed solids (m^3/kg FS)

V_{po} initial value of V_p (m^3/kg FS)

V_{ref} reference value of V (m^3/kg FS) [see Eq (2)]

V_S specific volume of fixed solids (m^3/kg FS)

V_t V at which $P_S(V)$ starts to curve upward above linear $\ln(P_S)$ versus V line

V_U V for fixed solids + non-expressible water (m^3/kg FS)

V_w specific volume of water (m^3/kg water)

v_i volume of inner cylinder per unit length (m^2)

w mass of fixed solids per unit area between neutral plane or ram and position in cake (kg FS/m^2)

w_c w at interface between liquid and feed slurry (kg FS/m^2)

w_c^- immediately upstream of w_c

w_c^+ immediately downstream of w_c

W total mass of fixed solids per unit area between ram or ram and outflow surface (kg FS/m^2)

X kg water/kg FS in press feed or cake

X_{ne} kg of non-expressible water per kg fixed solids

x distance in direction in which solids are conveyed (m)

Δx_n distance cake moves in x direction at nth computation step (m)

Y weight fraction of fixed solids in press cake or filter cake (kg solids/kg moist cake)

Y_e (volume of fluid expelled from particles in outflow)/(total outflow volume)

Y_S weight fraction of fixed solids in press feed or waste-treatment sludge

Y_w weight fraction of water in press feed

y distance in direction at right angles to z and x directions (m)

Z cake thickness or height or length of cylinder (m)

Z_a cake height at which $C_R = 1$

Z_c capillary rise obtainable with filter paper in capillary suction test (m)

Z_d effective air-free discharge-height of cake in roll mill (m)

Z_n cake thickness at plane between roll axes in roll mill (m)

Z_o initial length of cylinder (m)

Z_Θ cake height at angle Θ on two-roll mill (m)

z distance from ram surface or neutral plane in direction of liquid flow (m)

z_n z after cake moves nth step in x direction (m)

Greek Letters

α local, specific filtration resistance of cake (m/kg) [see Eq 16)]

α_a mean effective α in Buchner funnel filtration test (m/kg) [see Eq (73)]

α_b constant in $\alpha(V)$ Eq (114) and Eq (115)

α_o reference value of α in Eq (76) (m/kg)

β coefficient in Eq (94), an empirical consolidation equation

γ exponent in Eq (94), an empirical consolidation equation

ε fraction of cake volume not occupied by fixed solids

ε' fraction of cake volume not occupied by particles

ζ $(Z_o - Z)/(Z_o - Z_\infty)$

η pressing rate coefficient in $P_S(V,Z')$ and $P_S(V,V')$

η_K flow resistance for dashpot in Kelvin-Voigt element

η_J juice yield based on original mass of juice present [see Eq (67)]

η_S juice yield based on original mass of feed (kg juice/kg feed) [Eq (68)]

λ exponential coefficient in e versus P_S correlation Eq (4) (1/Pa)

λ_i exponential coefficient in Lanoiselle compaction equation Eq (95)

Λ creep coefficient in exponent in Eq (89) and (90) (1/s)

Θ field strength term (m/s^2)

Θ angle relative to plane passing through roll axes in a two-roll mill

Θ_a angle at which C_R becomes 1 in two-roll mill

Θ_c angle of contact of belt on roll

Θ_d angle on sugar cane roll mill where $Z_\Theta \cdot S \cdot \cos(\Theta) = \dot{Q}_f$

Θ_e negative Θ at which U becomes 0 in roll mill

Θ_s Θ at which cake first becomes completely saturated in two-roll mill

Θ_1 Θ at which sugar cane first contacts roll

Θ_2 Θ at which sugar cane leaves roll

μ viscosity $(kg/m \cdot s)$

υ exponent in Eq (93), an empirical consolidation equation

ξ function to correct $\ln(P_S)$ versus V curvature

ξ particle surface area per unit of particle volume (1/m)

ρ_F density of fluid

ρ_S density of fixed solids

τ $C \cdot t/W^2$ or $C_e \cdot t/\Omega^2$

τ_r relaxation time constant Eqs (124), (127) and (128) (s)

τ_o relaxation time coefficient $(s \cdot kg/m^3)$

τ_{ji} shear stress acting in j direction on plane normal to i direction

Φ Series in Eqs (98) and (99)

χ Vesilind's capillary suction test characterization parameter ($kg/m \cdot s^2$)

Ψ fraction of cake volume occupied by pores in particles

ω volume of fixed solids per unit between neutral plane or ram and position in cake (m)

ω angular velocity when centrifugal forces are important (1/s)

Ω total volume of fixed solids per unit area between ram or ram and outflow surface (m)

Subscripts

a average

app apparent

c sugar cane

eff effective

exp *due to expansion*

f final

I at node I or in slice I

m without cake present

max *maximum or maximum tolerable value*

n at nip in two-roll mill or at plane between roll axes or node n

o initial

R roll, relaxed

r radial

ref reference value

x in the x direction

y in the y direction

z in the z direction

∞ at equilibrium

18 LIST OF REFERENCES

1 Speichem Bulletin, "Continuous Extraction of Apple Juice", 1974

2 H.L. Crosby, in "Pulp and Paper Technology 2nd Edition.", K.W. Britt, ed., Van Nostrand Reinhold, New York, 1970, p.292

3 L.H. Tindale and S.R. Hill-Haas J. Am. Oil Chem. Soc. 53, 265 (1976)

4 D.K. Brederson The Roll of the Screw Press in a Modern Vegetable Oil Plant. paper 38d, AICHE National Meeting, Denver CO, Aug. 29, 1983

5 E.W. Lusas, L.H. Watkins and K.C. Separation of Fats and Oils by Solvent Extraction: Non-Traditional Methods in "Edible Oils and Fats Processing: Basic Principles and Modern Practices", D. Erickson, ed. Am. Oil Chem Soc., Champaign Il., 1990, p.56

6 A. Utvik, Liquid Solid Separation by Twin Screw Pressing, paper 38, 1983 Denver AIChE Mtg

7 Stord Bartz Bulletin, 1982

8 C. Buttersack, Zuckerindustrie, 119, 831 (1994)

9 Hubert C. Stollenwerk Inc. Bulletin, "The Stoll II Press". 1979

10 Fred S. Carver Inc. Bulletin CP-1963 Carver Cocoa Presses, 1963

11 G. Troost "Technologie des Weines", Vol. 1 in "Handbuch der Kellerwirtschaft", Verlag Eugen Ulmer, Stuttgart, 1972, p.82, 94, 106

12 H.G. Kessler "Food Engineering and Dairy Technology", Verlag A. Kessler, Freising, 1981, p.436

13 Bucher-Guyer Ltd. Bulletin HPX-5005-Bucher, 1991

14 Bucher-Guyer Ltd. Information, Practical experience gained in 1978 with the combined press/extraction process BUCHER, 1979

15 J.C.P. Chen, Raw Sugar Process and Extraction of Juice, Chap. 4 in "Cane Sugar Handbook", J. C. P.Chen and C.C. Chou, eds. J. Wiley, 1993, p. 48-86

16 Fulton Iron Works Company Bulletin, "Fulton Cane Mills" Fulton Iron Works Company, St. Louis, Missouri 63116

17 C.R. Murry and J.E. Holt, "The Mechanics of Crushing Sugar Cane" Elsevier, Amsterdam, 1967, p.1-5, p.34-94, p.101

18 B. Wahlstrom, Pressing, Chap. 9 in Pulp and Paper Science and Technology Vol II", ed. C.E. Libby, McGraw Hill, New York, 1962, p.229-237

19 I.W. Peters, Paper Machine - Press Section, Section 6-3, in "Handbook of Pulp and Paper Technology 2nd Edition.", ed. K.W. Britt, Van Nostrand Reinhold, New York, 1970, p. 419-429

20 T. Helle and T. Forseth, Tappi J. 77, No. 6, 171 (1994)

21 G. Hoffmann, "The Chemistry and Technology of Edible Oils and Fats and Their High Fat Products", Academic Press, London, 1989, p 78-79

22 M. Shirato, T. Murase and E. Iritani, F.M Tiller and A.F. Alciatore, Filtration in the Chemical Process Industry, Chap.6 in "Filtration, Principles and Practices, 2nd Ed,", eds. M.J. Matteson and C. Orr, Marcel Dekker, New York, 1987, p. 348-378

23 Larox Inc. Bulletin 103 GB 05/85, Larox Automatic Pressure Filters, Columbia, Maryland, 1985

24 CMMC Bulletin, RPF 30/40/50, Chalonnes sur Loire, 1994

25 Andritz, A Dewatering Profile, Andritz-Ruthner Inc. Arlingtom Texas, 1995, p. 6-11

26 Bellmer, Bellmer Winkelpress F, Gebr. Bellmer GmbH and Co., Niefern, Germany, 1992

27 Eimco, Eimco Filtration Equipment, Eimco, Salt Lake City, Utah, 1983

28 R.B. Dick and R.O. Ball, CRC Critical Reviews in Environmental Control, 10, 269 (1980)

29 I. Andreasen and B. Nielsen, Water Sci. Techn., 28, 37 (1993)

30 H.P. van der Roest, A.A. Salomé and E. Korneef, Water Sci. Techn., 28, 21 (1993)

31 Permutit Company Bulletin 5595A, Permutit Multi-Roll Sludge Dewatering Press, The Permutit Company, Paramus N.J. 1975

32 Stoelting Inc, Stoelting Flexipress, Stoelting Inc, Kiel Wisconsin, undated

33 Process Engineers Inc., P.E.I./Stoelting Drainpress Dejuicer, Process Engineers Inc. Hayward, Calif., undated

34 Bellmer, Bellmer Winkelpress W for Grapes, Gebr. Bellmer GmbH and Co., Niefern, Germany, 1992

35 Klein, Competence in Food Technology, Alb. Klein GmbH & Co., Niederfischbach, Germany, 1994

36 Enbom, Belt Presses, Helsinki, Finland, undated

37 J. Novak, W. Knocke, W. Burgos, and P. Schuler, Water Sci. Techn., 28, 11 (1993)

38 L. Thomas, G. Jungschaffer, and B. Sprössler, Water Sci. Techn. 28, 189 (1993)

39 A. Bähr, European Patent Application 0 398 131 A2, May 8, 1990

40 E. Muhlack, Zuckerind., 117, 525 (1990)

41 F. Pouillaude, J. Vetter, R. Plever and P. Delalandre, Zuckerind. 113, 38 (1988)

42 FMC, Citrus Juice Extractors, FMC Corporation, Citrus Machinery Div. Lakeland, Florida, undated

43 Brown, Brown Model 400 "Cushioned Reaming" Citrus Juice Extractor, Brown International Corp., Covina, California, undated

44 Anonymous, Filtr. & Sep., 32, 212 (1995)

45 Anonymous, Filtr. & Sep., 29, 121 (1992)

46 Alfa Laval Separations AB Bulletin IB 41279E, p. 12

47 S. Minett, Filtr. & Sep., 33, 25 (1996)

48 O.E. Albertson and E.E. Guidi, J. Water Pollut. Control Fed., 41, 607 (1969)

49 E. Lowe, E.L. Durkee, and W.E. Hamiltom, U.S. Patent No. 3,346,392 Oct. 10, 1967

50 J.A. Rowse, U.S. Patent No. 3,042,578, July 3, 1962

51 G.V. Laivins and E.M. Scallan Tappi J., 77, No. 3, 125 (1994)

52 K. Terzaghi and R.E. Peck, "Soil Mechanics in Engineering Practice", Wiley, New York, 1948, p. 48-78, 233-242

53 M. Shirato, T. Murase, H. Kato and S. Fukaya, Kagaku Kogaku, 31, 1125 (1967)

54 R.E. Olson, in "Consolidation Testing in Consolidation of Soils", eds. R.N Young and F.C. Townsend, ASTM, Philadelphia, 1988, p. 7-68

55 P.L.Berry and T.L. Poskitt, T.L., Geotechnique 18, No. 9, 27 (1972)

56 H.G. Schwartzberg, J.R. Rosenau and G. Richardson in "Drying and Concentration of Foods and Other Materials", AIChE Symp Ser. 163,

Vol. 73, eds. C.J. King and J.P. Clark, AIChE, New York, 1977, p. 177-190

57 H.G. Schwartzberg, T. Collyer, and L.F. Whitney, in "Food, Pharmaceutical and Bioengineering", AIChE Symposium Series 74, ed. G. Tsao, A.I.Ch.E., New York, 1978. p. 166-174

58 E.I. Vorob'ev and M.N. Shinkarik, M.N. Teor. Osn. Khim. Teknol., 22, 226 (1987) translation in Theor Found. Chem. Eng. 170 (1988)

59 H.P. Grace, Chem. Eng. Prog., 49, 303, (1963)

60 B.W. Huang, Pressing Tests with Sugar Beets, Internal report, Dept. of Food Engineering, University of Massachusetts. 1981

61 M.F. Ashby, Metall. Trans. A., 14A, 1755 (1983)

62 L.J. Gibson and M.F. Ashby "Cellular Solids", Oxford University Press, Oxford, England, 1988

63 M. Peleg, I. Roy, O.H. Campanella and M.D. Normand, J. Food Sci., 54, 987 (1989)

64 S. Swyngedau, A. Nussinovitchm I. Roy, M. Peleg, and V. Huang, J. Food Sci. 56, 756 (1991)

65 D. Leonhard, Water Sci. Techn., 28, 117 (1993)

66 P. Kos, D.D. Adrian, J. Environ. Eng. Div. Am. Soc. Civ. Eng., 101, 947 (1975)

67 D. Leonhard, "Eindickung und Entwässerung als Konsolidierungsvorgang, Thesis, University of Karlsruhe

68 F.M. Tiller and W.F. Leu, J. Chin. Inst. Chem Eng., 11, 61 (1980)

69 W. Leu, Cake Filtration, Ph.D. dissertation, Univ. of Houston, 1981

70 N. Deerr, "The Milling of Cane Considered in Relation to the Volume Occupied by the Fiber". Exp. Station Report Hawaiian Sugar Planters Assoc., 1912

71 P.G. Atherton, Proc. Queensland Soc. Sugar Cane Technologists, 21, 225 (1954)

72 C.R.D. Shannon, Proc. Meet. Br. West Indies Sugar Technol., 38, (1942)

73 W.L. Ingmanson, Chem Eng. Prog., 49, 577 (1957)

74 W.L. Ingmanson, letter to C.F. Gurnham, March 25, 1960

75 C.F. Gurnham and H.J. Masson, Ind. Eng. Chem., 38, 1309, (1946)

76 C.F. Gurnham, "The Compression of Fibrous Materials with Particular Reference to the Expression of Liquids", Ph.D. Thesis, New York University, 1942

77 C.F. Gurnham, "Preliminary Investigations of a Theory of Expression", M.S. Thesis, New York University, 1940

78 R.S. Spencer, C.D. Gilman and R.M. Wiley, J. Appl. Phys. 21, 527 (1950)

79 I. Kormendy, Act. Aliment. Acad. Sci. Hung. 1, 315 (1972)

80 E.C. Koo, Ind. Eng. Chem., 34, 342 (1942)

81 E.C. Koo, J. Chem. Eng. (China) 4, 15 (1937)

82 G.C. Mrema, "Mechanisms of Mechanical Oil Expression from Rapeseed and Cashew", Ph.D. Thesis, University College Dublin. 1979

83 H. D. Wilder "Compression Creep Properties of Wet Pulp Mass", Ph.D. Thesis, Institute of Paper Chemistry, Appleton, WI 1960

84 W.H. Baskerville and A.C. Wambie, Engineering Experiment Station Bulletin No. 12, University of Tennessee, 1942

85 H.G. Schwartzberg, Chapter 16 in "Physical Properties of Foods, eds. M. Peleg and E. Bagley, AVI, Westport, Connecticut, 1983, p. 423-471

86 D.W. Taylor, "Fundamentals of Soil Mechanics", Wiley, New York, 1948, p. 213, 238

87 C. Buttersack and W. Basler, Plant Sci. (Shannon Irel.), 76, 229 (1991)

88 J.A. Petty and M.A. Palin, J. Exp. Bot., 34, 688 (1983)

89 J.A. Petty, Holzforschung, 35, 95 (1981)

90 C.S. Spyropoulos, J. Membrane Biol., 76, 17 (1983)

91 M.T. Tyree, Can J. Bot., 46, 317 (1968)

92 U. Zimmermann and E. Steudle, Aust. J. Plant Physiol., 3, 1 (1975)

93 B. Alberts, D. Bray, J. Lewis, M. Raff, K. Roberts and J.D. Watson, Chapter 19 Special Features of Plant Cells in "Molecular Biology of the Cell", Garland Publishing Inc., New York, 1983, p. 1099-1146

94 B.S. Thomas, Pulp Properties, Section 3.9 in "Handbook of Pulp and Paper Technology 2nd Edition.", ed. K.W. Britt, Van Nostrand Reinhold, New York, 1970, p. 226

95 F.G. Dennis Jr., Apples, Sect 3-6. in "Handbook of Fruit Set and Development", ed. S.P. Manselise, CRC Press, Boca Raton, Florida, 1986, p. 5

96 C. Buttersack, P. Steinert, R. Gieringer and K. Bucholz, in Proceedings of 6th World Filtration Congress, Nagoya, 1993, p. 901

97 V. Tullin, Zucker, 5, 433 (1953)

98 R.G. Koegel, V.I. Fomin and H.D. Bruhns, Cell Rupture Properties of Alfalfa, ASAE Paper No. 72-309, ASAE, St. Joseph, Michigan

99 P. Steinert, G. Galling, C. Buttersack and K. Buchholz, Zuckerindustrie, 115, 840 (1990)

100 E. Holtz, I. Ohlson and H. Schwartzberg, Solute Separation by Selective Infusion, AIChE Annual Meeting, San Francisco, CA, 1984

101 H. Brüniche-Olsen, "Solid Liquid Extraction", NYT Nordisl Forlag, Arnold Busck, Copenhagen, 1962, p. 178

102 D.C. McIntosh, Section 1-5, "Handbook of Pulp and Paper Technology 2nd Edition.", ed. K.W. Britt, Van Nostrand Reinhold, New York, 1970, p. 36, 42

103 C. Buttersack, P. Steinert, R. Geiringer and K. Buchholz, Proc. 6th World Filtration Congress, Nagoya, 1993, p. 561

104 T. Addy, L.F. Whitney and C.S. Chen, Mechanical Parameters in Leaf Cell Rupture, ASAE Paper No 75-1057, 1975, ASAE, St. Joseph Mich.

105 N. Deerr, The Influence of the Structure of Cane on Mill Work in Sugar Factories, Expt. Station Report Hawaiian Sugar Planters Assoc., Honolulu, Hawaii, 1910

106 K. Sawamoto, M.S. Thesis Nagoya University, 1967

107 F.M. Tiller and W.M. Lu, AIChE J., 18, 569 (1972)

108 B.F. Ruth, Ind. Eng. Chem., 27, 708 (1935)

109 J.K. Mitchell, "Fundamentals of Soil Behavior", Chap. 12, Wiley, New York, 1993, p. 19, 228-246, 318

110 I. Kormendy, Act. Aliment. Acad. Sci. Hung. 3, 93 (1974)

111 P.B. Sorenson, P. Moldrup, and J.A. Hansen, Chem. Eng. Sci., 51, 967 (1996)

112 P.B. Sorenson and J.A. Hansen, Water Sci. Techn., 28, 133 (1993)

113 S. Rebouillat, H.G. Schwartzberg and LeClerc, "Proceedings of 6th World Filtration Congress", Nagoya 1993

114 I. Kormendy, J. Food Sci., 29, 631 (1964)

115 H. Gray, Trans. Am. Soc. Civ. Eng., 110, 1327 (1945)

116 M. Shirato, T. Murase, N. Hayashi and T. Fukushima, J. Chem. Eng. Jpn., 10, 154 (1977)

117 A.E.Z. Wissa, J.T. Christian, E.H. Davis and S. Heiberg, J. Soil Mech. Found. Div, Am. Soc. Civ. Eng., 97 No. SM10, 1393 (1971)

118 M. Shirato, T. Murase, M. Negawa and T. Senda, J. Chem. Eng. Jpn., 3, 106 (1970)

119 M. Shirato, T. Aragaki, R. Mori and K. Sawamoto, J. Chem. Eng. Jpn., 1, 86 (1968)

120 D.E. Smiles, Chem. Eng. Sci., 25, 985 (1970)

121 D.E. Smiles and J.M. Kirby, Sep. Sci. Technol., 22, 1405 (1987)

122 X. Wu, Chem. Eng. Sci., 49, 831 (1994)

123 I. Tosun, Chem. Eng. Sci., 41, 2563 (1986)

124 E.J. La Heij, P.J.A.M. Kerkhof, K. Kopinga and L. Pei, AIChE J., 42, 963 (1996)

125 K. Stamatakis, and C. Tien, Chem. Eng. Sci., 46, 1917 (1991)

126 R.J. Wakeman, Trans. Inst. Chem. Eng., 59, 260 (1981)

127 F.R. Tiller and N.B. Hsyung, Water Sci. Techn., 28, 1 (1993)

128 B.F. Ruth, Ind. Eng. Chem., 38, 564 (1946)

129 R.S. Gale, R.C. Baskerville and J.D. Swanwick, Water Pollut. Control, 66, 553 (1967)

130 A.E. Scheidigger, "The Physics of Flow Through Porous Media", McMillan, New York, 1960

131 P.C. Carman, Trans. Inst. Chem. Eng. (London), 16, 168 (1938)

132 S. Ergun, Chem. Eng. Prog., 48, 89 (1952)

133 M.K. Bo. D.C. Freshwater, and B. Scarlett, Trans. Inst. Chem. Engrs., 43, t228 (1965)

134 J. Happel and H. Brenner, "Low Reynolds Number Hydrodynamics", Prentice Hall, Englewood Cliffs, N.J. 1965

135 J. Happel, AIChE J., 4, 197 (1958)

136 H.G. Schwartzberg, B.W. Huang and C. Peri, Modelling Mechanical Expression of Fluid from Cellular Biological Solids, Paper 21e, 1994 AIChE Annual Meeting, San Francisco, CA, Nov. 13-18, 1994

137 M. Tokita, and T. Tanaka, J. Phys. Chem. 95, 4613, (1991)

138 J. Vallon and D. Humblot and H.G. Schwartzberg, paper IFT Annual Meeting, Anaheim, CA, June 1984

139 P.A. Vesilind "Treatment and Disposal of Wastewater Sludges", Ann Arbor Science, 1979

140 V. Lotito, G. Minimi, L. Spinosa. and F. Lore, Water Sci. Techn. 28, 103 (1993)

141 P.R. Karr and T.M. Keinath, J. Water Pollut. Control Fed., 50, 1911 (1978)

142 L. Olböter and A. Vogelpohl, Water Sci. Techn., 28, 149 (1993)

143 R.S. Gale, Water Pollut. Control, 66, 622 (1967)

144 E. Friedrich, H. Friedrich, W. Heinze, K. Jobst, H.J. Richter, and W. Hermel, Water Sci. Techn., 28, 145 (1993)

145 J.R. Feldkamp, Géotechnique, 39, 141 (1989)

146 R.C. Baskerville and R.S. Gale, Water Pollut. Control, 67, 233 (1968)

147 J-H. Tay and S. Jeyaseelan, Water Sci. Techn. 28, 249 (1993)

148 H.Z. Sarikaya, and S. Al-Mashoud, Water Sci. Techn. 28, 47, (1993)

149 H. Unno, H. Muraiso and T. Akehata, Water Res., 17, 149 (1983)

150 P.A. Vesilind, J. Water Pollut. Control Fed., 60, 215 (1988)

151 P. Walstra, The Syneresis of Curd, Chapter 5 in "Cheese Chemistry, Physics and Microbiology", Vol. 1, ed. P.F. Fox, p. 141-191

152 S. Rebouillat, Pressing of Casein Curds, Internal Report, Food Engineering Dept. University of Massachusetts, 1985

153 G.W. Jackson and D.P. James, Can. J. Chem. Eng., 64, 364 (1986)

154 I. Langmuir, Part IV in OSRRD No. 865, Ser. No. 353, W.H. Rodebush et al. ed., 1942.

155 J. Happel, AIChE J., 5, 174 (1959)

156 E.M. Sparrow and A.L. Loeffler Jr., AIChE J., 5, 193 (1959)

157 J.E. Drummond and M.I. Tahir, Int. J. Multiphase Flow, 10, 515 (1984)

158 S. Kuwabara, J. Phys. Soc. Jpn., 14, 527 (1959)

159 H. Hasimoto, J. Fluid Mech., 5, 317 (1959)

160 A.S. Sangani and A. Acrivos, Int. J. Multiphase Flow, 8, 193 (1982)

161 M.L. White, J. Phys. Chem., 64, 1563 (1963)

162 R. Viswanadham, C.D. Agarwal, and E.J. Kramer, J. Appl. Polym. Sci., 22, 1655 (1978)

163 K.H. Stenzel, A.L. Rubin, W. Yamayoshi, T. Miyata,, T. Suzuki, T. Sohde, and M. Nishizawa, Trans. Amer. Soc. Artif. Intern. Organs, 17, 293 (1971)

164 E.M. Johnson and W.M. Deen, AIChE J., 42, 1220 (1996)

165 H. bin Jamaluddin, "Alfalfa Protein Decolorization by Filtration", M.S. Thesis, University of Massachusetts, 1978

166 M.L. Agerbaek and K. Keiding, Water Sci. Techn., 28, 159 (1993)

167 D.W. Taylor and M. Merchant, J. Math. Phys., 19, 167 (1940)

168 S. Muruyama and T. Yamanouchi. Trans. Jpn. Soc. Civ. Eng. no. 14, 62 (1952)

169 Y. Ishii, S. Kurata, and S. Fukuya, Trans. Jpn. Soc. Civ. Eng. no. 30, 1 (1955)

170 R.E. Gibson and K.Y. Lo, Publication no. 41, Norwegian Geotechnical Institute, Oslo, 1961

171 T. Mogami in "Doshitsu Rikigaku", Iwanami, Tokyo, 1961, p. 92

172 M. Shirato, T. Murase, A. Tokunaga, and O. Yamada, J. Chem Eng. Jpn., 7, 229 (1974)

173 M. Shirato, T. Murase, M. Iwata and S. Nakatsuka, Chem Eng. Sci. 41. 3213 (1986)

174 M. Shirato, T. Murase and N. Hayashi, Proceedings World Filtration Congress III, Vol. I, 1982, p 280-287

175 M. Shirato, T. Murase, T. and T. Aragaki, "Slurry Deliquoring by Expression", Dechema Monographien, Vol 74, 1973 p 9-29, Dechema, Cologne

176 M. Shirato, T. Murase, K. Atsumi, T. Nagami and H. Suzuki, J. Chem. Eng. Jpn., 1, 334 (1978)

177 M. Shirato, T. Murase and N. Hayashi, Proceedings 2nd Pacific Chemical Engineering Congress, Vol. I, 1977, p. 667

178 S. Rebouillat, "Deshydration par Filtration Pressage" Doctoral Thesis, L'Institut National Polytechnique de Lorraine, 1983

179 S. Rebouillat, D. LeClerc and G. Baluais, Entropie, 21, No. 121, 13 (1985)

180 M. Shirato, T. Murase, K. Atsumi in "Proceedings, Second World Filtration Congress", London, (1979), p. 39

181 M. Shirato, T. Murase, F. Iritani, and S. Nakatsuka, J. Chem. Engng. Japan, 19, 587 (1986)

182 M. Shirato, T. Murase and M, Iwata, Mem. Fac. Engng. Nagoya Univ. 38, 42 (1986)

183 B.F. Ruth, G.H. Montillon and R.M. Montana, Ind. Eng. Chem, 25, 76 (1933)

184 H.S. Carslaw and J.C. Jaeger, "The Conduction of Heat in Solids", 2nd Ed. Clarendon Press, Oxford, 1959, p. 89, 282

185 J. Crank, "The Mathematics of Diffusion" 2nd Ed., Clarendon Press, Oxford, 1986, p. 286

186 J.R. Haight, "Moisture Diffusivity Determination for Filtration", Ph.D Dissertation, Univ. of Massachusetts, 1987

187 K. Rietema, "Study on Compressibility of Filter Cakes", Ph.D. Thesis, Delft University of Technology, 1953

188 M. Shirato and T. Aragaki, Filtr. & Sep., 9, 294 (1972)

189 G.G. Chase and M.S. Willis, Sep. Sci. Technol., 26, 117 (1991)

190 B.R. Bierck, S.A. Welis and R.I. Dick, J. Water Pollut. Control Fed., 60, 645 (1988)

191 F.M. Tiller, N.B. Hsyung, Y.L. Shen and W. Chen, Proc. World Filtration Congress, Nice, France, 1990

192 M.A. Horsfield, E.J. Fordham and L.D. Hall, J. Magn. Reson., 81, 583 (1989)

193 F.B. Hutto, Chem Eng. Prog., 53, 328 (1957)

194 M. Shirato, T. Murase, K. Atsumi, T. Aragaki and T. Noguchi, J. Chem. Eng. Jpn., 12, 51 (1979)

195 B. Sivaram and P.K. Swamee, J. Jpn. Soc. Soil Mech. and Found. Eng., 17, 48 (1977)

196 Torikato and T. Yano, Agric. Biol. Chem. 51, 2983 (1987)

197 C. Buttersack, Chem. Eng. Sci., 40, 1145 (1994)

198 G.C. Mrema and P.B. McNulty, in "Solids Separation Process", I. Chem. Eng. Symposium Series 59, London, 1980, p. 2/2

199 G.C. Mrema and P.B. McNulty, Ir. J. Food Sci. Technol., 8, 59 (1984)

200 P.B. McNulty, in "Progress in Food Engineering", eds. C. Cantarelli and C. Peri, Forster Verlag, Kusnacht, Switzerland, 1983, p. 61

201 J.L. Lanoiselle, E. Vorobyov and J.M. Bouvier, Entropie 30, No. 186, 39 (1994)

202 J.C. Akkerman, F.H.J. Fox and P. Walstra, Neth. Milk Dairy J., 48, 1 (1994)

203 V.H. Abularach, "A Study of Cake Porosities in Constant Rate Pressing, M.S. Thesis, University of Massachusetts", 1979

204 J.J. Hamilton, and C.B. Crawford, in "Papers on Soils", ASTM STP 254, Am. Soc. for Testing and Materials, Philadelphia, 1959, p. 254

205 C.B. Crawford in "Consolidation Testing in Consolidation of Soils", eds. R.N Young and F.C. Townsend, ASTM, Philadelphia, 1988, p. 79

206 R.E. Smith and H.E Wahls, J. Soils Mech. and Found. Div. Am. Soc. Civ. Eng., 85 SM2, 519 (1985)

207 B.W. Huang, "Flow-Induced Pressure Drop During Expression", M.S. Thesis, Univ. of Massachusetts, 1979

208 S. Rebouillat and H.G. Schwartzberg, in "Food Engineering and Process Applications, Vol 2, Unit Operations" eds. M. Le Maguer and P. Jelen, Elsevier Appl. Sci. Publ., 1986, p. 281

209 M. Ghizzardi, "Studio e Modellazione della Spremitura della Pasta de Olive", Tesi di Laureo, Università degli Studi di Milano, 1993

210 K.E. Basken, D.K. Shirer, K.C. Koegel and H.D. Bruhn, Reducing the Energy Requirements for Plant Juice Protein Production, ASAE Paper No 75-1056, 1975, ASAE, St. Joseph, Michigan

211 S. Rebouillat, "Pressing Characteristics of Different Apple Cultivars", Report, Food Engineering Dept. University of Massachusetts, 1985

212 F. De La Garza and R. Bolton, Am. J. Enol. Vitic., 35, 189, (1984)

213 S. Rebouillat, "Studies of Media Resistance", Report, Food Engineering Dept. University of Massachusetts, 1985

214 H. Schwartzberg, S. Rebouillat, J. Humblot, D. Humblot and K.H. Kim Analysis of Pressing Characteristics of Apples, Proceedings 5th World Congress of Chemical Engineering, San Diego, July 14-18 1996, Vol II, 1996, p. 221

215 N. Pollack, "Study of the Feasibility of Gas-Aided Expression", M.S. Thesis, Univ. of Massachusetts, 1978

216 C. Buttersack and D. Blecher, Optimization of the Mechanical Dewatering of Sugar Beet Pulp, Proceedings 5th World Congress of Chemical Engineering, San Diego, July 14-18 1996, Vol II, 1986, p. 215

217 H.G. Schwartzberg, B. Zanoni, C. Peri and E Pagliarini, A Mathematical Model for Olive Paste Expression (to be submitted to AIChE.J.), 1996

218 S.H.I. Al-Mashad and C.A. Zuritz, J. Food Eng., 20, 247 (1993)

219 P.J. Banks, Theory of Constant Rate Expression and Subsequent Relaxation, Fourth International Drying Symposium Vol. 1, Kyoto, Japan, 1984, p. 112

220 G. Belfort, Chap. 7, in "Advances in Solid-Liquid Separation", ed. H.S. Muralidhara, Battelle Press, Columbus, 1986, p. 165-189

221 M.A. Biot, J. Appl. Phys., 12, 155 (1941)

222 O.C. Zienciewicz and T. Shiomi, Int. J. Numer. Anal. Methods Geomech., 8, 71 (1984)

223 B.A. Schrefler and L.A. Simoni in "Numerical Methods in Geomechanics", ed. G. Swoboda, A.A. Balkema, Rotterdam, 1988, p. 205-212

224 S.P. Neuman in "Finite Elements in Fluids Vol. 1", eds R.H. Gallagher, J.T. Oden, C. Taylor and O.C. Zienciewicz, Wiley, London, 1975, p. 201-217

225 I. Kormendy, Fundamentals of Mechanical Expression with Aspects of Generalization of the Expression Theory, in "Progress in Food Engineering", eds. C. Cantarelli and C. Peri, Forster-Verlag, Küsnacht, Switzerland, 1981, p. 47

226 T. Murase, N. Hayashi, H. Suzuki and M. Shirato, Int. Chem. Eng., 25, 130 (1985)

227 T. Murase, N. Hayashi, H. Suzuki and M. Shirato, Kagako Kogaku Ronbunshu, 9, 549 (1983)

228 J.G. Loughran, Personal communication, 1988

229 J.G. Loughran, "Mathematical and Experimental Modelling of the Crushing of Prepared Sugar Cane", Ph.D. Thesis, University of Queensland, Australia, 1990

230 D.R.J. Owen, S.Y. Zhao and J.G. Loughran, Eng. Comp., 12, 281 (1995)

231 M. Shirato, T. Murase, N. Hayashi, K. Miki, T. Fukashima, T. Suzuki, N. Sakakibara and T. Tazima, Kagaku Kogako Ronbunshu, 3, No. 3, 303 (1977)

232 M. Shirato, T. Murase, M. Iwata, N. Hayashi, E. Funahashi, and A. Nishi, Kagaku Kogako Ronbunshu, 11, No. 3, 331 (1985)